THE INTERACTION OF INTERMEDIATE ENERGY NUCLEONS WITH NUCLEI

A study of (p,n) reactions on some 1p-shell nuclei at 98.5 MeV

A Thesis submitted for the degree of
Doctor of Philosophy in the University of Oxford

by

R.A. Bell, B.A.

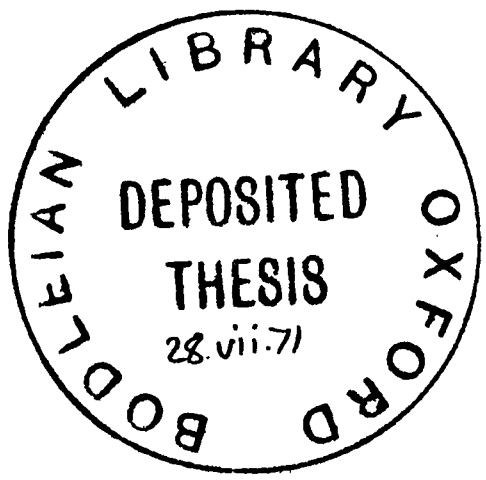

October,
1970.

Brasenose College,
Oxford.

ABSTRACT

Measurements have been made of the differential cross-sections for (p,n) reactions at 98.5 MeV on the 1p-shell nuclei ^{7}Li, ^{9}Be, ^{11}B, ^{12}C and ^{16}O over an angular range of 0° - 45° (lab). Angular distributions for transitions to excited states of the residual nuclei as well as their ground states were obtained. The energy resolution was ~ 1.2 MeV (f.w.h.m.) and the angular resolution 3.2° (f.w.h.m.). The angular distributions are subject to an error which varies systematically with angle and could be up to $\pm$ 10% at 12.5°, though it is thought likely to be less than this. The absolute normalization error is $\pm$ 14%.

The experiments were done using the neutron time of flight facility on the Harwell 2.79 m synchrocyclotron. Thin targets were bombarded with the internal proton beam of the synchrocyclotron and the neutron time of flight spectra determined using a 100 m flight path.

The experimental systems were considerably modified prior to the experiment and an investigation was carried out to determine the optimum energy resolution obtainable. It proved impossible to achieve the hoped for 0.5 MeV (f.w.h.m.).

An improved value was obtained for the degree of excitation of the 0.431 level in ^{7}Be in the $^{7}Li(p,n)$ reaction and this is compared with an impulse approximation prediction (Mahalanabis, 1964). The two values agree within experimental error, but the prediction is somewhat higher than the experimental value.

All the angular distributions established were discussed in terms of the structures of the states involved. The results are compared with previous (p,n) work at 100 MeV (Saltmarsh, 1965), 30 MeV and 50 MeV (Clough, 1969; Clough, 1970). Comparison is also made with results from $^{12}C(p,p')$ experiments (Hasselgren, 1965; Jacmart, 1964).

Shape fits to the angular distributions were made using a DWBA computer code (Friedman, 1966). The DWBA formulation is discussed, and the methods by which the code could be used to further analyse the results in order to determine the effective nucleon-nucleon interaction is explained.

It is thought that future developments in the study of (p,n) reactions at this energy are likely to be towards achieving considerably improved energy resolution, and a precise absolute normalization of the cross-sections.

PREFACE AND ACKNOWLEDGEMENTS

During the past four years, I have been working as a member of the Synchrocyclotron Group at A.E.R.E., Harwell. During the first year I was engaged on a study of p-p scattering at 98 MeV using the extracted proton beam of the 2.79 m synchrocyclotron, and during most of the second year, the synchrocyclotron was shut down for major modifications. Since the machine again became available for experiments, I have been working with the neutron time of flight group. Experiments undertaken by the group include a study of n-p bremsstrahlung, the study of (p,n) reactions which make up the bulk of this thesis, and, currently, an investigation of sub-threshold fission.

I would like to express my sincere thanks to the following people:

Dr. A. Langsford, my supervisor, for his invaluable advice and assistance throughout the experiment;

My colleagues Messrs. I.T. Belcher, G.C. Cox and especially P.H. Bowen who, like me, seemed to end up working most of the nights;

the operating staff of the synchrocyclotron and the staff of the Harwell central computer for their willing co-operation and assistance,

the engineering staff of the synchrocyclotron, Mr. K.C. Done, and in particular Mr. R.T.C. Smith, without whom the target changer would never have worked,

Dr. C.F. Clement and Mr. D. Jaques for a number of helpful discussions,

Dr. B. Rose for making arrangements for me to work on the synchrocyclotron,

The U.K.A.E.A. for providing me with a research grant, and, above all, I thank Sarah, my wife, without whose love I should never have finished.

CONTENTS

CHAPTER 1

INTRODUCTION

There has been considerable interest for many years in the study of nuclear reactions at intermediate energies (50 - 300 MeV). A great many experimental data have accumulated, and the theoretical understanding of the reactions has steadily improved. In the 1p-shell nuclei, the energy levels are now largely established, e.g. (Ajzenberg-Selove, 1968; Lauritsen, 1966), and interest centres round the angular distributions and magnitudes of the cross-sections.

Up to the present, (p,n) reactions have been little studied in this energy region, mainly because of difficulties in obtaining both good energy resolution and an adequate counting rate, and in determining the absolute normalization of the results. These problems have recently been partially overcome at Harwell, and the experiment which constitutes the bulk of the research presented in this thesis is a study of (p,n) reactions at about 98.5 MeV on the 1p-shell nuclei ^{7}Li, ^{9}Be, ^{11}B, ^{12}C and ^{16}O at laboratory angles in the range 0-45°, using the neutron time of flight facility on the Harwell 2.79 m synchrocyclotron. This work was an extension with improved energy resolution of the previous Harwell work at this energy by Saltmarsh (Saltmarsh, 1965).

The aims of the experiment are defined in section 1.1 and an account of the main features of nuclear reactions in general and (p,n) reactions in particular in the intermediate energy region is given in section 1.2. An account of recent major modifications to the synchrocyclotron and the time of flight system is given in section 1.3, and mention is made in section 1.4 of some other work carried out by the author during the period of this research.

The remaining Chapters of the thesis contain a detailed account of the experiment and its interpretation. The apparatus is described in Chapters 2 and 3 and the experimental runs in Chapters 4 and 5. The way in which the results were calculated from the basic experimental data is described in Chapter 6, and the results, together with their interpretation, are presented in Chapter 7. Chapter 8 gives an overall assessment of the experiment, and considers possibilities for future work in this field.

1.1 Aims of the experiment

The major aim of the experiment was to use the (p,n) reaction to study those states which are readily excited via direct interactions in the 1p-shell. The direct reaction mechanism is essentially simple, since processes in which the incoming particle interacts with more than one target nucleon may be ignored (see section 1.2), and so a simple interpretation of the results is hoped for in terms of the single particle structure of the states which are excited.

It was not the primary aim of the experiment to obtain a detailed understanding of the reaction mechanism in terms of DWIA, DWBA, or some other model, though shape fits to the angular distributions were made using a DWBA computer code (see Chapter 7, section 7.8). Rather the purpose was to obtain as comprehensive as possible a set of experimental data which would justify a subsequent detailed theoretical analysis.

An important secondary aim of the experiment was to investigate the properties of the time of flight system as used with the modified synchrocyclotron, and, in particular to determine the optimum energy resolution obtainable. These investigations, which were much more difficult and time consuming than was anticipated, are described fully in Chapter 4, where it is explained that the attempt to achieve a 0.5 MeV (f.w.h.m.) energy resolution failed, and that 1.2 MeV was the best that could be achieved.

1.2 (p,n) reactions at intermediate energies

1.2.1 Direct reactions

The main feature of reactions at intermediate energies is their "direct" character. Since the de Broglie wavelength of the incoming particle (~ 2.8 fm for a 100 MeV proton) is comparable with or less than the nucleon-nucleon spacing within a nucleus, it is expected to interact with only one target nucleon at a time, and, to first order, may be assumed to interact with one particle only during the whole reaction. This is the single scattering approximation.

The angular distributions of the cross-sections of such reactions exhibit particularly simple features. For a given transfer of orbital angular momentum, Δl, the shape depends much more on the size of the nucleus than on details of its structure. On the direct interaction single scattering model, the cross section is proportional to the matrix element

$$\int \chi_f^* \psi_f \; M(q) \; \psi_i \chi_i \; dV$$

where $\chi_{f,i}$ are the free particle wave-functions, $\psi_{f,i}$ are the nuclear wave-functions, and q is the momentum transfer.

Taking $\chi_{f,i}$ to be plane waves yields a term $e^{i\underline{q}.\underline{r}}$ which may be expanded in spherical harmonics:

$$e^{iq\cdot r} = \sum_{l=0}^{\infty} i^l \left(\frac{4\pi}{2l+1}\right)^{1/2} j_l(qr)\, Y_l^0(\Omega) \; .$$

By making simple assumptions about the nuclear wave-functions, see e.g. (Clegg, 1965), the main dependence of the angular distribution may be shown to be on the Bessel function, j_l, and to first order the angular distribution is given by

$$j_{\Delta l}(qR)$$

where R is the nuclear radius. The angle is kinematically determined by qR. In particular, $\Delta l=0$ transitions are forward peaked, $\Delta l=1$ transitions peak at $\sim 10^{o}$ for $1p$-shell nuclei at ~ 100 MeV, and for higher values of Δl, the distribution peaks first at higher and higher angles. Distortions of the Bessel function shapes occur but do not alter the gross features of the distributions, so that values of Δl may often be derived without a detailed description of the reaction. This determines the parity change, $(-1)^{\Delta l}$, of the nucleus, and the angular momentum selection rules restrict the change in total spin, ΔJ to be Δl or $\Delta l \pm 1$.

One of the earliest and most successful attempts to describe nuclear reactions was the optical model for elastic scattering which described the interaction of the incoming particle, not in terms of its interactions with individual nucleons, but in terms of an averaged potential due to the whole nucleus. This approach was successful at both low and intermediate energies, and in view of what has been said about the direct character of intermediate energy reactions, it ought to be possible to establish a relation between the two approaches. This was successfully achieved by Bethe (Bethe, 1958) following methods established by Watson et al (Watson, 1953; Francis, 1953; Riesenfeld, 1958). These ideas were extended by Kerman, McManus and Thaler (Kerman, 1959), who showed that both elastic and inelastic scattering could be formulated in terms of the nucleon-nucleon interactions within the nucleus. At the higher energies, the impulse approximation (IA) (Chew, 1950; 1952,A; 1952, B) is valid. This assumes that the nucleon-nucleon interaction is the same as that between free nucleons. This is a satisfying approach since it describes the reaction in terms of fundamental <u>experimental</u> quantities

- the free nucleon-nucleon scattering amplitudes - but at energies $<\sim 100$ MeV the assumption is likely to be invalid and a microscopic Born approximation (BA) approach is used which represents the nucleon-nucleon interaction within the nucleus in terms of a potential. It is assumed that there is no a priori knowledge about the strengths of the terms in this potential and that they must be determined from the direct reactions themselves. It is usual nowadays in IA and BA calculations to take as the wave functions for the incoming particles, waves which are distorted by a presumed optical potential, leading to the distorted wave models, DWIA and DWBA.

1.2.2 (p,n) reactions

In the reaction A(p,n)B, A and B are isobars and B has an atomic number, Z, which is one greater than that of A. The change in the third component of the isospin of the nucleus, ΔT_3, involved in the reaction is necessarily equal to -1 (adopting the convention that for the neutron $t_3 = +\frac{1}{2}$) but the change in total isospin, ΔT, depends on the isobaric quantum numbers of A.

If A is a $T=\frac{1}{2}$, $T_3 = +\frac{1}{2}$ nucleus, as was the case in the present experiment for ^{7}Li, ^{9}Be and ^{11}B, then A and B are mirror nuclei, and $\Delta T = 0$ transitions to analogues of the $T=\frac{1}{2}$ ground and excited states of A are allowed. Transitions to $T = 3/2$ states of B may also occur with consequently greater values of ΔT.

In the case of the T=0 nuclei ^{12}C and ^{16}O, no analogue can exist in B of T=0 states of A. Therefore the transitions are necessarily $\Delta T \geq 1$ to $T \geq 1$ states in B. The ground state of B will be the analogue of the first T=1 excited state of A.

The (p,n) reaction to a level in B clearly has similarities to the (p,p') transition to the analogous level in A. Consider first an "analogue transition", i.e. a transition between the analogous ground states of mirror nuclei. This corresponds to elastic scattering, and such reactions have been successfully analysed by extending the optical model to include an isospin dependent term, as first proposed by Lane (Lane, 1962). Thurlow has performed such an analysis (Thurlow, 1968) of the previous Harwell data (Saltmarsh, 1965).

Similarly the impulse approximation may be applied to (p,n) reactions simply by using the appropriate scattering amplitudes, and the Born approximation by including isospin dependent terms in the nucleon-nucleon potential. A DWBA computer calculation was used to fit the angular distributions from the present experiment, and further details of the formulation of the potential are given in Chapter 7, section 7.8.

It is also possible to derive some general conclusions about comparisons between (p,n) and (p,p') cross-sections. This is discussed further in Chapter 7, section 7.6.

1.3 Recent modifications to the Harwell 2.79 m synchrocyclotron and to the neutron time of flight facility.

The synchrocyclotron was extensively modified during the period 1967 - 8 and improvements were made to the time of flight system. Many of the synchrocyclotron modifications were not strictly relevent to the present experiment, but as reference is made throughout the thesis to the effects on the experiment of various aspects of the modifications, it was felt desirable to present a coherent outline here of the reasons behind them. A complete account of the facilities currently available from the synchrocyclotron has recently been published (Taylor, 1970).

Prior to the modifications, the synchrocyclotron accelerated protons only, at a repetition rate of 200 Hz. Internal beams up to 1.5 μA were obtainable, but an extremely inefficient extraction method was used, consisting of scattering the internal beam from a tungsten target into a magnetic channel. The extraction efficiency was $\sim 10^{-5}$.

The main aims of the modifications were to achieve much higher internal beams of protons, also deuterons, helium-3 particles and alpha particles; and to achieve a much higher extraction efficiency ~0.1. A regenerative extractor was designed, and for this to operate effectively, it was necessary to achieve good internal beam quality, in particular, small radial betatron oscillations.

The internal beam intensity is limited by the "space charge", consisting of particles which fail to accelerate, which exists at the machine centre during operation. Consequently to increase the beam intensity, the space charge was reduced by increasing the dee voltage, and consequently the repetition rate. The repetition rate was also made variable up to ~1600 Hz.

To obtain high beam quality, a Calutron ion source was used which injected most of the particles into similar orbits. In addition, since far fewer particles failed to accelerate, the space charge limit was reduced even further.

To reduce the r.f. power requirements at the new repetition rate to within acceptable limits, it was necessary to reduce the capacitance of the dee. This was achieved by altering the shape to a non-180° "cut-back" form. However it has become apparent, both theoretically and experimentally, that the cut-back at small radius resulted in off-centering forces on the protons which induced radial oscillation amplitudes up to 100 mm - far larger than was appreciated at the design stage. As a result, the beam quality is still relatively poor, and the extraction efficiency far worse than was hoped.

The study of (p,n) reactions using the synchrocyclotron involved bombarding a suitable thin target with the internal proton beam, and using the neutron time of flight spectrometer to measure the energy spectrum of the resulting neutrons. Since the extracted beam was not used, the major benefit of the modifications from the point of view of the present experiment was the increased internal beam current.

During the modification period, additional neutron flight paths were constructed, the longest being 100 m. It was not expected that the time resolution obtainable with the modified synchrocyclotron would be improved, but with internal beam properties expected to be much the same as before, the increased length of flight path available was expected to improve the energy resolution for 90 MeV neutrons from 2 MeV (f.w.h.m.) to 0.5 MeV.

1.4 Other research

During the period 1966-7, the author was engaged with others in an experiment (Wigan, 1967; Wigan, 1968) to measure the differential cross-section and the polarization in elastic proton-proton scattering at 98 MeV, and he also carried out an experiment (Bell, 1968) which used the 147 MeV extracted proton beam of the synchrocyclotron as a non-destructive probe to measure very small density fluctuations in a graphite disc, and to assess this technique for possible further applications.

CHAPTER 2

OVERALL DESIGN OF THE EXPERIMENT

This chapter gives an account of the overall design and layout of the experiment, and of the functional relationships between the components of the apparatus. These are the pulsed proton beam, the targets and target changing mechanism, the collimation and counter arrangements whereby a beam of neutrons was defined for a range of neutron production angles, and the electronic system for determining the neutron times of flight.

A detailed account of the apparatus and the experiments appears in Chapters 3, 4 and 5.

2.1 Basic Experimental Requirements

Chapter 1 established that the experimental method was essentially one of bombarding a target containing the nuclear species under investigation with a nearly mono-energetic proton beam whose mean energy was ~100 MeV, and determining the energy spectra of the neutrons emitted at various angles to the proton beam.

Due to the difficulty of wholly absorbing a neutron's energy in a detector in such a way as to produce a proportional response, the usual method of measuring neutron energies, and the one chosen for this experiment, is a time of flight technique. The energy of a neutron may be calculated if the time taken to traverse a given distance be known.

The principles of time of flight spectrometry using the Harwell Synchrocyclotron have been described elsewhere (Scanlon, 1957), the experimental requirements being a suitably collimated neutron beam, a detector at some distance from the target (109.17 m in this experiment), a pulsed beam to enable the time at which a detected neutron left the target to be known, and a system to measure the time interval between

this "start" time and the time of detection of the neutron.

The beam of a synchrocyclotron has an intrinsically pulsed structure, so that the Harwell 2.79 m synchrocyclotron used for this experiment is a particularly suitable machine for neutron time of flight experiments in this energy region.

2.2 Layout inside the synchrocyclotron

During the acceleration cycle of the synchrocyclotron, a phased bunch of protons spirals outwards, their mean radius and energy increasing monotonically. The full energy of the protons, attained at a radius of 1.39 m, is 150 MeV, but, in this experiment, a lower incident energy was achieved by placing the target under investigation inside the synchrocyclotron at a smaller radius, so that the beam was intercepted part way through the acceleration cycle. The targets were placed at a radius of 927 mm and the incident energy was measured, and found to be in the range 96 - 99 MeV, the precise value depending critically on the experimental conditions (see Chapter 6).

To achieve a short pulse of protons on the target such as is necessary for time of flight spectrometry, it was essential that the whole proton bunch should be incident on the target during a single orbit. There is no orbit separation on the synchrocyclotron, so that it was not acceptable to simply place the target in the plane of the beam - the median plane - and allow the protons to expand onto it. To overcome this problem, the target was placed below the median plane; and, when the protons were orbiting directly above the target, they were deflected downwards by means of an electrical pulse applied to a pair of plates placed one above and one below the median plane, so that the subsequent trajectory of the protons passed through the target.

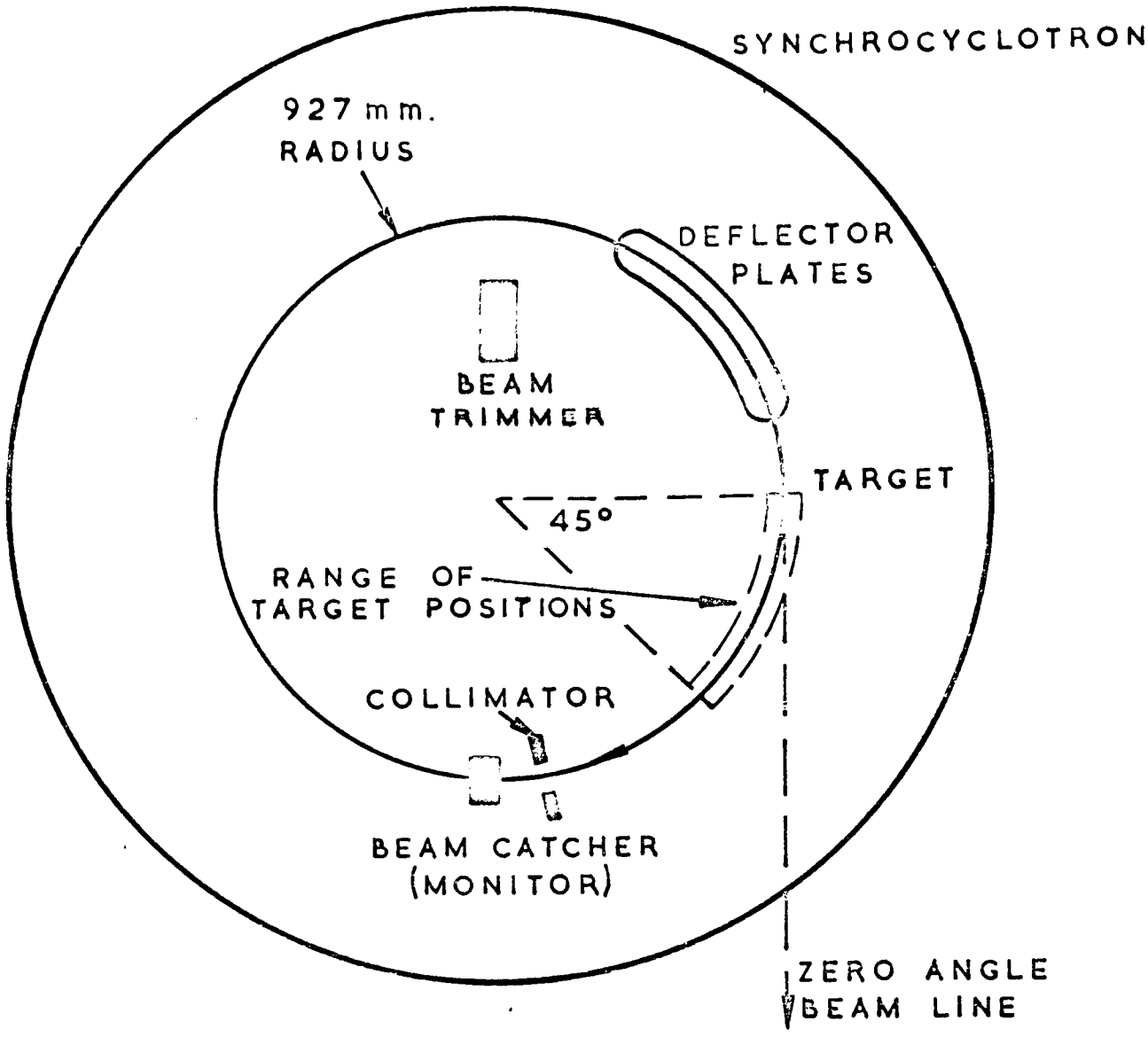

FIG. 2.2.A. LAYOUT INSIDE THE SYNCHROCYCLOTRON

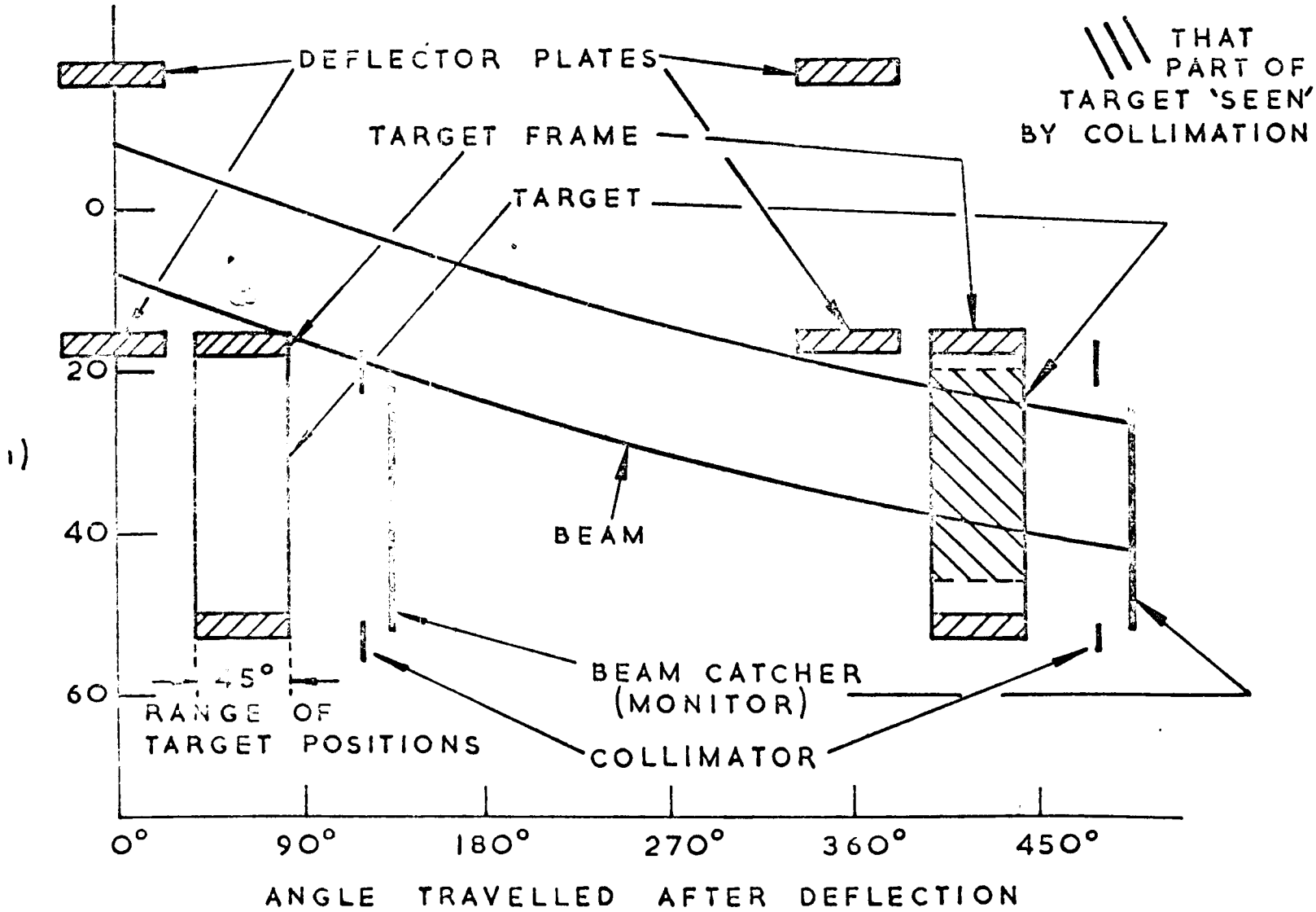

FIG. 2.2.B. TRAJECTORY OF PROTON BUNCH

To prevent multiple traversals of the target by the beam on subsequent orbits, a "beam catcher" which completely absorbed the protons was placed downstream of the target. The beam catcher was also used in an only partially successful attempt to monitor the integrated intensity of the internal beam by measuring the total charge collected during any one measurement.

The layout inside the synchrocyclotron used in this experiment is shown in fig. 2.2.A. The azimuthal position of the target was variable over a 45° range to allow observation of neutrons at different production angles as explained in the following section.

After deflection, the protons made a little over one further orbit of the synchrocyclotron before hitting the target. The calculated (Scanlon, 1957) trajectory of the bunch is illustrated in fig. 2.2.B in which its vertical extent and position is plotted as a function of the angular distance travelled after deflection. On the first post-deflection orbit the bunch passed over the target and the beam catcher; after one complete orbit it passed under the lower deflection plate; and on the second orbit it was incident on the target and the beam catcher.

It was necessary to limit the vertical extent of the bunch to 16 mm to ensure that no part of it was incident on the target or beam catcher on the first orbit. This was achieved by placing a block of carbon, the "beam trimmer", with its top 8 mm below the median plane at a smaller radius than the plates so that the deflected beam should not hit it. The vertical oscillations of the protons within the bunch ensured that the block trimmed the beam symmetrically about the median plane.

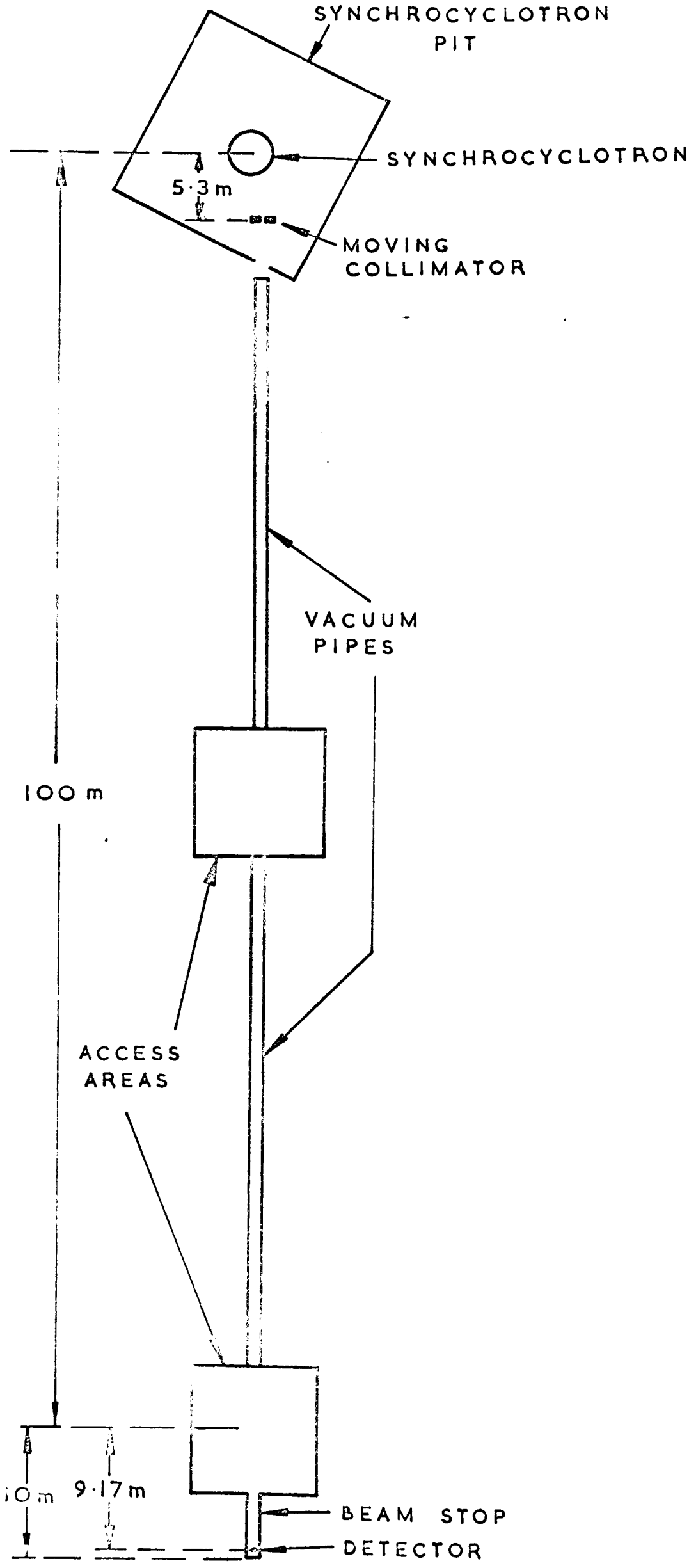

FIG. 2.3.A. THE OVERALL LAYOUT

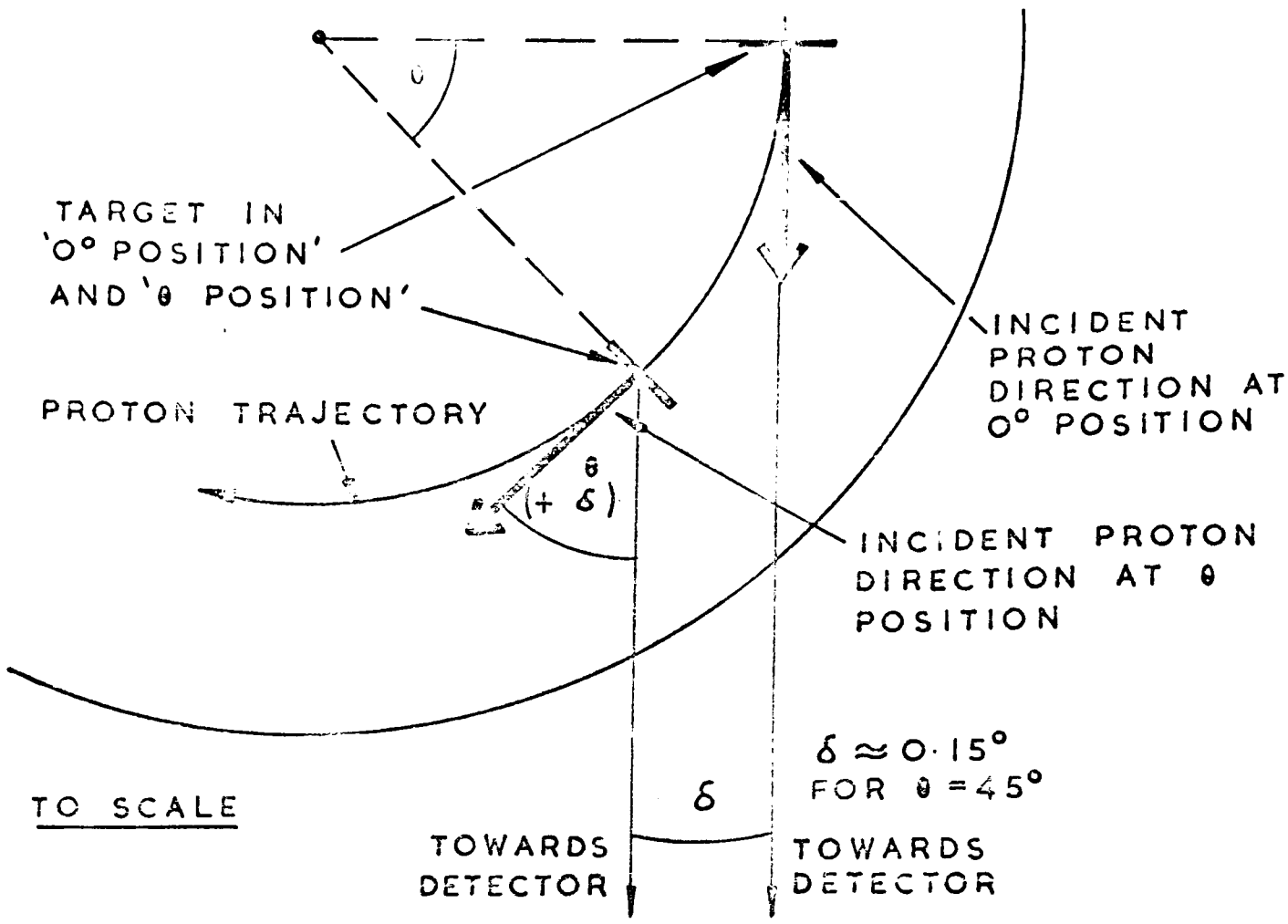

FIG. 2.3.B. OBSERVATION OF NEUTRONS AT DIFFERENT ANGLES

NOT TO SCALE

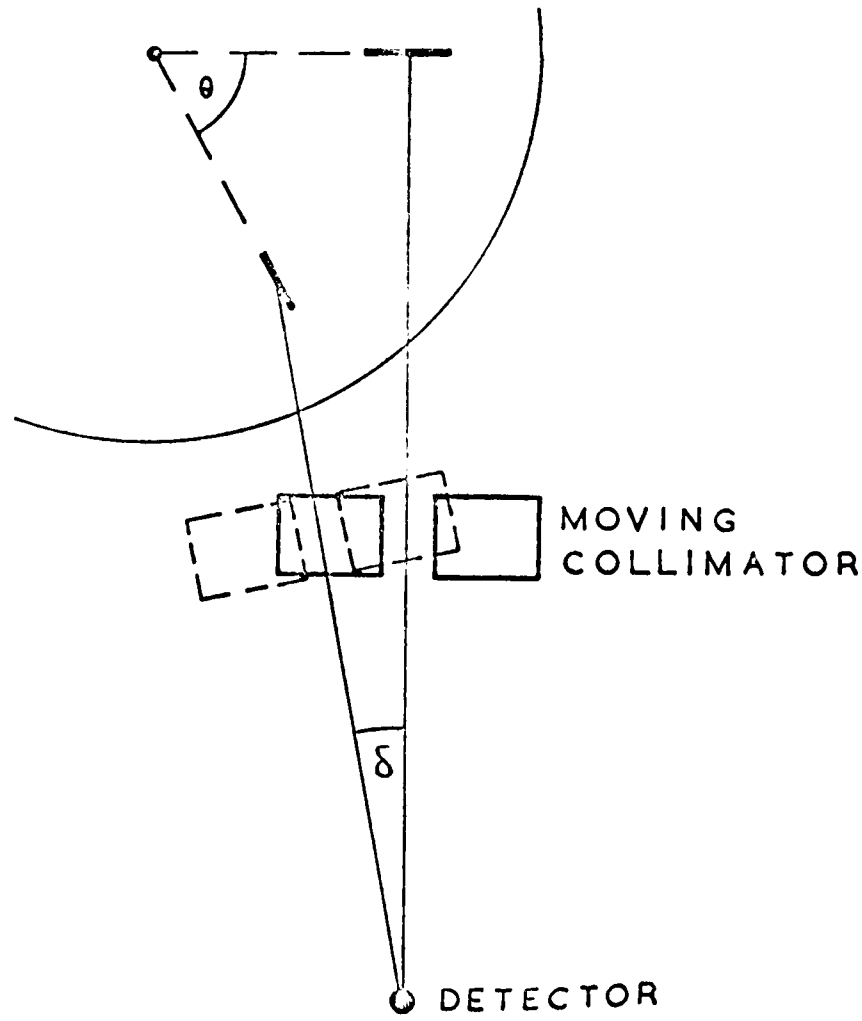

FIG. 2.3.C. MOVEMENT OF THE MOVING COLLIMATOR

2.3 The Overall Layout

The overall layout of the beam line is illustrated in fig. 2.3.A. The synchrocyclotron is in an underground pit and tunnels have been constructed for the neutron flight paths.

To obtain the longest possible flight path and therefore the best energy resolution, the detector was placed at the end of the 5 m long tunnel downstream of the 100 m access area as shown in fig. 2.3.A. This short length of tunnel was constructed as a "beam stop" to prevent back scattering from the walls leading to high backgrounds in experiments which observe scattered neutron beams in the 100 m area. Such backgrounds in the present experiment were negligible because the counter was in the main neutron beam.

The pipes lying along the flight path were evacuated to reduce the attenuation of the neutron beam.

Only one defining collimator was used, at a distance of 5.3 m from the target. The neutron beam was defined by this collimator and the detector.

The usual method of observing the products of a nuclear reaction at different scattering angles is to keep the incident beam and the target fixed, and to swing the detector round so that the scattered beam line pivots about the target. This was clearly impossible in the present experiment - the size of the beam pipes limited the range of angular movement to 0.15°. Hence the observed scattering angle was changed by varying the azimuthal position of the target inside the synchrocyclotron and keeping the detector fixed. This is illustrated in figs. 2.3.B and 2.3.C where it can be seen that while the final neutron direction changed by at most 0.15°, the incident proton direction changed as the protons swung further round in their orbit before hitting the target. The beam

line pivoted about the detector. The size and position of the vacuum pipes limited the range of observable angles to 0^{o} - 45^{o}.

Because of this movement of the beam line, it was necessary for the defining collimator to move laterally to follow the target as illustrated in fig. 2.3.C, which is not drawn to scale. Also, as the direction of the beam line changed by up to 0.15^{o}, it was desirable for the 610 mm long collimator to rotate by up to 0.15^{o} so as to remain parallel to the beam as illustrated in the figure. The moving collimator is described in detail in Chapter 3.

In addition to the need to move the target azimuthally inside the synchrocyclotron, it was also necessary to have all the targets under investigation inside the synchrocyclotron at once, and to position automatically a selected target at the required radius. The reason for this was to avoid the excessive delays involved in opening the synchrocyclotron vacuum tank and the consequent changes in running conditions which would have made relative normalization of the spectra from target to target very difficult. The device used to perform this function and to effect the azimuthal movement, was called the "target changer" and is described in Chapter 3.

Both the target changer and the moving collimator were remotely controllable from the laboratory.

The time of flight of a detected particle was determined from the time of application of the deflection pulse and the time at which the particle was detected. The electronic timing and display system used for this purpose is described in Chapter 3.

2.4 Summary

This chapter has sought to explain the purpose of the apparatus used in the experiment.

The incident proton energy was fixed at less than the full energy of the synchrocyclotron by placing the targets in the synchrocyclotron so that the beam was incident on them part way through the acceleration cycle. The neutron energy spectra were determined using a time of flight technique, and the necessary short incident pulse of protons was achieved by deflecting the whole proton bunch downwards onto the target.

The observed neutron production angle was varied by moving the target azimuthally. This necessitated the movement of the defining collimator and the construction of a device to effect the azimuthal movement of the target.

The construction and operation of the apparatus is described in detail in the next chapter.

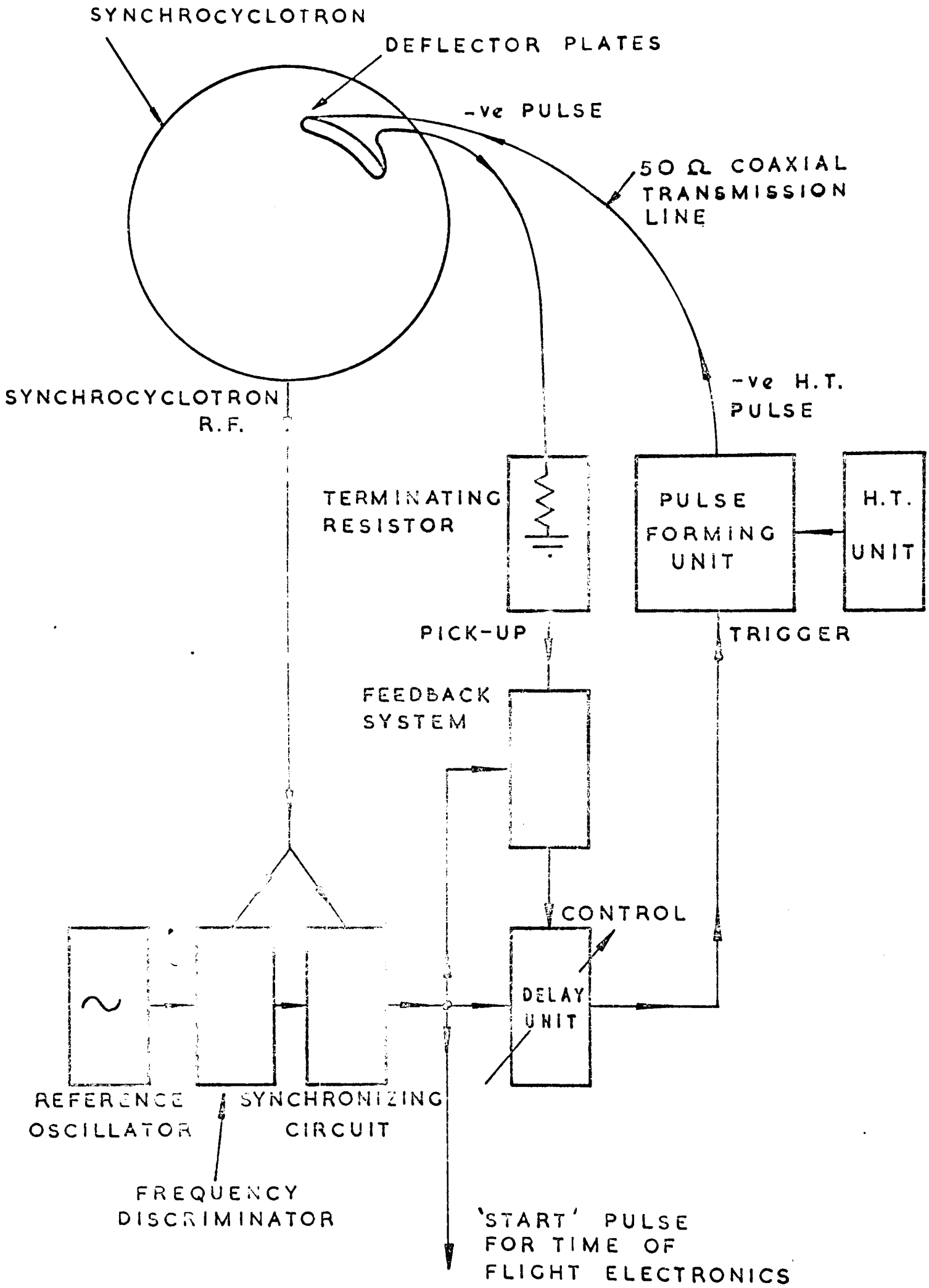

FIG. 3.1.A. THE DEFLECTION SYSTEM

CHAPTER 3

THE APPARATUS

This Chapter describes the apparatus in detail and gives an account of how it was used. Further details about the experiments are given in Chapter 5.

The apparatus described consists of the deflection system, the target changer, the targets, the moving collimator, the vacuum pipes, the detection system, and the electronic time of flight spectrometry system.

3.1 The Deflection System

This section outlines the system used for deflecting the proton bunch inside the synchrocyclotron downwards onto the target. The principles of such a system have been described by Scanlon et al (Scanlon, 1957) and it is anticipated that a full description of the present system will appear elsewhere (Bowen, 1970).

The deflection system was completely redesigned prior to the experiment, which was the first to make use of it. The earlier experimental runs therefore served partly to commission the new system.

The system is illustrated schematically in fig. 3.1.A. Since the synchrocyclotron is frequency modulated, the frequency of the r.f. accelerating voltage could be used to determine the point in the acceleration cycle at which the protons were orbiting at the required radius. To effect this, the r.f. was fed into a frequency discriminator ( ), as shown, which output a pulse when the frequency of the r.f. became equal to that from a reference oscillator. The pulse was then phased to the r.f. by the synchronizing circuit (Langsford, 1965,A), and after passing through a controlled delay was used to trigger the pulse forming unit which applied the H.T. pulse to the deflection plates. The output of the

synchronizing circuit was also used as the "start" pulse for the time of flight electronics.

When suitably triggered, the pulse forming unit, whose main component was an English Electric CX1168 Thyratron, applied a negative H.T. pulse to the lower deflection plate via a 50 Ω co-axial transmission line. The deflection plates formed part of this line, which was terminated in a 50 Ω load resistor. Information about the time of arrival of the pulse at the plates was derived from a pick-up from this terminating resistor, and was input to a feed-back system, which controlled the delay in order to compensate for drifts in the operating time of the pulse forming unit.

Protons passing between the plates experienced a downwards force due to the interaction of the beam current with that flowing in the plates, in addition to that caused by the electrostatic field between the plates (Langsford, 1965,B).

To set up the system, the feed back unit was switched off, and the oscillator frequency set to approximately the correct value (21.75 MHz for a radius of 927 mm). The phasing delay was then manually varied to give maximum deflected beam. The frequency of the reference oscillator was then varied, the phasing delay being optimised after each change, and set at the value which gave maximum beam. The feedback system was then switched on to hold the phase constant.

The optimum value of the voltage supplied by the main H.T. unit was determined in a similar way to be 40 kV.

3.2 The Target Changer

The purpose of the target changer was to allow any one of a number of different targets to be positioned inside the synchrocyclotron at the required radius of 927 mm, and at a range of azimuthal angles covering 60^{o}.

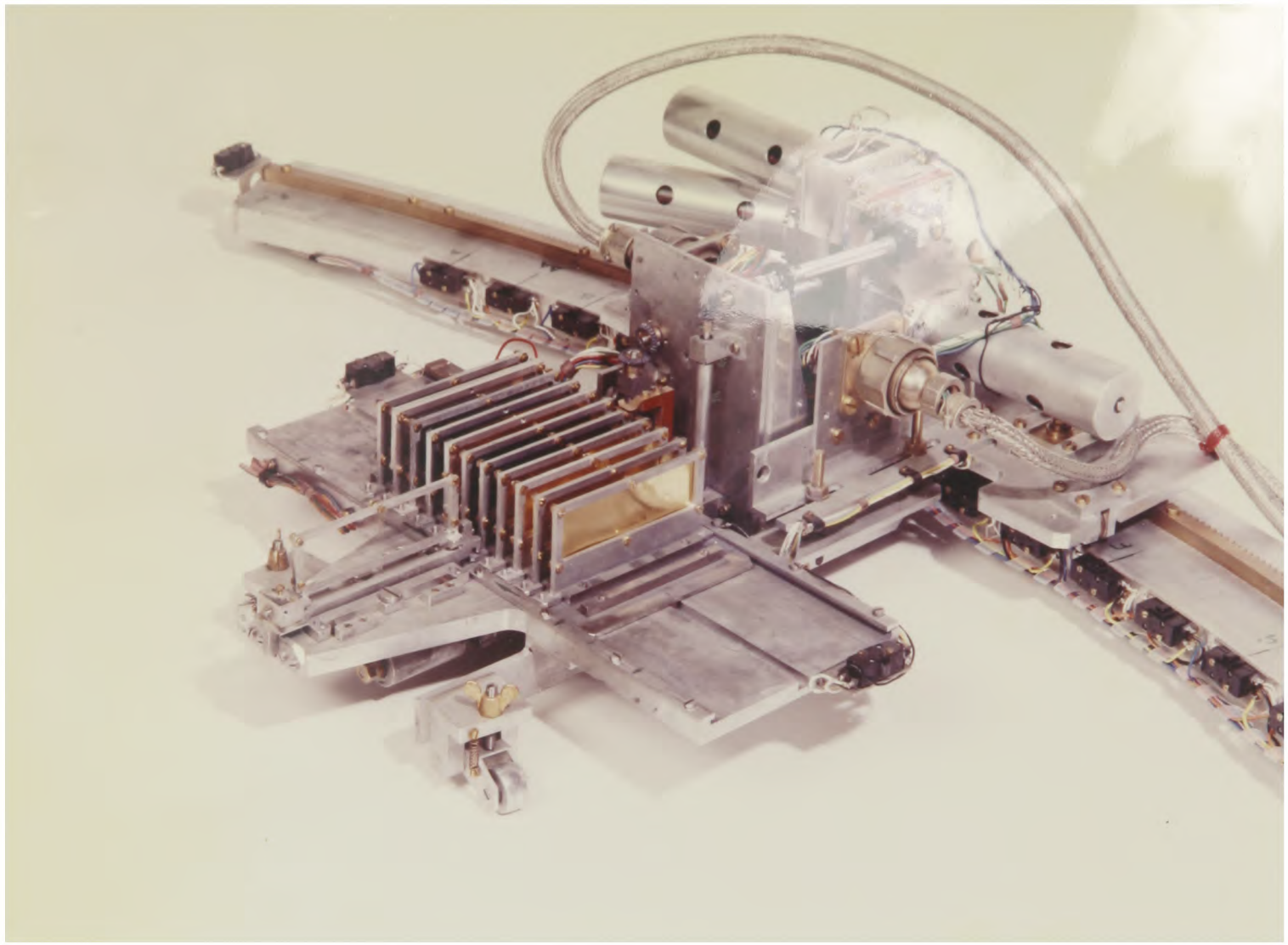

(i)

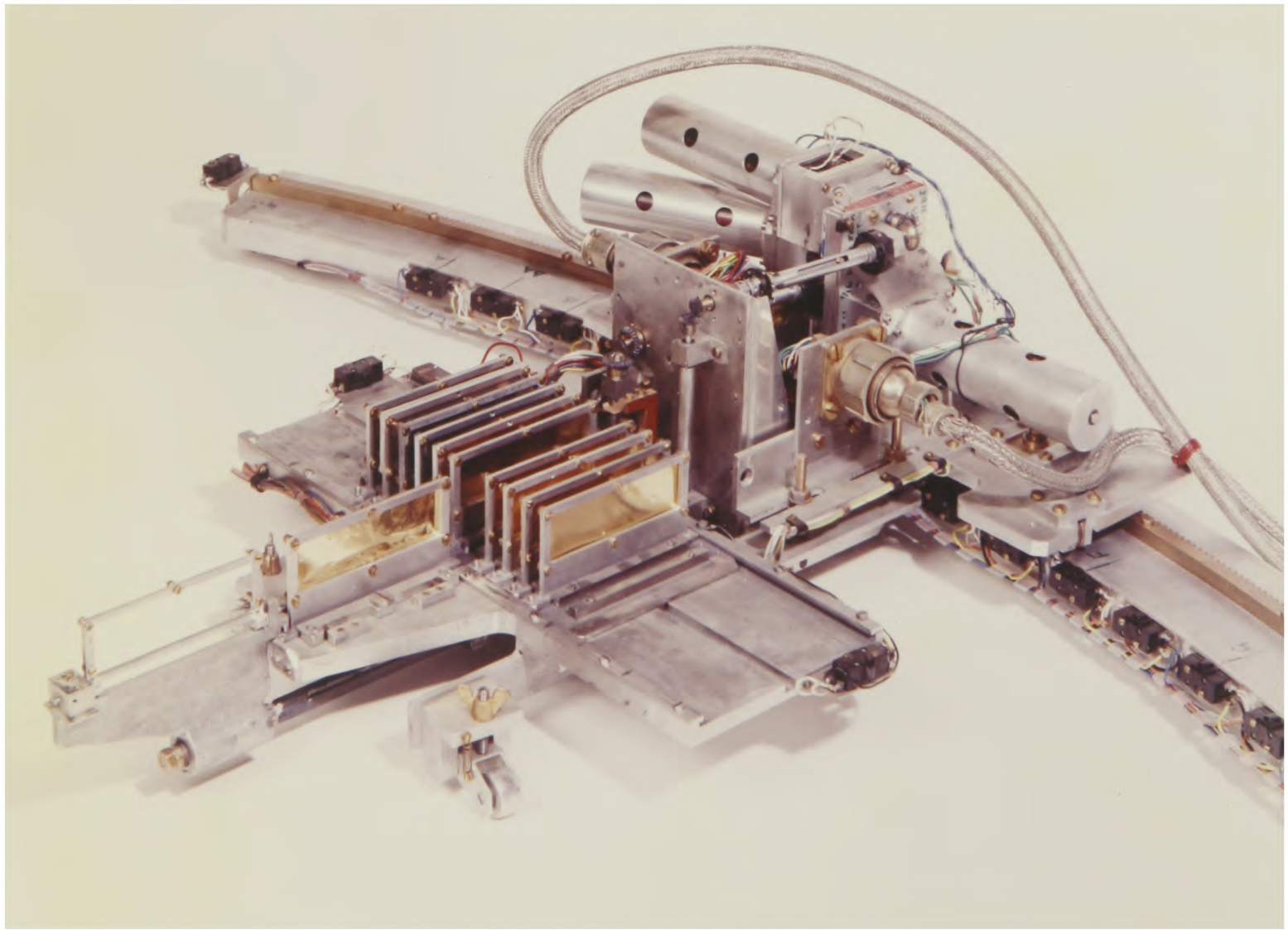

(ii)

FIG. 3.2.A. THE TARGET CHANGER

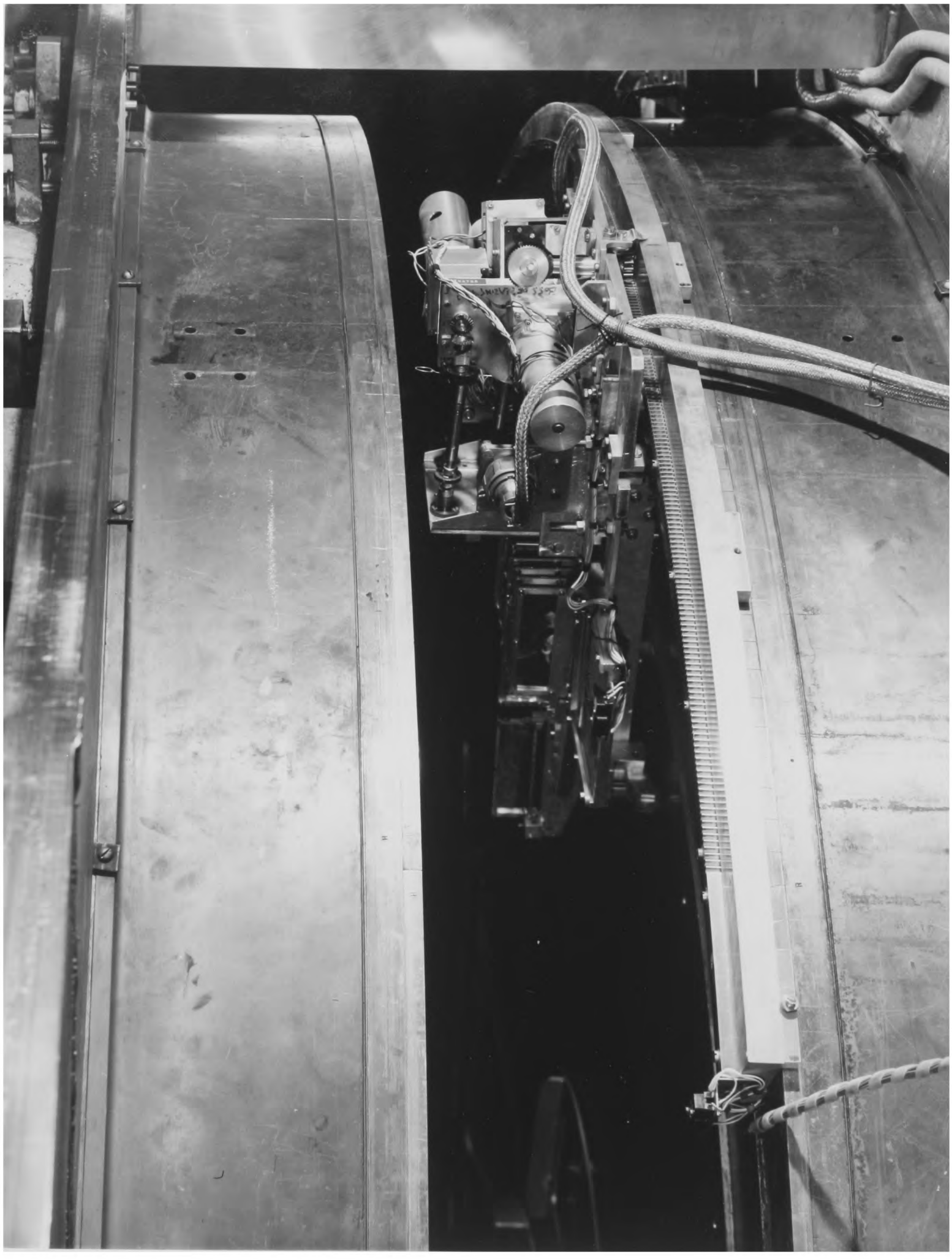

FIG. 3.2.B. THE TARGET CHANGER IN THE WORKING POSITION

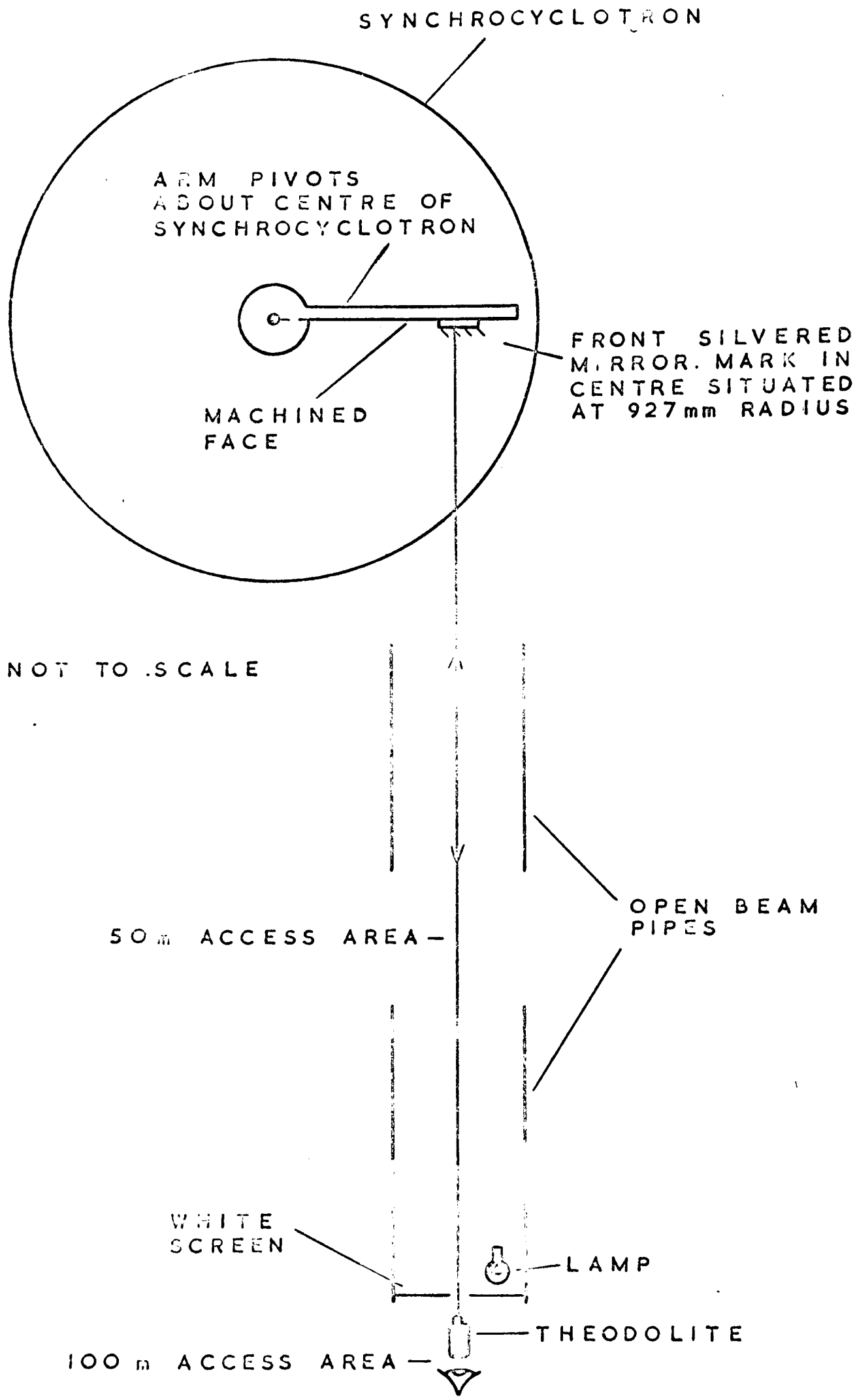

FIG. 3.2.BB. DETERMINATION OF THE 'ZERO-ANGLE' AZIMUTHAL POSITION

Power for the device was derived from motors specially constructed to operate inside the synchrocyclotron where the working conditions were a high vacuum and a magnetic induction of 1.5 T (15 k gauss). The motors consisted of bare armatures with no field windings, and utilised the magnetic field of the synchrocyclotron.

Overall views of the target changer are shown in fig. 3.2.A., and a view in the working position inside the synchrocyclotron is shown in fig. 3.2.B. The main assembly positioned the selected target at the required radius, and its azimuthal position could be varied by moving the assembly along a curved track clamped to the outer edge of the lower pole face of the synchrocyclotron.

3.2.1 The Azimuthal Movement

The target changer was driven azimuthally along the track by means of a rack and pinion. The rack, which can be seen in fig. 3.2.A running along the centre of the track, was engaged by a pinion fixed to the main assembly and driven by one of the motors via a 250:1 reduction gear box. The assembly was constrained to remain radially oriented as it moved along the track, and in use the rate of charge of azimuthal angle was $\sim 0.05^{o}\ s^{-1}$.

The "zero-angle" azimuthal position inside the synchrocyclotron was determined by means of a theodolite situated on the beam line in the 100m access area as shown in fig. 3.2.BB. The image of the screen with a dark hole in the centre could be clearly seen reflected in the mirror. The zero-angle azimuth was then found by rotating the arm holding the mirror about the centre of the synchrocyclotron until the image of the hole was superimposed on the mark on the mirror at the required radius of 927 mm. It was found necessary to use a front silvered mirror, since small non-uniformities in the glass of a back silvered mirror caused considerable distortion and blurring of the image over the 200 m light

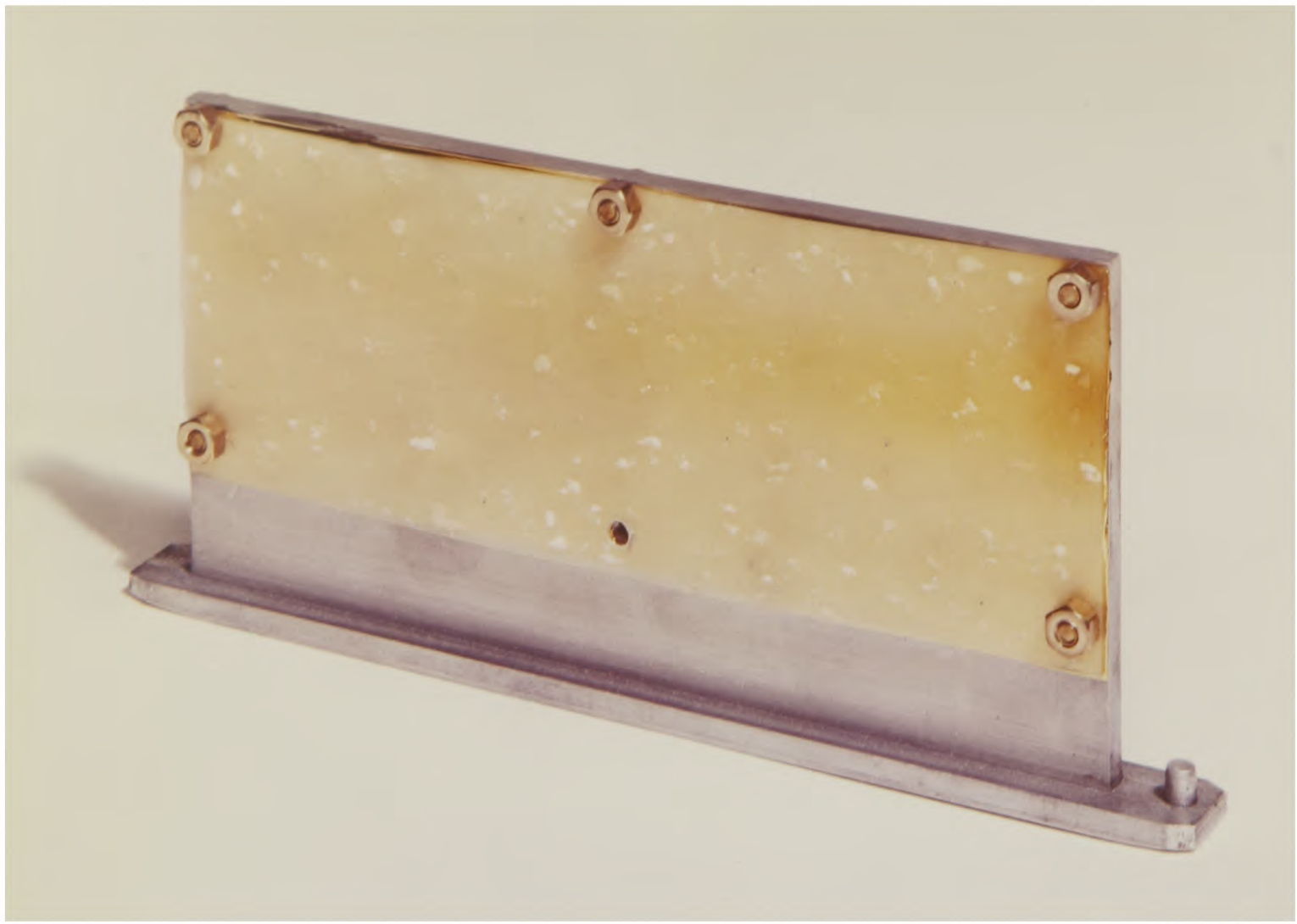

FIG. 3.2.C. THE DEUTERATED POLYTHENE TARGET

NOTE: THE OVERALL GOLD COLOUR IS DUE TO THE GOLD BACKING OF THE TARGET, BUT, IN ADDITION, CHARRING OF THE DEUTERATED POLYTHENE DUE TO HEATING CAUSED BY THE BEAM MAY BE SEEN, MAINLY TOWARDS THE RIGHT HAND SIDE.

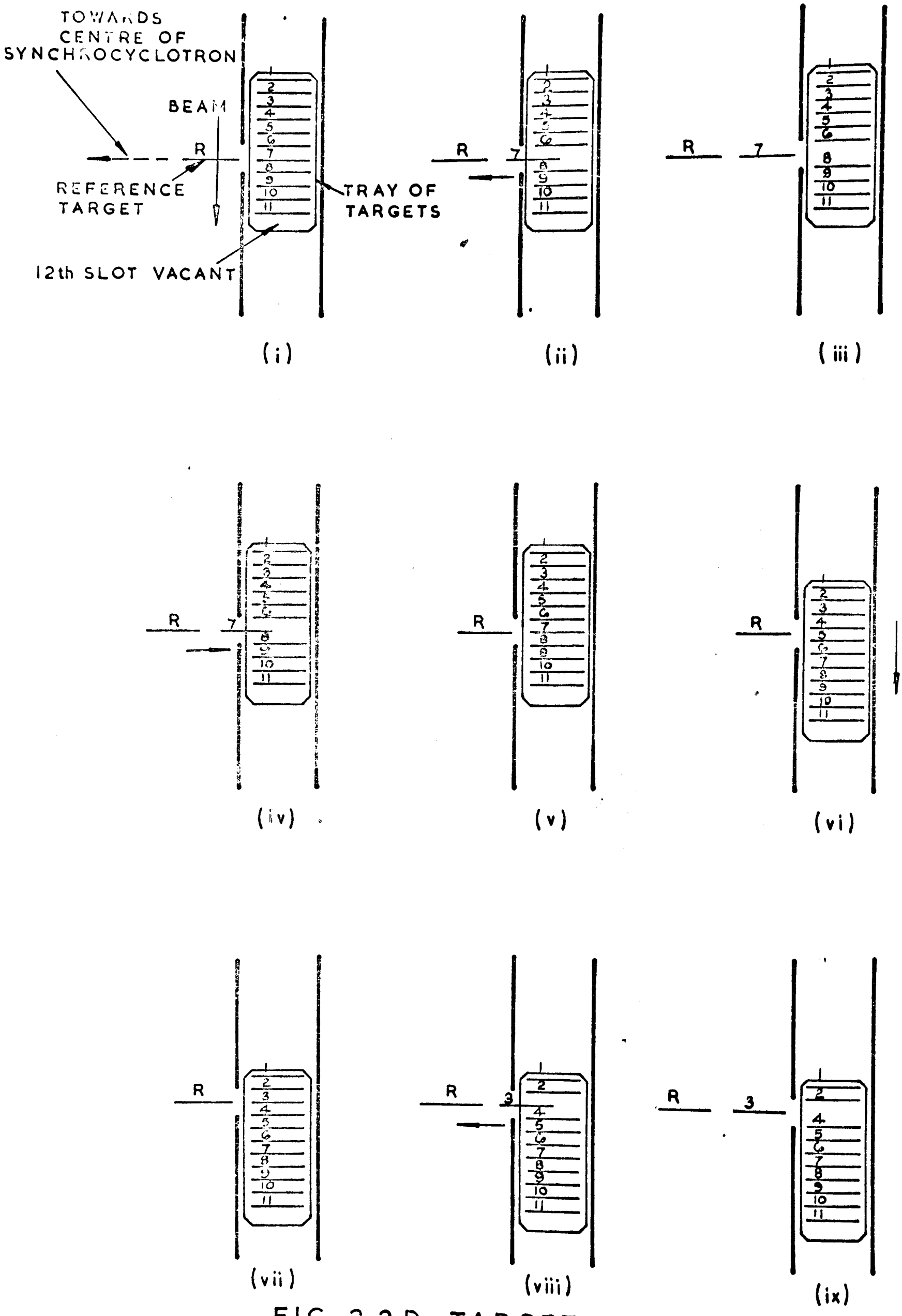

FIG. 3.2.D. TARGET SELECTION

path. From the estimated error in radial orientation of the mirror, it was calculated that the azimuth had been found to 0.02°.

The azimuthal position of the target changer was determined by means of a series of microswitches set at roughly 2.5° intervals along the track and actuated by the passage of the target changer. It could be stopped at a microswitch position with a reproducibility of 0.1°.

3.2.2 Target Selection

The method used for inserting the selected target to the required radius was similar to that used in some semi-automatic slide projectors. Each target was fixed to a target frame, and the flat bottoms of the frames were slotted into a tray so that the targets stood upright one behind the other. The targets were 30 mm high and 100 mm wide and the tray could hold up to 12 targets. A single target (deuterated polythene) is shown in fig. 3.2.C and the tray of targets is visible in the overall views shown in 3.2.A.

In addition to the targets in the tray, a further target known as the "reference target" was used for normalization purposes. Its position relative to the other targets, and the method of target selection may be inferred from fig. 3.2.D. (i) shows the reference target in the beam, and (ii) - (iii) show the insertion of target number 7 into the beam, the reference moving out of the beam to a lower radius. (iv) - (ix) show the subsequent selection of target 3. Fig. 3.2.A (i) and (ii) show views of the target changer with the target respectively extracted and inserted, the reference target being respectively in and out of the beam position. It should be noted that changing between a target from the tray and the reference target and vice versa only involved a single extraction or insertion and was much more rapid than changing between two other targets. This enabled frequent rapid

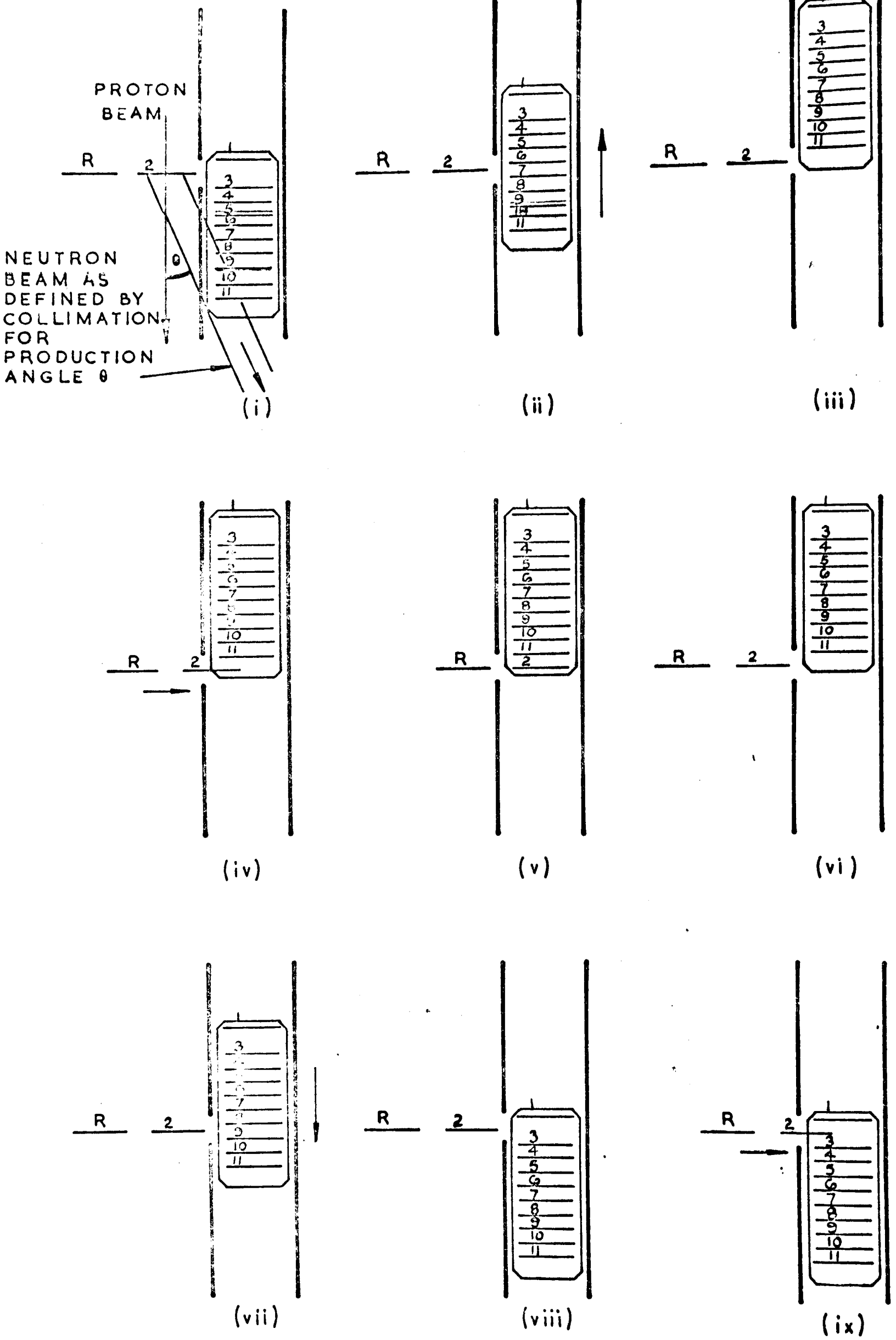

FIG. 3.2.E. TARGET SELECTION AT LARGER ANGLES

investigation of the reference target, which was chosen to be lithium because the intense narrow peak of neutrons resulting from the $Li^7(p,n)^7Be$ (g.s.) reaction provided a good energy resolution and incident proton energy check throughout the experiment (see Chapter 4).

It may be seen from fig. 3.2.E (i) that at certain target positions and neutron production angles, the neutron beam passed through the targets in the tray. Fig. 3.2.E (ii).- (ix) show how this problem was overcome by moving the tray laterally. Slot number 12 was left vacant so that the reference target could be rapidly investigated after this lateral movement, as shown in the figure.

The lateral movement of the tray, and the insert/extract mechanism were separately driven by the motors, so that, including the one for the azimuthal drive, three motors were used in all.

3.2.3 The Target Changer Control Unit

The target changer was operated by remote control from the laboratory using a purpose built control unit. This unit provided a visual indication of the state of the target changer, and interlocked the drives so that it was impossible to carry out any procedure which would damage the mechanism, e.g. driving the tray laterally when a target was only half inserted. There was also a facility for automatically stopping the azimuthal drive at a microswitch position.

The unit could also be switched from manual control to control by an on line computer via the CAMAC interface system. It was originally intended to control the target charger using a Honeywell DDP-516 computer and a considerable amount of software was written for the purpose. However, it became apparent that the operating system of the computer was not going to be ready in time, and the project was abandoned.

NOTES.

1. THE TARGETS SHOWN WERE USED FOR DATA TAKING. SOME THICKER TARGETS WERE ALSO USED FOR COMPARISON PURPOSES.

2. THE kg-atom IS DEFINED ON THE SCALE $^{12}C = 12$.

3. 1 kg m^{-2} = 0·1 g cm^{-2}.

TARGET MATERIAL		AREA DENSITY (kg m^{-2})	AREA DENSITY OF MAIN ISOTOPE (kg-atom m^{-2})	PROTON ENERGY LOSS (MeV)
CD_2	D	0·569	0·0710	0·393
	C		0·0351	
Li	OCT./NOV. 1969	0·666	0·0878	0·395
	DEC. 1969	0·594	0·0783	0·353
Be		0·603	0·0669	0·359
B	OCT./NOV. 1969	0·483	0·0348	0·295
	DEC. 1969	0·517	0·0373	0 316
C		0·522	0·0430	0·398
Li OH. H_2O	O	0·593	0·0284	0·409
	Li		0·0131	

TABLE 3.3 A

TARGETS

However, the facility was modified and Chapter 5.4 explains how for part of the experiment, the control unit was interfaced to a system of scalers which automatically operated the insert/extract mechanism, and gave more reliable monitoring of the experiment than an entirely manual system would have provided.

3.3 Targets

The targets used were all fixed to frames of standard construction which measured internally 100 mm wide and 30 mm high. This size and shape was chosen to coincide roughly with that of the beam. A target in its frame was shown in fig. 3.2.C.

The thicknesses of the targets were chosen so that the 0.33 MeV energy loss of the proton beam in passing through the targets should only very slightly worsen the energy resolution of 1.2 MeV achieved in the experiment. Thicker samples of many of the targets were also used to allow a useful comparison between thick and thin versions of the same element in energy resolution investigation.

Excepting deuterium, samples of the natural elements were used as the neutron spectra from the minority isotopes had a negligible intensity with respect to the main isotope either overall, or in the energy region of interest.

Lithium, beryllium, boron and carbon were studied in elemental form, oxygen in the form of lithium hydroxide, and deuterium in the form of deuterated polythene. The lithium, beryllium and deuterated polythene targets were strong enough to be bolted to the target frame. The brittle carbon targets were slotted into an aluminium holder bolted to the target frame. It was almost impossible to obtain solid samples of lithium hydroxide and boron of sufficient size, thickness and strength, and the method of manufacture of these targets from the powdered substances is described in Appendix A.

It was necessary to have a reasonably high yield of gamma rays to determine both the origin of the time of flight spectrum, and the time resolution function as explained in Chapter 6. To achieve this, all the targets were backed with

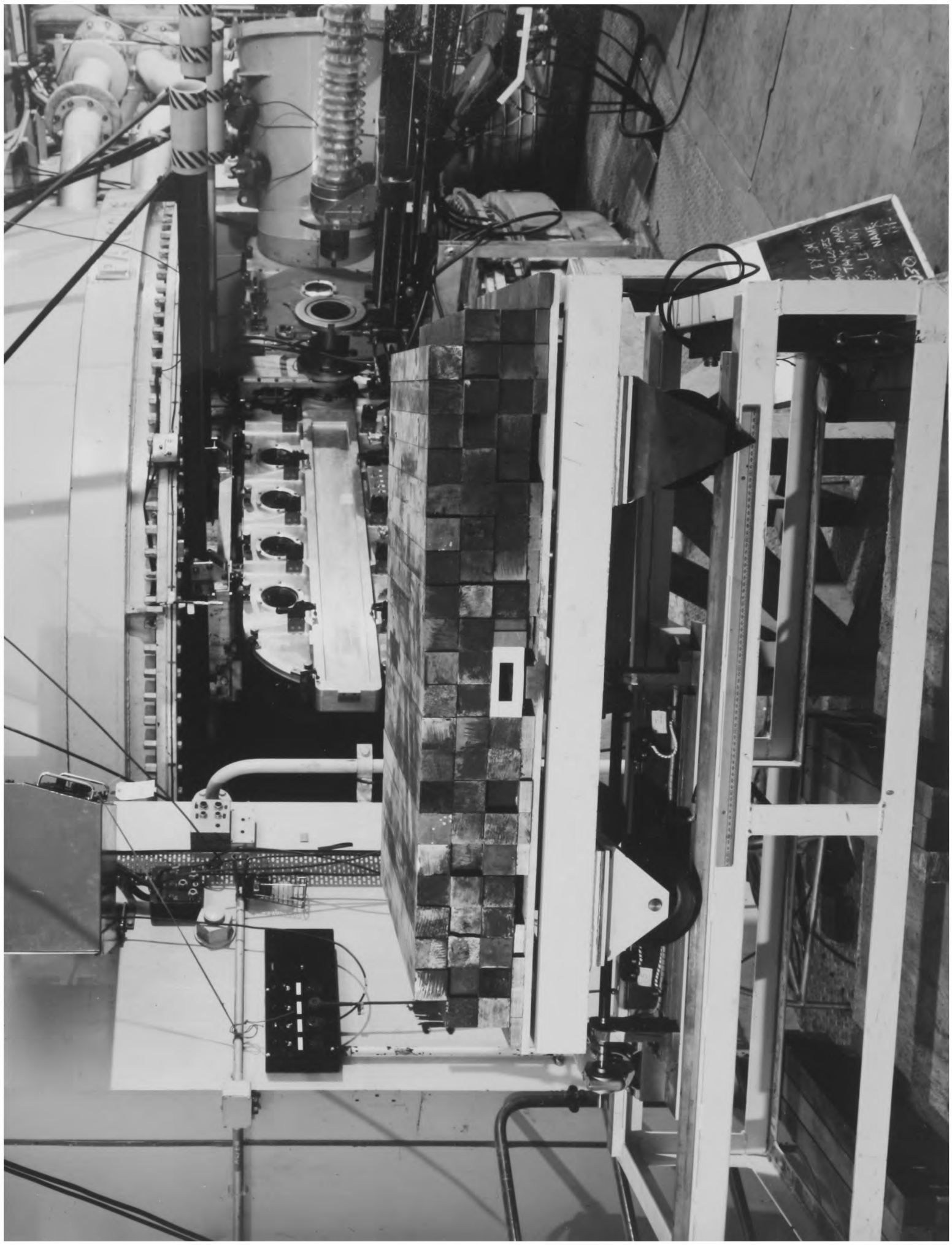

FIG. 3·3.A. THE MOVING COLLIMATOR

50 μm thick gold foil.

A list of the targets used, and their thicknesses is given in table 3.3.A.

3.4 The beam catcher/monitor

The beam catcher was situated inside the synchrocyclotron downstream of the target, as shown in fig. 2.2.A, to prevent multiple traversals of the target by the beam.

It was also used to monitor the intensity of the incident proton beam, and consisted of an electrically insulated and shielded block of copper 32 mm high, 130 mm wide and 65 mm long. A collimator, 70 mm wide and 24 mm high, was placed in front of it. A cable from the copper block to the laboratory was connected to earth through a 100 kΩ resistor and the voltage developed across the resistor was a measure of the current deposited on the block. An integrating digital voltmeter (IDV) was connected across the resistor and measured the total charge deposited during any one measurement.

The monitor was an extremely useful tool for determining short term variations in the internal beam intensity, but was found to be deficient for normalizing the data. This is discussed in section 5.3.

The beam catcher/monitor is henceforth referred to as "the monitor".

3.5 The Moving Collimator

Section 2.3 explained that as the target was moved inside the synchrocyclotron to allow observation of neutrons at different production angles, it was necessary to move the defining collimator laterally by up to 270 mm to follow the beam line, and desirable to rotate it by up to 0.15^{o} so that it remained parallel to the beam line.

An overall view of the moving collimator with the synchrocyclotron in the background is shown in fig. 3.5.A in which it may be seen that the collimator and its associated steel shielding was built up on a trolley running on rails attached to a steel framework. The collimator aperture, which may be seen towards the bottom of the shielding, was 20 mm high and

80 mm wide. Its width could be reduced to 60, 40, 20 or 10 mm by the insertion of suitable steel plugs.

The shielding was 610 mm (2 feet) long and transmitted only 7×10^{-5} of a 100 MeV neutron beam.

The lateral extent of the shielding was 1.22 m, and was wide enough to obscure the slot in the wall of the synchrocyclotron pit downstream of the collimator from background neutrons for all lateral positions of the collimator. Such neutrons were emitted, in particular, from the target, the monitor and the deflector plates.

The lateral movement of the trolley on its rails was driven by a lead screw fixed to the frame and powered by a mains A.C. electric motor.

The top plate, upon which the shielding was situated, could rotate about a vertical axis through its centre, and was driven by a short lead screw placed tangentially 480 mm from the axis, and powered by a second mains A.C. motor.

The moving collimator was controlled from the laboratory, and the control unit was designed for computer as well as manual control. The facility for computer control was not used.

The lateral position of the collimator was determined in the laboratory by means of a closed circuit television system which viewed a pointer moving over a millimeter scale. The position could be set to 0.2 mm. The position corresponding to the zero-angle position of the target changer was determined by viewing the target with a theodolite placed on the beam line in the 100 m access area, and driving the collimator until the aperture was in line with the target. Positions corresponding to the other angles were calculated, and the calculations confirmed using the theodolite.

The angular position was determined by means of a scale fixed to the end of the top plate, but since a second television system was not available, a given angular position was reached from the laboratory by driving the motor for an empirically calibrated length of time, taking the point at which an end-stop microswitch shut off the motor as the starting point. The "zero-angle position" was determined using the theodolite and the other positions calculated. The position could be set to 0.02^{o}.

3.6 The Vacuum Pipes

The pipes lying along the flight path were evacuated to reduce the attenuation of neutrons in the air. There is a 26% attenuation for 100 MeV neutrons in 100 m of air and this was reduced to 11% lost in the remaining 27.46 m of air and the thin aluminium windows. Further attenuation in the door of the synchrocyclotron led to an overall loss of 17%. The attenuation increased with decreasing neutron energy, being 25% for 60 MeV neutrons.

Thin, 3 mm thick, aluminium "windows" in the blanking plates at the ends of the pipes were used in preference to plastic film windows to avoid the danger of an implosion resulting from their comparatively large size. The size had to be sufficient to completely contain the whole range of beam lines.

3.7 The Detection System

The detector consisted of a piece of NE 102A plastic scintillator viewed by a G.E.C. 56 AVP photomultiplier tube.

The output pulse from the photomultiplier was input to a discriminator to eliminate most of the small pulses resulting from electronic noise, and the output pulse from the discriminator was used as the "stop" pulse for the time of flight electronics. To obtain good time resolution, a

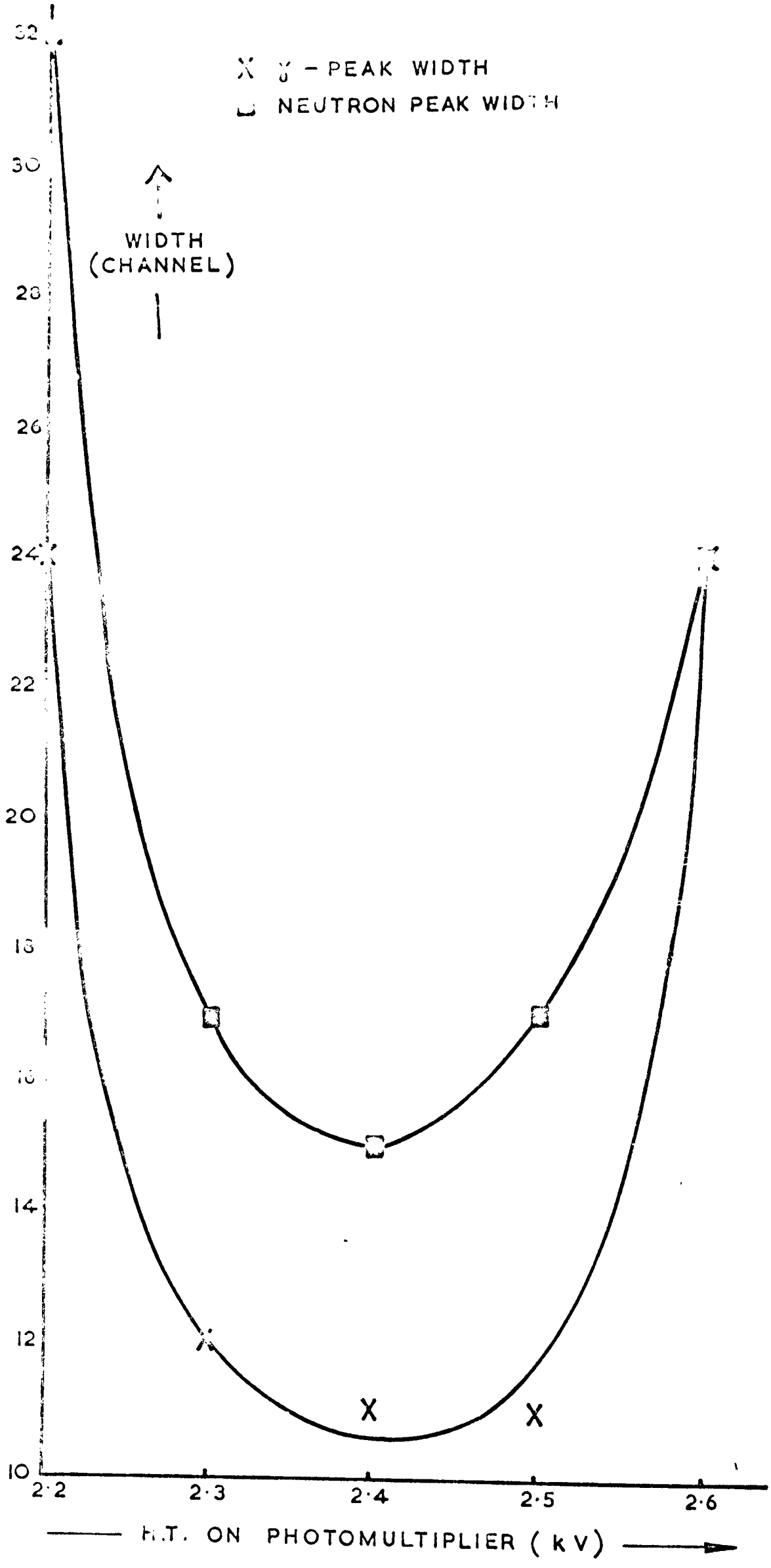

FIG. 3.7.A. VARIATION OF RESOLUTION WITH PHOTOMULTIPLIER H.T.

"zero-crossing" type of discriminator, a Harwell unit, type 2125 A, was used, since it produced an output pulse which was well timed relative to the input pulse over a very wide range of input pulse amplitudes.

The detector was placed at the maximum possible distance of 109.17 m from the target to obtain the best possible energy resolution.

A number of different sizes of scintillator were available, and the optimum one was determined experimentally, the criterion being that it should be as large as possible in order to give a high counting rate, but should not significantly worsen the energy resolution. A very large scintillator can lead to poor energy resolution because of the differences between the times taken by light flashes produced in different parts of the scintillator to reach the photomultiplier.

The widths of the γ-ray peak and the main neutron peak in the spectrum from lithium were used as measures of the resolution. This is discussed in Chapter 4.

A cylindrical piece of scintillator 114 mm in diameter and 203 mm long was found to be the best of those available. Using a smaller scintillator did not improve the resolution, whereas using a larger cuboidal piece 457 mm long by 100 mm x 200 mm under similar operating conditions broadened the neutron peak from 3.3 ns to 4.5 ns (f.w.h.m.) and produced a "bump" at one side.

The effect on the resolution of varying the bias level of the discriminator and the potential (H.T.) on the anode of the photomultiplier was also determined. Variation of the bias level had no detectable effect and the level was set at a convenient value as described in Appendix B. However the widths of the γ-peak and neutron peak varied with the photomultiplier H.T. as shown in fig. 3.7.A, and as a result the H.T. was set at the value of 2.4 kV corresponding to the position of the minimum.

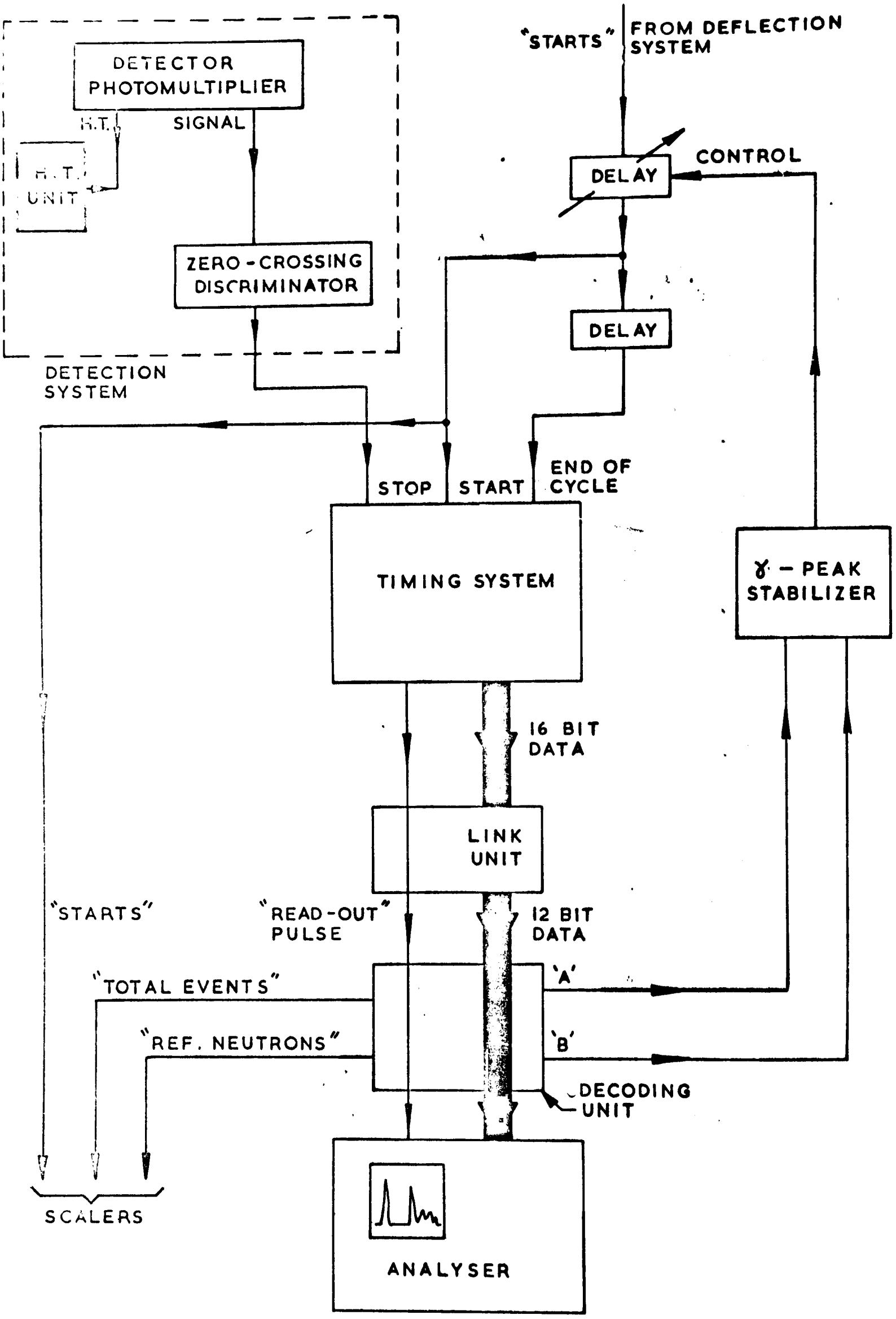

FIG. 3.8.A. THE MAIN ELECTRONICS.

The experimental determination of the variation with energy of the efficiency of the detector is described in Appendix C.

3.8 Time of Flight Electronics

The information about the time of flight of a detected particle (γ-ray or neutron) was contained in the times of arrival of the start pulse, derived from the deflection system triggering electronics, and the stop pulse, resulting from the detection of the particle and coming from the output of the zero-crossing discriminator. The time of flight electronics converted this information into digital form suitable for addressing the Intertechnique BM96 4096 channel analyser used to store and display the time of flight spectrum.

A block schematic diagram of the electronics is shown in fig. 3.8.A. and the parts are described in the following subsections.

3.8.1 The Start Delay

The absolute time of flight of a γ-ray could be calculated from the speed of light and the known length of the flight path. This determined the time origin of the system, making it unnecessary to know by how much the start and stop pulses had been delayed in the cables etc., and enabling a further arbitrary delay to be introduced into the start system as shown in fig. 3.8.A. The value of this delay was adjusted so that the start-stop time interval corresponding to the detection of a γ-ray was small and corresponded to some convenient channel near the beginning of the analyser. To compensate for fluctuations and drifts, the start delay was controlled by a feed-back unit known as the γ-peak stabilizer which reacted to changes in the position of the γ-ray "peak" in the analyser.

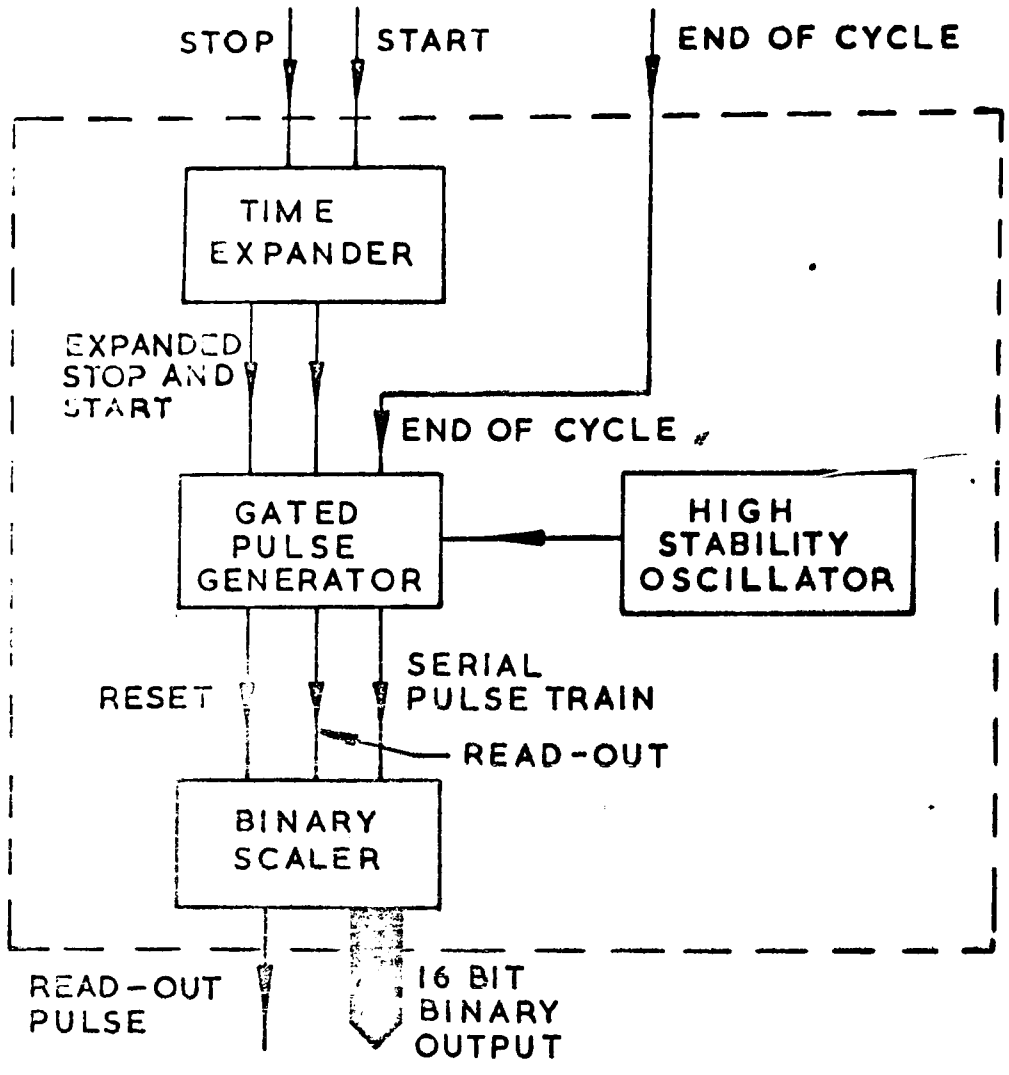

FIG. 3.8.B. THE TIMING SYSTEM

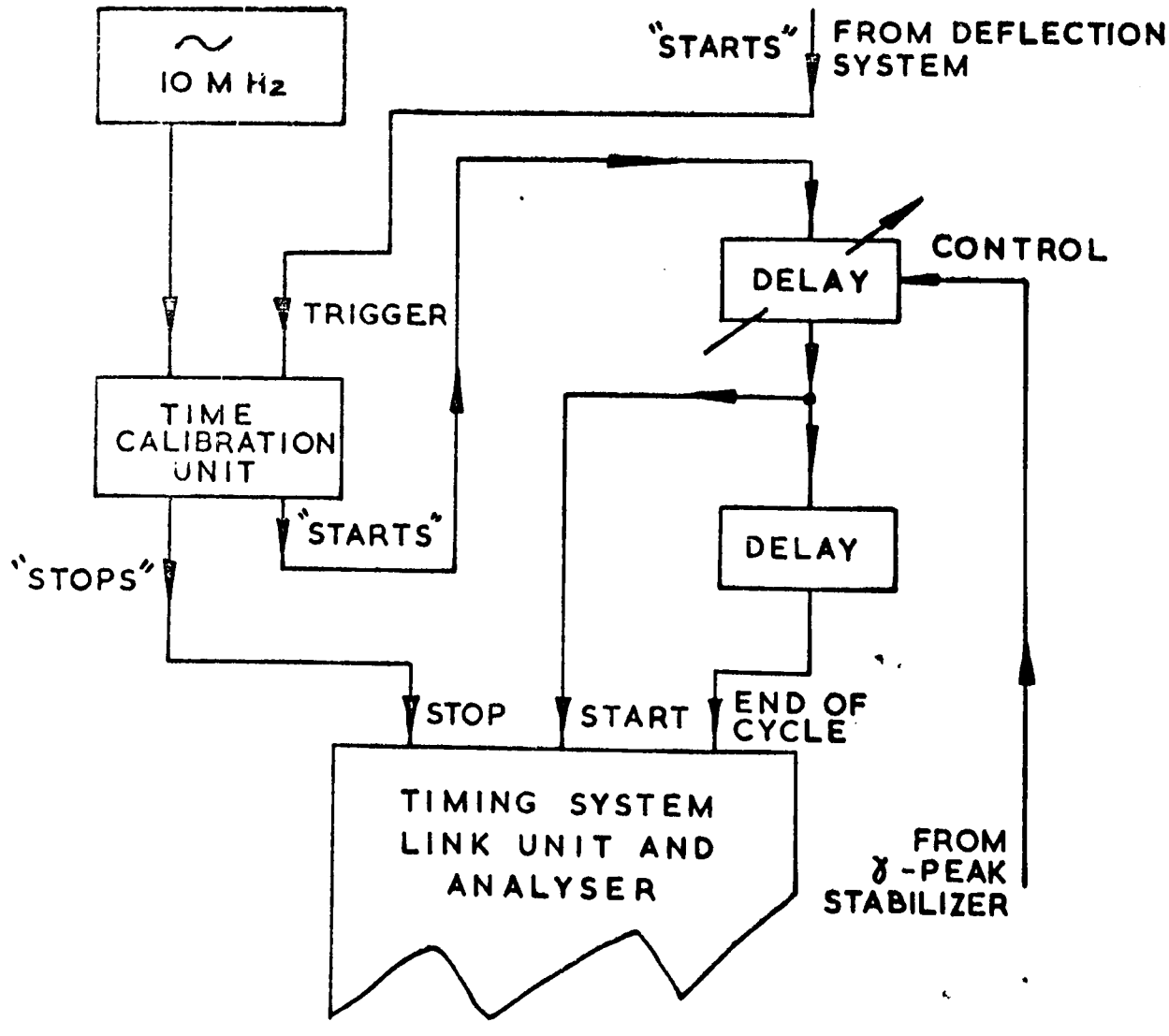

FIG. 3.8.C. TIME CALIBRATION.

3.8.2 The Timing System and the Link Unit

The timing system converted the start-stop time interval into a proportional 16 bit parallel binary number together with a "read-out" pulse which was used to strobe the number into the analyser. The link unit was used as an interface between this 16 bit output and the 12 bit input required to address the 4096 ($= 2^{12}$) channel analyser as described below.

A block schematic diagram of the timing system electronics is given in fig. 3.8.B. The start and stop pulses were fed into a time expander, a Harwell unit, type 95/2119-1/6, causing it to produce output start and stop pulses whose separation was proportional to that of the input pulses. The constant of proportionality could be set to be 25, 50 or 100 and was chosen to be 50 since it was found that this gave the best resolution. The standard unit was modified to run at repetition rates up to 1.5 kHz.

The expanded output pulses were fed into a stabilized 300 MHz gated pulse generator, a Harwell unit, type 95/2187-1/6. Pulses appeared at the output socket only during the time interval between receipt of the start and stop pulses by virtue of an internal gate opened by the start pulse and closed by the stop pulse. The numbers of pulses output was proportional to the start-stop time interval, and the datum was converted from serial to parallel binary form by means of a binary scaler. The stop pulse, as well as closing the gate, caused the emission of a read-out pulse which strobed the datum into the analyser, and a reset pulse which cleared the scaler in readiness for the next event. In the event of no stop pulse appearing within the desired analysis time, an end of cycle pulse was supplied a fixed time after the start pulse as shown in the

figures. This inhibited data transfer and cleared the scaler.

The longest pre-expansion start-stop time interval of interest was ~ 1 μs, being the difference between the times of flight of a ~ 30 MeV neutron and that of a γ-ray. The time expander increased this interval to 50 μs which led to 15000 pulses accumulating in the 16 bit binary scaler. The link unit was used to drop two bits from the least significant end, thereby dividing the number by 4 and allowing start-stop times up to 1.33 μs to be stored.

3.8.3 The Decoding Unit and the Gamma Peak Stabiliser

The output from the link unit was passed through the decoding unit before entering the analyser (fig. 3.8.A.). The decoding unit did not change the number, but simply inspected it and produced pulses at its output sockets when the number satisfied certain conditions. It was a complex unit and has been described in Appendix II of Saltmarsh' thesis (Saltmarsh, 1965). Only those outputs used in this experiment will be described.

The "total events" socket output pulses whenever a number passed through. The pulses were counted by a scaler and used to check that information had not been lost from the store of the analyser before or during its being punched out.

The "reference neutrons" socket output pulses whenever the number lay within a certain region chosen to encompass a block of high energy neutrons. The pulses were counted by a scaler and were a useful monitor of the neutron counting rate.

Another two sockets, A and B, were used to feed information about the position of the γ-peak to the γ-peak stabilizer which controlled the start delay. The delay was set so that the median point of the γ-peak was mid way between channels 383 and 384, this

position being chosen so that γ-rays originating from protons incident on the target on the synchrocyclotron orbit before the main deflection orbit should appear close to the beginning of the spectrum. Socket A output pulses when the address was in the range 380-383 and B when it was in the range 384-387, and the γ-peak stabilizer reacted so as to equalize the counting rate from the two sockets, thereby centering the γ-peak.

3.8.4 Time Calibration

An empirical calibration of the timing system was performed periodically throughout the experiment in order to detect drifts and to determine the slight non-linearity of the system.

The experimental start and stop pulses were replaced by pulses from a purpose built unit known as the time calibration unit (Langsford, 1967) as shown in fig. 3.8.C. When suitably triggered, this produced a start and stop pulse whose time separation was given by

$$t = a + n\tau$$

where n is an integer, a is constant and τ is the period of the r.f. input. The value of n swept up and down in a saw-tooth way with a $\sim$ 1s period and the resulting "spectrum" in the analyser consisted of a series of sharp spikes, separated in time by τ. The separation in terms of channels gave the desired calibration.

Previous experience had shown that the calibration of such timing systems may be start rate dependent, so, to ensure a start rate equal to that used in the experiment, the experimental start pulses were used to trigger the time calibration unit as shown in the figure.

The widths of the peaks resulted from jitter in the time calibration unit and in the timing electronics. However the peaks were at most 2 channels wide and this was small compared to the 12 channel timing width attributable to other causes.

The positions of the peaks could be determined to 0.02 channels (10 ps).

CHAPTER 4

INVESTIGATIONS OF THE ENERGY RESOLUTION

This Chapter describes the investigations into the energy resolution obtainable with the new neutron time of flight system, which were carried out during the middle part of 1969. Details of the modifications to the synchrocyclotron which were made prior to the experiment, and of the reasons behind them, are given in Chapter 1, and an understanding of this is desirable as a background to the present Chapter. The modifications led to considerably changed operating characteristics, and it proved impossible to obtain adequate resolution with a technique used successfully prior to the modifications and suggested by a rather superficial examination of synchrocyclotron theory. This will be termed the "traditional technique", and its failure necessitated an experimental investigation into the problem, which led to the discovery of a technique which reduced the f.w.h.m. of the resolution function to $\sim$ 1.2 MeV. It had been hoped to achieve a width of 0.5 MeV.

Section 4.1 describes the experimental methods used during the investigations, 4.2 discusses the traditional technique and suggests reasons for its failure, and 4.3 describes the partially successful technique and attempts an explanation of the phenomena observed. Section 4.4 suggests possible future improvements, and the Chapter is summarized in section 4.5.

It should be appreciated that, although much theoretical work has been carried out in recent years on the behaviour of the internal beams of synchrocyclotrons, many of the conclusions are difficult to verify experimentally. Consequently, some of the explanations attempted here require further testing before being regarded as fully established.

The importance of this work in relation to the experiment is that it established the method of obtaining the optimum resolution, suggested the reasons why it was worse than anticipated, and pointed the way to possible future improvements; however, it stands also in its own right as a contribution to the continuing investigation into the characteristics of the modified synchrocyclotron.

The data on (p,n) reaction for the main experiment were taken during two subsequent experimental runs which are discussed in Chapter 5.

4.1 Experimental techniques

These studies of the resolution were made during the period March - September, 1969. Most of the work was done before the target changer was fully commissioned, and a simplified method of holding the targets was used. Only two targets were used and they were placed at the working radius of 927 mm near to the 0° azimuthal position. The mounts pivoted about a horizontal axis, and either target could be "flipped" up and into the beam, or down and out of the beam by means of a coil attached to the pivot and energized by an electric current which interacted with the magnetic field of the synchrocyclotron.

One of the targets was 3 mm thick aluminium, chosen to give a very high yield of γ-rays, and the other was a thin (0.33 MeV energy loss) lithium target backed with gold foil, as was used for the main experiment. Lithium was chosen since the neutron energy spectrum resulting from its bombardment with intermediate energy protons is dominated by the transition from the ground state of Li^7 to that of Be^7, and consists

of a very intense narrow peak of neutron energies plus a small smooth background. There was a further peak near to the beginning of the time of flight spectrum resulting from the detection of γ-rays as explained in the previous chapter. The neutron spectrum was distant from this γ-peak, lying entirely within the second half of the stored spectrum.

Information about the resolution of the system was contained in the shapes of the γ-peak and the $Li^7(p,n)Be^7$ neutron peak. Since γ-rays of all energies travel with the same speed, the width of the γ-peak, Γ_γ, from either of the two targets, directly gave the time spread of the initial proton bunch (neglecting detection jitter and electronic jitter which were shown to be small). This time spread also contributed to the width of the lithium neutron peak, Γ_n, but this was further increased by the energy spread of the incident protons, the energy loss in the target, and the natural width of the Be^7 ground state.* This natural width was negligible, and the energy loss in the target was small, constant, and known. Γ_n was the parameter which determined the resolution of the experiment, but useful information about the characteristics of the synchrocyclotron could be obtained from a comparison of Γ_n and Γ_γ. Furthermore one of the experimental aims was to reduce the energy spread of the protons to a very small value, so that $\Gamma_n \approx \Gamma_\gamma$. This would have simplified the analysis of the data by enabling the resolution function for the neutrons to be calculated from the shape of the γ-peak. This aim was not achieved.

The experimental method was to use the aluminium target to set up the time of flight electronics and then switch to the lithium target. Counting was carried on for long enough to determine Γ_γ and Γ_n ($\sim$20s), and the effect on Γ_γ and Γ_n of varying the parameters controlling the synchrocyclotron was determined with a view to minimising Γ_n, and if

* In fact, Γ_n was further broadened by the unresolved excitation of the first excited state of ^7Be at 0.431 MeV (Chapter 7), but the effect of this was not large enough to invalidate the conclusions of this section.

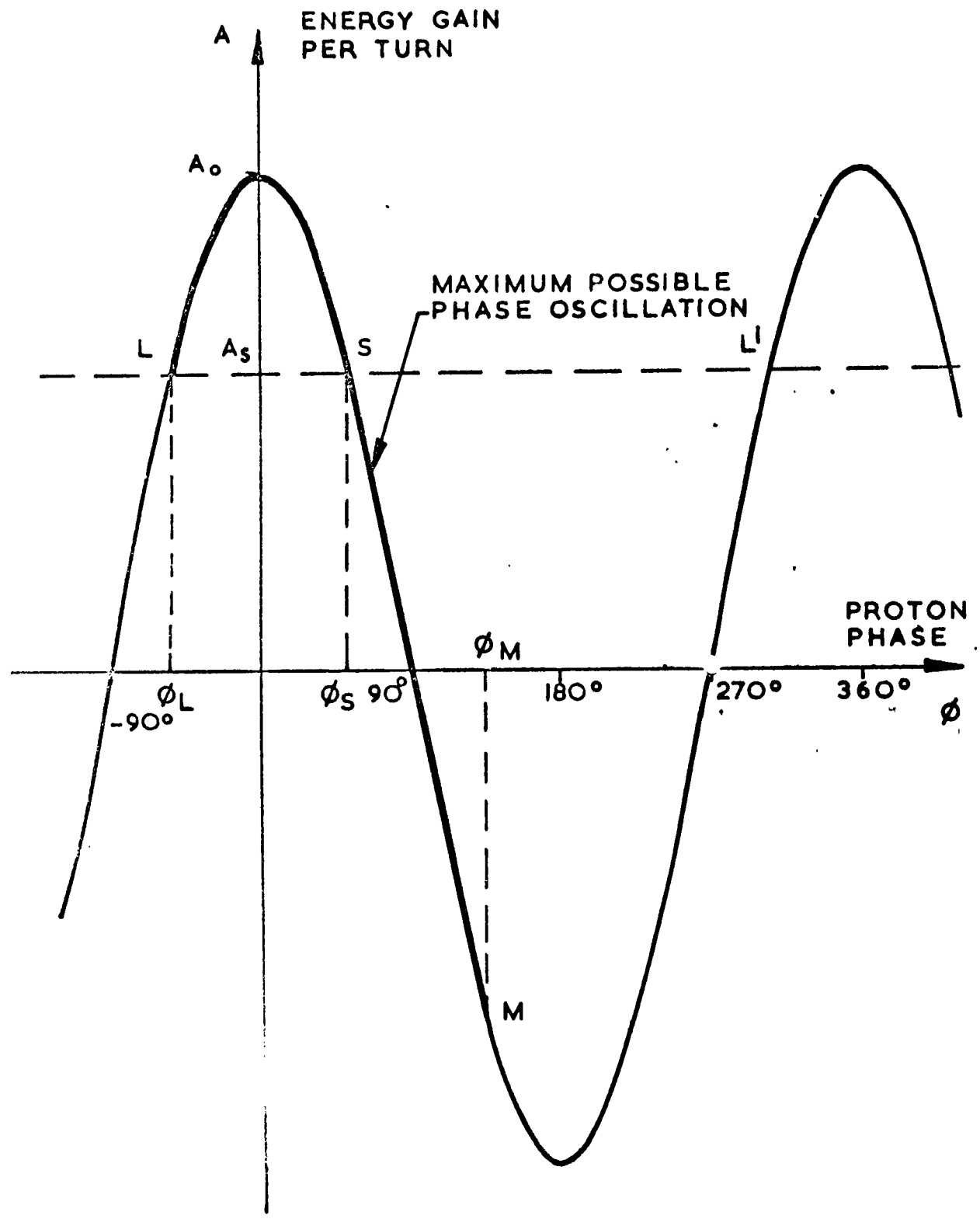

FIG. 4.2.A. PHASE OSCILLATIONS IN THE SYNCHROCYCLOTRON.

possible causing Γ_γ and Γ_n to become equal.

It will be appreciated from the following sections that the number of variable parameters was large and it was therefore impossible to explore the whole of parameter space fully.

4.2 The traditional technique and reasons for its failure

An outline of synchrocyclotron theory as it effects energy resolution is given here as a basis for the subsequent discussion. Full details of the basic theory have been published by Bohm and Foldy (Bohm, 1946; Bohm, 1947), and in the past five years, work aimed at improving the performance of synchrocyclotrons has been carried out at CERN (published in the form of CERN MSC internal reports) and at Harwell (Scanlon, 1970,A).

The protons inside a synchrocyclotron spiral outwards in a very roughly monoenergetic bunch, the r,f. accelerating voltage applied to the dee being modulated in frequency to compensate for the increasing relativistic mass of the protons and the radial decrease of the magnetic field.

The phase, ϕ , of a proton relative to the r.f. may be generally defined so that the proton experiences the maximum possible energy gain per turn, A_o, when $\phi = 0^\circ$, and zero energy gain per turn when $\phi = \pm 90^\circ$, the sense being defined so that a proton falling behind the r.f. increases its relative phase. Fig. 4.2.A shows the sinusoidal variation of A, the energy gain per turn, with ϕ. It should be noted that this phase convention is different from that used by Bohm and Foldy.

The synchronous phase, ϕ_s, is defined so that a proton remains synchronous with the r.f., i.e. remains at the point S in fig. 4.2.A, provided that its phase is equal to ϕ_s and its orbital frequency, f, is equal to that of the r.f., f_s. At a particular radius, ϕ_s is determined by the rate of frequency modulation, the characteristics of the magnetic field and the maximum possible energy gain per turn, A_o.

If, however, a proton does not have both the synchronous phase and the synchronous frequency, then there is the possibility of phase oscillations about ϕ_s. Suppose that $\phi = \phi_s$, but $f > f_s$, so that the proton is gaining on the r.f. and ϕ is decreasing, i.e. moving towards the point L in fig. 4.2.A. In this case, the energy gain per turn becomes greater than the synchronous value, A_s, with a consequent decrease in f and a slowing of the movement of ϕ. There is a converse restoring tendency on the other side of S. If, however, ϕ decreases beyond the point L, the energy gain per turn becomes less than A_s and the decrease in ϕ accelerates and continues without limit so that the proton is lost from the beam. The greatest allowed excursion to low phases is therefore to the point L in fig. 4.2.A and the corresponding upper limit is to a point M to the right of S. The region between L and M is termed the "phase bucket" and only particles which remain within the bucket can be accelerated.

Phase oscillations may be regarded as both azimuthal oscillations and energy oscillations. The time length of the proton bunch contributes to Γ_γ and the energy spread constitutes most of the extra broadening which leads to Γ_n.

The phase bucket may be reduced in size, thereby "spilling out" protons with the highest phase oscillation amplitudes, either by decreasing the r.f. voltage or by increasing the repetition rate. Referring to fig. 4.2.A, the former has the effect of reducing A_o keeping A_s constant, and the latter of increasing A_s keeping A_o constant. Both procedures cause ϕ_s to move towards 0^o. It is therefore expected that either procedure should improve the resolution at the expense of loss of beam intensity as more and more protons fail to be accelerated.

This was precisely the behaviour observed by Saltmarsh (Saltmarsh, 1965) in previous work using the unmodified synchrocyclotron. However, the

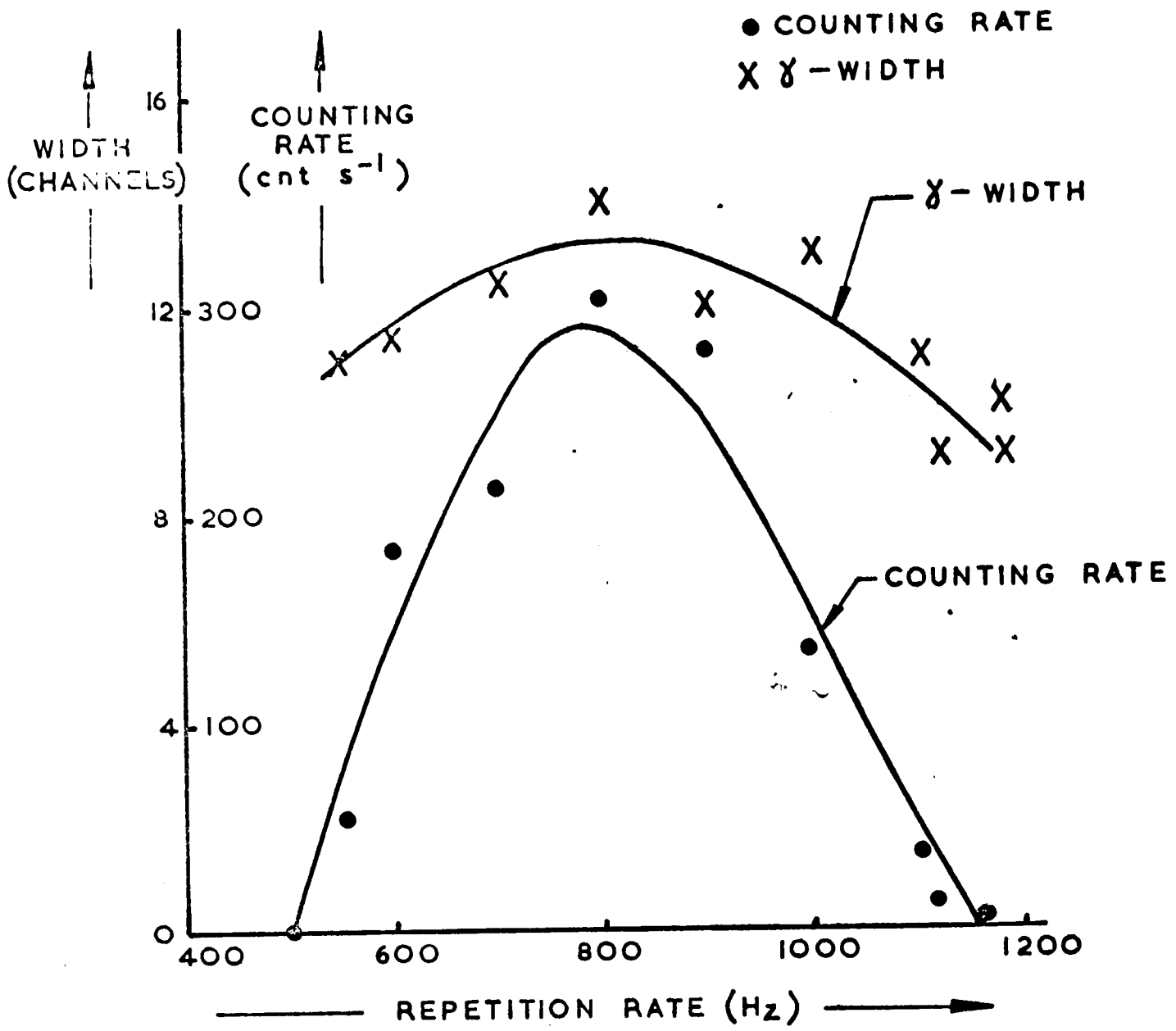

(i). "BEST" GRAPH

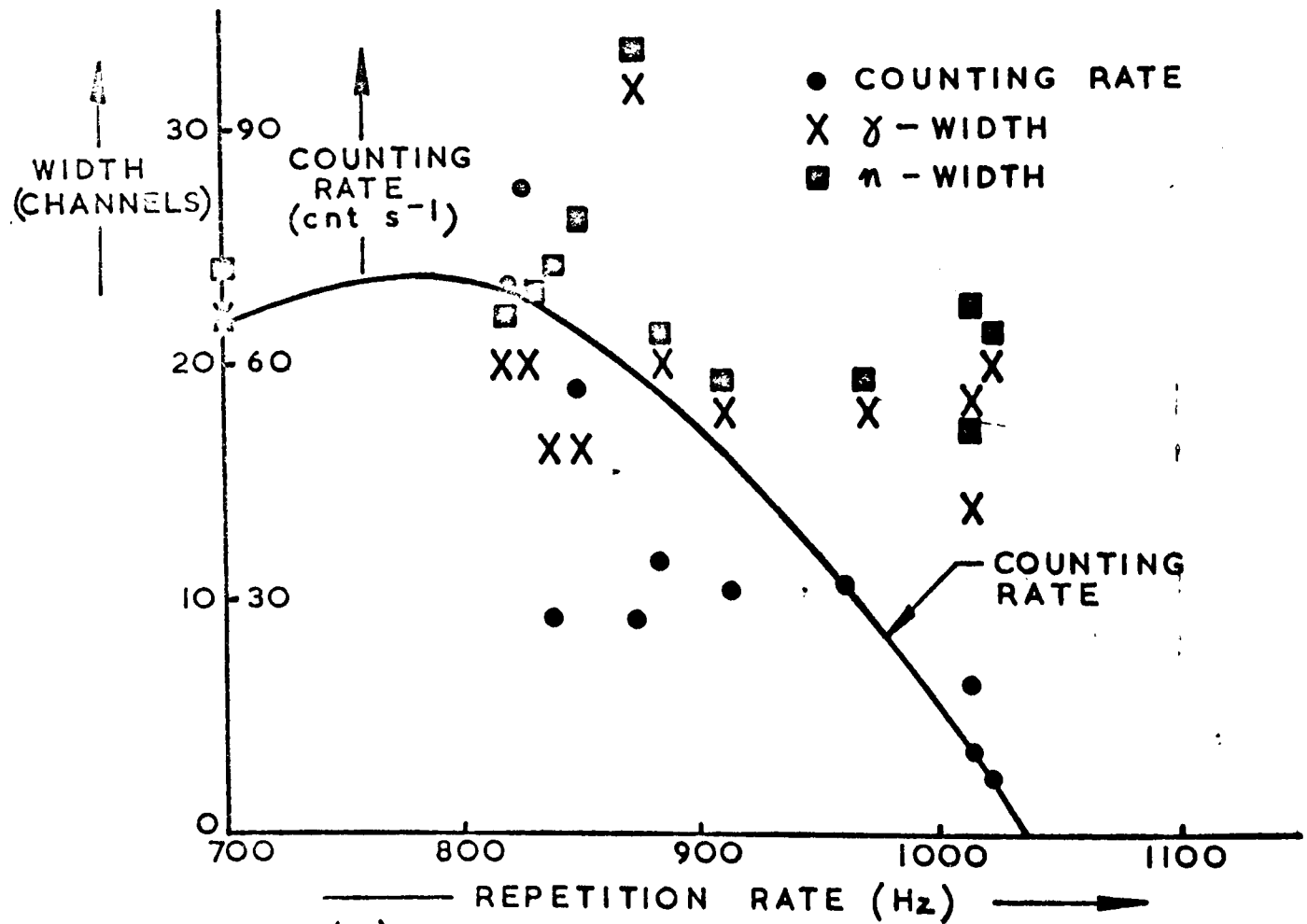

(ii). TYPICAL GRAPH

FIG. 4.2.B. VARIATION OF RESOLUTION WITH REPETITION RATE.

present investigations failed to yield the expected improvement in a consistent manner. Fig. 4.2.B (i) shows the best set of data obtained using this techniques. The counting rate and Γ_γ exhibited the expected decrease with increasing repetition rate, though the decrease in Γ_γ was not as great as expected. The decrease of counting rate and Γ_γ at low repetition rates is discussed below. The neutron width was not measured for this set of data, but subsequent experience suggests that Γ_n corresponding to the lowest value, 9 channels, of Γ_γ would have been $\sim$ 14 channels giving an energy resolution of 0.9 MeV. However the counting rate was exceedingly low, the synchrocyclotron running conditions were extremely unstable, and the results were not reproducible - not even immediately after the data had been taken! The fairly random behaviour shown in fig. 4.2.B (ii) was much more typical of the investigations. Similar inconclusive behaviour was observed as the r.f. voltage was reduced.

It was clear that the resolution was not exhibiting the expected strong dependence on repetition rate or r.f. voltage, and that such variations as were observed depended on synchrocyclotron operating parameters whose values were not being monitored. This led to an investigation into the effects of these parameters, which is described in the next section (4.3). The remainder of this section attempts an explanation for the failure of the traditional technique.

There are two possible reasons for the failure. The first is connected with the phase space population caused by the ion source, and the second with details of particle dynamics around a minimum in the curve of ϕ_s v. radius.

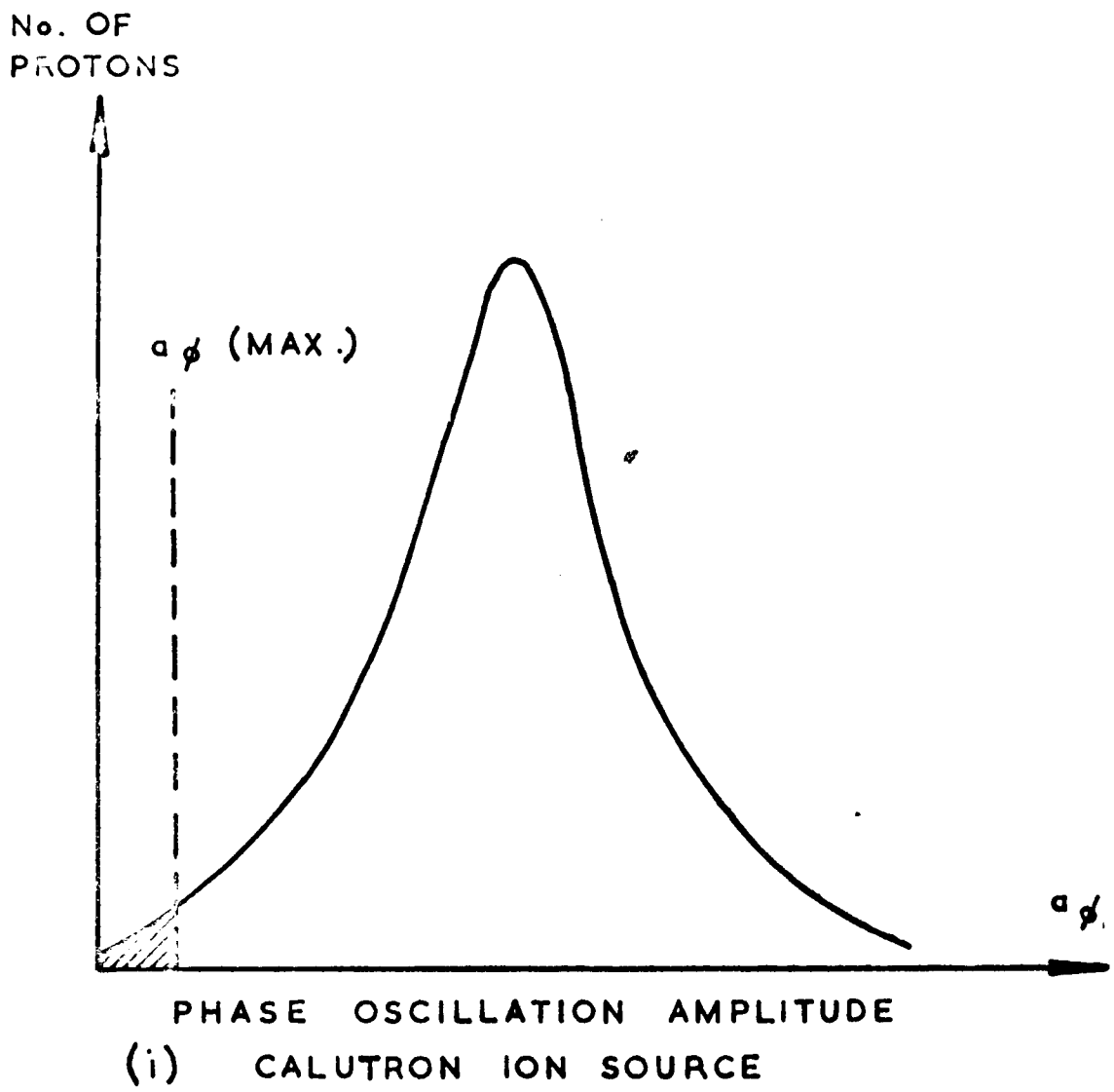

FIG. 4.2.C. PHASE OSCILLATION DISTRIBUTIONS.

The ion source used during most of the present work was a "Calutron" type, whereas that used by Saltmarsh was "open". An open ion source produces a cloud of very low energy protons at the centre of the synchrocyclotron and only a small proportion of these gain energy and acquire suitable phases to carry on being accelerated efficiently. By contrast, a Calutron source has a narrow tube, containing a vertical slit, which protrudes into the median plane. An applied r.f. field extracts protons from the slit and injects them into the phase bucket so that a very much higher proportion of the protons are accelerated, leading to increased beam intensity.

However, at the centre of the synchrocyclotron, $\phi_s \approx 80^\circ$, whereas the Calutron source injects protons in the range 0° - 40°. The protons, therefore, nearly all commence with large phase oscillation amplitudes, the phase bucket possibly being populated as shown in fig. 4.2.C (i). This could account for the experimental results, since reducing the size of the phase bucket so as to remove from the beam all protons with amplitudes greater than, say, a_ϕ (max) would leave only a negligible beam intensity, as shown by the shaded portion of the figure.

However, it was expected that the open ion source would populate the phase bucket more uniformly, perhaps as shown in fig. 4.2.C (ii). Removing protons with amplitudes greater than a_ϕ (max) would now leave a much greater intensity, so that the traditional technique would be expected to be more successful with the open source.

(It should be stressed that the curves shown in fig. 4.2.C are intended only to illustrate qualitatively the nature of the differences in the distributions expected to be produced by the two sources. The curves as drawn do not represent the results of theory or experiment, and details of the shapes of the actual distributions may be considerably different from those shown).

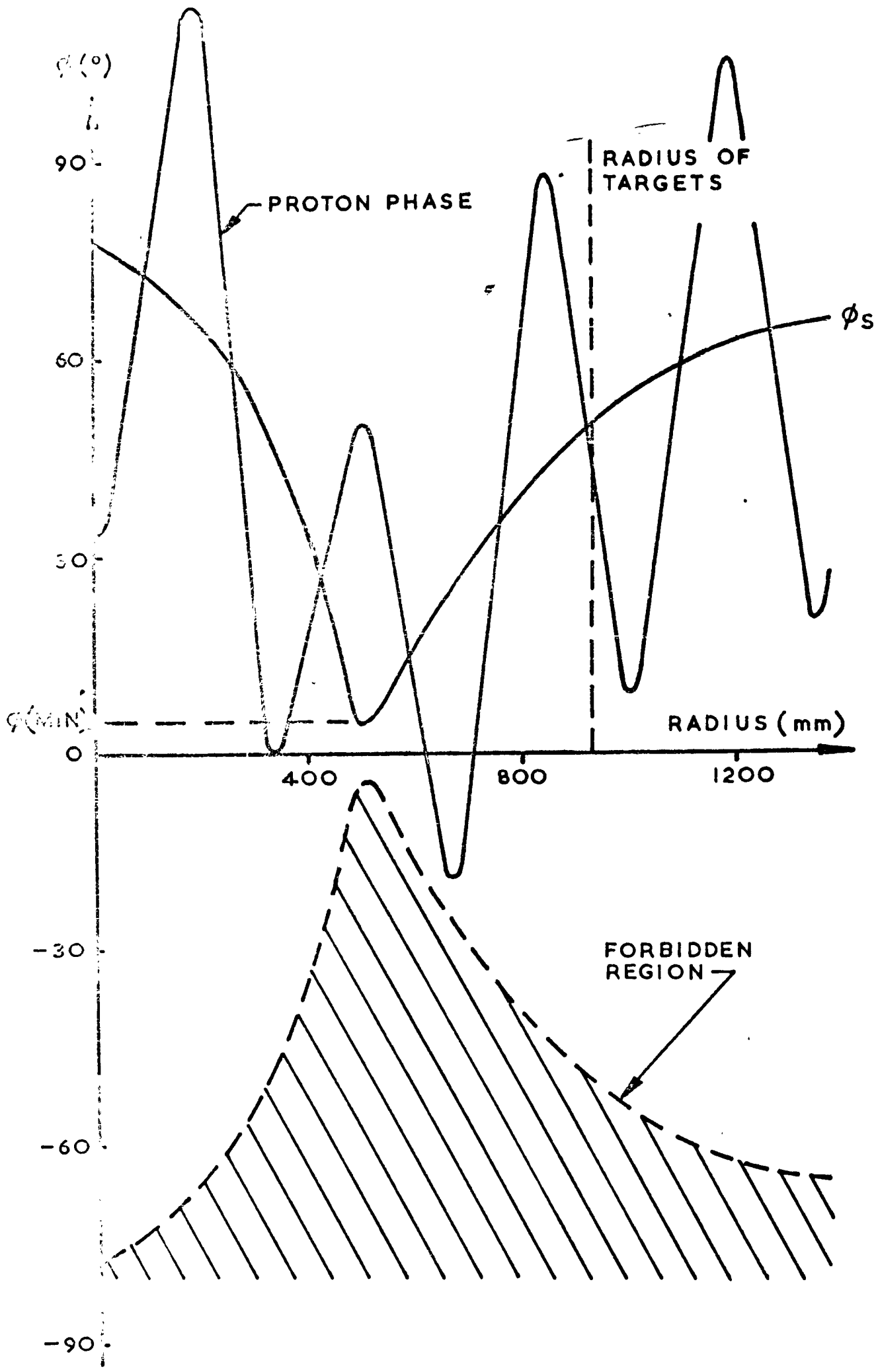

FIG. 4.2.D. "BOTTLENECK JUMPING".

NOTE: THE PHASE OSCILLATION HAS BEEN DRAWN AS SHOWN FOR THE SAKE OF CLARITY AND CONVENIENCE. A MORE REALISTIC DIAGRAM WOULD SHOW ABOUT TEN COMPLETE CYCLES, WITH THE PERIOD DECREASING TOWARDS LARGER RADII, BUT INCREASING NEAR THE MINIMUM OF ϕ_s.

The likelihood that the Calutron source would fail to populate the centre of the phase bucket was realised at an early stage, and, as a result, a new open ion source was manufactured. However, no improvement in resolution was observed using this source, indicating that the above explanation is incomplete. However, there was insufficient time available to redesign the open source for the new operating conditions, and the new source was manufactured to the old specifications. It proved very unreliable and difficult to work with, and consequently its characteristics were not investigated as fully as had been hoped. It is therefore possible that the resolution could be improved by using the traditional technique with a reliable open ion source.

The second possible reason for the failure of the traditional technique for improving resolution, which would account for its failure with both types of source, is connected with the variation of ϕ_s with radius. This variation is shown in the upper half of fig. 4.2.D and is typical of synchrocyclotrons. Referring back to fig. 4.2.A, the low phase limit of the phase bucket was the point L at a phase of $-\phi_s$, and in the present figure this is represented by the dotted reflection about 0°. A proton which leaves the phase bucket and enters the shaded "forbidden" region is lost from the beam.

The phase bucket diminishes as the protons accelerate towards the minimum of ϕ_s and protons are spilled from it. The traditional method for improving energy resolution has the effect of lowering the minimum towards 0°, and its success depends on the assumption that no proton with a phase oscillation amplitude greater than 2ϕ (min) can pass the bottleneck without entering the forbidden region.

However, if the period of phase oscillation is not small compared with the rate of change of ϕ_s, then a proton's phase can oscillate about ϕ_s as shown in the figure (4.2.D). It may be seen that the proton, whilst having a large oscillation amplitude, is nevertheless accelerated past the bottleneck without entering the forbidden region.

The phase oscillation period relative to the period of frequency modulation varies as the square root of the repetition rate, so that the situation would have been worse at 800 Hz than at the repetition rate of 200 Hz used by Saltmarsh.

An attempt was made to investigate low repetition rates, where this bottleneck jumping effect would be less important, and as was seen from fig. 4.2.B (i) there was some evidence for a slight improvement. However, it was impossible to usefully use the Calutron source below ~500 Hz, since, in order to reduce the size of the phase bucket, it would have been necessary to reduce the r.f. voltage below the minimum (~9 kV) at which the Calutron source would operate.

It was found to be also very difficult to accelerate any beam below ~ 500 Hz using the open ion source, and in view of this, and its previously mentioned unreliability, it was considered to be the wisest course of action to abandon the traditional technique and to investigate the effects of other synchrocyclotron operating parameters.

4.3 The Successful Method

After a considerable amount of investigation using the Calutron source, the method found to be most effective for improving the resolution consisted of altering the point near the beginning of the acceleration cycle at which the firing pulse was applied to the ion source. This is discussed in sub-section 4.3.1. Further dependence of the resolution on the deflection

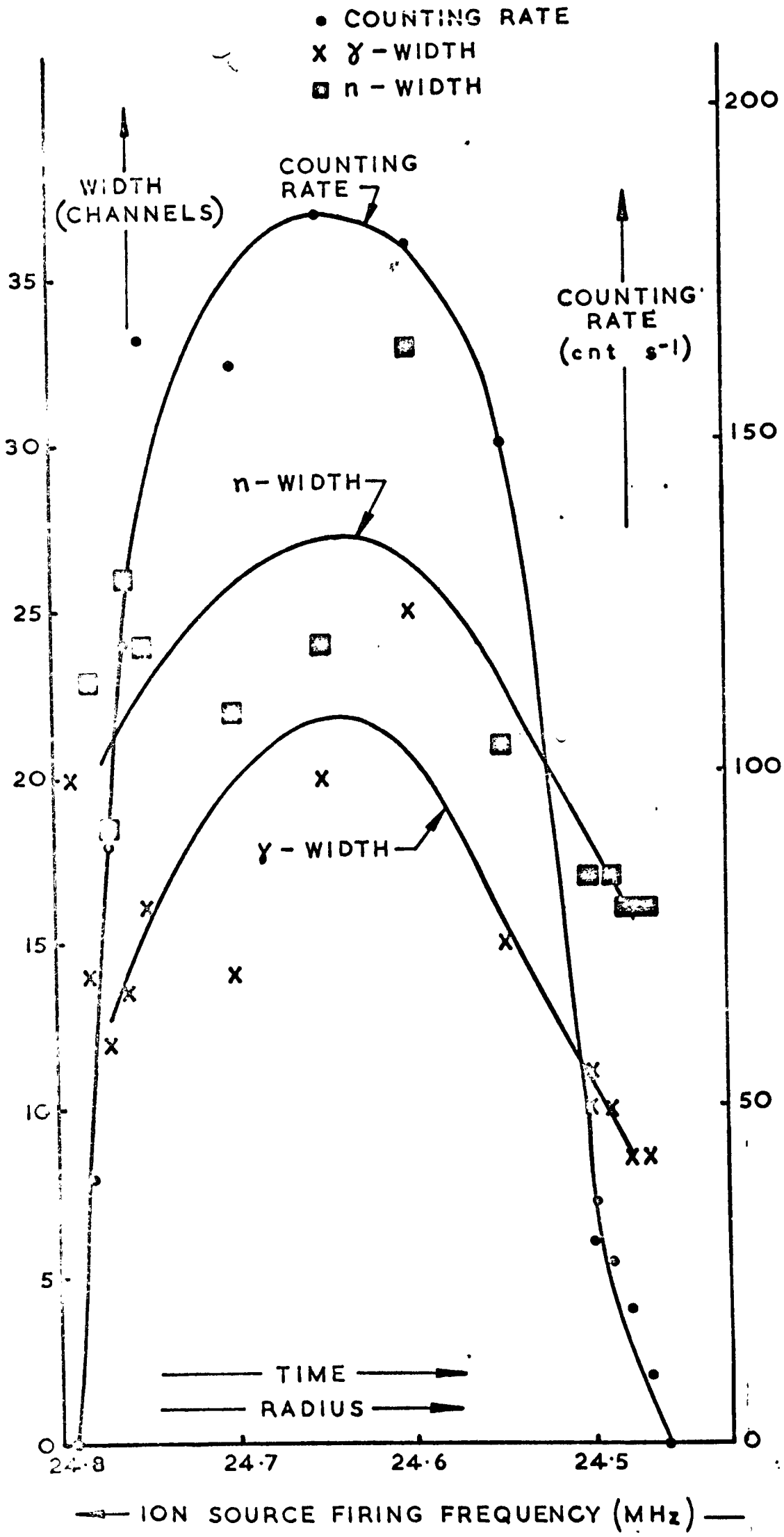

FIG. 4.3.A. VARIATION OF RESOLUTION WITH ION SOURCE FIRING TIME.

frequency is discussed in sub-section 4.3.2 and on other parameters in 4.3.3. A résumé of the practically used resolution optimising technique is given in 4.3.4.

4.3.1 Ion Source Firing Time - Phase Oscillation Bunching

The timing of the trigger pulse used to fire the ion source was derived in the same way as that for the deflection pulse, i.e. by means of a frequency discriminator coupled to a pick up from the r.f.

Fig. 4.3.A shows Γ_γ, Γ_n, and the counting rate plotted as a function of the r.f. frequency at which the ion source was fired. The abscissa is scaled from right to left, so that the time of firing and the current radius of the synchronous orbit increases from left to right.

The resolution improved for both early and late firing, but the improvement was greater, and the situation more stable in the case of late firing. Widths of $\Gamma_\gamma = 2.3$ ns and $\Gamma_n = 3.8$ ns could be consistently achieved. However it was not possible to maintain these widths over long periods of time, and $\Gamma_\gamma = \sim 3$ ns, $\Gamma_n = \sim 5$ ns was the best which could be stably used, leading to the energy resolution of 1.2 MeV achieved in the experiment. Although equally low widths were occasionally achieved without using this technique, the situation was invariably erratic and unstable, and a resolution of ~ 1.8 MeV would have been the best that could have been used over sufficiently long periods.

A possible reason for the success of the technique is connected with a phenomenon which will be termed "phase oscillation bunching". With the open ion source, most of the phase bucket is populated, and the energy and time spread of the bunch corresponds to the dimensions of the bucket. The Calutron source, however, injects particles into a

limited region of phase space (0° - 40°) initially, with a spread of amplitudes in the range 40° - 80°. Protons leaving the source towards the end of the acceptance period tend to have larger amplitudes, and vice versa. There is therefore a tendency for a large fraction of the protons to be concentrated in a limited region of the bucket, and to oscillate <u>together</u>, so that at any one time the energy, time, and phase <u>spread</u> of the bunch will be smaller than that corresponding to the bucket size. This effect may be mitigated by the fact that phase oscillation frequency is slightly amplitude dependent, introducing an overall debunching effect.

Firing the ion source late, so as to only overlap the end of the acceptance period, may therefore have lead to further improvement by reducing the range of phase oscillation amplitudes, thereby reducing the spread of the bunch, and, in addition, reducing the debunching effect. There would be a theoretical advantage in firing the ion source early and using the beginning of the acceptance period, in that smaller phase amplitudes would be selected. However, in practice, much better control could be achieved by using late firing since the initial rise of the ion source arc pulse was much better defined than its extinguishing.

Evidence for phase bunching has been obtained by measuring the time distribution of the particle current deposited on a probe inserted into the circulating beam.

The phenomenon could be investigated further by deflecting the beam at different points in the acceleration cycle and determining the change in incident proton energy (e.g. by measuring the shift in position of the lithium neutron peak). If the change were in accord with the calculated smooth increase of energy with radius, this would indicate the absence of an appreciable amount of phase bunching, whereas

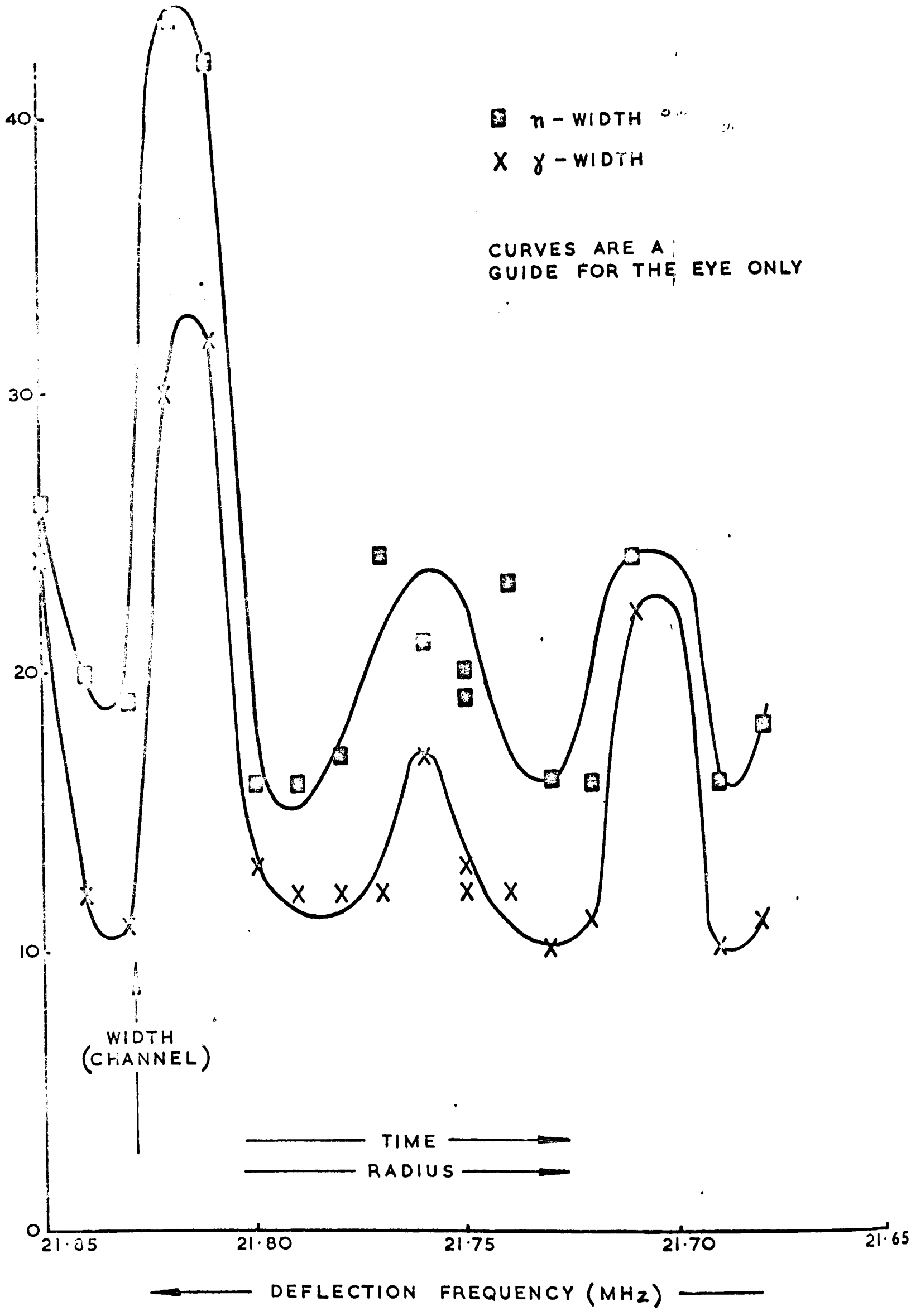

FIG. 4.3.B. VARIATION OF RESOLUTION WITH DEFLECTION FREQUENCY.

an oscillatory variation about this value with a period equal to that of the phase oscillations would confirm its presence. The phase oscillation period is difficult to calculate precisely since it depends on ϕ_s, but it is at least several hundred microseconds. As a result, the change in deflection time, and hence in the deflection radius which would have been required to show up the effect was too large for this to be possible without changing the radius of the deflection plates. However, the relatively small changes which were attempted did show up another phenomenon, which is described in the next sub-section.

4.3.2. Variation of the deflection frequency - precessional phase bunching

It was found that Γ_γ and Γ_n depended on the deflection frequency (i.e. the point in the acceleration cycle at which the beam was deflected onto the target) in an oscillatory manner as shown in fig. 4.3.B. The period of the oscillations in terms of change of deflection frequency was 49 $\pm$ 5 kHz. The repetition rate was 800 $\pm$ 10 Hz and at this rate and at the radius of the targets, the modulation rate is 11.4 $\pm$ 0.4 GHz s^{-1}, leading to a period for the oscillations in Γ_γ and Γ_n of 4.3 $\pm$ 0.6 μs. This is much less than the period of phase oscillation. However, there are two other modes of oscillation open to an accelerating proton: vertical oscillations about the magnetic median plane, and radial oscillations. Both are at constant energy. Radial oscillations in the present synchrocyclotron are the result mainly of off-centering forces in the cut-back region of the dee which cause the orbit centre to shift from the geometrical centre. The orbit centre then precesses round the geometrical centre.

The periods of vertical oscillation and of the precession of the orbit centre are given by

$$\tau_{\text{vertical}} = \frac{\tau_{\text{orbital}}}{\sqrt{n}}$$

$$\tau_{\text{precessional}} = \frac{\tau_{\text{orbital}}}{1 - \sqrt{1 - n}}$$

where $$n = - \frac{r}{H} \frac{dH}{dr} ,$$

r is the orbit radius, and H is the magnetic field strength.

At the radius of the targets,

$\tau_{\text{orbital}} = 46.01 \pm 0.02$ ns and $n = 0.0226 \pm 0.0002$.

Evaluation of the formulae yields

$$\tau_{\text{vertical}} = 305 \text{ ns},$$

which is much less than the observed period, but

$$\tau_{\text{precessional}} = 4.03 \pm 0.04 \ \mu\text{s},$$

in good agreement with the observed period.

It therefore seems extremely probable that the phenomenon is connected with the precessional motion of the orbit centres, and such an oscillatory variation could be caused if either the amplitude or phase of the precessional motion were bunched. Such bunching could well be caused by the established strong coupling between phase oscillations and radial oscillations. As a result of this bunching, the orbit centres would be distributed within a fairly long sausage-shaped region of space, and the maxima of the curves would occur when the "sausage" was parallel to the tangent at the targets at the point of

deflection so that the length of the proton bunch was increased. Scanlon (Scanlon, 1970, B) estimates that variations in bunch length up to 150 mm - in reasonable agreement with the observations - could occur but at twice the precessional frequency since the "sausage" would be parallel to the tangent twice during a complete period. This prediction of the frequency of the variations is in conflict with the observations, and this conflict has so far not been resolved.

4.3.3 Dependence of the resolution on other parameters

No evidence was found for a significant dependence of the resolution on any of the following:

1) the amount by which the beam was "trimmed" in the vertical direction by means of an adjustable carbon absorber placed at a low radius,
2) the operating voltage of the ion source,
3) the duration of the firing pulse applied to the ion source,
4) the rate of hydrogen supply to the ion source, or
5) the vertical position of the median plane within the synchrocyclotron.

It was found that the resolution depended slightly on the position and orientation of the ion source, probably because the protons were injected in a way more likely to produce the phase bunching effect previously described. The optimum position was stable from run to run and, once found, could simply be set at the beginning of a run.

4.3.4 The technique for optimizing the resolution

As a result of the foregoing investigations, the technique finally adopted for optimization of the resolution was as follows.

1) The position and orientation of the ion source were set to the previously determined optimum values.
2) The repetition rate was set at 800 Hz to give maximum beam.

3) The deflection frequency was varied and set to give maximum beam.

4) The ion source firing frequency was varied so as to minimise Γ_n.

5) The deflection frequency was again varied, by small amounts, to minimise Γ_n.

4.4 Possibilities for future improvement

It is intended that the shape of the dee used with the synchro-cyclotron should undergo further modification so that the dee angle should be 180° out to a radius of 508 mm. There is nothing in the foregoing analysis to suggest that this would necessarily improve the resolution obtainable, but it should be appreciated that any fairly major change in the operating characteristics might well lead to a change in the resolution.

There are two other possible ways of effecting an improvement which could be attempted. The first is simply to attempt to reproduce as far as possible the running conditions used by Saltmarsh. If the time spread of 2 ns which he achieved could be reproduced, the increased length of the flight path would lead to an energy resolution of 0.5 MeV. This would involve further work on the open ion source to improve its reliability, and running the synchrocyclotron at a repetition rate of 200 Hz.

Secondly, the most obvious way of improving the resolution is to use a redesigned Calutron ion source which would inject protons into orbit at the stable phase angle of 80°. There should then be hardly any tendency for phase oscillations to occur, with a consequent improve-ment in resolution. However such a redesign is exceedingly difficult, since to inject protons at high phase angles would require extra

positively charged electrodes to produce the correct electrostatic field configuration, and their presence is expected to lead to severe electrical breakdown problems. This approach has been tried at CERN, but with little success to date.

4.5 Summary

The "traditional" method for improving the time and energy resolution of the synchrocyclotron, by either decreasing the dee voltage or increasing the repetition rate, failed when attempted with the modified synchrocyclotron. Since the failure occurred with both a Calutron and an open ion source, it has been suggested that it was due to a "bottleneck jumping" effect whereby particles with large phase oscillations can escape past a minimum in the stable phase angle without being lost, this effect being exacerbated by the increased repetition rate at which the modified synchrocyclotron was operated.

The method by which an improvement in the resolution was achieved was to adjust the timing of the ion source pulse so that particles were captured into orbit at a late time in the acceleration cycle. It has been argued that the improvement arose from the increased degree of "phase oscillation bunching" which reduced the azimuthal extent of the proton bunch.

Further small improvements were made by selecting the deflection frequency so as to enhance the effect of "precessional phase bunching" which it is suggested was induced by the strong coupling between phase oscillations and radial oscillations resulting from the cut-back dee.

The best reproducible resolution achieved was 1.2 MeV (f.w.h.m.) for 95 MeV neutrons.

CHAPTER 5

THE MAIN EXPERIMENT - (p,n) REACTIONS AT ABOUT 98 MeV

The main (p,n) experiment was carried out during two major data taking runs on the synchrocyclotron which took place after the investigations into the energy resolution described in Chapter 4. The first, held during the late part of October and the early part of November, 1969, was known as the ON69 run, and the second, held during December, 1969, as the D69 run.

A set of data covering all the targets over the full range of angles was obtained during the ON69 run, but it was shown that the monitor was not operating reliably, and that this presented a problem in normalizing the data. This problem was overcome during the D69 run during which the detection efficiency measurement described in Appendix C was also carried out.

Section 5.1 summarizes the preliminary and routine checks and adjustments carried out during the experiment, the ON69 run is described in section 5.2, the deficiencies of the monitor in section 5.3, and the D69 run in section 5.4.

The analysis of the data is described in Chapter 6.

5.1 Routine checks and adjustments

Methods of setting up and adjusting the apparatus are described mainly in Chapter 3. This section outlines the routine procedures carried out before and during the data taking runs.

5.1.1 Optimization of the energy resolution

Before data taking commenced, the energy resolution was optimized as explained in Chapter 4.

5.1.2 Counter gain

The gain of the main neutron counter and its associated electronics was set at the half height of the Compton recoil edge from the

γ-decay of Cs^{137}. The procedure is standard, and is described briefly in Appendix B. The gain was set immediately before data taking commenced, and it was checked and maintained constant at periodic intervals.

5.1.3 Time calibration

The procedure for calibrating the timing system is described in sub-section 3.8.5. The calibration was performed frequently, usually before and after each series of counts. The time calibration "spectrum" on the analyser was punched on paper tape and kept for subsequent accurate analysis.

5.2 The ON69 run

During the ON69 run, the taking of data for a particular target at a particular angle went as follows:

1) The analyser, the scalers, and the integrating digital voltmeter (IDV) attached to the monitor were reset to zero.
2) All the above were started simultaneously.
3) Counting was stopped automatically after a preset time.
4) The readings of the scalers and the IDV were noted and the contents of the analyser were punched on paper tape.

The scalers recorded the following information:

1) "Starts" i.e. the number of repetitions of the acceleration cycle. The repetition rate was $\sim$ 800 Hz.
2) "Events" i.e. the total number of events recorded by the analyser.
3) "Reference neutrons" - i.e. the total number of events recorded in a particular block of the analyser, this block being chosen to include the high energy neutrons.
4) "Time" - This scaler recorded the time in milliseconds.

The order in which data were taken consisted of investigating a particular target over a range of angles between 0^{o} and 40^{o}, and then changing to another target and covering the same angular range and so on. The alternative to this procedure, i.e. investigating a number of targets at a particular angle before changing the angle, was adopted during the D69 run.

Changing to a different angle involved:

1) driving the target changer azimuthally and stopping it semi-automatically when the appropriate microswitch was actuated.
2) driving the moving collimator laterally to the correct position by observing the television monitor, and
3) driving the moving collimator angularly for the appropriately determined length of time.

During the angular sweep for a given target, the reference lithium target was periodically investigated so that the spectrum of the target under investigation could be compared with that from the reference under what were assumed to be similar conditions. In particular, the reference spectrum provided a monitor of the incident energy, and information on the current energy resolution.

5.3 The deficiencies of the internal beam monitoring system

The internal beam monitor (section 3.4) was potentially an invaluable tool, for providing both absolute normalization of the data, and a rapid direct measurement of the incident beam intensity. It was, for example, very useful for determining the optimum phase delay (see section 3.1), since this had to be done frequently, and the direct determination of counting rate was slower than simply reading the voltmeter attached to the monitor. (This voltmeter was used in addition to the integrating voltmeter mentioned in section 3.4). Plots of the monitor reading, M,

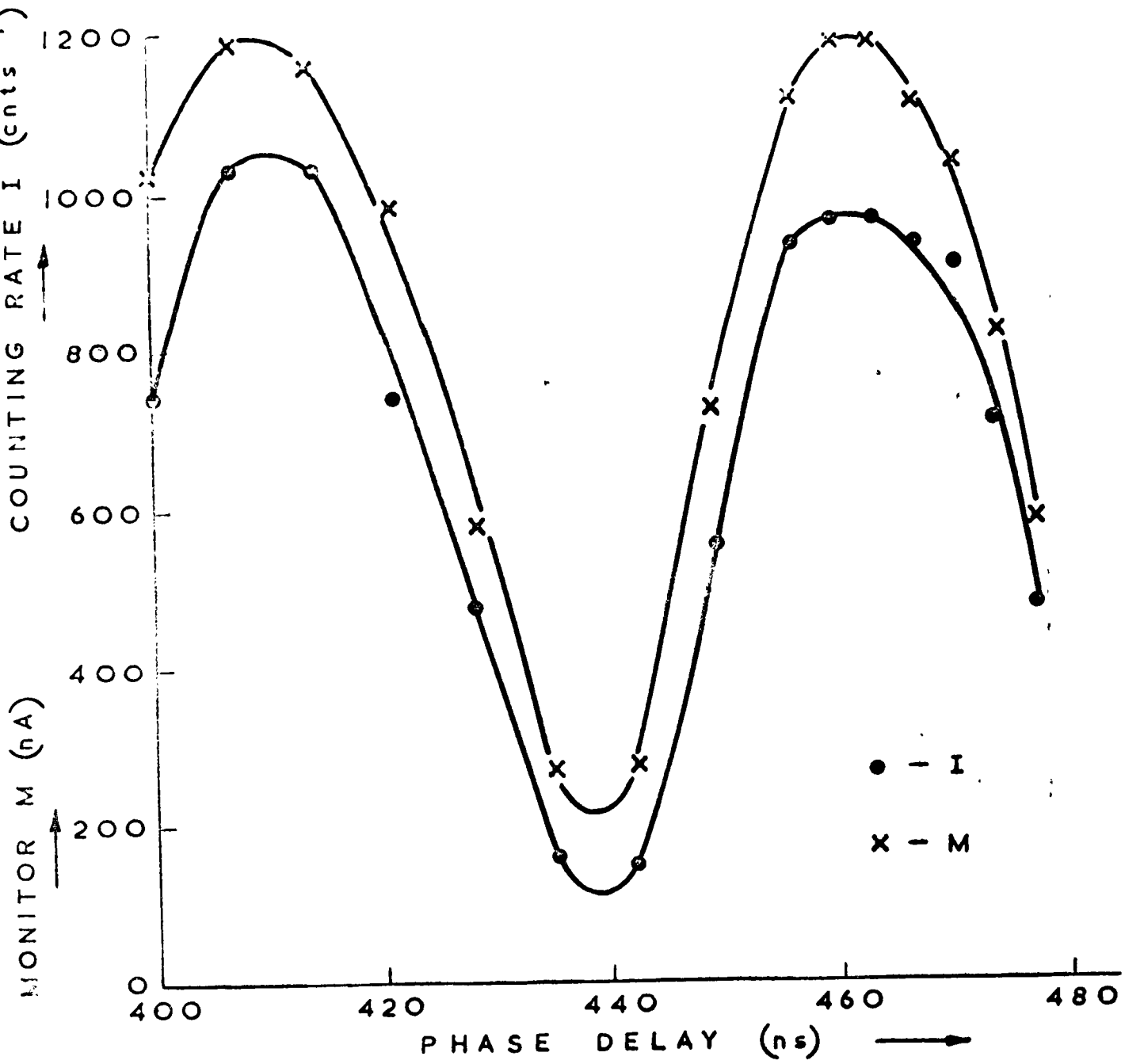

(i)

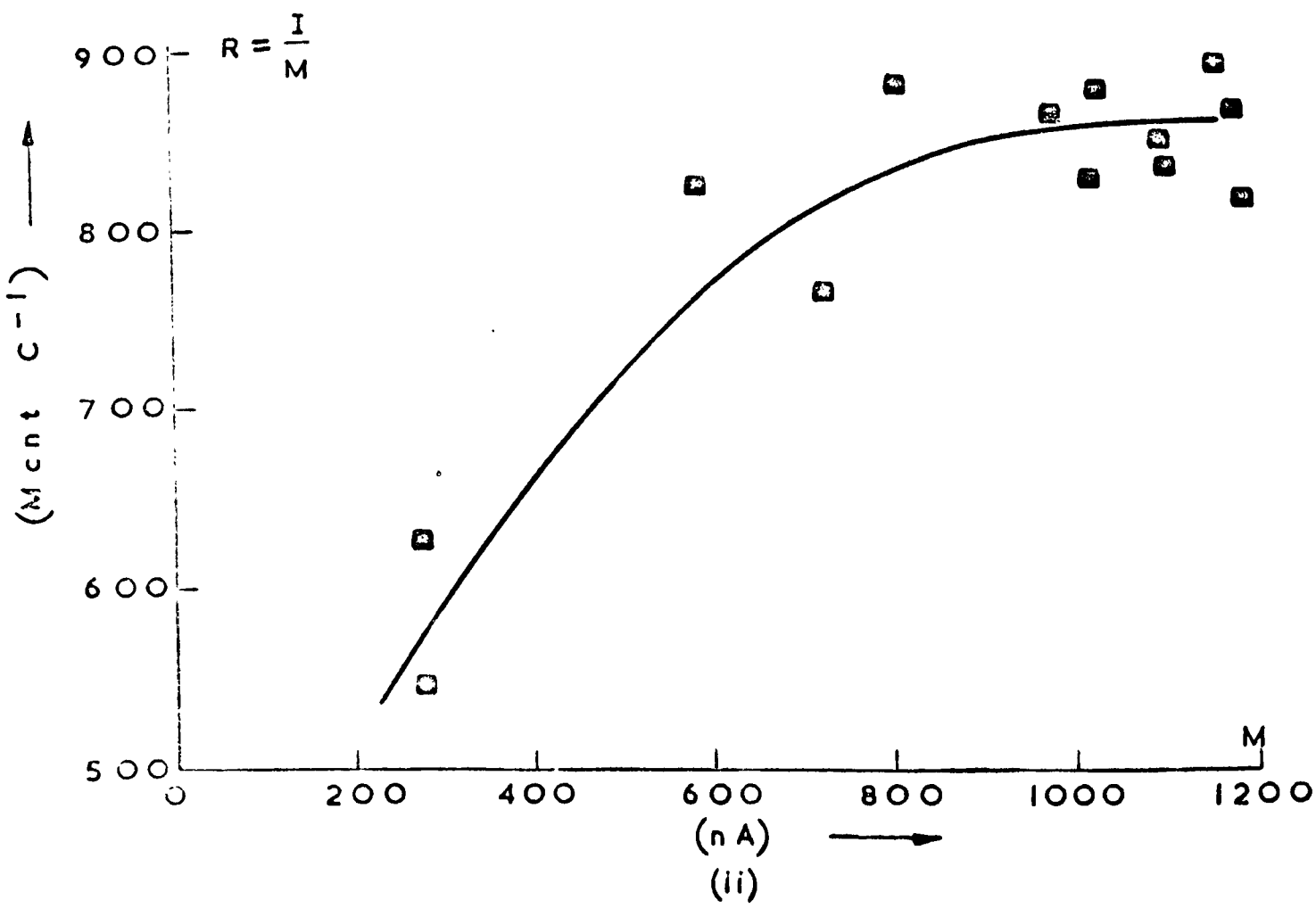

(ii)

FIG. 5.3.A. EFFECT OF MIS-PHASING ON THE MONITOR

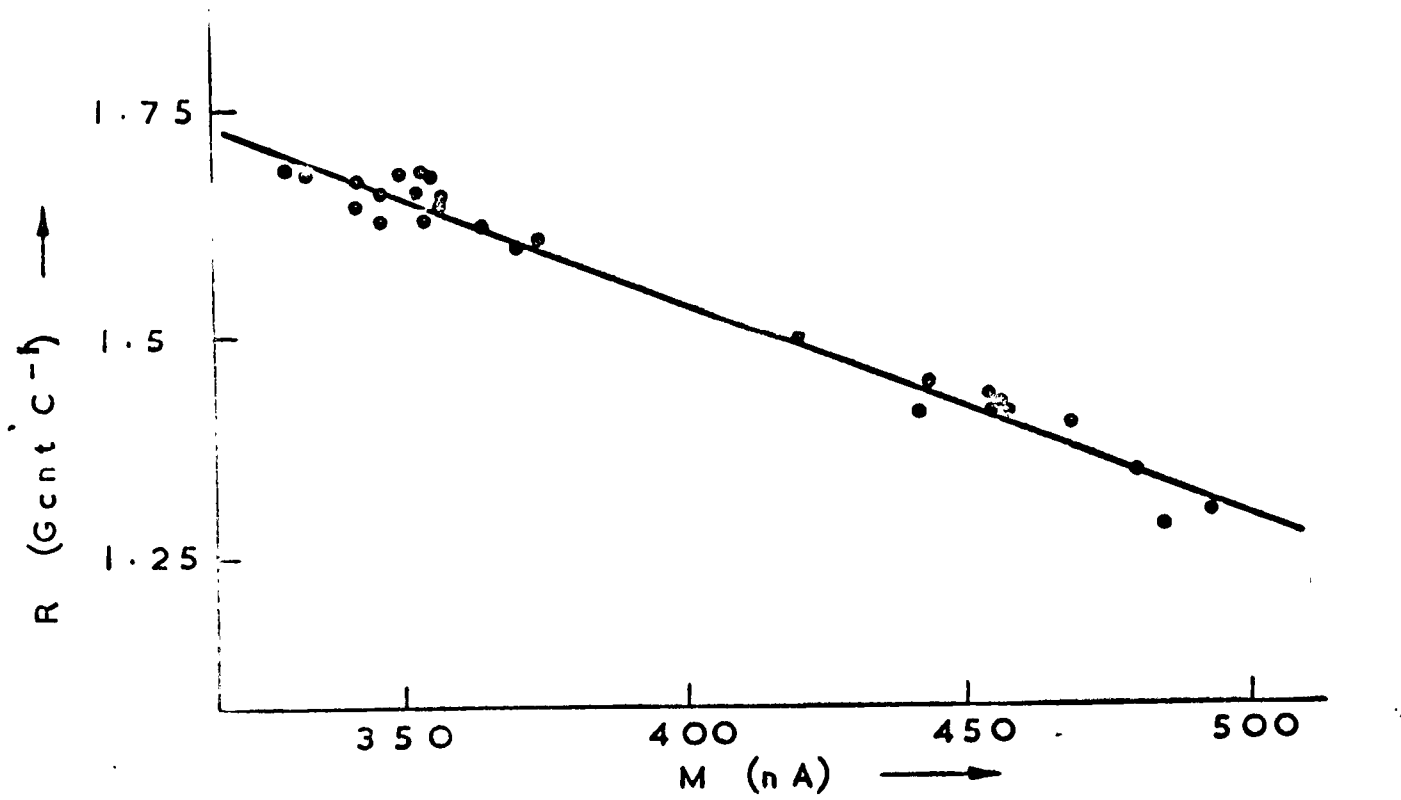

FIG. 5.3.B. VARIATION OF R WITH M DURING SERIES OF 10s COUNTS, FOR Li 0° SPECTRUM

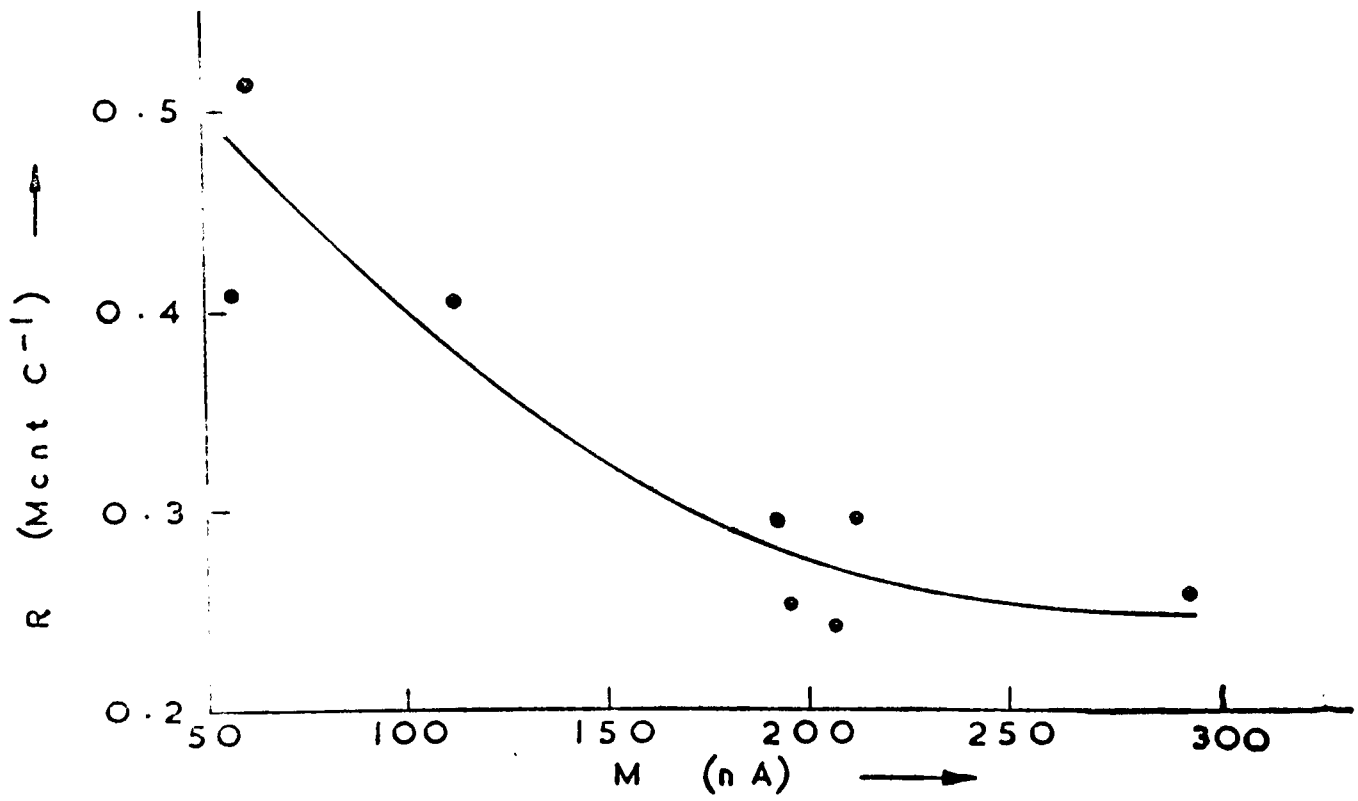

FIG. 5.3.C. VARIATION OF R WITH M FOR ALL ON69 0° Li NEUTRON PEAKS

and the counting rate, I, (corrected for the dead-time of the electronics as explained in Chapter 6) as functions of the phasing delay are shown in fig. 5.3.A(i), and the fact that the two curves were accurately in phase both indicated that the apparatus was well set up, and justified the use of the monitor for finding the positions of the maxima.

However, the ratio R, where

$$R = \frac{I}{M}$$

was fairly constant when the phasing delay was close to the optimum setting, but diminished as the degree of mis-phasing increased. A plot of R v. M is shown in fig. 5.3.A(ii).

Furthermore, when the counting rate varied for reasons other than mis-phasing, R was found to decrease with increasing M - the reverse of the trend evident in fig. 5.3.A. The results of a series of consecutive 10s counts are shown in fig. 5.3.B, and it may be seen that the variation of R with M was reproducible and linear within experimental error. (It should be noted that values of R from figure to figure are not directly comparable as different targets were used.) The data shown in fig. 5.3.B form part of a set taken during the angular normalization experiment described in sub-section 5.4.2.

The reproducibility of the variation of R with M was, however, valid only in the short term. Fig. 5.3.C shows results for the eight spectra from the reference lithium target taken at 0° during the ON69 run. Observations of the spectra were chronically spaced throughout the run, and though the general trend of decreasing R with increasing M is again evident, it may be seen that fluctuations up to ~ 30% occurred. Similar fluctuations were observed at other angles, and were shown to occur well within the time taken (~ 6h) for an angular sweep.

'OLD' BEAM PROFILE SHOWN DOTTED ALONG WITH 'NEW'
N.B. 'OLD' AND 'NEW' PROFILES SHOWN NORMALISED TO SAME HEIGHT, AND THEREFORE NOT ON SAME SCALE

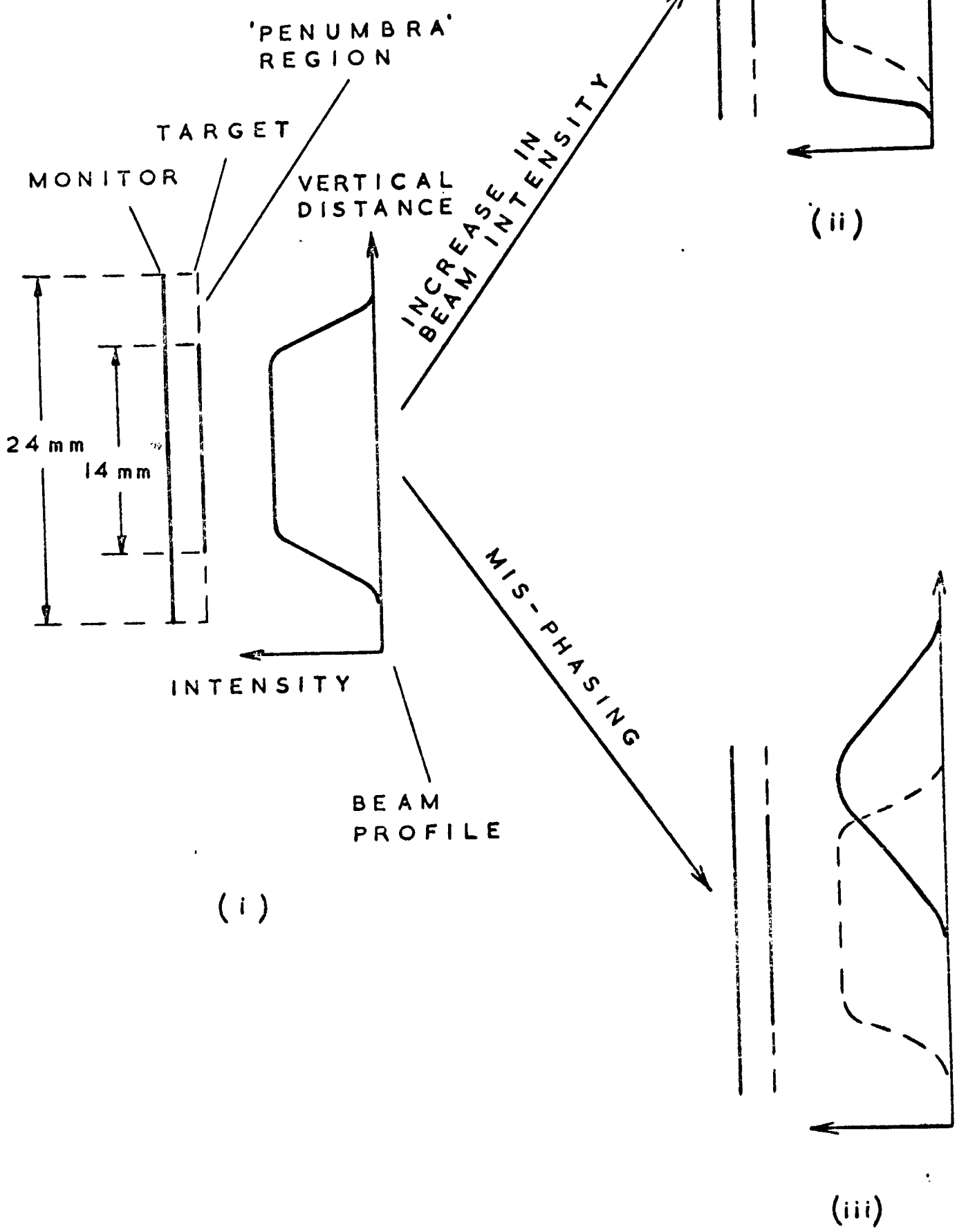

FIG. 5.4.D. POSSIBLE EXPLANATION OF DEFICIENCIES OF MONITOR

The variation of R with M did not of itself preclude the use of the monitor for angular normalization (see section 5.4.2), but the random variations would have led to errors up to 30% if the monitor readings had been used to normalize the whole of the angular data. (See Chap. 6, sub-section 6.5.2 for discussion, and solution).

However, the observed variations in R, by up to a factor of three, almost entirely precluded the use of the monitor for absolute normalization, since it would clearly have been impossible to accurately calculate the relation between the monitor reading and the absolute intensity of the effective beam incident on the target.

The reasons for these phenomena are imperfectly understood. It is thought unlikely that there were deficiencies in the apparatus itself. The most likely defect would have been imperfect electrical insulation, but the leakage resistance was measured on a number of occasions and found to be in excess of 20 MΩ.

The size of the collimator in front of the monitor was chosen to be equal to the limits of the area of the target "seen" by the collimation. In particular, its height was 24 mm, coinciding with the limits of the "penumbra" defined by the collimation. However, the "umbra" was only 14 mm high, so that over 10 mm of the height, the beam contributed fully to M but only partially to I. The beam trimmer (Chapter 2, section 2.1) constrained the beam to be 16 mm high at a synchrocyclotron radius of ~600 mm, but by the time the deflection radius of 927 mm was reached, this would have spread out so that the beam profile might have been as shown in fig. 5.3.D (i). An increase in the beam intensity might well have caused a "filling in" of the wings of the distribution, as shown in fig. 5.3.D(ii), leading to a greater proportion of the beam being within the "penumbra" region with a consequent decrease in R. Mis-phasing,

though reducing the beam intensity and causing the profile to become more rounded, would also cause the beam incident on the target to rise, since the beam would have passed between the deflection plates under inefficient deflection conditions. The change, therefore, might have been as shown in fig. 5.3.D (iii) leading again to a greater proportion of beam in the penumbra region and a reduction in R.

These considerations are no more than "plausibility arguments" and, though they account qualitatively for the observations, it is very difficult to account for the observed magnitudes of the variations in R.

Some improvement in the situation might have been effected by choosing dimensions for the collimator in front of the monitor, which were partway between those of the "umbra" and "penumbra", but the best solution for the future would almost certainly be to collimate the beam before it is incident on the target, to a size smaller than the "umbra". This would have the disadvantage of reducing the counting rate, but in addition to removing the dependence of R on M would increase the accuracy of absolute normalization by making possible a direct calculation of particle flux from the value of M, independently of the shape of the beam profile. Unfortunately, the desirability of such a solution was not realised early enough for it to be implemented in the present experiment.

5.4 Data taking during the D69 run - Normalization

If the monitor had worked effectively, it would have provided absolute normalization of all the data. Its deficiencies presented three distinct normalization problems:

(a) relative normalization between different targets at the same angle,

(b) relative normalization between different angles for the same target, and

(c) absolute normalization.

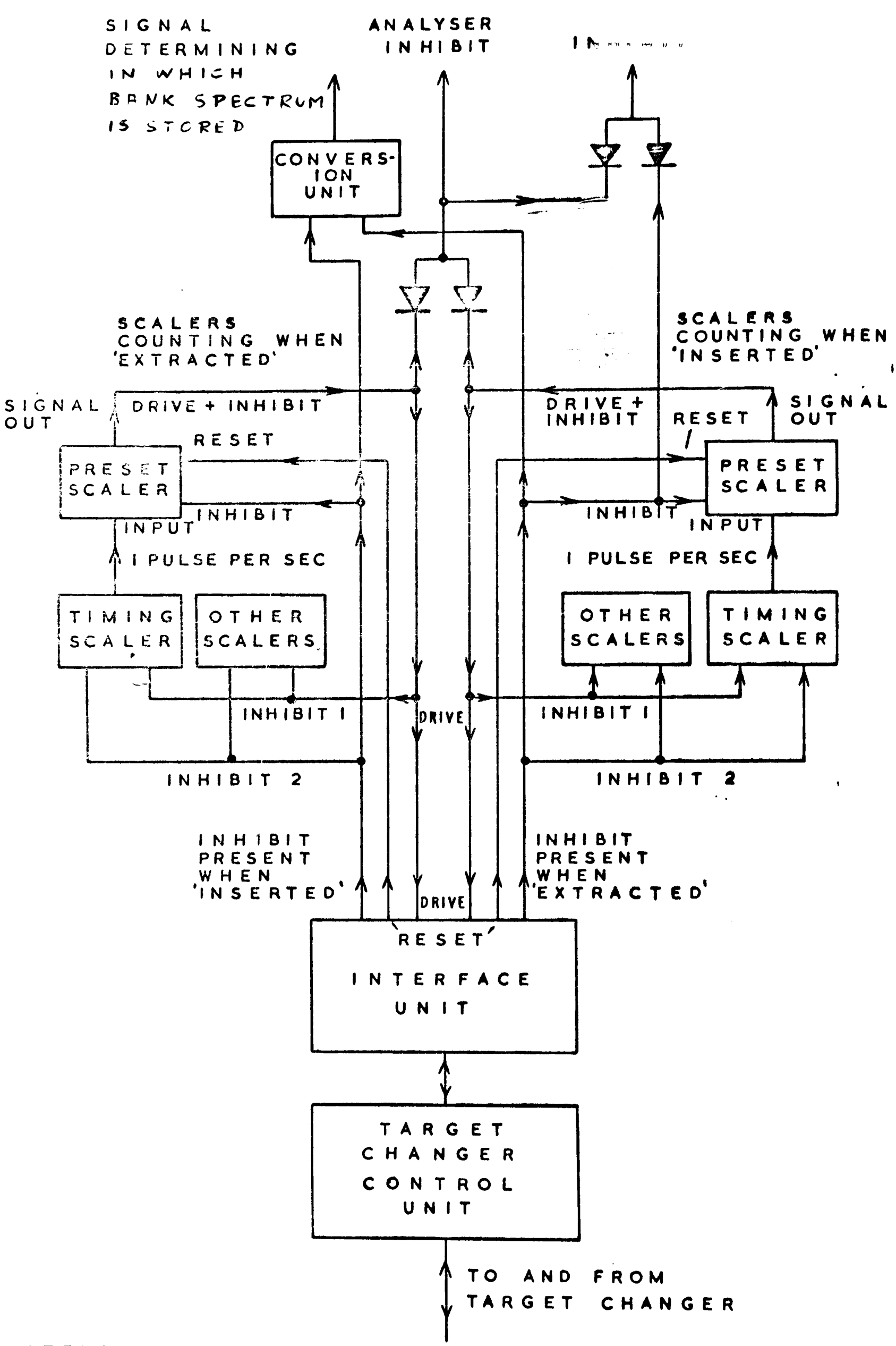

NOTES :—

1. INPUTS TO MOST SCALERS NOT SHOWN.
2. TIMING SCALERS INPUT FROM CLOCK PULSE GENERATOR.
3. WHOLE SYSTEM INHIBITED BY 'TOTAL TIME' PRESET SCALER – NOT SHOWN.
4. NEGATIVE SIGNALS USED, SO DIODES PASS SIGNALS AGAINST THEIR ARROWS.

FIG. 5.4.A. SCALER/TARGET CHANGER INTERFACE SYST

The target to target normalization was determined for all the targets at a selection of angles during the D69 run and is described in the first sub-section. Having done this, it was necessary to determine the angular normalization for only one target, and a partially successful attempt to do this experimentally is described in the second sub-section, though an alternative method for angular normalization is discussed in Chapter 6, sub-section 6.6.2.

Absolute normalization was achieved by normalizing each spectrum to that from the deuterated polythene target, and using a previous measurement (Langsford, 1967, B) of the absolute cross-section for the d(p,n)2p reaction (see Chapter 6).

5.4.1 Target to target normalization, data taking

The relative normalization between two targets could be achieved simply by comparing the magnitudes of their spectra normalized to a fixed time, provided that the mean internal beam level was the same for each target. In practice, the internal beam fluctuated too much to allow this for consecutively investigated targets, and this problem was overcome during the D69 run by interleaving a series of alternate counts from the target under investigation and the reference target.

The system devised to do this is illustrated schematically in fig. 5.4.A. The scalers used during the ON69 run were duplicated, and a third bit was dropped from the address produced by the timing system so that the spectrum was stored in 2048 of the 4096 channels of the analyser. The scaler system was interfaced to the "computer" socket of the target changer control unit via a specially built unit.

When the target changer insert/extract mechanism was in the "insert" position (target from the tray in the beam, see Section 3.2),

one bank of scalers only counted and the spectrum stored in the lower bank of 2048 channels; when it was "extracted" (reference target in beam), the other bank of scalers counted, and the spectrum stored in the upper half. The monitor was retained, and the I.D.V. counted only in the "insert" position.

The alternate insertions and extractions of the target were automatically operated by signals from two preset scalers which counted millisecond pulses from a clock pulse generator. The time of a single "insert" count was determined by the setting of one of the scalers and vice versa. All counting was inhibited while the target changer was driving. The overall counting time was set on a third preset scaler.

The scalers and the analyser were not reset between individual counts, and the counts and spectra were allowed to build up.

For most of the data taking, 30s "extract" counts were alternated with 60s "insert" counts, these times being a compromise between achieving the most accurate normalization and not driving the target changer so often that the mechanism siezed.

The system was operated so that the first and last counts of a series were either both "insert" or both "extract" so that the normalization would be correct for a steady one way drift of beam intensity. In general, the procedure was adequate provided that drifts in the internal beam intensity were slow compared with a single "insert" or "extract" time, and that more rapid fluctuations summed to zero for both. This was believed to be the case from inspection of the behaviour of the beam monitor, and it is shown in Chapter 6 from self consistency arguments that, though a few counts had to be rejected, the normalization was good to $\sim$10%.

Data were taken only at 0^{o}, 5^{o}, 10^{o}, 15^{o}, 20^{o} and 30^{o} since it was possible to interpolate the normalization between angles.

An undesirable feature of the D69 data was the presence of high "spurious" background not resulting from reactions taking place in the target. This was caused by the deflection plates overheating and buckling so that they bowed downwards and could be "seen" by the collimation. This effect was zero at the 0^{o} position since the deflection plates were situated horizontally a little way from the 0^{o} beam line, but was appreciable at 5^{o} and became steadily worse at higher angles. It also exhibited quite considerable variation over relatively short periods of time as the amount by which the deflection plates bowed varied according to the degree of overheating. The effect was also present for some of the elements studied towards the end of the ON69 run, though to a much smaller degree. Since the experiment, the technical problem of avoiding the overheating has proved difficult to solve, and experience has shown that with the deflection plate design in use during the experiment, it was the ON69 run, relatively free from spurious background, which was atypical.

The spurious background did not seriously detract from the main purpose of the D69 run which was to determine the target to target normalization of the peak areas, since the spurious background spectrum was relatively smooth and the peaks could be separated relatively easily. It did, however present problems in subtracting the spectra from the gold backings of the targets, and in calculating the angular normalization. (see following sub-section and Chapter 6).

5.4.2 Experimental determination of the angular normalization

It is explained in detail in Chapter 6 that the angular normalization may be determined by performing a theoretical calculation of the area of the background under the peaks using statistical theory. It was desirable, however, to perform an experimental determination of the angular normalization as a check on the validity of the assumptions made in the calculations.

This sub-section describes the experiment, but a discussion of the results is deferred until Chapter 6.

The simplest method of determining the angular normalization without a monitor is to perform a series of counts at different angles sufficiently rapidly so that the incident beam intensity does not change during the angular sweep. The requirement that the data be taken rapidly precluded the use of the analyser since the time taken (4 min) to punch a single spectrum would have slowed the data taking by an unacceptable amount.

The electronics system was therefore slightly modified so that counts from sockets in the decoding unit were recorded in four scalers. The decoding unit was set so that one scaler recorded the counts corresponding to the first half of the store of the analyser, a second recorded counts in the third quarter and a third counts in the fourth quarter. The fourth scaler recorded total events as a check that counts were not lost from any scaler.

Lithium was chosen as the element to be investigated both because it had been used as a reference throughout the experiment, and because the ratio of peak area to background was greatest for this element.

Since energy resolution was no longer of any concern, the synchrocyclotron running conditions were changed so as to increase

the beam intensity and make it more stable.

It was found, nevertheless, that the beam level still fluctuated too rapidly to enable a reproducible angular distribution to be obtained without the use of the monitor, and it was therefore necessary to use the monitor in such a way that the variation of R with M could be accurately determined at each angle.

The scaler system was therefore set so that at each angle a series of 10 s counts was taken, the scaler contents being automatically recorded and reset after each count. It was found that R varied reproducibly and linearly with M at each angle, the results at 0° having already been presented as fig. 5.3.B. It was therefore possible to normalize the data to a fixed value of M, and, after making certain geometrical corrections, to calculate the angular distributions of the counting rates in those sections of the spectrum recorded by the scalers.

The main $Li^7(p,n)Be^7$ (g.s.) peak was contained in the third quarter of the observed spectrum at all observed angles, and its area was inferred from the counts in the appropriate scaler. However, the presence of spurious background introduced errors into this calculation since the ratio

$$\frac{\text{peak area}}{\text{3rd quarter area}}$$

at a particular angle varied during the D69 run.

The results, errors, and the way in which they were calculated are discussed fully in Chapter 6.

CHAPTER 6

CALCULATION OF THE RESULTS

The data analysis was carried out to obtain values for the cross-sections of the transitions observed in the experiment at the observed range of angles, and, where they were not already established, values of the excitation energies of the corresponding levels. The data input to this analysis were the uncorrected time spectra, and the first task was to produce fully corrected time spectra from which energy spectra could be calculated. Such an energy spectrum consisted of a number of peaks corresponding to the states of the residual nucleus, on a smooth background resulting from breakup processes.

Section 6.1 describes how the data were handled, an account of the corrections made to the time spectra is given in section 6.2, and section 6.3 explains how excitation energies and Q-values were calculated from the positions of the peaks.

The cross sections were calculated from the areas of the peaks, and section 6.4 explains how these areas were determined by a specially written computer program. It was sometimes possible to determine separate areas in cases where peaks were too close together to be resolved by eye, and in some of these cases, the positions of the peaks were also determined using this program. The way in which cross sections were calculated from the peak areas is explained in section 6.5.

6.1 Data Handling

Because of the enormous number of data produced in the experiment, almost the whole of the analysis had to be performed by computer. The two hundred and twenty seven paper tapes containing the uncorrected time spectra were transferred to 7-track magnetic tapes using a Honeywell DDP-516 computer. The program checked the data, and allowed on-line

correction at a teletype of any paper tape punching errors. The contents of the 7-track tapes were then transferred to 9-track tapes using the Harwell I.B.M. 360/75. This computer was used for the whole of the subsequent analysis.

The programs written to perform the analysis were as follows.

i) The main correction program

ii) The background subtraction program

These two programs between them performed all the corrections described in section 6.2.

iii) The kinematics program

This predicted the expected positions of the peaks as explained in section 6.3.

iv) The fitting program

See section 6.4.

Programs were also written to find the centroid of regions of the spectra, and to calculate ratios of the areas of such regions. Much of the coding of the kinematics program was also included in some of the other programs, in particular, the fitting program.

6.2 Correction of the time spectra

Before peak positions and areas could be determined, the energy dependent corrections had to be made to the time spectra. Energy independent corrections affected only the overall normalization of a spectrum and these were made to the cross section values rather than to the contents of each channel.

Conversion between position in the time spectra and neutron energy had to be performed frequently throughout the analysis, and the way in which this was done is described in sub-section 6.2.1. The subsequent sub-sections describe the energy dependent corrections, which were as follows:

(i) the dead-time correction,

(ii) the counter efficiency correction,

(iii) the beam attenuation correction, and

(iv) subtraction of the spectra from the gold foil backings.

6.2.1 Neutron energy calculation

The time of flight of neutrons recorded at a particular position, C_n, in a spectrum was calculated using a knowledge of the position of the γ-peak, C_γ, and the time calibration of the system. If t' was the time interval corresponding to the interval $(C_n - C_\gamma)$, then the time of flight of the neutrons, t, was simply given by

$$t = t' + \frac{p}{c} ,$$

where p is the length of the flight path and c is the velocity of light. The energy of the neutrons was then calculated using the relativistic formula.

C_γ was taken to be the position of the centroid of the γ-peak, and this was computed for each spectrum by the main correction program.

The time calibration was determined by computing the positions of the centroids of the "spikes" in the time calibration "spectra" (see Chapter 3, sub-section 3.8.4). One of the "spikes" had been adjusted to be as close as possible to the position of the γ-peaks, and the mean time width per channel between this spike and the sixth was computed. The sixth spike was chosen because its position was close to that of the neutron peaks resulting from a number of analogue transitions. When necessary, account was taken of the slight non-linearity of the system by plotting the deviations of the actual positions of the other "spikes" from the positions calculated on the assumption of a constant channel width. This deviation was not

greater than 0.5 channels over the region of interest, and interpolation between "spike" positions could be performed to ~0.05 channels or ~13 ps. Timing drifts throughout a run necessitated interpolation between the times at which the time calibration "spectra" were taken. This introduced an extra error of ~20 ps leading to an overall uncertainty of ~25 ps or ~6 keV for 90 MeV neutrons. This was insignificant in comparison with the precision with which the position of a neutron peak could be determined.

6.2.2 The dead-time correction

The dead-time correction arose because the counting electronics was capable of recording only one event in any one synchrocyclotron burst (repetition cycle). The recording of an event therefore prevented the recording of subsequent events in the same burst, and created a bias against late events. It may be shown (Saltmarsh, 1965) that the correction factor at the junction between the n th and (n + 1)th channels is given by

$$f'_n = \frac{B}{B - \sum_{i=0}^{n} y_i}$$

where y_i is the uncorrected contents of channel i, and B is the number of bursts. Taking

$$f_n = \tfrac{1}{2}\,(f'_{n-1} + f'_n)$$

was an extremely close approximation to the correction factor for the whole of channel n.

The formula is valid provided that the intensity (and spectrum shape) of the neutrons produced in each burst is constant. Errors due to this being invalid were usually small, except that it was known that a number of bursts contained hardly any neutrons owing to

the proton bunch failing to start acceleration. In this case, B should be the number of bursts containing neutrons, or "effective" bursts. Previous determinations of the ratio, R, of effective bursts to bursts had shown that it fell as low as 0.7 when the machine was running unstably as in this experiment. This could lead to a possible absolute error of up to 2%.

This would have affected the absolute normalization obtained using the monitor had this been possible. However as the method in fact used (sub-section 6.5.3) depended upon a comparison between spectra, error arose only from the difference in the corrections to the two spectra, and from one part of a spectrum to another, and this error was not greater than 0.05%. Consequently, it was not necessary to determine the ratio R.

6.2.3 The counter efficiency correction

The variation with neutron energy of the detection efficiency of the counter was determined, as described in Appendix C, by comparing it with a standard counter whose absolute efficiency had been previously determined (Bowen, 1962).

The fitting program (sub-section 6.4.3) was used to fit an analytic function to the results, viz:

$$f_c(T) = \frac{1}{(1 + 7.245 \times 10^{-3}(T - 90))(1 - 6.916 \times 10^{-4}(T - 90))},$$

where T MeV is the kinetic energy of the neutron. Since only the energy variation was of current concern, the normalization was arbitrarily adjusted for convenience to give $f_c(90) = 1$.

The energy corresponding to each channel was calculated, and hence the number of neutrons recorded in each channel divided by the appropriate value of f_c to normalize the spectrum to that which

would have been recorded by a detector whose efficiency was energy independent.

6.2.4 The beam attenuation correction

The neutron beam was attenuated by its passage through the 25.4 mm of aluminium and 27.46 m of air between the target and the detector.

The transmission as a function of neutron energy was calculated from published total cross-section data (Hughes, 1955) and an analytic function fitted to the results using the fitting program. This fit gave a neutron transmission function

$$f'_T(T) = \frac{0.8155}{1-2.172\times10^{-3}(T-90) - 1.044\times10^{-5}(T-90)^2 - 9.646\times10^{-7}(T-90)^3}$$

where $f'_T(T)$ is the transmission for neutrons of energy T MeV. The normalization was again adjusted to give a correction factor of unity for T = 90.

6.2.5 Subtraction of the spectra from the gold foil backing

In order to determine the background from the gold backings of the targets, a lone gold target was also investigated, and this was subtracted before further analysis was carried out. However, problems were encountered in determining the factors by which the gold spectra should be multiplied, and a discussion is deferred to section 6.5, since the method used was based on the same principles as the normalization methods described therein.

6.2.6 Conversion to energy spectra

All further calculation of the results was performed using the fully corrected time spectra, and conversion of some of the time spectra to neutron energy spectra was carried out for display purposes only. It was achieved by calculating a new set of abscissae by converting each channel number to a neutron energy, and by multiplying

the contents of each channel by dT/dn where T is the neutron energy, and n is the channel number.

6.3 Calculation of incident energies, Q-values, and excitation energies

This section describes how the incident proton energy, and the Q-values and excitation energies corresponding to the observed transitions were determined from the positions of the peaks in the spectra. Sub-section 6.3.1 discusses how the peak positions were determined, sub-section 6.3.2 describes the relativistic kinematics computer program, and sub-section 6.3.3 explains how it was used to perform the calculations.

6.3.1 Determination of peak positions

For purposes of this analysis, the "position" of a peak was defined to be the centroid of the top 40% of the peak in terms of height. This definition was chosen so that the position was independent of changes in the "wings" of the resolution function. Also, it often enabled precise direct computation of the position even when the peak was not completely separated from its neighbours.

In the case of unresolved peaks, determination of the positions had to be made using the fitting program (section 6.4).

6.3.2 The relativistic kinematics program

The function of the relativistic kinematics program was to calculate the laboratory energy, T_n, of neutrons emitted at laboratory angle θ resulting from the reaction A(p,n)B(+ Q MeV), and to predict the position in a time of flight spectrum of the resulting peak. T_n depended on the incident proton energy, T_p, as well as on Q and θ. The position of the peak in the spectrum was calculated from T_n using a knowledge of the γ-peak position and the time calibration.

The neutron energy threshold for a reaction of the form $A(p,n)B_1,B_2$, ... leading to a three or more body final state was

similarly calculated by assuming a single residual particle with a rest mass equal to the sum of the separate masses of B_1, B_2 ....

6.3.3 The calculations

Since the position of a peak depended on both T_p and Q, there was no way of calculating the separate values of these variables simply from inspection of a single spectrum. However, Q-values for all the analogue transitions were already well established, and this allowed T_p to be calculated by making a series of predictions of peak positions for stepped values of T_p, comparing with the actual position, and interpolating where necessary.

Having assigned a value of T_p to each spectrum, it was then possible to predict the positions all peaks resulting from transitions to known states of the residual nucleus. The important variable determining the excitation energy (as opposed to the Q-value) of a level was the difference, δ, between the position of the corresponding peak and that corresponding to the ground state. The quantity δ was not sensitive to small errors in T_p.

In the case of resolved, narrow, well known levels, the position invariably agreed with the prediction within the $\pm$ 0.05 MeV limits of experimental error. In the case of previously unknown levels, or levels whose excitation energy was uncertain, the excitation energy was determined by interpolating between predicted positions.

One further point remains to be made. The cross-sections were calculated from the areas of the whole peaks, so that to quote values of T_p derived from the position of the top 40% of the peak as "the energy of the experiment", would strictly speaking, be incorrect. However, the small difference ($\sim$ 0.1 MeV) between the "top 40%" position and that of the centroid of the whole peak was less than the

variation (~ 0.5 MeV) of T_p during the relevent runs, and so could be neglected for this purpose.

6.4 Determination of the areas and positions of peaks and background

The peaks in the time spectra corresponding to transitions to states of the residual nucleus were superimposed on a smooth background resulting from breakup processes. In nearly all cases the peaks were not well separated, and in a number of cases were not resolvable at all by eye.

The shapes of a single peak and of the background could be determined or predicted in terms of analytic functions, and in order to analyse the spectra, a computer code was written to fit sums of these functions to the spectra. The fitting was performed using the fully corrected time spectra.

The first two sub-sections consider the expected form of the spectra, the third describes the fitting program, and the fourth explains the way in which it was used.

6.4.1 Shape of the background

In the absence of a final state interaction, statistical theory may be used to calculate the shape of the energy spectrum of one of the particles of a transition to a final state consisting of more than two particles. The energy spectrum in the centre of mass is simply given by the appropriate phase space integral.

For example, in the case of three body breakup

$$p + A \longrightarrow n + B_1 + B_2 ,$$

the relativistically invariant phase space integral is given by (Kretzsman, 1961),

$$\frac{dR}{dT} \propto \frac{1}{W^2} \left[T\,(2M_2+T)(W^2-M_2^2+M_1^2)^2 - 4W^2 M_n^2 \right]^{\frac{1}{2}}$$

where M_n, M_1, M_2 are the masses of the neutron, B_1 and B_2 in MeV/c^2, T MeV is the kinetic energy of the neutron, and

$$W^2 = E_{TOT}^2 + M_2^2 - 2 E_{TOT} (T + M_2)$$

where E_{TOT} is the relativistic total energy of the system.

The non-relativistic approximation is

$$\frac{dR}{dT} \propto \frac{1}{T_{MAX}} \left[T (T_{MAX} - T) \right]^{\frac{1}{2}}$$

where T_{MAX} is the neutron threshold energy. A comparison was made between the shapes given by the two formulae, and at the energy of the experiment they were found to be the same to within 1%. The simpler non-relativistic form was therefore used.

The non-relativistic four-body phase space integral is given by

$$\frac{dR}{dT} \propto T^{\frac{1}{2}} (T_{MAX} - T)^2 .$$

Before these functions could be fitted to the time of flight spectra, they had to undergo a kinematical transformation to the laboratory system and a conversion to time of flight co-ordinates.

The proton bombardment of ^{9}Be may be taken as an example to show how the functions were chosen. As well as the transition to the ^{9}B + n final state, other possible transitions leading to the emission of a neutron include

$$^9\text{Be} + p \longrightarrow \begin{cases} (\ ^4\text{He} + {}^4\text{He} + p + n,\ Q = -1.57\ \text{MeV}\ ) & \text{4-body} \\ (\ ^8\text{Be} + p + n\ ,\ Q = -1.67\ \text{MeV}\ ) & \\ (\ ^4\text{He} + {}^5\text{Li} + n\ ,\ Q = -3.54\ \text{MeV}\ ) & \text{3-body} \end{cases}$$

Numerous other final states were possible, but with lower Q-values. (All the Q-values involved in this experiment were negative, but the terms "lower" and "higher" are used in their strictly correct sense, e.g. a Q-value of -2 MeV is lower than one of -1 MeV.) The Q-values

were taken either from the nuclear spectroscopy data of refs. (Ajzenberg-Selove, 1968; Lauritsen, 1966) or from the nuclidic mass excess data of ref. (König, 1962).

No information was available about the relative magnitudes of the cross-sections of these breakup modes.

6.4.2 Shapes of the peaks

The shape of a single peak corresponding to a transition to a state whose natural width was negligible was simply given by the resolution function of the system. The shape of a peak corresponding to a naturally broad state was the resolution function broadened by a Lorentzian.

As explained in Chapter 4, the shape of a γ-peak directly gave the time resolution function, but the overall resolution function was a compound of this time resolution function, the energy loss of the protons in the target, and the incident energy distribution of the protons. It proved impossible to reduce the energy spread of the incident protons to a negligible amount, and since this energy distribution was not known, it was impossible to calculate the resolution function directly from the shape of the γ-peak.

It was therefore necessary to use the neutron peaks to define the resolution function. There was no peak which was known to be narrow, single and completely separated from other peaks, but the resolution function was successfully determined from overlapping peaks as explained in sub-section 6.4.4.

6.4.3 The fitting program

The object of the fitting program was to fit a function representing the expected shape of the spectrum to the experimental data using a "chi-squared minimization" technique. The experimental data

consisted of a series of channel numbers, n_i, $n_i + 1$, ... n, ...n_f, and channel contents, y_n, with standard deviation δ_n. The function, F, to be fitted was defined in terms of a series of parameters, a_1, a_2, ..., so that

$$F = F(n_1 A),$$

where

$$(A) = (a_1, a_2, a_3 .....).$$

χ^2 was defined by

$$\chi^2 = \sum_{n=n_i}^{n_f} \left[\frac{y_n - F(n, A)}{\delta_n} \right]^2 = \sum_{n_i}^{n_f} \Delta_n^2$$

and the fitting procedure consisted of varying (A) so as to minimise χ^2. If the functions accurately represent the experimental curve, then, subject to statistical error, the value of χ^2 at the minimum should be equal to the number of fitted points (Guest, 1961). If the function is a poor representation, the value of χ^2 per point will be greater than unity; conversely if the function has too many variable parameters, it is possible for it to "follow" the positions of the points more closely than the experimental curve, leading to values of χ^2 per point of less than unity.

The kernel of the fitting program was a sum of squares minimization routine named VA02A. This is a member of the Harwell Subroutine Library and was written by M.J.D. Powell. The method (Powell, 1965) is iterative, and does not require user-supplied derivatives. The values of Δn were computed by the fitting program

NOTES:-

1. IN ALL FUNCTIONS, $x = m - a_1$,
   $\therefore a_1$ IS THE 'POSITION' OF THE FUNCTION.

2. IN f_9 AND f_{10} a_1 IS IN PRACTICE ALWAYS ZERO, SO THAT $x = n$

FUNCTION	NAME	USE
$f_1(n, a_1, a_2, a_3) = a_2 / (1 + x^2 / 4 a_3^2)$	LORENTZIAN OF WIDTH (F.W.H.M.) a_3	'NATURAL' SHAPE OF PEAK, ONLY USED IN CONJUNCTION WITH f_4
$f_2(n, a_1, a_2, a_3, a_4, a_5, a_6) = \frac{a_2}{1 + a_3 x + a_4 x^2 + a_5 x^3 + a_6 x^4}$	RECIPROCAL OF QUARTIC (ROQ)	USED TO REPRESENT THE RESOLUTION FUNCTION
$f_3(n, a_1, a_2) =$ $f_2(n, a_1, a_2, p, q, r, s)$	ROQ WITH FIXED SHAPE PARAMETERS	DITTO ABOVE WHEN SHAPE NO LONGER VARIABLE
$f_4(n, a_1, a_2, a_3) =$ $\int_{-\infty}^{\infty} f_1(x-\omega, a_2 a_3) f_3(x, 1) d\omega$	ROQ BROADENED BY LORENTZIAN	REPRESENTED PEAK WITH FINITE NATURAL WIDTH
f_5, f_6, f_7, f_8	————	NOT USED
$f_9(n, a_1, a_2)$, $f_{10}(n, a, a_2)$ — FORMULAE IN TEXT SECTION 6.4.1.	3- AND 4- BODY PHASE SPACE INTEGRALS	REPRESENTED SHAPES OF BACKGROUND

TABLE 6.4.A. FUNCTIONS USED WITH THE FITTING PROGRAM

externally to VA02A, and VA02A then varied (A) so as to minimise χ^2.

F(n,A) was expressed as the sum of a series of basic functions representing peaks and background shapes.

$$F(n,A) = \sum_i \sum_j f_i(n,A_{ij})$$

where f_i is one of the basic functions, and A_{ij} is a series of parameters defining the jth example of the ith functional form. Up to ten functional forms were catered for, and up to nine examples of each form.

The functional forms used to fit the time of flight spectra are shown in Table 6.4.A. A set of parameters (a_1, a_2, ...) represents a single (A_{ij}), the subscripts i and j having been omitted for clarity. The "reciprocal of a quartic" (ROQ) (f_2 in the Table) was found to be adequate for fitting almost any shape of peak, usually giving values of minimum χ^2 per point close to unity in the range 0.9 - 1.3.

It was not usually desirable to vary <u>all</u> the parameters of the functions, and it was possible to specify precisely which parameters should be varied during any one fit. The statistical errors were calculated from the variance-covariance matrix, V, defined to be the inverse of the matrix, G,

$$V = G^{-1},$$

$$G_{IJ} = \sum_{n=n_i}^{n_f} \frac{\partial \Delta_n}{\partial a_I} \frac{\partial \Delta_n}{\partial a_J}$$

where a_I and a_J are two of the variable parameters. A close approximation to V was calculated by another Harwell Subroutine, SV01A,

according to the formulae given as eqn. (33) of ref. (Powell, 1965). The standard deviation of a single parameter a_I was simply the square root of the variance, V_{II}. For functions of more than one parameter, more complicated expressions involving the off-diagonal covariance elements, as well as the diagonal variance elements had to be used (Guest, 1961).

The program was structured to allow easy alteration of the basic functional forms, so that it could be applied to other data.

The program contained a module for producing graphs showing the experimental data, the fitted function, F, and/or the separated basic functions or any summed combinations.

6.4.4 The way in which the fitting program was used

This sub-section describes the overall way in which the fitting program was used, and takes as illustrations examples from the fits to the spectra from the $^{11}B(p,n)^{11}C$ reaction. The analysis of these spectra was particularly easy and the conclusions particularly clean cut. Fits to the other spectra often produced far less conclusive results, and this is brought out in the overall presentation of the results given in Chapter 7.

Backgrounds

The first problem was to fit the background, and an attempt was made to determine in what proportions each of the possible break-up modes contributed to the whole. A region of the spectrum where there was no peak was used for the fit, and the fitted function taken as the sum of a number of three and four body break-up modes with the highest Q-values. The general conclusion was that it was possible to distinguish between three body modes and four body modes since the

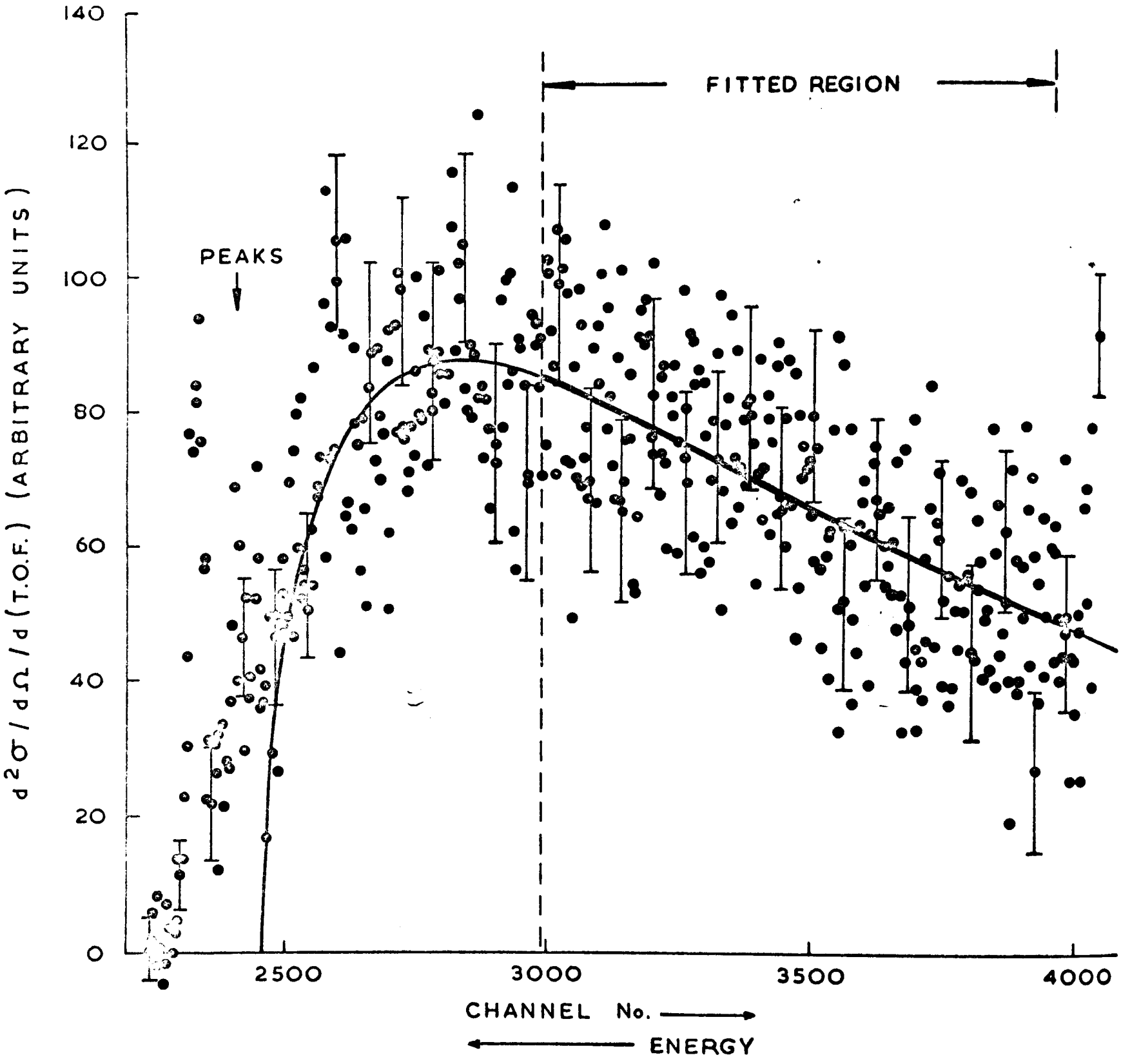

FIG. 6.4B FIT OF 3-BODY PHASE SPACE INTEGRAL TO 30° BORON SPECTRUM.

shapes were quite different, but not between different three body modes, say, since the difference in shape involved only small shifts along the abscissa resulting from the different Q-values, and were negligible except in the threshold region. Here the shape was obscured by the presence of peaks.

The $^{11}B(p,n)^{11}C$ spectrum shape was found to overwhelmingly favour a three body breakup mode, the contribution from the four body mode being indistinguishable from zero. Fig. 6.4.B shows the fit to the 30^{o} spectrum in which most of the "peak" excitation is absent because of the relatively high angle. It should be emphasised that only the comparitively small region indicated was used for the fitting. The remainder of the curve is an extrapolation of the phase-space integral, and the fact that the data were extremely well fitted in the extrapolated region gave considerable confidence that a similar extrapolation at other angles into regions with the considerable "peak" excitation was valid.

The resolution function

The next problem was to determine the resolution function for each spectrum. It was hoped to do this using the main neutron peak in the $^{7}Li(p,n)^{7}Be$ spectra, but the presence of the unresolved transition to the first excited state of ^{7}Be at 0.431 MeV changed the shape too much to allow this. The spectrum which could be used to provide the most accurate resolution function was the $^{11}B(p,n)^{11}C$ spectrum in which the first two peaks, though overlapping, were sufficiently far apart from each other and from the other peaks to allow a clear cut fit to be made. In addition, the background in this region was zero. The sum of two ROQs was used to represent the peaks, and the position of the second was calculated from the known

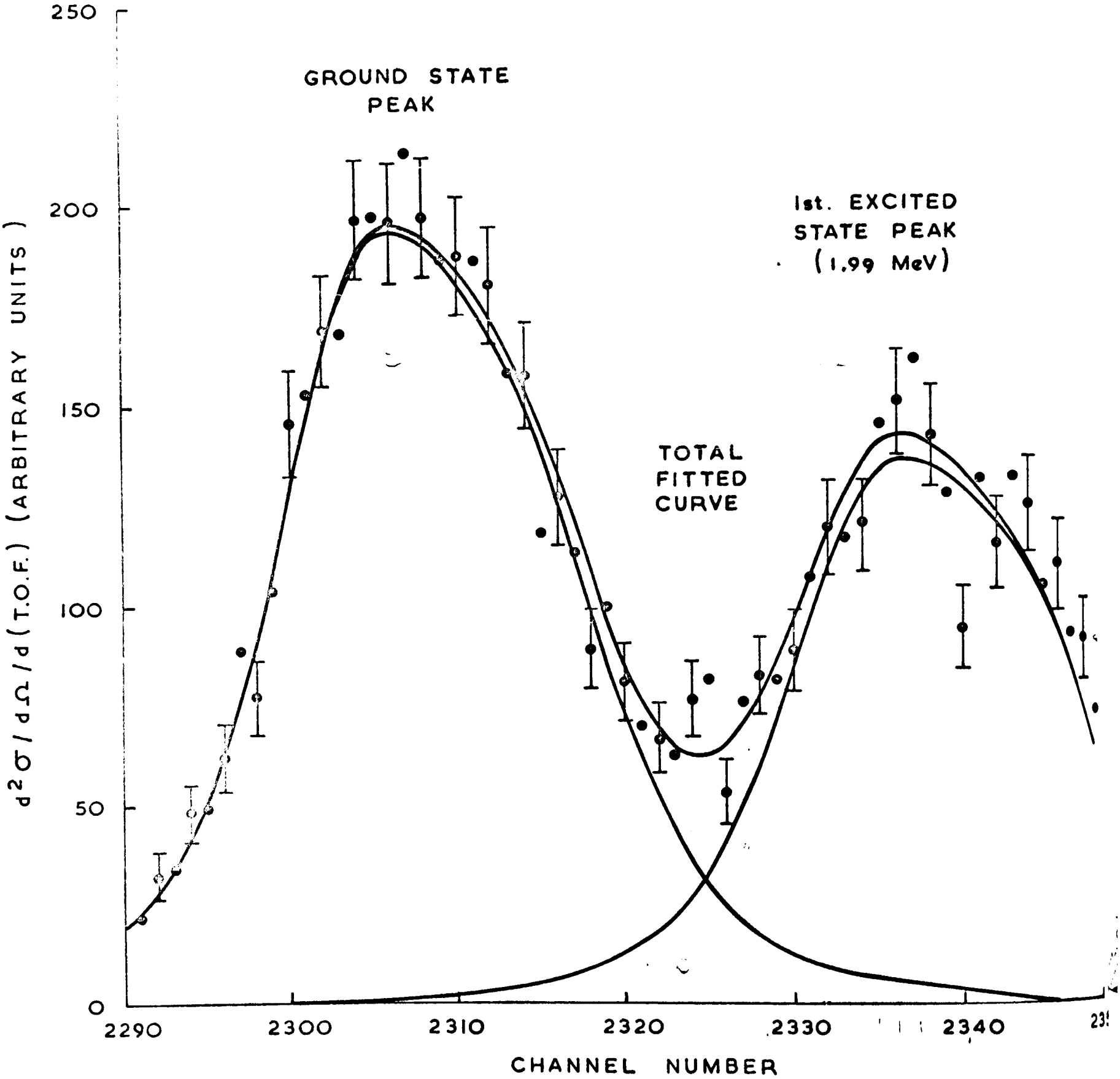

FIG. 6.4C DETERMINATION OF RESOLUTION FUNCTION FROM 0° BORON SPECTRUM.

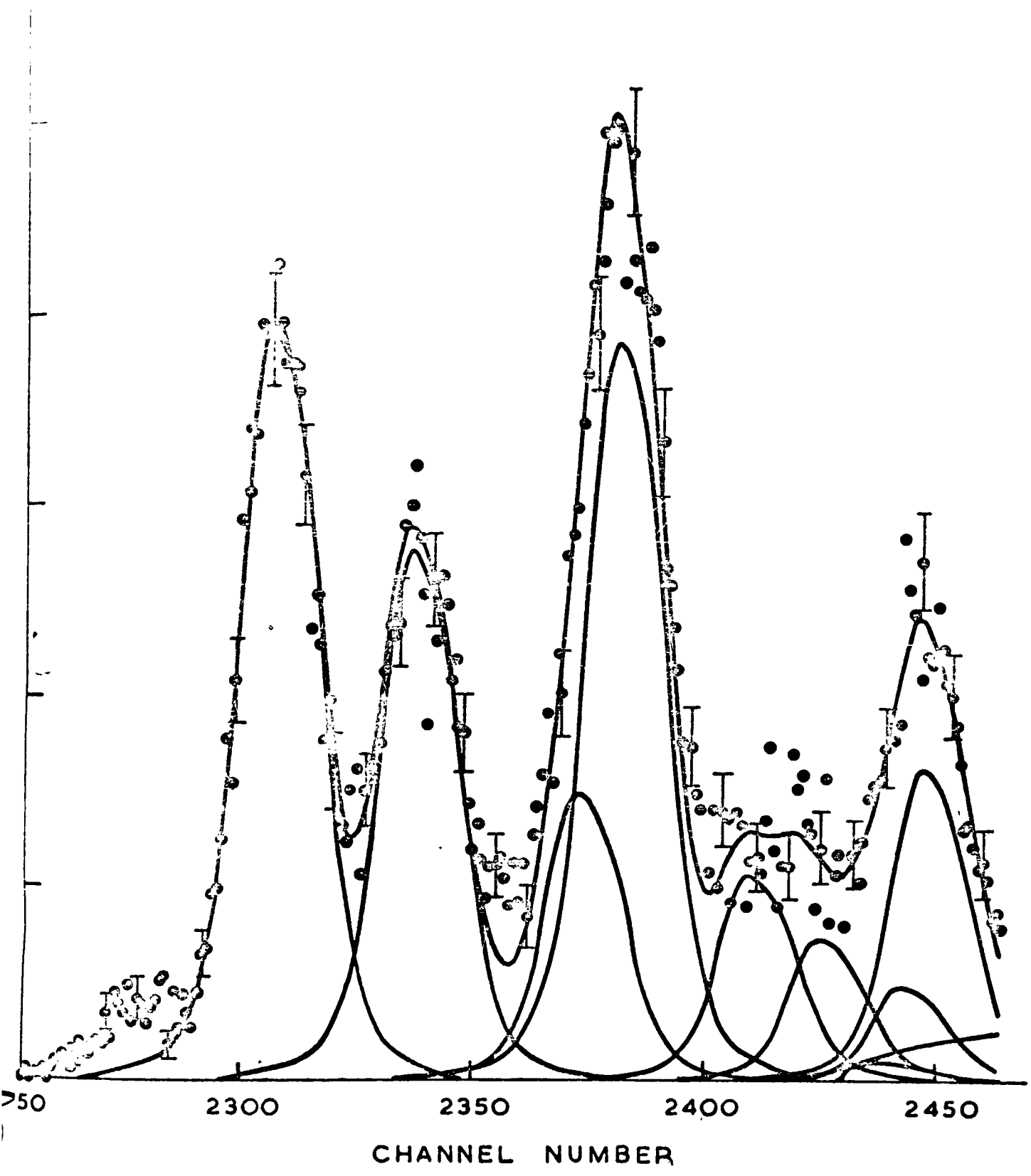

FIG. 6.4D FIT TO PEAKS IN 0° BORON SPECTRUM

excitation energy (1.995 MeV) of the first excited state of ^{11}C. The heights of the peaks and the shape parameters of the ROQs were allowed to vary during the fitting process, excepting that the program was modified slightly so that the shape parameters of one ROQ were constrained to remain equal to those of the others. The positions of the peaks were kept fixed. (A trial fit which allowed the position of the second peak to vary in addition to the other parameters produced almost identical ROQ shape parameters, and a position for the second peak which was negligibly different from that predicted.). The results of such a fit to the ON69 0^{o} spectrum are shown in fig. 6.4.C in which the overall function and the two separate peaks are shown.

Peaks

Having determined the resolution function for the $^{11}B(p,n)^{11}C$ spectrum it was then possible to apply it to all the peaks in this spectrum. First it was confirmed that the positions of the peaks as predicted by the kinematics program coincided with the positions estimated visually, and the function to be fitted was defined as the sum of the previously determined background functions and ROQs with fixed shape parameters at each of the predicted positions. The only variable parameters were the heights of the peaks. The results of such a fit are shown in fig. 6.4.D. It may be seen that the third peak is broader than the rest and has been fitted with two close narrow peaks at the expected positions of transitions to the second and third excited states of ^{11}C at 4.305 MeV and 4.794 MeV. It was not possible to establish on purely experimental grounds whether this peak resulted from a single naturally broad state or two unresolved states (though it was shown, using randomly scattered manufactured data, that such a procedure was possible in principle). However the

positions and small widths of these ^{11}C states are firmly established, and it was felt that evidence of the separate cross sections for transitions to the two states had been obtained.

The other spectra were fitted in a similar way, except that it was necessary to use as the resolution function, the ROQ shape parameters obtained from the $^{11}B(p,n)^{11}C$ spectrum. This did not usually lead to serious errors. Sometimes it was necessary to use broadened ROQs, and in a few cases, the position of a peak was also allowed to vary so as to more accurately determine the excitation energy.

Modifications to increase speed

In its original form, the program was very inefficient since all the separate functions making up the whole were recalculated from the basic function definitions every time any parameter was changed during the fitting procedure. In this form it took about five minutes computing time to completely analyse a single spectrum, so that it would have been prohibitively expensive to attempt to analyse all two hundred and twenty seven spectra. Consequently, two important modifications were made which increased the speed by about a factor of ten. This made the analysis of all the spectra possible, but, even so, several hours computing time were used.

The first modification consisted simply of not recalculating a basic function if none of its parameters had been altered, and the second of using a rapid recalculation method if only the height of a function had been changed, as was the case with a large majority of the fits.

6.5 Calculation of the differential cross-sections

Terminology

Before introducing the subject matter of this section, some terms and symbols will be defined, as follows:

Composite spectrum: spectrum from a target complete with gold foil backing, symbol "C" used for the area of the whole or part of the spectrum;

gold spectrum: spectrum from the gold foil backing of a target or from the lone gold target, symbol "G";

bare spectrum: spectrum from the target material without the gold foil backing, symbol "B".

$$C = B + G.$$

The term "background" is used in three different ways as follows:

gold background: synonymous with "gold spectrum", used when the gold spectrum is being regarded as a "background" to the composite spectrum;

breakup background: that part of a spectrum other than the peaks, which results mainly from nuclear breakup processes in the target,

spurious background: that part of an observed spectrum other than the peaks or the breakup background, which probably resulted mainly from nuclear reactions taking place in the deflection plates, symbol "S", may be subscripted.

The presence of spurious background is indicated by the appropriate symbol being primed, so that, e.g.

$$C' = C + S.$$

Introduction

This section describes how the differential cross-sections were calculated from the areas of the peaks found by the fitting program. In the absence of a reliable monitor, many of the calculations relied on the target to target comparisons performed during the D69 run. The target to target normalization and the way in which it was used to subtract the gold backgrounds from the composite spectra for the D69 data is described in subsection 6.5.1.

The presence of high spurious backgrounds during the D69 run caused difficulty in subtracting the gold spectra in particular from the ON69 data, and the way in which this was overcome and the angular normalization performed by using a theoretical calculation of the angular variation of the area of the breakup backgrounds is explained in 6.5.2.

Absolute normalization of the data is discussed in 6.5.3, and the section is summarized in 6.5.4.

6.5.1 Target to target normalization and subtraction of the gold background from the D69 composite spectra

During the D69 run, the spectrum from each target was compared with that from the reference lithium target in such a way that the internal beam intensity could be assumed equal for each. It was therefore only necessary to divide by the counting time to obtain the relative normalization between each target spectrum and the reference lithium spectrum, and hence the normalization between all the targets.

As the area of the peaks could be determined reasonably accurately even in the presence of spurious background, the D69 data therefore gave the target to target normalization for all peaks, i.e. for all cross sections of transitions to well defined states of the residual nucleus, for all the elements at each angle. This did not, however, provide angular normalization.

The normalization between each composite spectrum and the gold spectrum from the lone gold target also enabled the gold backgrounds to be subtracted. The subtraction was valid even in the presence of high spurious background provided that the spurious backgrounds were constant, for

$$C' = G + B + Sc \qquad (1)$$

$$G' = G + Sg \qquad (2)$$

Since the thicknesses of the gold backings and of the lone gold target were equal, we can write

$$Sc = Sg \qquad (3)$$

$$\therefore B = C' - G' \qquad (4)$$

However, the normalization factors, essentially the ratios C'/G', could not be applied to the ON69 data since S in eqns. (1) and (2) was not the same (in fact S was negligible for most of the ON69 data). Furthermore, for many of the D69 data, the spurious background intensity was <u>not</u> constant from target to target, almost certainly because the deflection plates moved up and down as they expanded or contracted. This led to errors in background subtraction from some of the D69 data, and led to the D69 data's not being used for the angular normalization for reasons which are made clear in the following subsection.

Although most of the background subtraction factors could not be applied to the ON69 spectra, it was established, by investigating the spurious background directly by observing the spectrum obtained with no target in the beam, that there was a negligible amount of spurious background at 0^{o}. It was therefore possible to apply the D69 0^{o} factors to the ON69 0^{o} data and this enabled the whole of the ON69 data to be corrected as explained in the following subsection.

6.5.2 Angular normalization and subtraction of the gold backgrounds from the ON69 composite spectra

Both the angular normalization and the subtraction of the gold backgrounds from the ON69 composite spectra relied mainly on a theoretical calculation of the angular variation of the area of the breakup background (see 6.4.1).

The statistical theory, used to predict the shape of the breakup background, also predicts that the angular distribution should be isotropic in the centre of mass system. On this assumption, and given the shape of the spectrum, determination of the angular variation in the laboratory system involved a purely kinematical calculation.

The angular normalization of a peak, and hence the angular distribution of the corresponding cross-section, was therefore obtained by comparing the area of a peak with that of a fixed section of the breakup background in a region where there was no peak, and assuming that the angular distribution of the latter was given by the above mentioned theory. It was because of the dependence of the angular normalization on the area of the breakup background that it was important to subtract the gold background accurately, since in the breakup background region of the spectrum, the gold background constituted between 20 and 50% of the composite area.

The choice of exactly which region of the breakup background spectrum to use in the calculations was governed by the following considerations. The predicted isotropic centre of mass distribution depends essentially on the assumption that the interaction leading to the breakup has no direct character, i.e. that the incoming particle interacts with many target nucleons and that the interaction time is relatively long. This is most likely to be true when the final state neutron energy is low, so that the choice of a low energy

region of the spectrum was desirable. It was also necessary to choose a region where there was no peak of significant area, and one which was included in the observed spectra for all elements at all angles. These considerations led to the choice of a region of the spectrum corresponding to neutron energies which would result from interactions leading to two body final states with Q-values in the range -30 to -50 MeV.

Confidence that the predictions were valid was gained from the fact that the shape of the experimental breakup background was well fitted by the phase space integral (see sub-section 6.4.4 and in particular, fig. 6.4.B) and that this has been confirmed by other workers (Bonner, 1970). Since the shapes were usually found to be fitted by three body rather than four or more body phase space integrals, the three body integral corresponding to the breakup mode with the highest Q-value was used, since it was shown that that inclusion of other breakup modes negligibly affected the shape of the spectrum particularly in the low energy region defined above. The difference between three and four body integrals in this region was also small.

Subtraction of the gold background from the ON69 composite spectra was performed by first applying the D69 0° factors to the ON69 0° data. This enabled the ratio of the area of the gold spectrum to that of the composite spectrum over the standard breakup background region to be evaluated for the 0° spectra. The theory was then used to calculate the way in which this ratio varied with angle and enabled the subtraction factors to be calculated. The variation of the ratio with angle was, e.g., 11.8% over 30° for lithium, and was a kinematical effect resulting from the difference in the masses of the gold nucleus and that of the other elements.

It should be noted that this method depends only on the assumption that the angular distributions of the breakup backgrounds in the centre of mass were very similar for both the gold spectra and the bare spectra, and not upon the correctness of the postulated isotropic distribution as such. That this assumption was valid at least to ~ 10% was shown by the target to target normalization of the peaks determined at all angles during the D69 run. Given the 0^{o} target to target normalization, and angular distributions independently calculated for each element, it was possible to obtain target to target normalization which depended only on the D69 0^{o} data and the theoretical calculations. Comparison with the D69 non-0^{o} data confirmed that the calculations were valid to 10%. It was felt that the assumption that this result also applied to the gold spectra was also valid at least within the above limits of error.

The only direct experimental confirmation of the validity of the predicted angular distribution as such obtained in the present experiment was the angular distribution investigation described in Chapter 5, section 5.4.This established the angular distribution of the counting rate in the third quarter of the observed lithium spectrum, but because of the possible presence of spurious background, there was some difficulty in calculating the area of the neutron peak from the "3rd quarter area". The amount of spurious background was fairly low when the "3rd quarter" distribution was determined, and so the ratios

$$\frac{\text{peak area}}{\text{3rd quarter area}}$$

for the ON69 data were used in the calculations. This gave an angular distribution which was slightly more forward peaked than that obtained using the "background method", being (8 + 10)% low at

12.5° (lab.), but this difference was within experimental error. However, the exact amount of spurious background present was not known, and its presence would make the experimental angular distribution more strongly forward peaked, and the agreement worse. For example, if the amount of spurious background had been equal to that present for the main D69 10° lithium spectrum, the experimental result at 10° would have been (17 ± 10)% low. This evidence therefore suggests that the angular normalization method produces results which may be slightly high at non-zero angles, but the error at 12.5° (lab.) (~ 14° C.M.) are probably less than 10%.

It is very likely that any deviation from the predicted angular distributions of the breakup background are towards some degree of forward peaking, so that systematic error from this source would make the quoted cross-sections too high at non-0° angles - in agreement with the experimental indications.

6.5.3 Absolute normalization

The absolute cross-section for the d(p,n)2p reaction at 96 MeV and 0° has been previously measured (Langsford, 1967, B). The cross-section in the laboratory system for production of neutrons in the energy range Tn (Max) to (Tn(Max) - 8 MeV) was found to be 34.1 ± 3.4 mb sr^{-1}. The D69 0° target to target normalization factors were used to compare the 0° peak areas with the area of the d(p,n)2p peak from the deuterated polythene target over the above mentioned energy range to achieve the absolute normalization. The contribution to the deuterated polythene spectrum from the carbon was zero over this range.

The error on the target to target normalization factors was estimated to be ±10% leading to an overall normalization error of ±14%.

6.5.4 Summary

The D69 comparisons between the spectra from the reference lithium target and that from each other target in turn allowed target to target normalization of all the cross-sections over the whole angular range. It also enabled subtraction of the gold background from the D69 spectra, excepting that in some cases errors were introduced by the variation in the amount of spurious background observed from target to target.

The presence of spurious background prevented the straightforward application of the D69 normalization factors to the subtraction of the gold background from the ON69 spectra. This was overcome by using a theoretical calculation of the angular distribution of a region of the breakup background. This calculation was also used to perform the angular normalization.

Absolute normalization was achieved by reference to a previous determination of the absolute cross section at 0° of the d(p,n)2p reaction.

6.6 Angular resolution

The angular resolution of the experiment was the result of the very small divergence of the neutron beam resulting from the finite sizes of the target and the detector, and the very much greater divergence of the incident proton beam resulting from radial oscillations.

The divergence of the proton beam in the Harwell synchrocyclotron at the radius of this experiment has been calculated by Saltmarsh (Saltmarsh, 1965) to be 3.2° (f.w.h.m.). The relevant conditions in the present experiment were probably fairly similar, and as the only important consequence of the finite angular resolution was to cause a small shift in the quoted mean angle for some of the cross-sections, it was considered acceptable to use Saltmarsh' results.

CHAPTER 7

THE RESULTS AND THEIR INTERPRETATION

All the experimental results are presented in the Chapter, along with the whole of the interpretation. An overall assessment of the experiment is given in Chapter 8.

The first five sections of the Chapter discuss the results from each of the five nuclei studied, and the experimental angular distributions are presented in the form of graphs and tables adjacent to the appropriate section. Diagrams of the known energy levels of the nuclei concerned are also shown, and mention in the text of levels A, B ... refer to the levels in the residual nucleus which are indicated on these diagrams. A typical neutron energy spectrum from each element is also presented, and it should be emphasized that this is the only occasion where energy spectra are presented. All other spectra illustrated in this thesis are time of flight, or channel spectra, and in these, the corresponding neutron energy increases from right to left.

The errors shown are random errors only, and it should be remembered that the data are also subject to the following normalization errors

Absolute normalization : $\pm$ 14%
Angular normalization :
The error is likely to increase systematically with angle.
It is thought to be small but could be up to 10% at 12.5° (lab.)

Section 7.6 - 7.8 discuss aspects of the results common to more than one element. Section 7.6 compares the present data with other experimental results, section 7.7 briefly discusses the analogue transitions, and section 7.8 discusses a DWBA analysis of the results. The angular distributions predicted by the analysis are shown along with the appropriate

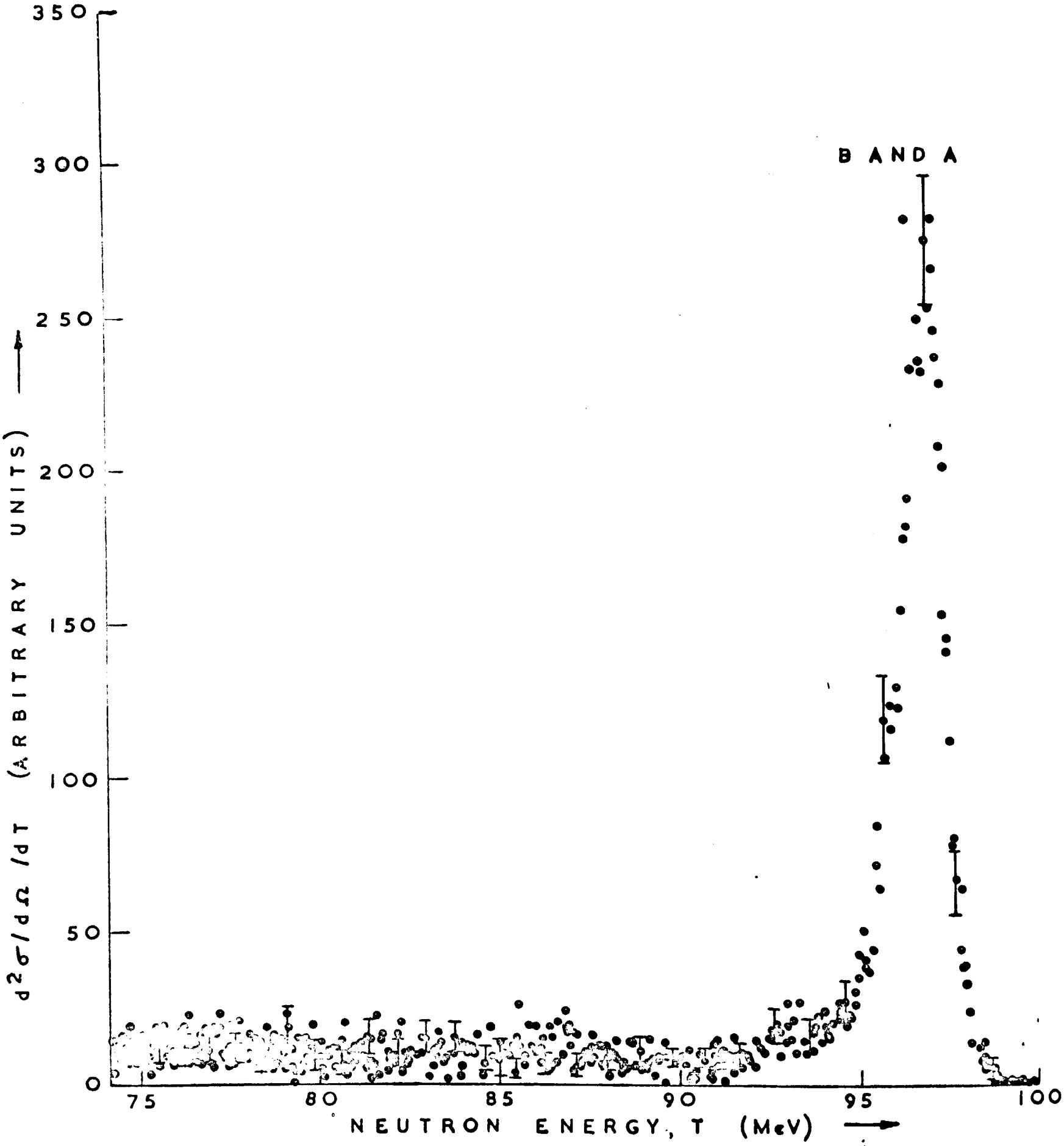

FIG. 7·1.A. 0° ENERGY SPECTRUM FROM LITHIUM

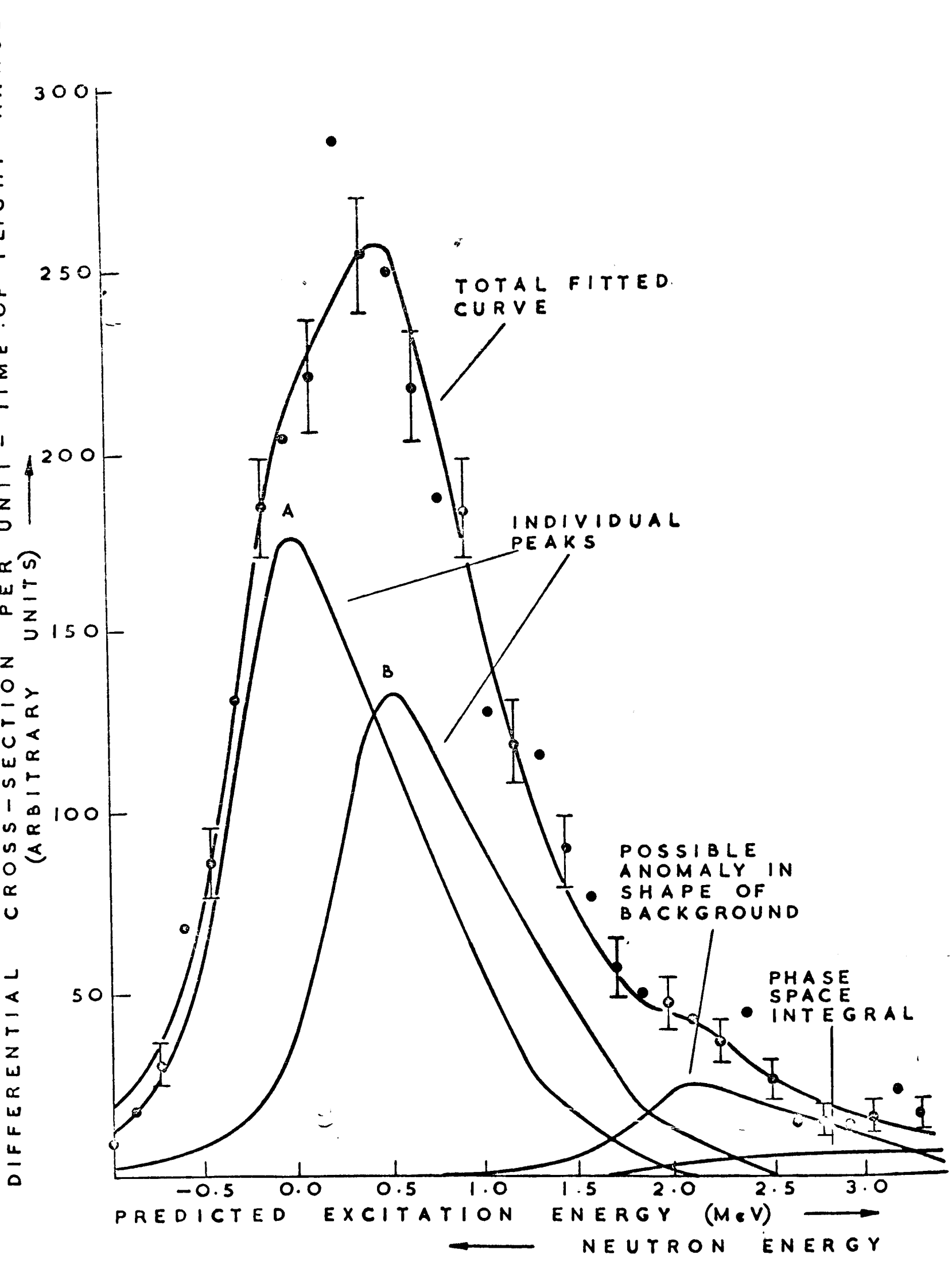

FIG. 7·1.B. FIT TO MAIN NEUTRON PEAK IN 0° LITHIUM SPECTRUM

$^{7}Li\ (p,n)\ ^{7}Be$

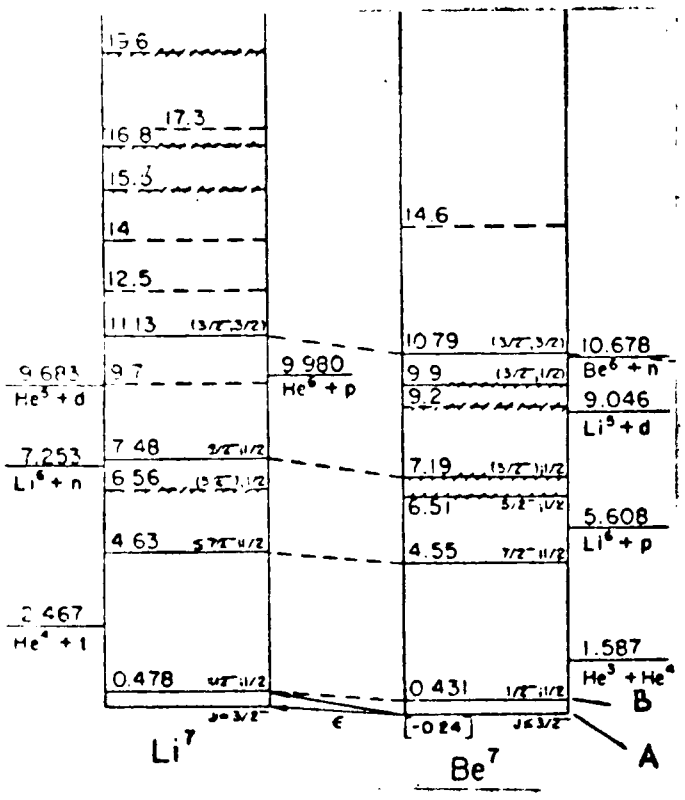

REF (LAURITSEN 1966)

(i)

C.M. ANGLE (o)	CROSS SECTION (mb sr⁻¹)	ERROR
1·5	27·9	0·4
3·3	25·4	1·9
5·9	26·6	1·0
8·6	21·9	0·6
11·7	16·5	0·4
14·6	11·5	0·2
17·5	9·0	0·2
23·2	2·5	0·4
29·0	1·4	0·2
34·6	0·83	0·16
40·4	0·66	0·20
46·0	0·51	0·20
51·8	0·39	0·20

(ii) LEVELS A (G.S) + B

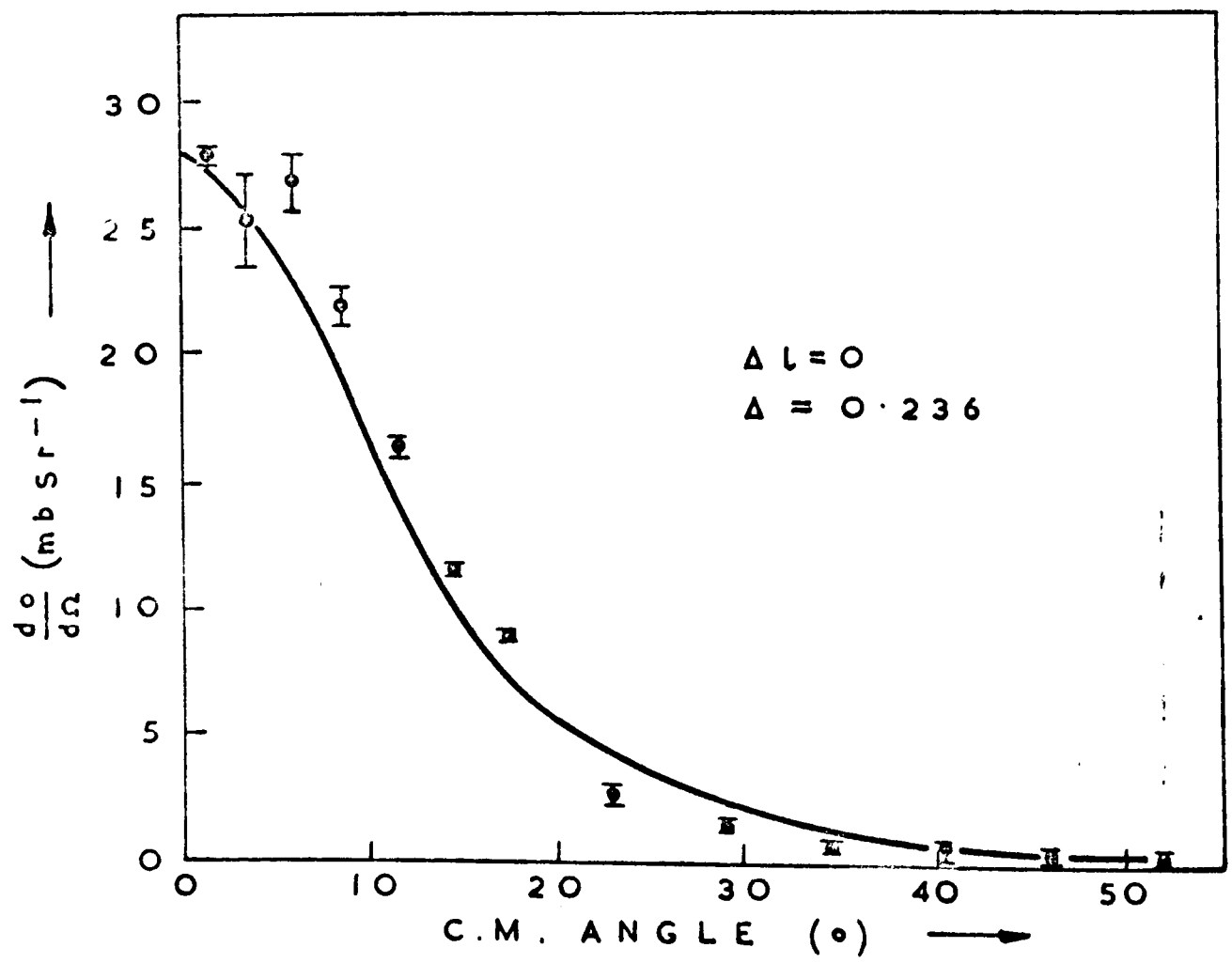

FIG. 7·1.C.

experimental data in sections 7.1 - 5.

7.1 Lithium

The energy spectrum from lithium is shown in fig. 7.1.A, and its main features are the very intense neutron peak at the high energy threshold, and, apart from the background, the almost complete absence of evidence for the excitation of more highly excited levels. From the known Q-value of the reaction and the energy level diagram of ^{7}Be (fig. 7.1.C(i)), the main neutron peak consists of unresolved transitions to the ground state (A), and first excited state (B) at 0.431 MeV of ^{7}Be, and the analysis of the separate contributions of these two transitions is discussed in subsection 7.1.1. Evidence for a possible further contribution to the peak is discussed in sub-section 7.1.2.

The summed cross-sections for the two transitions, showing the expected strong forward peaking of the angular distribution, are given in fig. 7.1.C.

A possible anomaly on the trailing edge of the composite peak is discussed in subsection 7.1.2.

7.1.1 Evidence for a transition to the 0.431 MeV level in ^{7}Be

It has in the past been very difficult to measure the degree of excitation of level B in the ^{7}Li(p,n) reaction in the 100 MeV region, because of the low excitation energy (0.431 MeV) compared with the width of the experimental neutron energy resolution function. The present resolution enabled an improved measurement to be made of the ratio

$$\frac{\left(\frac{d\sigma}{d\Omega}_{CM}\right)_{\text{(transition B)}}}{\left(\frac{d\sigma}{d\Omega}_{CM}\right)_{\text{(transition A)}}}$$

and this is described in subsections 7.1.1.1 and 7.1.1.2. Comparison of the result with the predictions of theory and with previous results is made in sub-section 7.1.1.3.

The experimental determination of R in the present experiment was more difficult than the apparently similar problem of resolving the two transitions in the $^{11}B(p,n)^{11}C$ reaction mentioned in sub-section 6.4.4. In that case, both the resolution function and the absolute positions of the component peaks were accurately known by reference to the two resolved peaks (g.s. and 1.995 MeV) in the same spectrum. Neither of these points held for the $^{7}Li(p,n)$ spectra, and it was necessary to use the D69 $^{11}B(p,n)$ spectra to infer the resolution function and absolute peak positions for those $^{7}Li(p,n)$ spectra with which they were paired. This depended on two assumptions.

Assumption 1 The mean incident proton energy when bombarding the lithium target was the same as that when bombarding the boron target.

Assumption 2 The resolution functions for the paired spectra were the same.

The D69 data taking technique (see section 5.4) was designed to minimise the failure of these assumptions. Two major effects on the composite $^{7}Li(p,n)^{7}Be$ (g.s. + 0.431 MeV) peak of the presence of the second component may be identified.

(i) The position of the centroid of the peak is shifted. To use this to determine R depends only on the validity of Assumption 1.

(ii) The shape of the peak is changed; in particular, it is broadened. To use this to determine R depends only on the validity of Assumption 2.

These two approaches are considered separately in sub-sections 7.1.1.1 and 7.1.1.2, where it is shown that the most reliable results were obtained using the shift of the centroid; and that, although the results using the change in peak shape had to be rejected, the method nevertheless confirmed that R was substantially greater than the value of 0.1 suggested by previous work.

7.1.1.1 Shift of the centroid

R was calculated from the D69 paired spectra from the boron and lithium targets by first calculating, directly from the experimental data, the positions of the centroids of the $^{11}B(p,n)^{11}C$ (g.s.) single peak and of the $^{7}Li(p,n)^{7}Be$ (g.s. + 0.431 MeV) composite peak. In each case the centroid was calculated over that region where the height of the peak was not less than 0.2 times the maximum height, i.e. the region W in fig. 7.1.D (i) and the region Ω in fig. 7.1.D(iv). The reasons for this choice of region are given below. Assumption 1 was then used to infer the position of the $^{7}Li(p,n)^{7}Be$ (g.s.) peak from that of the $^{11}B(p,n)^{11}C$ (g.s.) peak, taking into account the very small difference in energy loss (0.037 ± 0.006 MeV) suffered by the protons in passing through each target. The separation, δ, of this inferred position of the g.s. peak from the directly computed position of the composite peak was determined, and R finally calculated using the relation

$$\delta = \frac{R}{1 + R} S, \qquad R = \frac{\delta}{S - \delta},$$

where S is the separation corresponding to the excitation energy of 0.431 MeV.

The calculations were performed for the 0°, 5° and 10° D69 paired $^{11}B(p,n)/^{7}Li(p,n)$ spectra since only these three had sufficient statistical accuracy to define the regions W and Ω (fig. 7.1.D) with confidence. The values of R found were respectively

$$0.47 \pm 0.10,\ 0.22 \pm 0.11,\ 0.88 \pm 0.17$$

These errors are solely those derived from the statistical errors in the number of counts in each channel, according to the following formulae. The position, C, of the centroid of a peak is given by

$$C = \frac{\sum_i i\, n_i}{\sum_i n_i} = \frac{\sum_i i\, n_i}{N}$$

where n_i is the number of counts in the ith channel, and the summation is over the desired region. N is the total number of counts, or "area" of the region. The standard deviation in C, $\delta(C)$ may be shown to be given by

$$\delta(C) = \frac{1}{N} \sqrt{\sum_i \left[(i^2 + C^2 - 2\, i\, C)\ \mathrm{var}\ n_i\right]}$$

where var n_i is the variance (square of the standard deviation) of n_i. For a count obeying Poisson statistics, var $n_i = n_i$. However, in this case, those corrections detailed in section 6.2 (dead-time correction, etc.), had previously been made to the channel contents, so that the relation var $n_i = n_i$ no longer held.

The remainder of this section:

(i) discusses the magnitudes of errors arising from a possible failure of Assumption 1, and suggests that this is the reason why the spread of the above results is larger than would be expected solely on the basis of the statistical errors;

(ii) explains the reasons for the choice of peak region over which the centroid was calculated, considers possible errors, and shows them to be negligible; and

(iii) quotes what is considered to be the best value of R which may be derived in this way from the present data.

Failure of Assumption 1

It is possible to make only a very rough estimate of the errors resulting from the invalidity of Assumption 1. A single count lasted either 0.5 or 1.0 min, so that errors arise from the component in the incident energy fluctuations with a period of the order of 1 min. Let the magnitude of such fluctuations be A. Then, since a complete count was made up from 10 individual counts, the overall error is $A/\sqrt{10}$. This error applies to each of the two associated spectra, so that the error on the energy difference is $\sqrt{2}\ (A/\sqrt{10}) = A/\sqrt{5}$.

To account for the spread in the results requires A to be of the order of 0.1 MeV - a value of $\delta = 0.13 \pm 0.05$ MeV leads to $R = 0.43^{+0.29}_{-0.20}$. Two pieces of evidence suggest the actual magnitude of A.

(i) During several hours of data taking, the mean incident energy was observed to vary by typically 0.5 MeV. It is not possible to argue from the magnitude of this drift to a knowledge of the magnitude of fluctuations, but this at least shows that relatively large changes could and did occur.

(ii) Typically, during a count lasting several minutes, a neutron peak was observed to broaden by about 2 - 3 channels (f.w.h.m.), i.e. 0.2 MeV. This was almost certainly caused by incident energy fluctuations, and since the broadening took place over a period of minutes rather than seconds, this is good evidence that fluctuations of about the right magnitude and periodicity did occur.

Choice of peak region

It is therefore likely that the failure of Assumption 1 wholely accounts for the spread of the results. However, a possible further source of error, connected with the choice of region over which the centroids of the peaks were calculated, will now be considered. It will be shown in particular that:

(i) the method chosen minimised the errors,

(ii) such errors as remained were unlikely to be systematic,

(iii) the magnitudes of the errors in this particular case were negligible.

Ideally, the region chosen for the computation of the centroids should include the whole of the peaks, and exclude all excitation resulting from other transitions; no error would then be introduced. However, in practice, it was impossible to simultaneously fulfil both these requirements, and it was

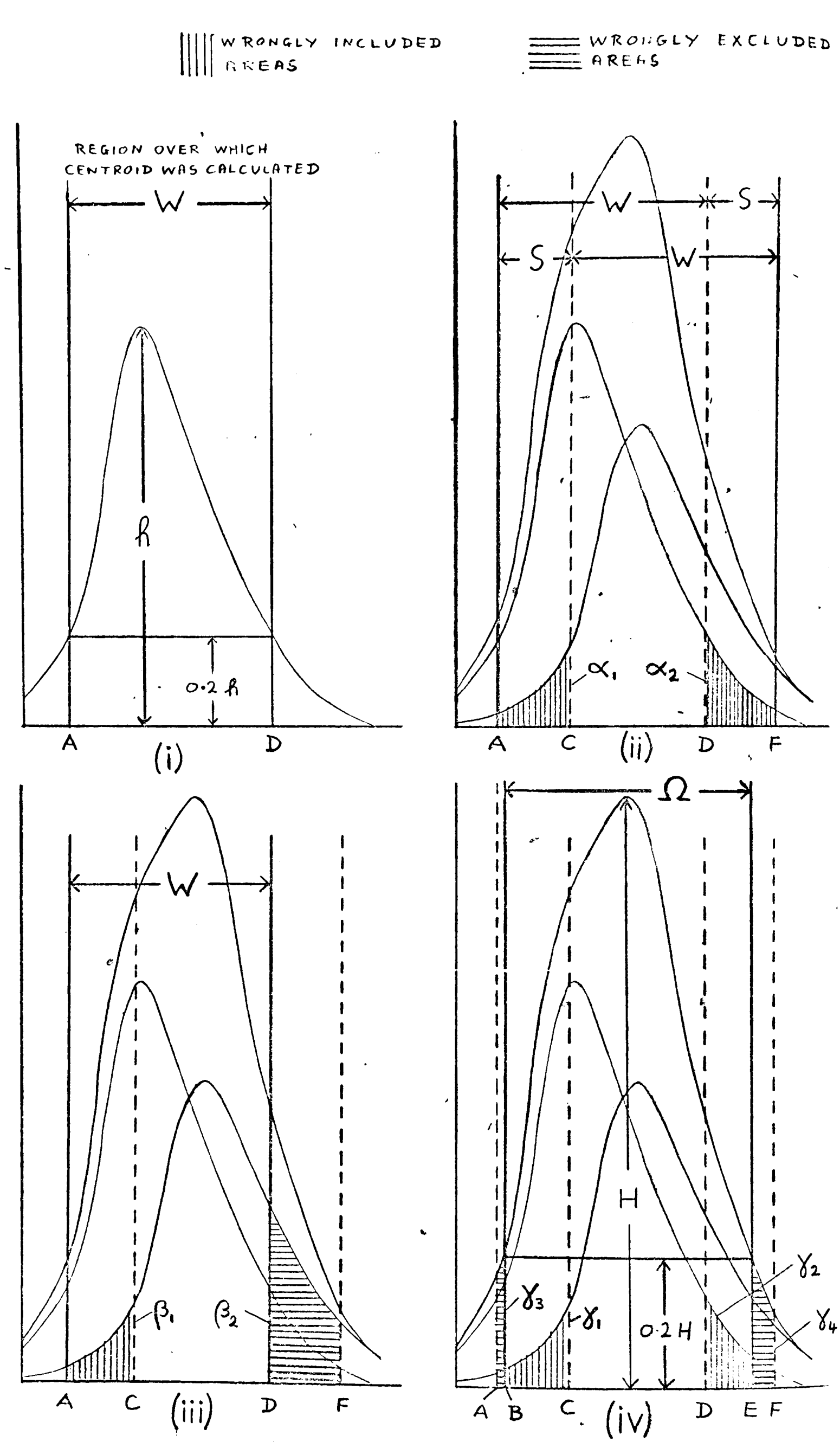
WRONGLY INCLUDED AREAS
WRONGLY EXCLUDED AREAS
REGION OVER WHICH CENTROID WAS CALCULATED
W
h
0·2 h
A
D
(i)
W
S
S
W
α1
α2
A
C
D
F
(ii)
W
β1
β2
A
C
D
F
(iii)
Ω
H
γ3
γ1
0·2 H
γ2
γ4
A
B
C
D
E
F
(iv)

FIG. 7.1. D.

necessary to exclude the outermost wings of the peaks in order to exclude

(i) the second peak in the $^{11}B(p,n)$ spectrum, and

(ii) that region in the $^{7}Li(p,n)$ spectrum interpreted in subsection 7.1.2 as a possible anomaly in the background.

Subject to (i) and (ii), the region should be as wide as possible, and the 0.2 x (maximum height) cut off illustrated in fig. 7.1.D(i) was the best compromise.

However, having fixed the region W for the single $^{11}B(p,n)^{11}C$ (g.s.) peak, the question arises as to how to treat the composite $^{7}Li(p,n)^{7}Be$ (g.s. + 0.431 MeV) peak. Since those parts of the component peaks which should be included overlap parts which should be excluded, the possibility of error is inevitable, and fig. 7.1.D (ii), (iii) and (iv) illustrate three possible approaches. In (ii), the region W, centred on the first component is extended by an amount S corresponding to the known excitation energy of 0.431 MeV, so as to take in the correct amount of the second component. In (iii) the region W is not extended at all, and in (iv) the same cut-off criterion is applied to the composite peak as was applied to the single peak, to give the region Ω (this was the method actually used).

The shaded areas show those regions which are wrongly included or excluded, and it may be shown that the resultant errors are given by

$$\varepsilon_{(ii)} = \frac{\alpha_1 x_1 - \alpha_2 x_2}{A}$$

$$\varepsilon_{(iii)} = \frac{\beta_1 y_1 + \beta_2 y_2}{A}$$

$$\varepsilon_{(iv)} = \frac{\gamma_1 z_1 - \gamma_3 z_3 + \gamma_4 z_4 - \gamma_2 z_2}{A}$$

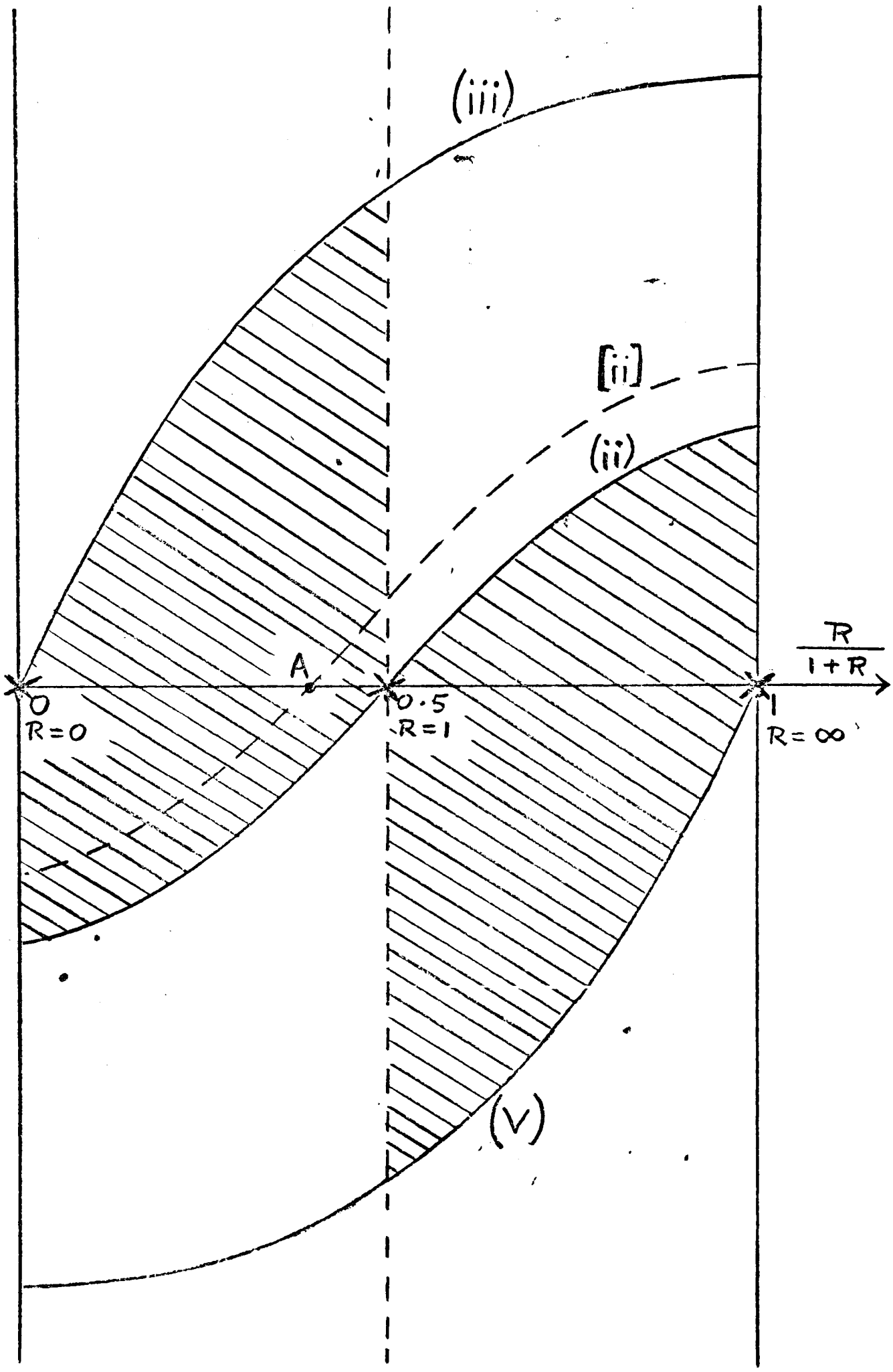

FIG. 7.1.E.

The ε are the true position of the centroid minus those directly computed, A is the total area after changing the spurious regions and is the same in each case, and the x, y and z are the distances of the areas from the computed centroids. A sign convention has been used so that all quantities are positive, on the presumption that the centroid lies between the regions on the left wing and those on the right.

The formulae may be used to infer the general behaviour of $\varepsilon_{(ii)}$ and $\varepsilon_{(iii)}$, and plots as a function of R/(R + 1) for a symmetrical peak shape are shown as the full lines in fig. 7.1.E. The curve marked (v) is for a region W centred on the second component peak. The crosses indicate that $\varepsilon_{(iv)} = 0$ for R = 0, 1 and ∞, and it may also be shown that $\varepsilon_{(iv)}$ is constrained to lie within the shaded region. The actual behaviour of $\varepsilon_{(iv)}$ depends on the peak shape (the shape remaining symmetric), but it is likely to lie close to the abscissa for all values of R. Moreover, there is no general reason to expect the sign of $\varepsilon_{(iv)}$ to be either $+_{ve}$ or $-_{ve}$, so that the error may be treated as random rather than systematic. The major effect of an asymmetry of the type shown in fig. 7.1.D is to cause $\varepsilon_{(ii)}$ to shift to the position indicated by the dotted line in fig. 7.1.E.

The peaks shown in fig. 7.1.D are taken from an actual fit to a ^{7}Li(p,n) spectrum as described in sub-section 7.1.1.2, and for this particular case, ε may be computed directly to give a percentage error in δ as follows

$$\frac{\varepsilon_{(ii)}}{\delta} = -\ 2.0\%$$

$$\frac{\varepsilon_{(iii)}}{\delta} = +\ 43.1\%$$

$$\frac{\varepsilon_{(iv)}}{\delta} = +\ 1.4\%$$

In this particular case $\varepsilon_{(ii)}/\delta$ is small because the value of R indicated, 0.75, happens to be close to the point A in fig. 7.1.E. The final value of R obtained is 0.44, and for this probably more realistic value, $\varepsilon_{(iv)}$ would stand out even more clearly as the best choice.

The error represented by $\varepsilon_{(iv)}$, even if it were several times larger in the actual case than in the above example, may be neglected compared with the ~ 40% error associated with the failure of Assumption 1.

(iii) Final value of R

It may be concluded, then, that the spread in the previously quoted results is almost entirely the result of a failure of Assumption 1, but that it is not possible to determine the resultant error accurately. Consequently, the final value of R was calculated by taking the mean of the three results weighted by their statistical precision, and assigning an error equal to the root mean square deviation of the results about the mean. This calculation yields

$$\boxed{R = 0.44 \pm 0.28}$$

7.1.1.2 Shape of the peak

It was clear, simply from inspection, that the peaks in the spectra from lithium were broader than peaks in other spectra known to be single, and that therefore the $^{7}Li(p,n)^{7}Be(0.431\ MeV)$ transition was contributing significantly. During both runs, single peaks were typically 1.2 MeV wide, and lithium peaks 1.5 MeV. However, for a quantitative determination of R, it was necessary to take the detailed peak shape into account, and to use the fitting program.

For the most useful fits, the D69 paired spectra from boron and lithium were again used. The resolution function was determined from the $^{11}B(p,n)$ spectrum (see sub-section 6.4.4) and then used to fit the $^{7}Li(p,n)$ spectrum assuming the validity of Assumption 2.

As a check, the $^{7}Li(p,n)$ peak was first fitted with a single peak. The fit was very poor, the peak being far too wide, thus confirming the significant contribution of the second peak. (The previously determined phase space background was also included in this fit as in all subsequent ones. Its amplitude was small over the peak region).

Fits using two peaks were then attempted, a number of different approaches being considered. The following combinations of parameters may be varied during the fitting process:

(i) the positions and heights of both peaks,

(ii) as (i) but subject to the constraint that the separation of the peaks be kept fixed at the amount, S, corresponding to the known excitation energy of 0.431 MeV.

(iii) the peaks may be kept fixed at the positions indicated by Assumption 1, and only the heights varied.

(i) and (ii) depend only on Assumption 2, (iii) depends in addition on Assumption 1. Method (ii) is theoretically the most reliable since it imposes all necessary, but no unnecessary constraints, but it would have been necessary to alter the fitting program to permit such fits to be made.

The first conclusion from the two-peak fits was that there was an anomaly on the trailing edge of the composite peak that could not be fitted without the inclusion of a small third peak as shown in fig. 7.1.B. The interpretation of this is considered in section 7.1.2. The presence of this peak in all subsequent fits is assumed.

The D69 pairs were fitted using methods (i) and (iii). Values of χ^2 at the minimum varied from 1.2 to 3.0 per point indicating reasonably good fits and a reasonable validity of Assumption 2. The method (iii) fits gave similar results to the method (i) fits, but since they were subject to an unnecessary constraint, the results were ignored. The method (i) results gave values for the positions which were consistent with a separation of S, and the values of R found for the three D69 spectra considered in the previous sub-section were

$$0.37 \pm 0.15, \quad 0.38 \pm 0.27 \text{ and } 0.96 \pm 0.38$$

These are clearly compatible with the shift of the centroid results, which were

$$0.47 \pm 0.10, \quad 0.22 \pm 0.11 \text{ and } 0.88 \pm 0.17,$$

but exhibit somewhat larger errors. It should be noted that, although the program calculated the errors in a purely statistical way (see sub-section 6.4.3), the above errors necessarily include a contribution from any failure of Assumption 2.

The ON69 spectra and those D69 spectra not paired with $^{11}B(p,n)$ spectra were fitted using method (i) only, using the resolution function obtained from the 0^{o} $^{11}B(p,n)$ spectra. Values of χ^2 varied between 2.5 and 15.0 per point, indicating, as expected, rather worse fits, since the resolution function used was not so realistic. Values of R varied from 0.3 to 1.5 and large errors were indicated. In a number of cases, the program indicated spuriously enormous errors up to 10^{8}%, and it was clear that, in this case, with a badly defined minimum of χ^2, the program was operating near the limits of its capability.

In view of this, it was felt that the D69 paired results also had to be viewed with some suspicion. To improve the situation, it would have been necessary to make a proper study of the performance of the program in such limiting cases, and of the detailed behaviour of χ^2 as the parameters were varied. Had this been done, it might then have been worth altering the program to allow method (ii) fits to be made.

However, no matter how much the techniques were refined, the results could only represent an <u>improvement</u> over the shift of the centroid method if Assumption 2 were significantly better than Assumption 1. Consequently, since any failure of Assumption 1 was in fact likely to <u>cause</u> a failure of Assumption 2, and in view of the considerable difficulties

involved, the results from the fitting program were rejected, save for the observation that they confirmed the significant contribution of the $^{7}Li(p,n)^{7}Be$ (0.431) peak.

7.1.1.3 Comparison of the present result with theoretical predictions and previous data

The value of R in the 100 MeV region has been uncertain for some time. Mahalanabis (Mahalanabis, 1964) used the plane wave impulse approximation to obtain angular distributions for transitions to levels A and B at 143 MeV, and Saltmarsh (Saltmarsh, 1965) used her formulae to calculate the 0^{o} cross-sections for 94 MeV. He predicted a value of R of 0.65 and compared it with his experimental value of $0.09^{+0.41}_{-0.09}$. (Saltmarsh quoted R = $0.08^{+0.30}_{-0.08}$, but there was an error in his definition of R, and he had in fact calculated the ratio R/(R+1)).

The present experimental value of R = 0.44 $\pm$ 0.28 is therefore somewhat lower than the value of 0.65 predicted by Mahalanabis formulation, but agrees within experimental error. Mahalanabis assumed an extreme L - S coupling model in which the overlap between the ground state of ^{7}Li and both states A and B of ^{7}Be was assumed to be complete. This assumption is likely to be valid for state A whatever model is used since it is the analogue of the ground state of ^{7}Li, but not for state B. Reducing the overlap would therefore lower the predicted value of R and agree better with the experimental value.

The present result may also be compared with those of Clough et al (Clough, 1969) for the same reaction at 30 and 50 MeV. They found R = 0.34 $\pm$ 0.03 at 30 MeV and R = $0.15^{+0.35}_{-0.15}$ at 50 MeV.

The data may also be compared with Mahalanabis' predictions of the differential cross-section at 0^{o}. Extrapolating the present experimental graph shown in fig. 7.1.C(ii) to 0^{o} and taking $R = 0.44 \pm 0.28$ yields a cross-section for the ground state transition of $19.4^{+4.5}_{-2.5}$ mb sr^{-1}. This is lower than Mahalanabis' prediction, but, again this is just within experimental error. Agreement with experiment would be improved by taking into account the effects of absorption neglected by Mahalanabis.

7.1.2 Evidence for an anomaly in the shape of the background

Examination of fig. 7.1.B shows excitation in the region of 2 MeV excitation energy, which has been fitted with a small third peak. Its presence was confirmed with most of the other lithium spectra examined. There is no known state of either ^{7}Be or ^{7}Li near this excitation energy, but the neutron energy is quite close to the threshold for breakup of the ^{7}Be nucleus to ^{3}He + α as indicated by the phase space integral corresponding to this breakup mode shown in the fig. It is possible that the shape of the background deviates from the phase space integral and exhibits a peak, or at least an enhancement, near the threshold. Such peaks have been observed by other workers and this question is discussed further in section 7.2. It should be stressed, however, that this apparent enhancement of the excitation could be simply the result of a low energy "tail" of the resolution function. Such a tail would be obscured in the other spectra because of the presence of more highly excited states. The experimental evidence for the anomaly must therefore be regarded as weak.

7.2 Beryllium

The spectrum from beryllium was the most difficult to analyse. The 0^{o} spectrum is shown in fig. 7.2.A, and the ground state transition, A, is clearly visible as well as a further strong excitation which peaks at 2.5 $\pm$ 0.1 MeV. This excitation falls off slowly towards lower energies suggesting the excitation of further states.

The known energy levels of ^{9}Be and ^{9}B are shown in fig. 7.2.B(i). The spectra were fitted with a single narrow peak at each of the positions corresponding to the known states.

The expected forward peaked angular distribution for the ground state transition is shown in fig. 7.2.B(ii).

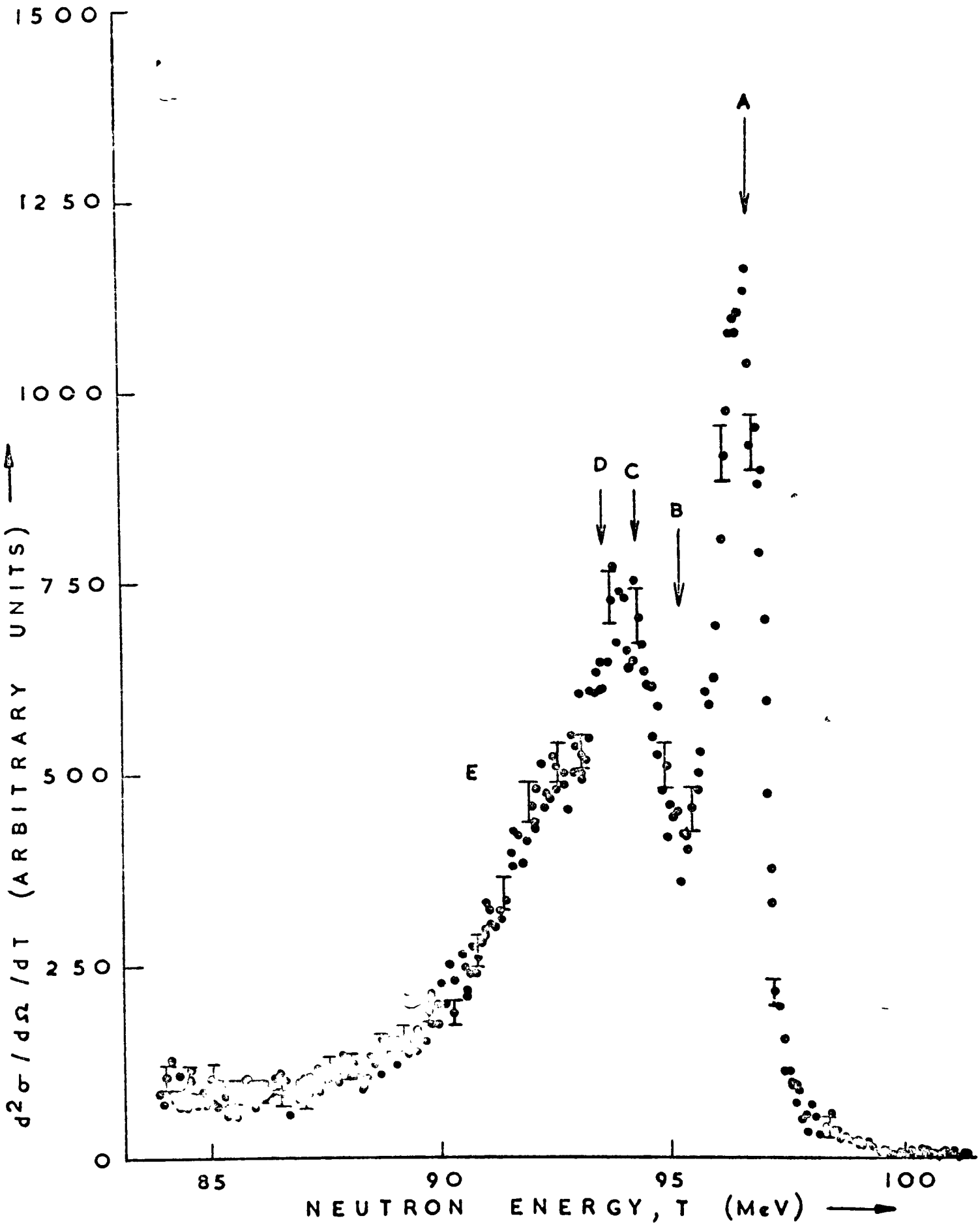

FIG. 7·2.A. O° ENERGY SPECTRUM FROM BERYLLIUM

^{9}Be (p, n) ^{9}B

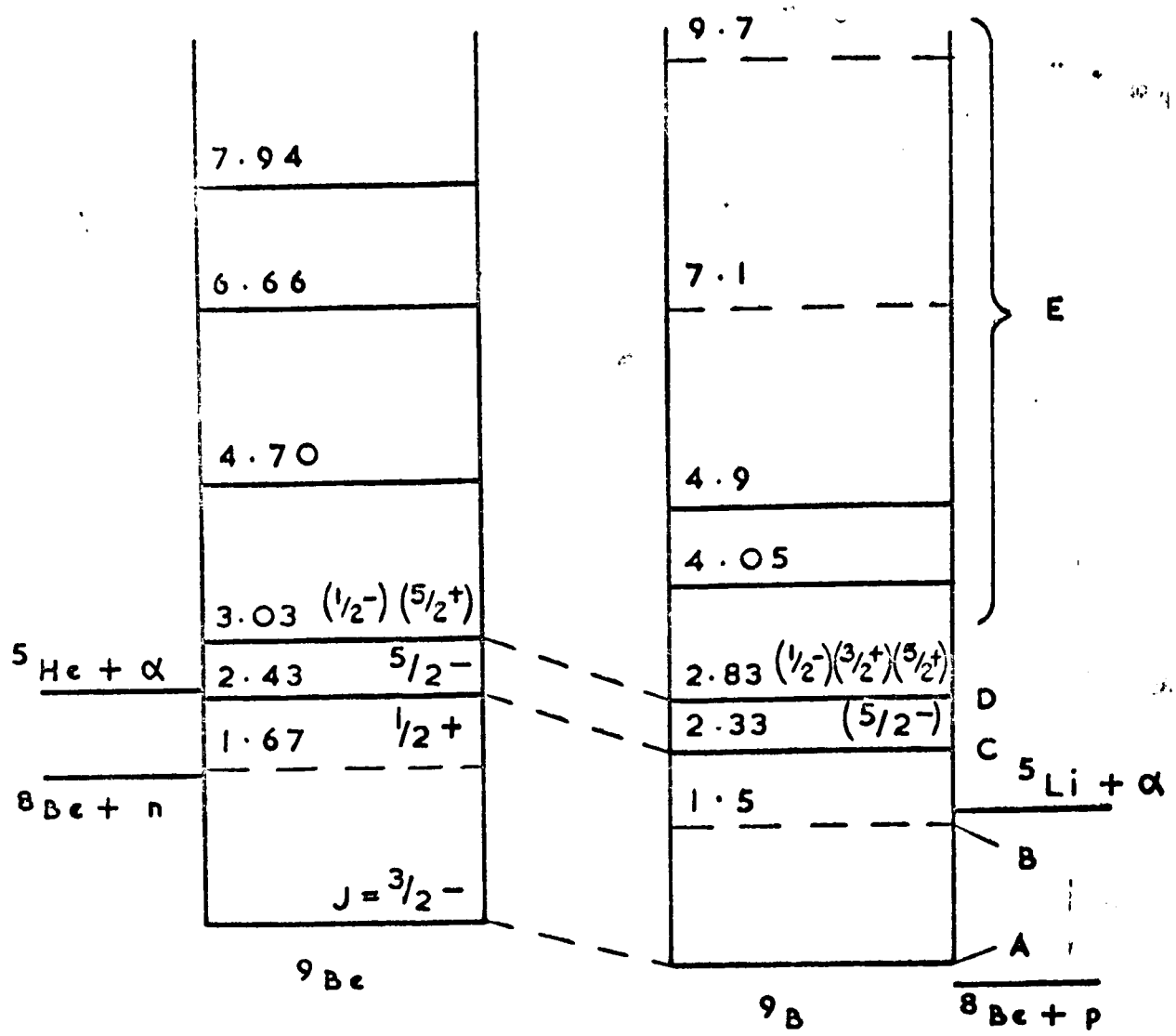

REFS (LAURITSEN 1966)
(SANADA 1970) (1)

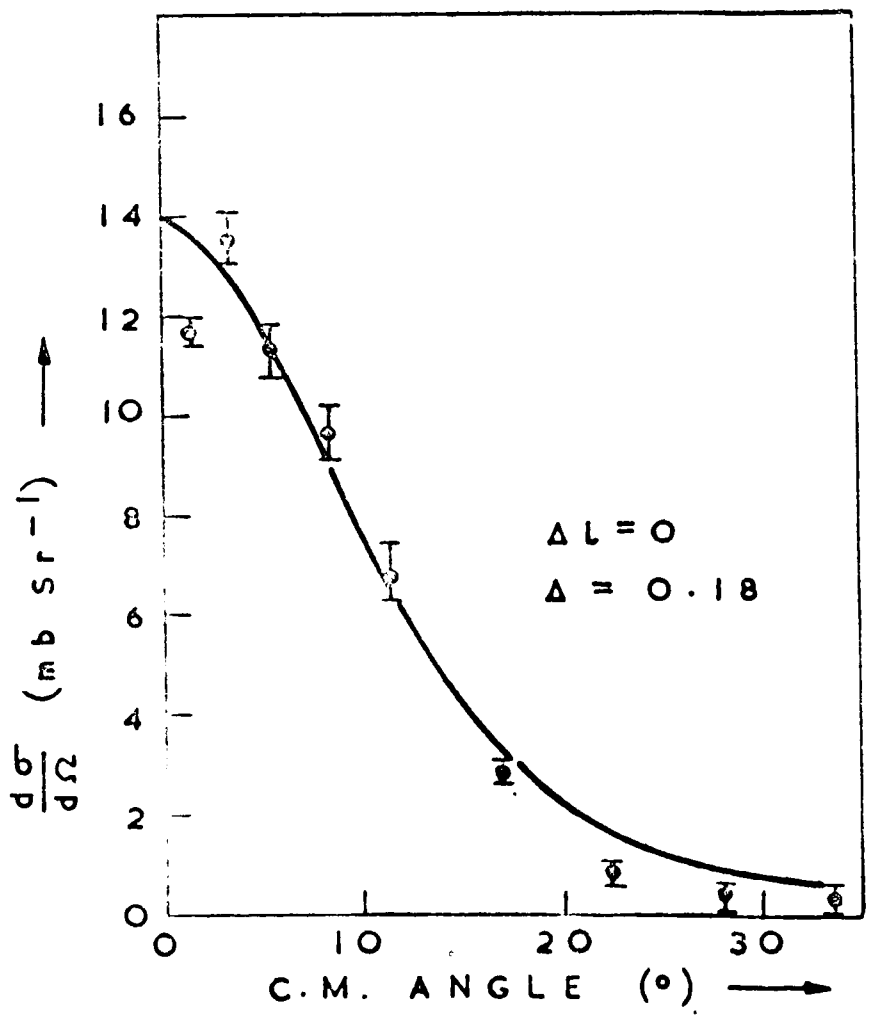

C.M. ANGLE (°)	CROSS SECTION (mb sr⁻¹)	ERROR
1·5	11·7	0·3
3·3	13·7	0·5
5·7	11·3	0·5
8·5	9·6	0·5
11·3	6·8	0·5
17·0	2·8	0·2
22·5	0·8	0·2
28·1	0·3	0·2
33·7	0·3	0·3

(ii) LEVEL A (G. S.)

FIG. 7·2.B.

$^{9}Be\ (p, n)\ ^{9}B$

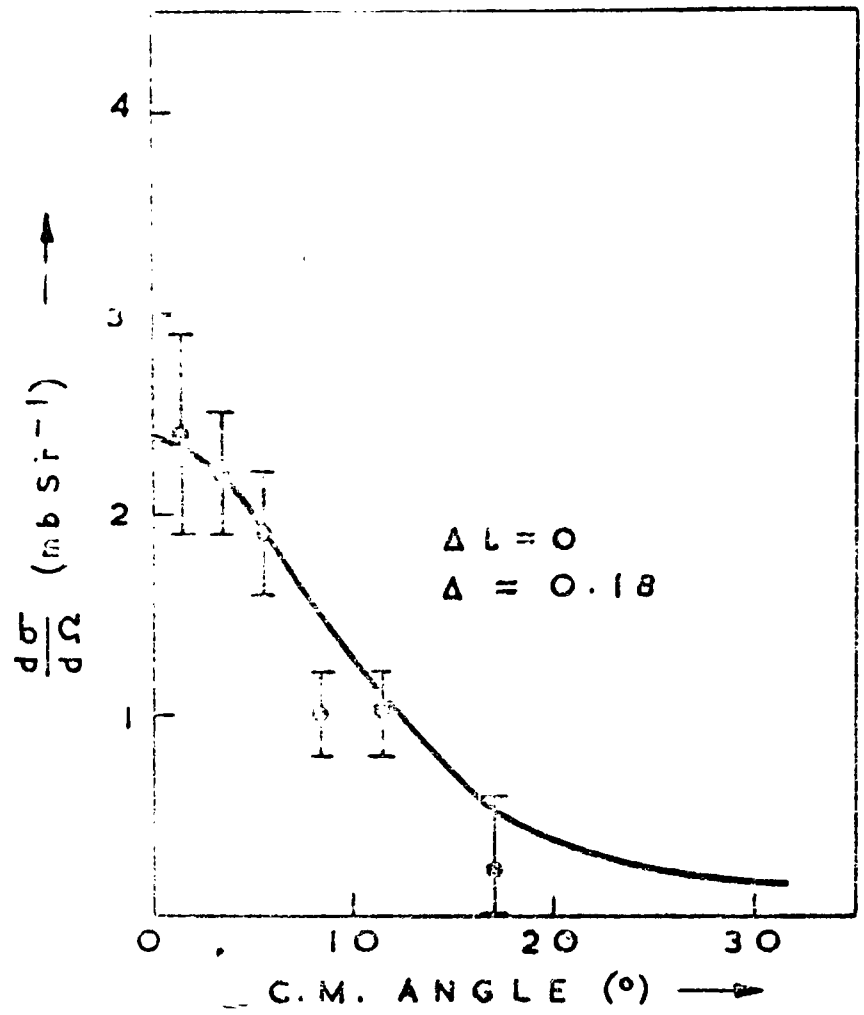

C M ANGLE (o)	CROSS SECTION (mb sr^{-1})	ERROR
1·5	2·4	0·5
3·3	2·2	0·3
5·7	1·9	0·3
8·5	1·0	0·2
11·3	1·0	0·2
17·0	0·2	+0·4 −0·2
22·6	—	—
28·1	—	—
33·7	—	—

(i) LEVEL B

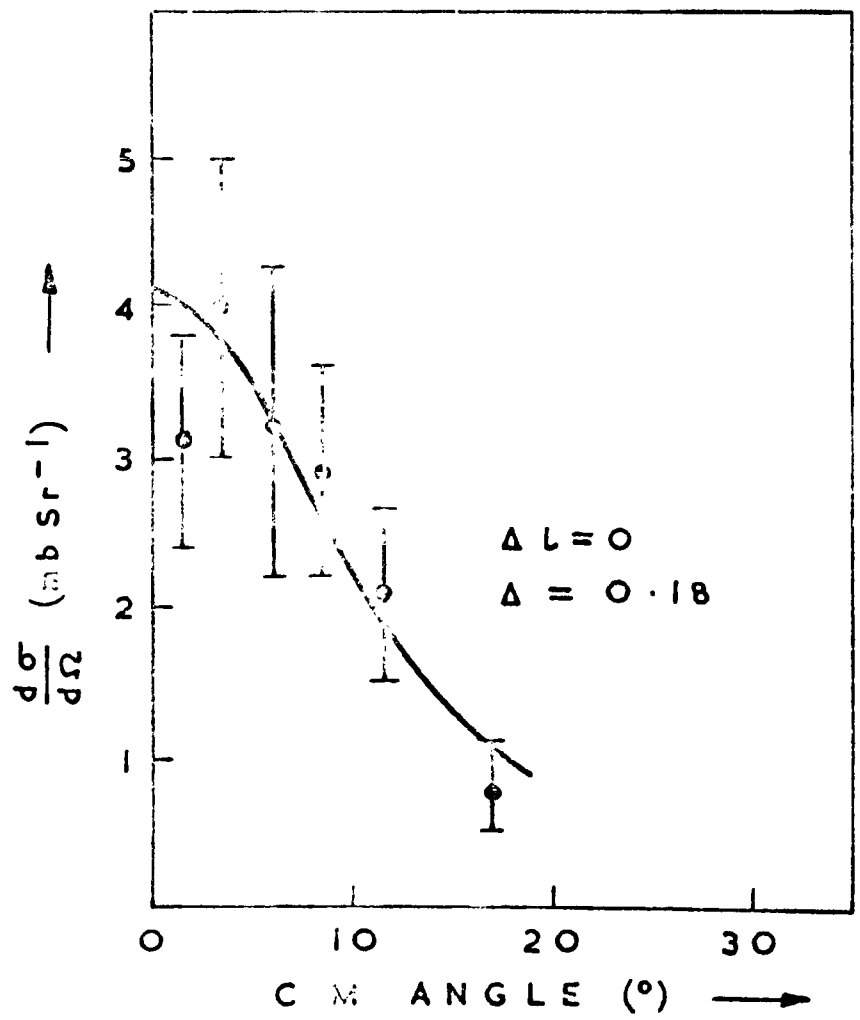

C.M. ANGLE o	CROSS SECTION (mb sr-1)	ERROR
1·5	3·1	0·7
3·3	4·0	1·0
5·2	3·2	1·0
8·5	2·9	0·7
11·3	2·1	0·6
17·0	0·8	0·3
22·6	—	—
28·1	—	—
33·7	—	—

(ii) LEVEL C

FIG. 7.2.C.

^{9}Be (p.n) ^{9}B

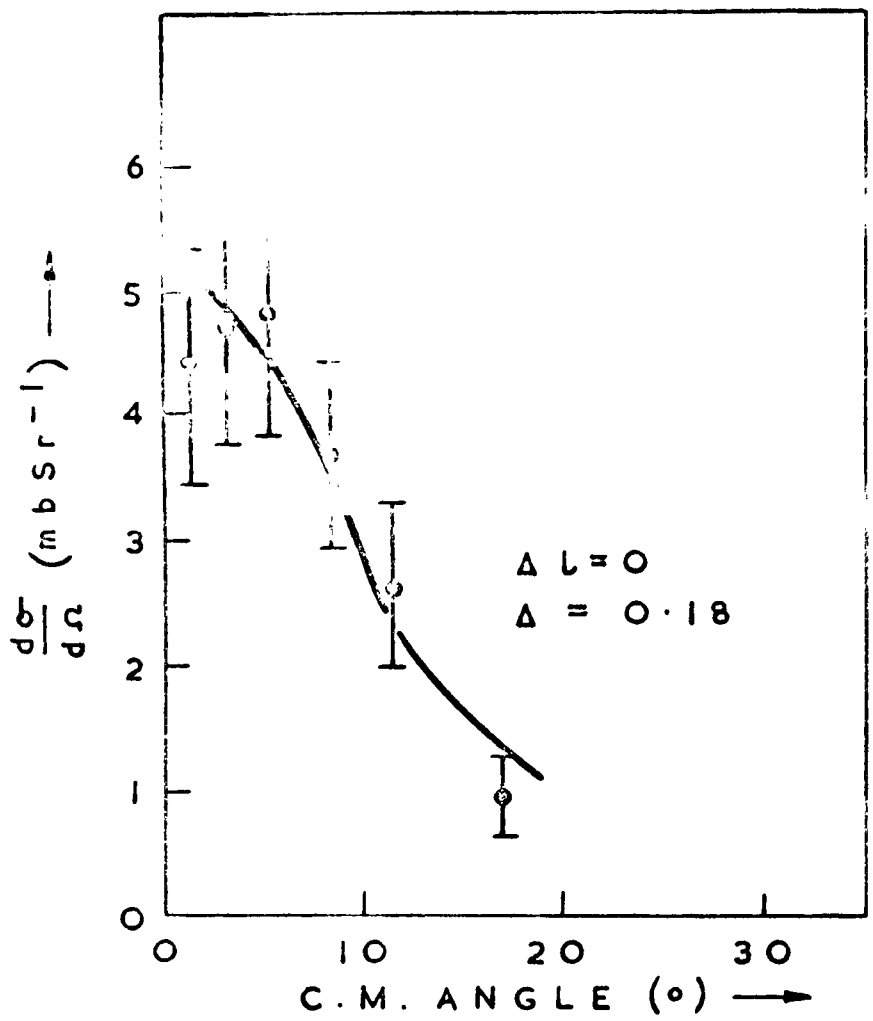

C.M. ANGLE (°)	CROSS SECTION (mb sr^{-1})	ERROR
1·5	4·4	1·2
3·3	4·7	1·2
5·2	4·8	1·2
8·5	3·7	0·9
11·3	2·6	0·8
17·0	1·0	0·4
22·6	—	—
28·1	—	—
33·7	—	—

(i) LEVEL D

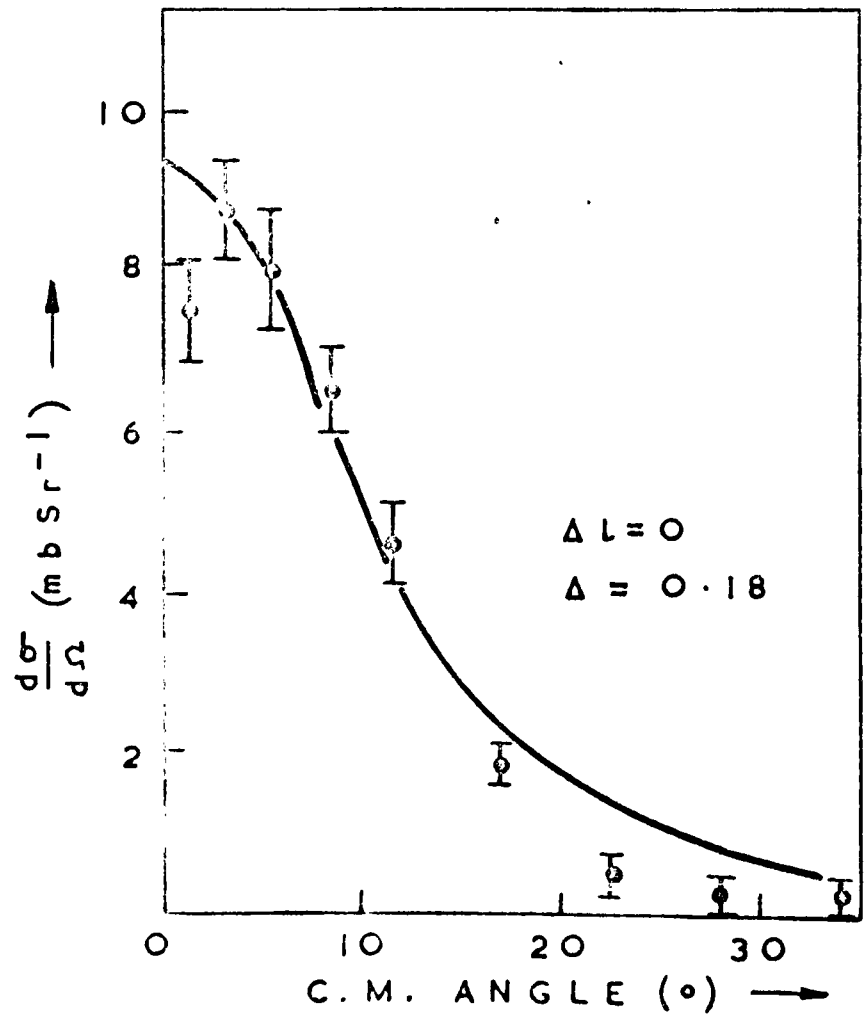

C M ANGLE (°)	CROSS SECTION (mb sr^{-1})	ERROR
1·5	7·5	0·6
3·3	8·6	0·6
5·7	8·0	0·7
8·5	6·6	0·5
11·3	4·7	0·5
17·0	1·9	0·2
22·6	0·5	0·2
28·1	0·3	0·2
33·7	0·3	0·3

(ii) LEVELS C + D

FIG. 7.2.D.

$^{9}Be\ (p,n)\ ^{9}B$

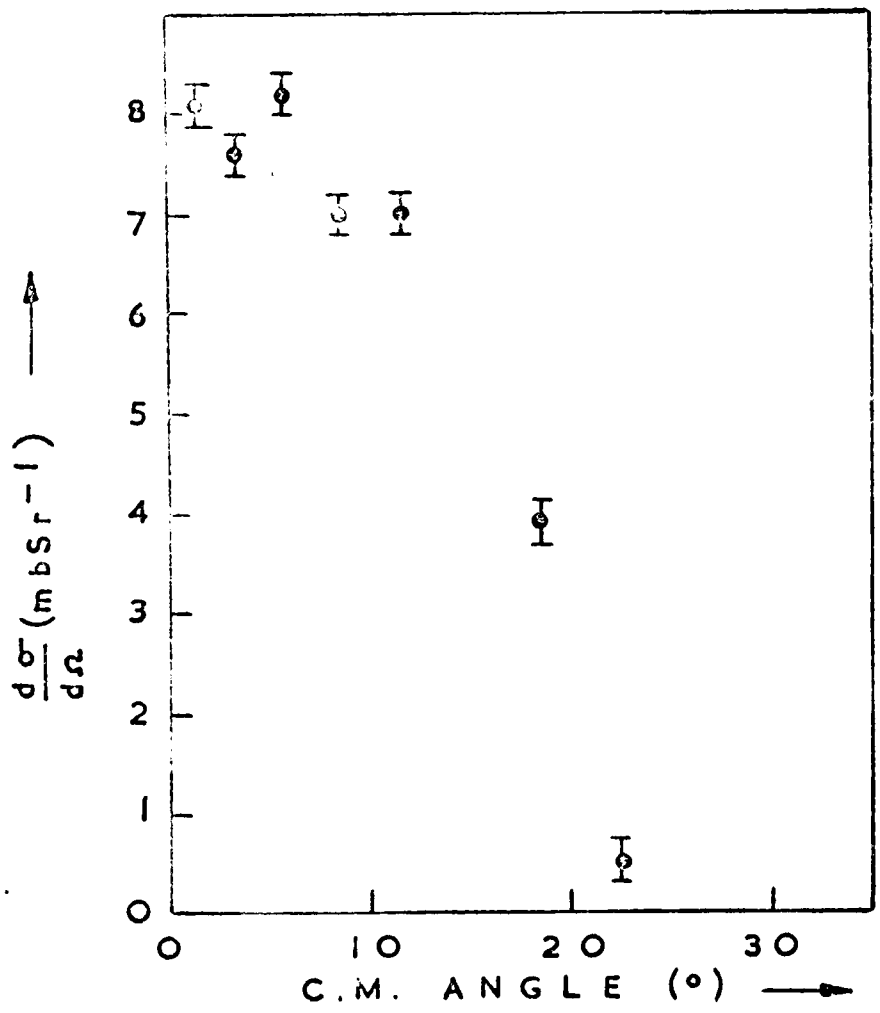

C.M. ANGLE (o)	CROSS SECTION ($mb\,sr^{-1}$)	ERROR
1·5	8·1	0·2
3·3	7·6	0·2
5·7	8·2	0·2
8·5	7·0	0·2
11·4	7·0	0·2
17·0	3·9	0·2
22·6	0·5	0·2
28·1	—	—
33·7	—	—

GROUP E

FIG. 7·2.E.

It was not possible to derive conclusions about the separate cross sections for transitions to levels higher than D, and these have been summed to give the angular distribution shown in fig. 7.2.E. The broad forward peaking is consistent with the excitation of both natural and unnatural parity states.

The existence of level B is uncertain. However, it proved very difficult to fit the spectra without the presence of a transition to this level to partially "fill in" the trough between the peaks, and when it was included in the fit, the angular distribution shown in fig. 7.2.C(i) was obtained. The forward peaked distribution, suggesting $\Delta l=0$, is inconsistent with the identification of this state as the analogue of a $1/2^+$ level at 1.67 MeV in ^{9}Be since the parity change implies an odd value of Δl, and as the "peak" could hardly be said to be "resolved", these results must be viewed with suspicion - but see below.

The second maximum in the spectrum occurs between the position predicted for levels C and D, indicating either that some other state is being excited, or that transitions to both C and D occur strongly. Angular distributions on the latter assumption are shown in fig. 7.2.C(ii) and 7.2.D(i) The precise relative magnitudes of the cross-sections are sensitive to details of the shape of the resolution function and may be in error, but the forward peaking of both transitions is not in doubt. The more accurate sum of the cross-sections is shown in fig. 7.2.D(ii).

Until recently, state D was regarded as having positive parity in both ^{9}Be and ^{9}B and the $1/2^-$ state predicted by the shell model (Kurath, 1956) was regarded as "missing". However Macefield (Macefield, 1969) has reported a $1/2^-$ state in ^{9}Be at 3.0 MeV excitation, i.e. just below, but very close indeed to state D. One interpretation of the present data is that neither state C nor state D is strongly excited and that the transition is to the analogue of this $1/2^-$ state in ^{9}B at an excitation of 2.5 MeV. The spectrum

was equally well fitted on this assumption provided that the excitation of state B was increased.

However, the evidence for the levels of ^{9}Be and ^{9}B has recently been reviewed by Sanada (Sanada, 1970), and he comes to the conclusion that the assignment of positive parity to state D is in error and that this is in fact the "missing" $1/2^-$ state. The 1.67 MeV excitation in ^{9}Be observed by e.g. Nguyen Ngoc et al (Nguyen Ngoc, 1963) is probably associated with the threshold of the breakup into (^{8}Be + n) (whether or not it is a "state" in the usual sense - see (Spencer, 1960; Baz, 1958; Inglis, 1962) for discussion) and Sanada suggests that the previous assignation of positive parity to level D might have been similarly associated with the broad 2^+ excited state (Blair, 1961) in ^{8}Be. The excitation of state B found necessary to fit the spectra may be similarly associated with the threshold of the (^{5}Li + α) breakup. It would also be not surprising to find a different angular distribution for this than found in ^{9}Be associated with the quite different (^{8}Be + n) breakup. Evidence for a similar "peak" near a breakup threshold in the lithium spectra has already been mentioned in sub-section 7.1.2.

Sanada's interpretation of state D is entirely consistent with the present data. On an extreme shell model picture of the nuclei, the transition to the $5/2^-$ state, C, can only proceed via $\Delta l=2$, but its excitation may be understood either in terms of a mixing of the $1/2^-$ and $5/2^-$ levels or of the impurity of the ground state in terms of the L-S coupling description - see section 7.8.

7.3 Boron

The 0° boron energy spectrum is shown in fig. 7.3.A. A number of peaks are clearly visible, and their positions corresponded well with those expected on the basis of the energy level diagram shown in 7.3.B(i). Fits to the boron spectra have already been discussed in Chapter 6, section 6.4.

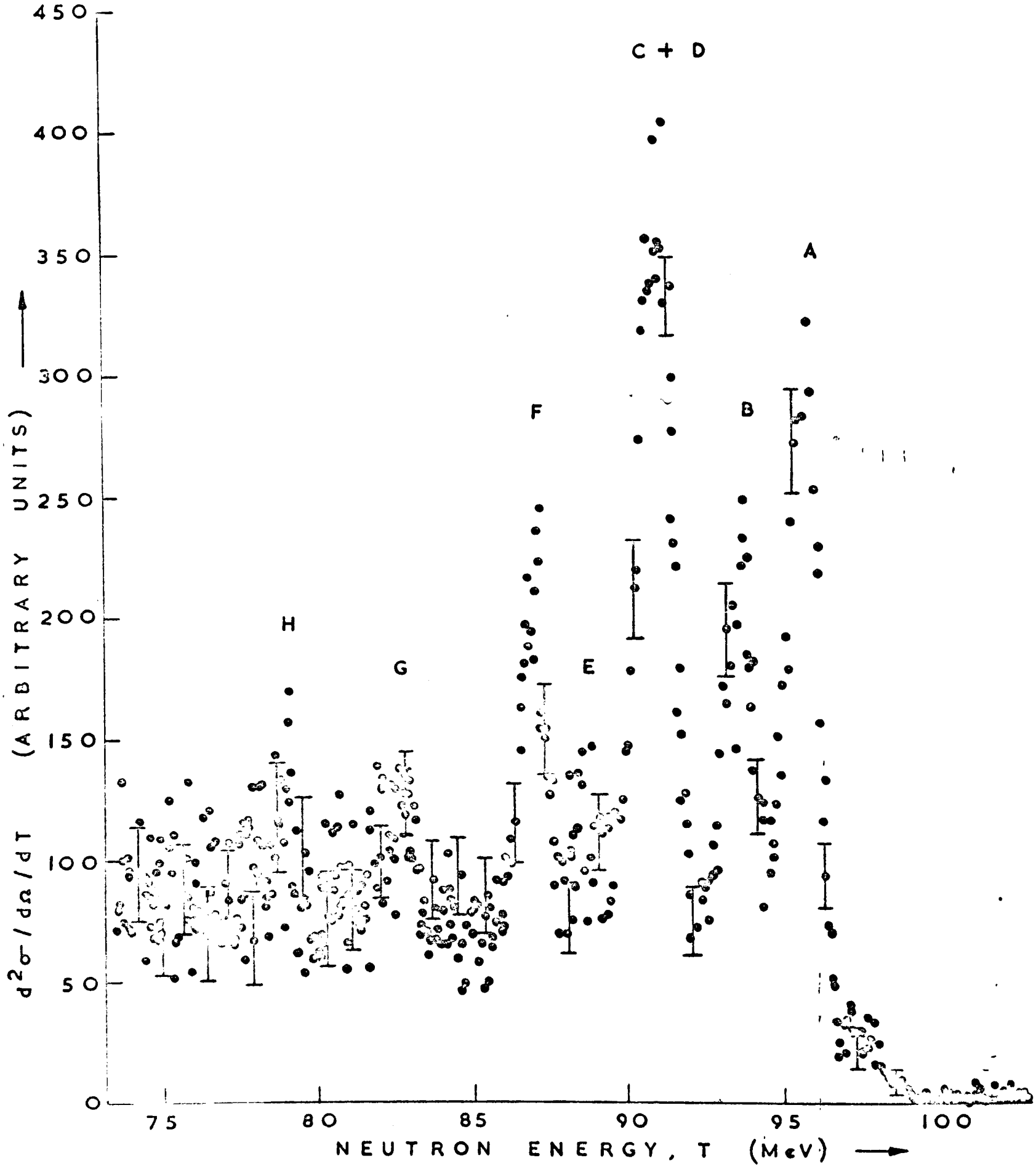

FIG. 7·3.A. 0° ENERGY SPECTRUM FROM BORON

$^{11}B\ (p,n)\ ^{11}C$

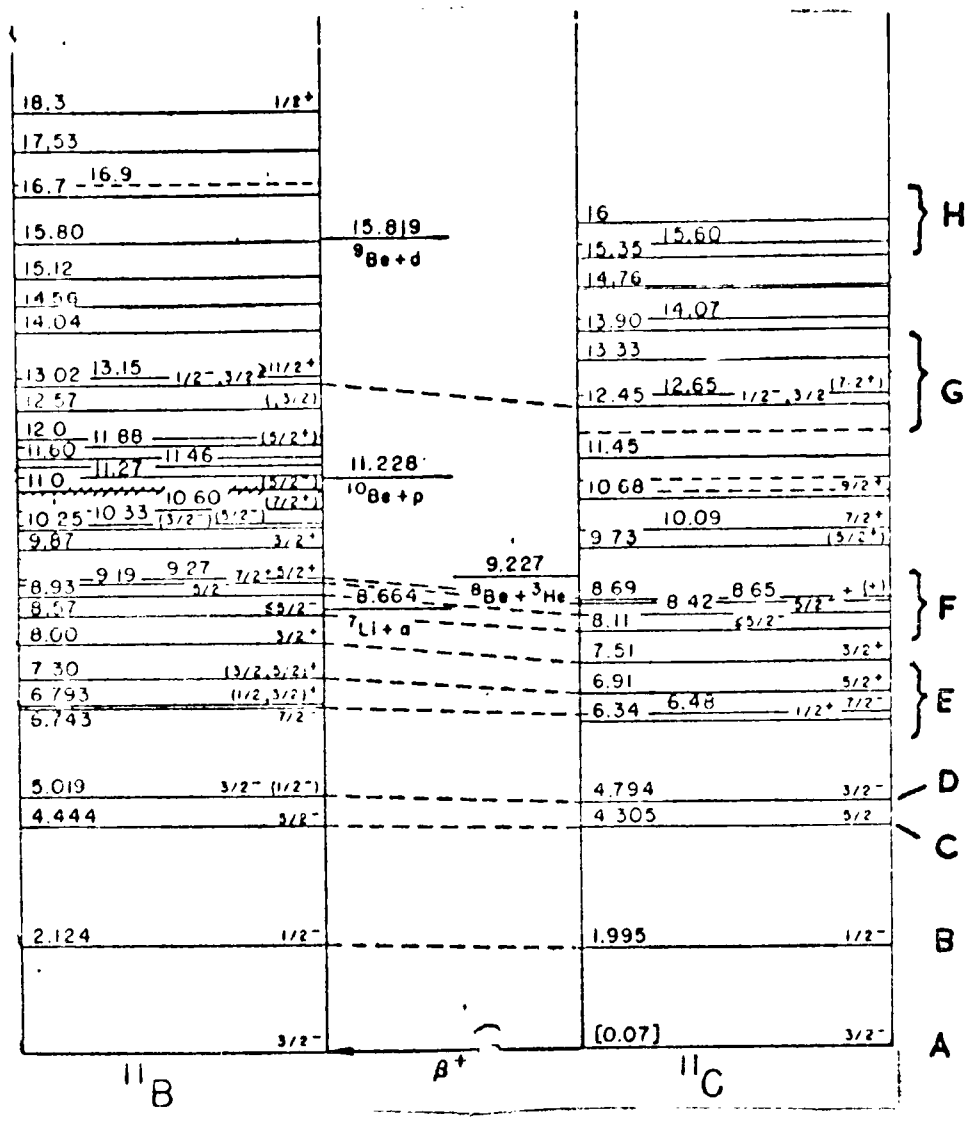

REF. (AJZENBERG-SELOVE, 1968)

i

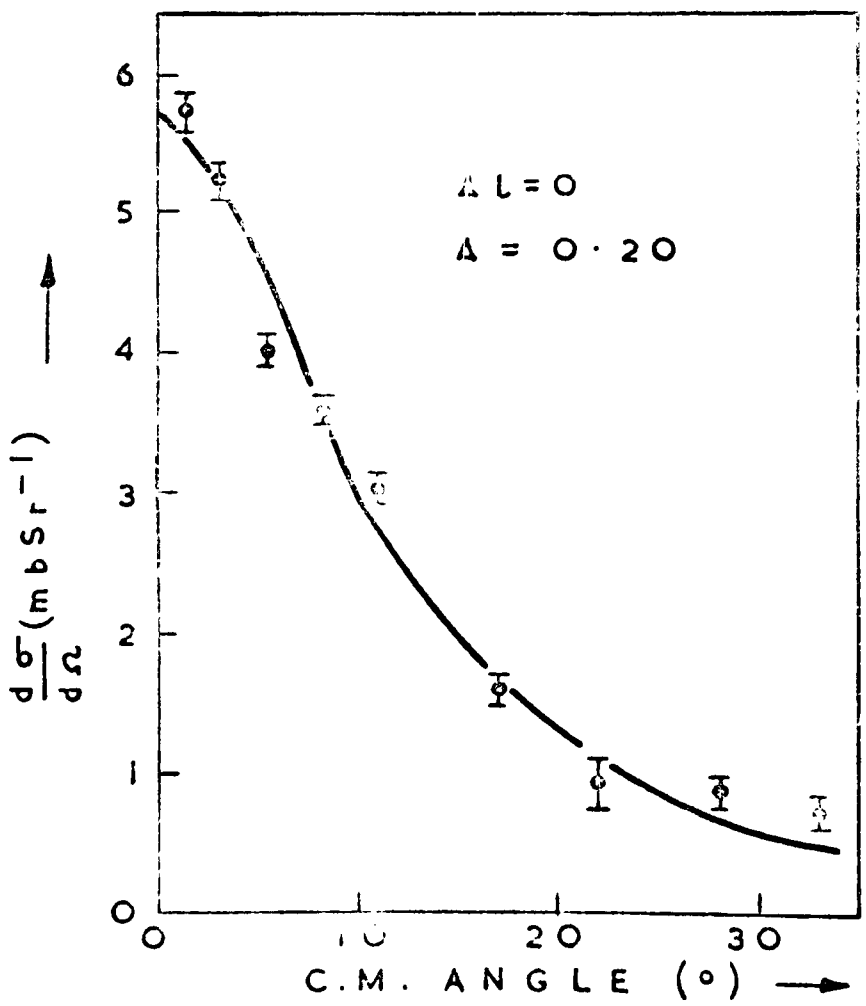

C.M. ANGLE (°)	CROSS SECTION (mb sr^{-1})	ERROR
1·5	5·73	0·12
3·2	5·23	0·21
5·6	4·04	0·09
8·3	3·57	0·08
11·1	3·02	0·08
16·6	1·61	0·06
22·1	0·96	0·11
27·6	0·89	0·05
33·0	0·74	0·04

(ii) LEVEL A (G.S.)

FIG. 7·3. B.

$^{11}B\ (p,n)\ ^{11}C$

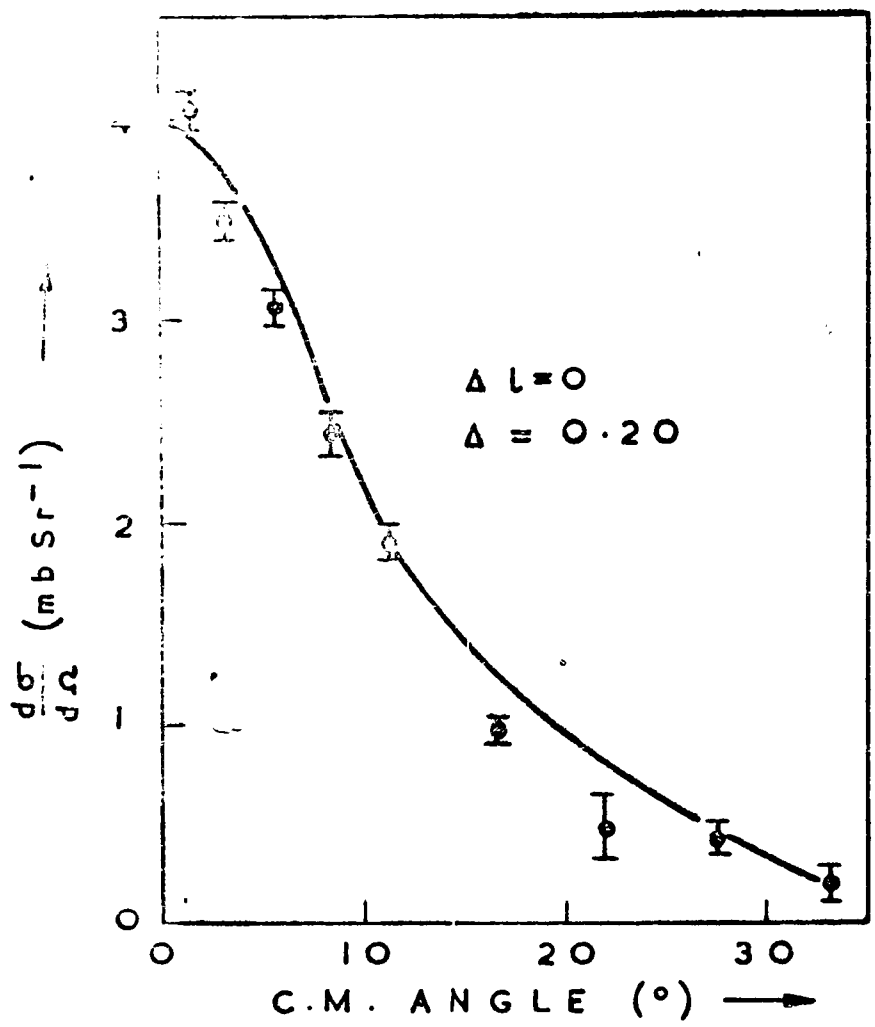

C M ANGLE (o)	CROSS SECTION (mb sr^{-1})	ERROR
1·5	4·03	0·10
3·2	3·51	0·10
5·6	3·07	0·05
8·3	2·44	0·08
11·1	1·89	0·07
16·6	0·96	0·05
22·1	0·48	0·16
27·6	0·43	0·07
33·1	0·20	0·07

(i) LEVEL B

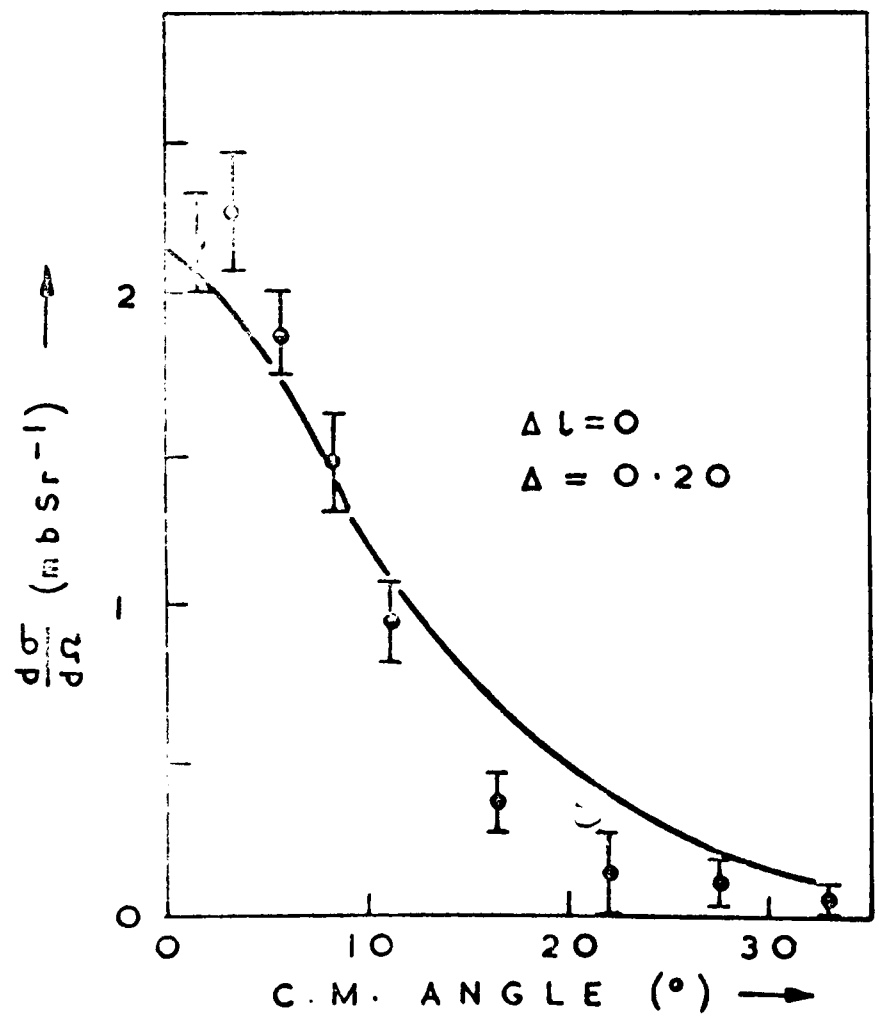

C M ANGLE (o)	CROSS SECTION (mb sr^{-1})	ERROR
1·5	2·17	0·16
3·2	2·28	0·20
5·6	1·90	0·14
8·3	1·46	0·16
11·1	0·93	0·14
16·7	0·36	0·11
22·1	0·14	0·14
27·7	0·10	0·07
33·1	0·03	+0·07 −0·03

(ii) LEVEL C

FIG. 7·3.C.

$^{11}B\ (p,n)\ ^{11}C$

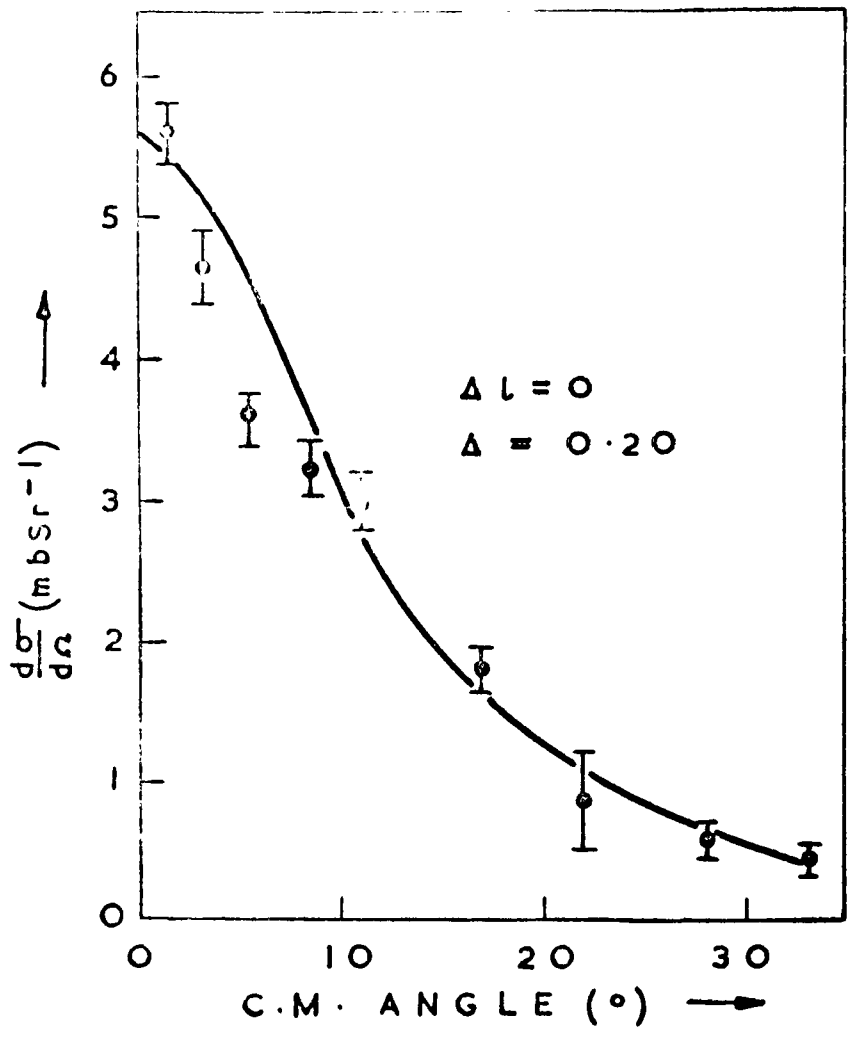

C.M. ANGLE (o)	CROSS SECTION (mb sr⁻¹)	ERROR
1·5	5·61	0·18
3·2	4·65	0·24
5·6	3·58	0·15
8·3	3·24	0·16
11·1	3·05	0·15
16·7	1·79	0·12
22·1	0·84	0·38
27·7	0·54	0·08
33·1	0·46	0·07

LEVEL D

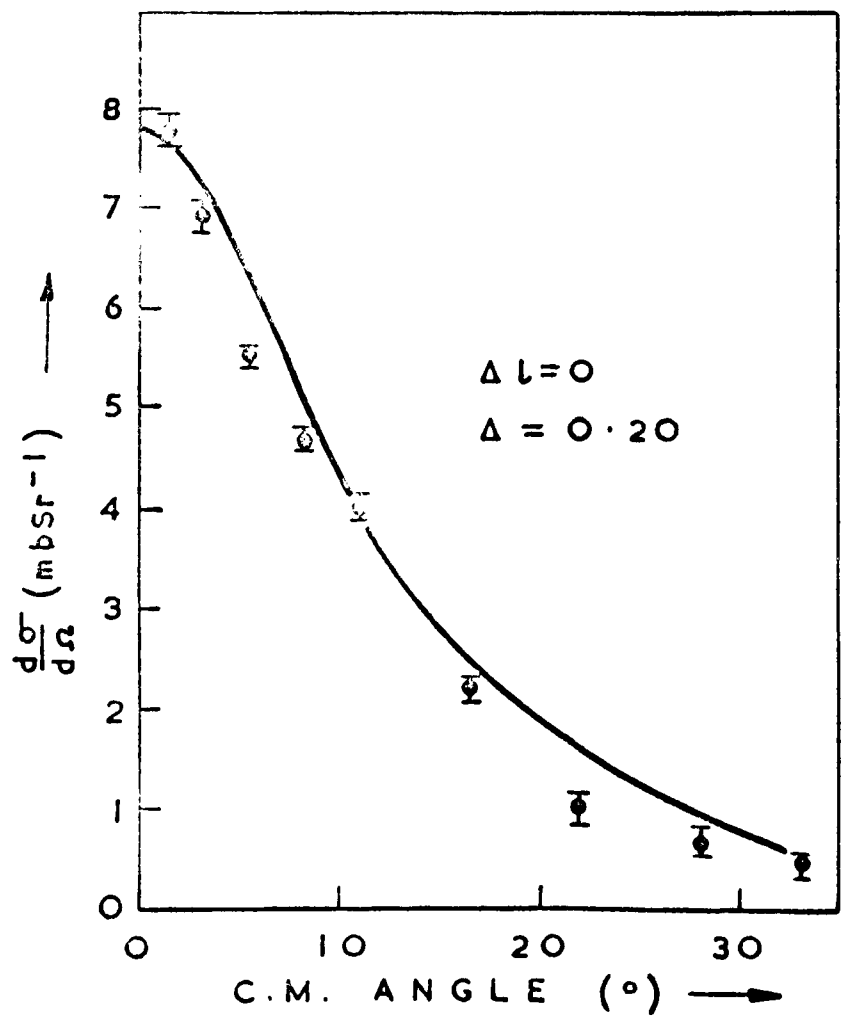

C.M. ANGLE (o)	CROSS SECTION (mb sr⁻¹)	ERROR
1·5	7·78	0·10
3·2	6·94	0·12
5·6	5·49	0·10
8·3	4·70	0·10
11·1	3·98	0·10
16·7	2·16	0·10
22·1	0·97	0·12
27·7	0·64	0·10
33·1	0·49	0·10

LEVELS C + D

FIG. 7·3.D.

^{11}B (p, n) C

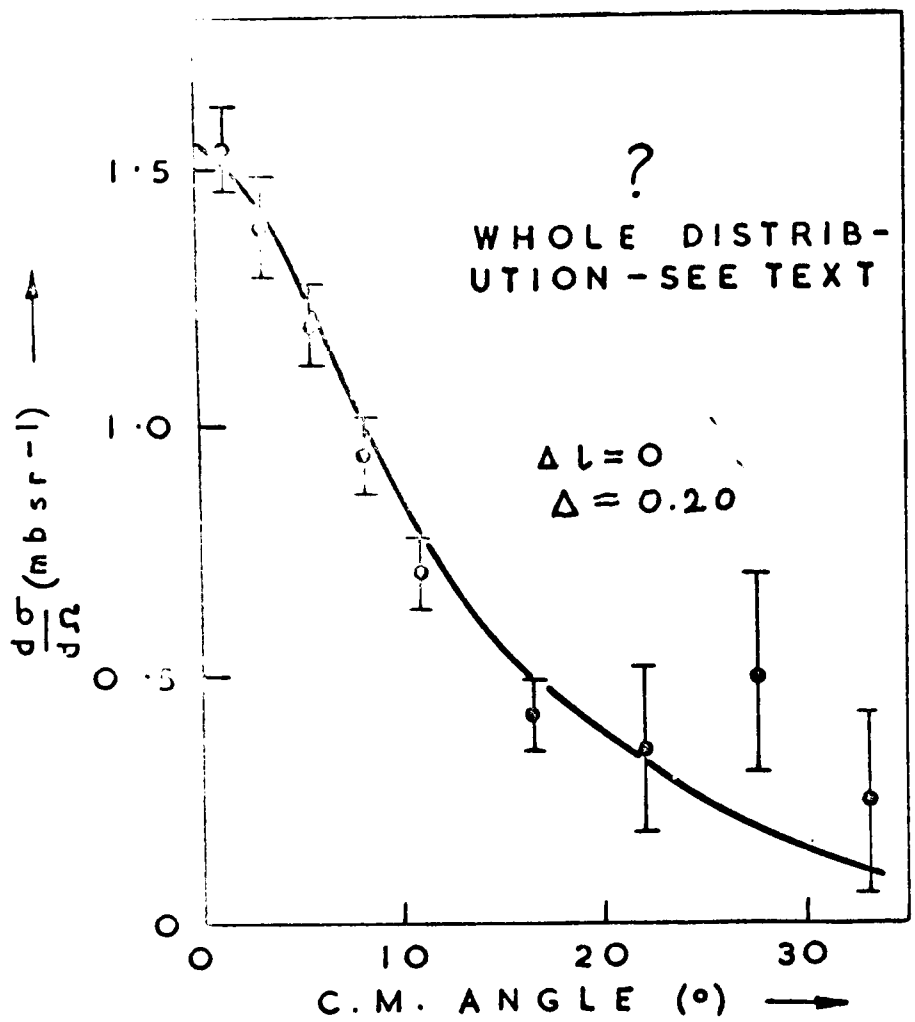

C.M. ANGLE (o)	CROSS SECTION ($mb\,sr^{-1}$)	ERROR
1·5	1·54	0·06
3·2	1·39	0·10
5·6	1·20	0·08
8·4	0·94	0·08
11·1	0·70	0·07
16·7	0·42	0·07
22·2	0·35	0·17
27·7	0·50	0·20
33·1	0·24	0·18

(i) GROUP E

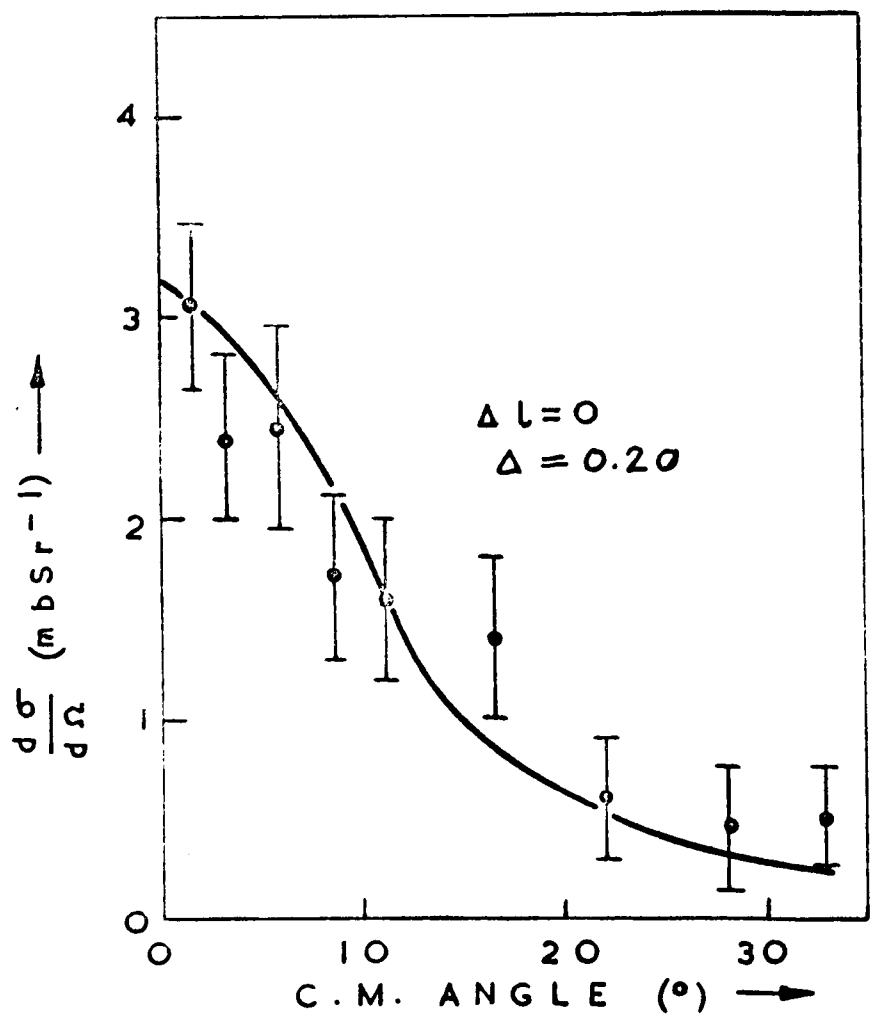

C.M. ANGLE (o)	CROSS SECTION ($mb\,sr^{-1}$)	ERROR
1·5	3·05	0·40
3·2	2·39	0·41
5·6	7·43	0·46
8·4	1·70	0·38
11·2	1·60	0·43
16·7	1·40	0·35
22·2	0·60	0·29
27·7	0·46	0·29
33·2	0·50	0·24

(ii) GROUP F

FIG. 7·3. E.

Angular distributions for transitions to levels A, B, C and D, and to groups of levels E and F were obtained and are presented in figs. 7.3.B-E. Excitation at about 13 MeV (G) and 17 MeV (H) was also observed but it was not possible to determine angular distributions.

The forward peaking of the transitions to A, B, C and D is to be expected from the known values of J^{π} on the assumptions discussed further in section 7.8, and so is that to group F on the assumption that it is the 8.11 MeV level ($\leq 5/2^-$) and 8.42 MeV level ($5/2^-$) which are strongly excited. However, group E is composed of two positive parity levels, implying odd values of Δl, and a $7/2^-$ level, which can only be reached via a $\Delta l=2$ transition from the $3/2^-$ ground state of ^{11}B. It may be seen from fig. 7.3.A that this neutron group (E) was badly defined, and it is possible that it was caused simply by the overlapping of groups (C+D) and F and was spuriously resolved by the fitting program. The angular distribution shown in fig. 7.3.E(i) is therefore of doubtful validity.

The strong excitation of a number of states in this reaction is in interesting contrast to the lithium spectrum (section 7.1) where only the ground and first excited states are strongly excited. This point is discussed in detail in section 7.8.

This spectrum shows clearly that $\Delta l=0$ transitions are favoured in direct reactions at this energy even at angles corresponding to the maxima of the expected distributions for $\Delta l \geq 1$.

7.4 Carbon

Fig. 7.4.A shows the 5° energy spectrum from carbon. (This particular spectrum was chosen for display simply because it had the greatest statistical accuracy). The known energy levels of ^{12}N are shown in fig. 7.4.b(i). Levels C, D and E are from (Clough, 1970) and the rest from (Ajzenberg-Selove, 1968). Ajzenberg-Selove et al also show a possible

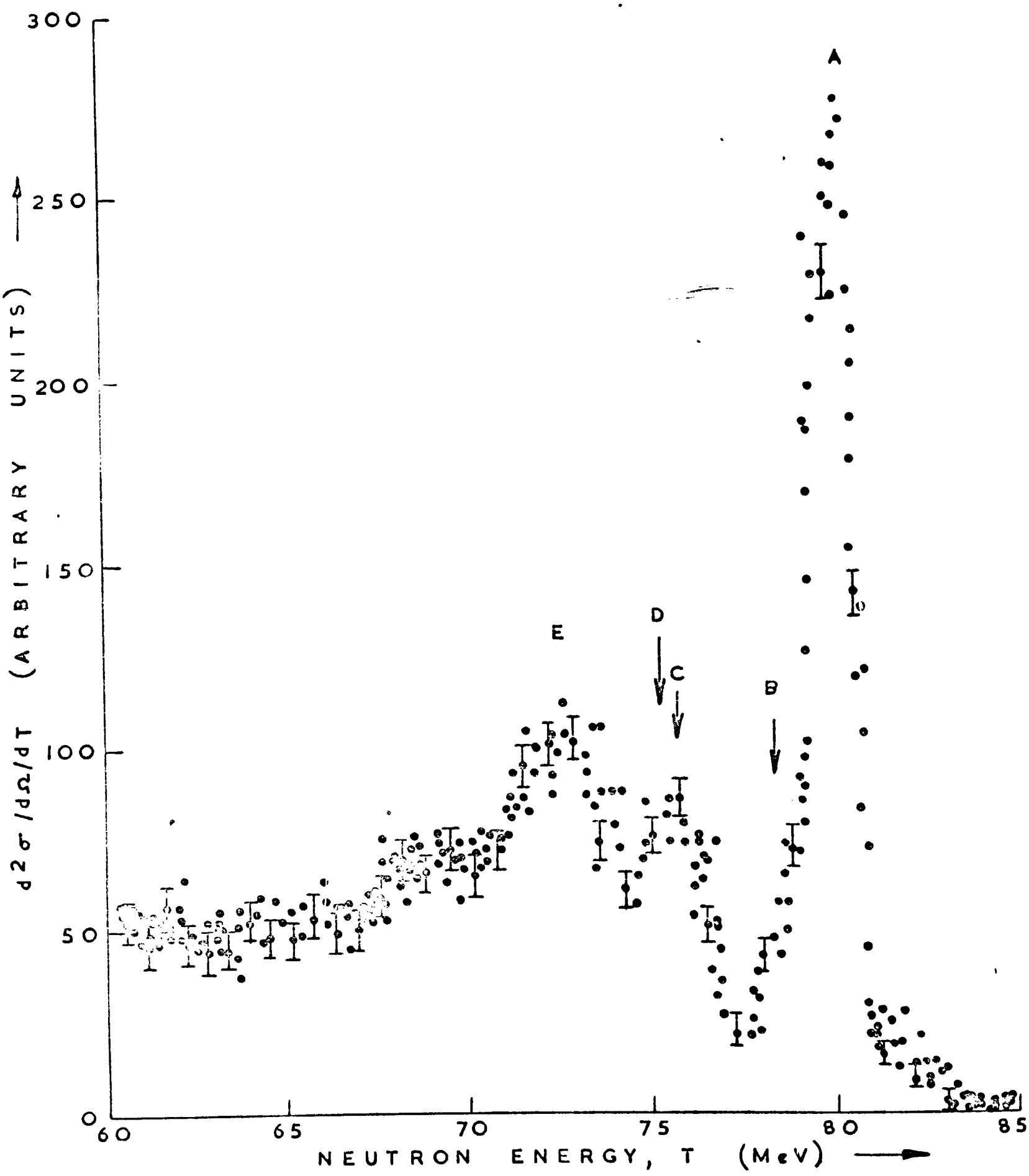

FIG. 7·4.A. 5° ENERGY SPECTRUM FROM CARBON

^{12}C (p, n) ^{12}N

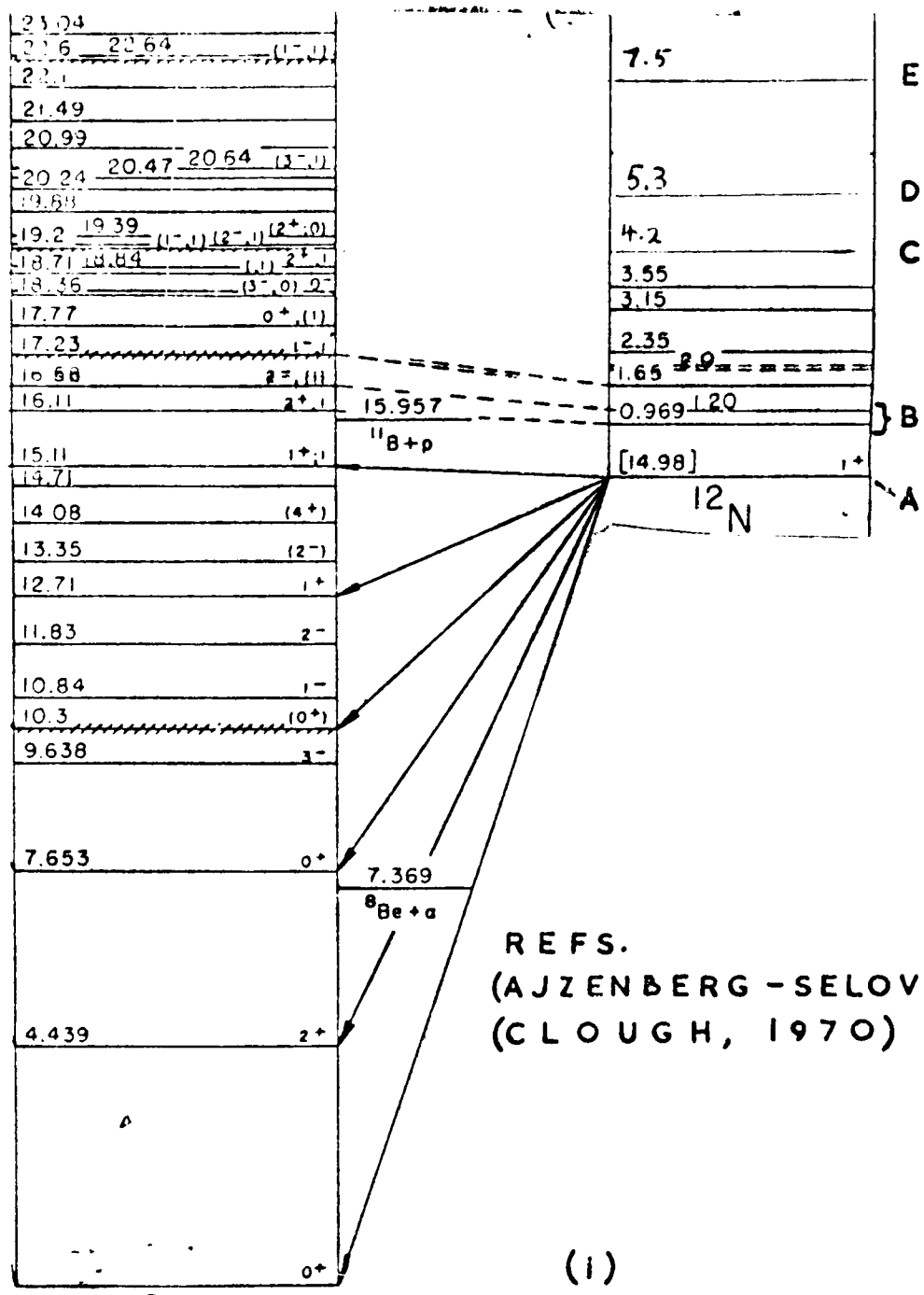

REFS.
(AJZENBERG-SELOVE, 1968)
(CLOUGH, 1970)

(i)

^{12}C

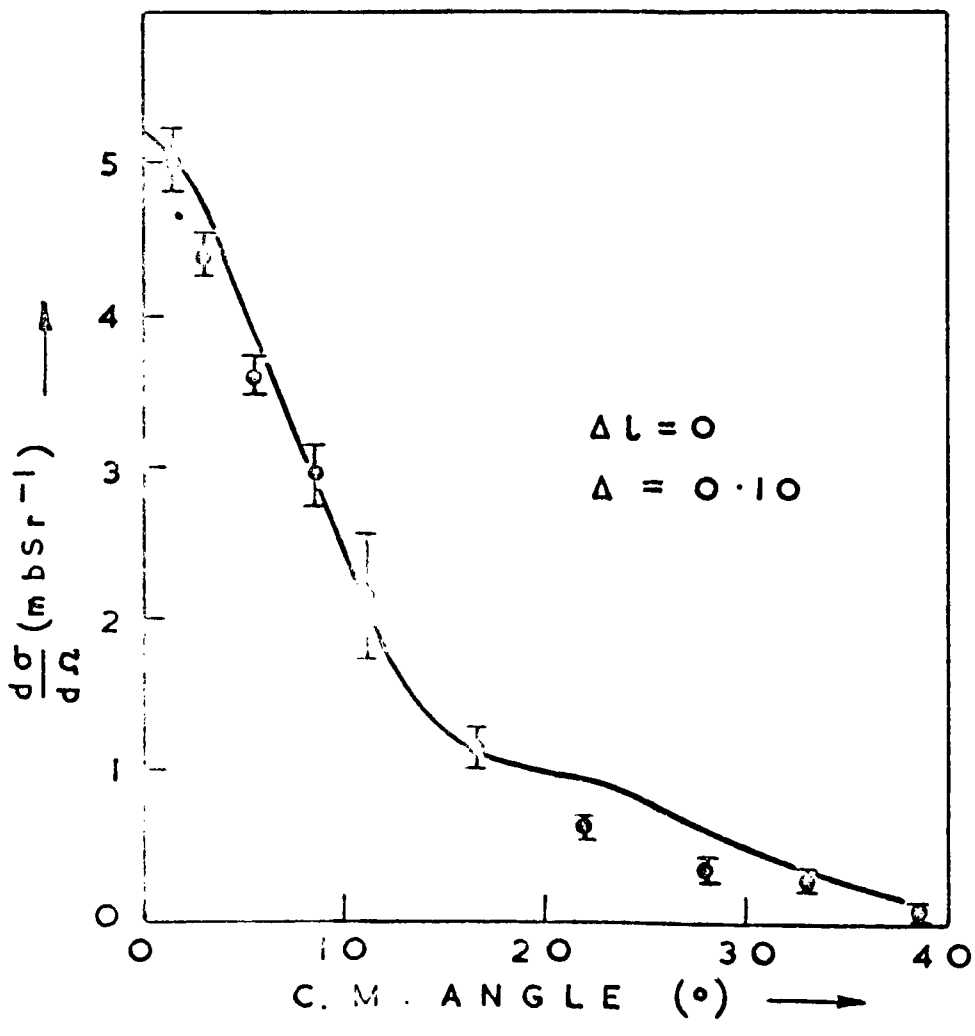

C.M. ANGLE (°)	CROSS SECTION (mb sr⁻¹)	ERROR
1·5	5·02	0·18
3·2	4·44	0·12
5·6	3·63	0·10
8·3	2·93	0·20
11·1	2·14	0·37
16·6	1·13	0·10
22·1	0·58	0·06
27·6	0·35	0·05
33·0	0·24	0·04
38·5	0·09	0·09

(ii) LEVEL A (G.S.)

FIG. 7·4.B.

$^{12}C\ (p, n)\ ^{12}N$

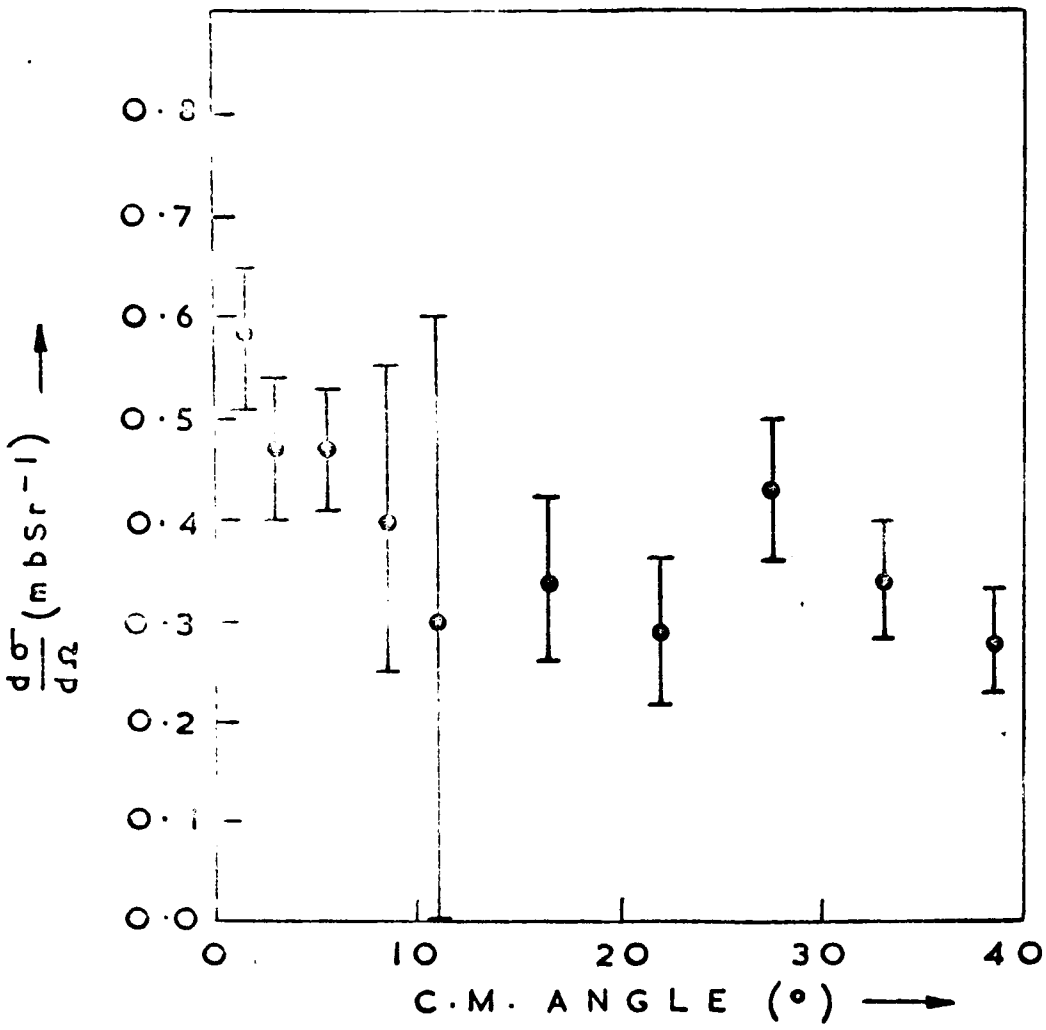

C.M. ANGLE (o)	CROSS SECTION (mb sr⁻¹)	ERROR
1·5	0·58	0·07
3·2	0·47	0·07
5·6	0·47	0·06
5·3	0·40	0·15
11·1	0·30	0·30
16·6	0·34	0·08
22·1	0·29	0·07
27·6	0·43	0·07
33·0	0·34	0·06
38·6	0·28	0·05

(i) GROUP B

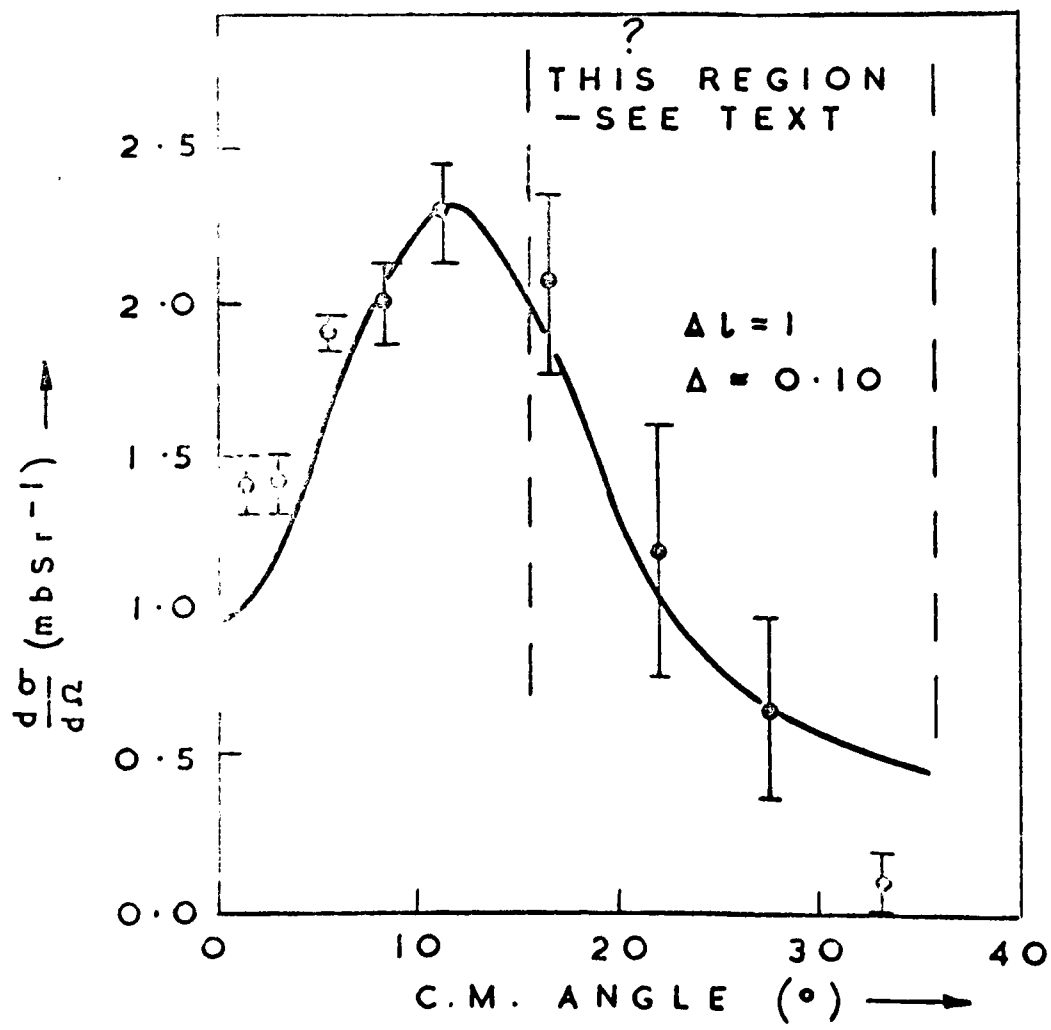

C M ANGLE (o)	CROSS SECTION (mb sr⁻¹)	ERROR
1·5	1·41	0·10
3·2	1·41	0·11
5·6	1·91	0·07
8·3	1·98	0·12
11·1	2·29	0·15
16·7	2·06	0·31
22·1	1·18	0·41
27·6	0·65	0·31
33·0	0·10	0·10
38·6	—	—

(ii) LEVEL C

FIG. 7·4. C.

$^{12}C\ (p,n)\ ^{12}N$

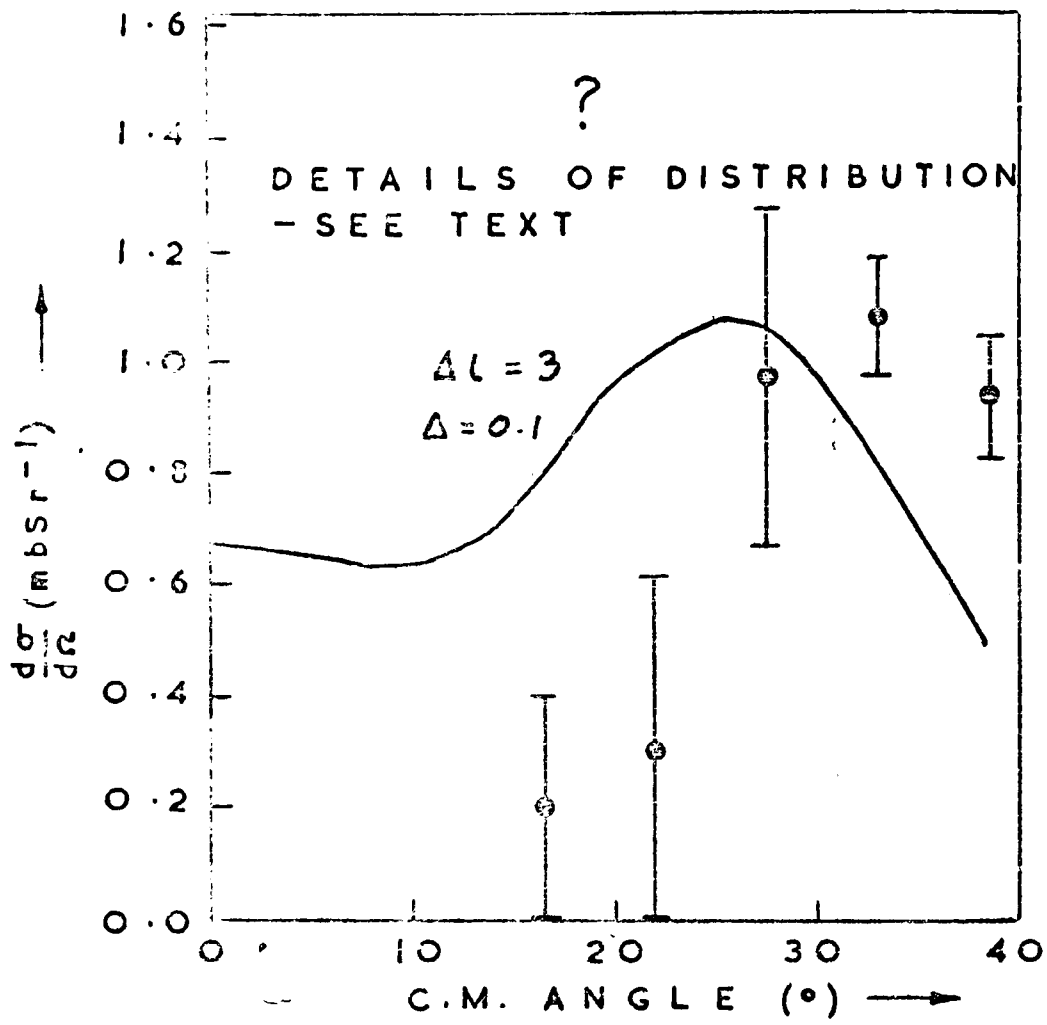

C.M. ANGLE (°)	CROSS SECTION (mb sr⁻¹)	ERROR
1·5	—	—
3·2	—	—
5·6	—	—
8·3	—	—
11·1	—	—
16·7	0·20	0·20
22·1	0·31	0·31
27·6	0·97	0·31
33·0	1·08	0·10
38·6	0·94	0·10

LEVEL D

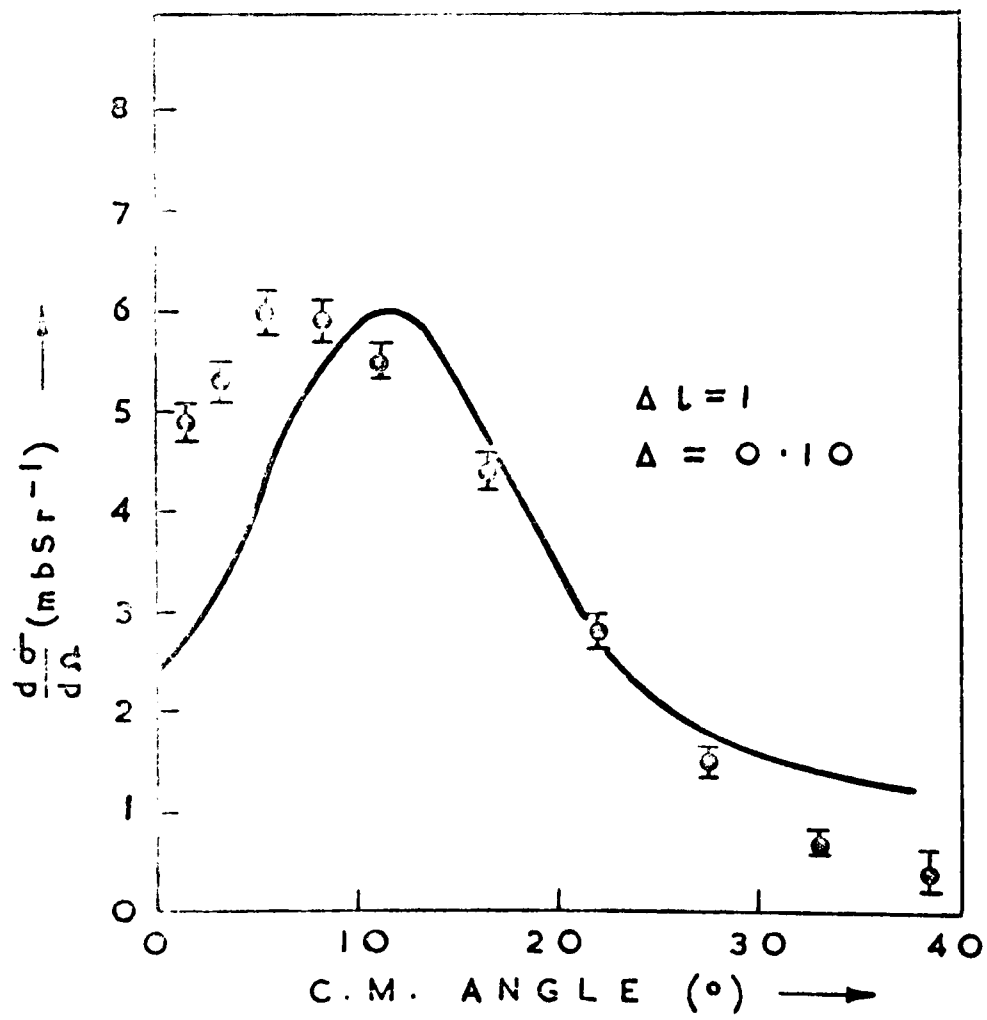

C M ANGLE (°)	CROSS SECTION (mb sr⁻¹)	ERROR
1·5	4·92	0·20
3·2	5·28	0·20
5·6	5·98	0·21
8·3	5·93	0·21
11·1	5·49	0·17
16·7	4·45	0·18
22·1	2·79	0·15
27·6	1·49	0·12
33·0	0·73	0·10
38·6	0·37	0·21

LEVEL E

FIG. 7.4.D.

level at 6 MeV which has been omitted from the present figure. The transition to the ground state, A, may be clearly seen in fig. 7.4.A as well as two broad peaks at excitation energies of 4.3 ± 0.2 MeV (C) and 7.1 ± 0.4 MeV (probably E). There is also evidence for excitation of at about 1 MeV. On the assumption of a single narrow peak in this region, the fitting program found the excitation energy to be 1.18 ± 0.05 MeV but it almost certainly consists in fact of unresolved transitions to the two levels comprising group B in fig. 7.4.B(i).

The position of the excitation at 4.3 MeV shows a definite shift to lower energies relative to the other peaks between 20° and 35° (lab.). This strongly suggests the existence of another state, and on the assumption that the shift is complete by 35°, its excitation energy is 4.8 ± 0.3 MeV. This is very probably the 5.3 MeV state (D) found by Clough et al, and, if so, the discrepancy in the excitation energy suggests the shift from one to the other is not complete by 35° as assumed.

Levels C, D and E all appear to be naturally broad and were fitted with broadened resolution functions. The widths were found to be respectively 1.3 ± 0.2 MeV, 2.5 ± 0.5 MeV and 3 ± 1 MeV.

The angular distributions are shown in figs. 7.4 B - D. The section between 20° and 35° for levels C and D is in some doubt as it is based on a rough estimate of the separate contributions to the unresolved peak.

The angular distribution for the ground state transition, A, is strongly forward peaked suggesting $\Delta l=0$, consistent with the expected $0^{+} \longrightarrow 1^{+}$. The transitions to B would be expected to have $\Delta l=2$ ($0^{+} \longrightarrow 2^{+}$) and $\Delta l=1$ ($0^{+} \longrightarrow 2^{-}$) and therefore to be not forward peaked. The rather inconclusive behaviour exhibited in fig. 7.4.C(i) is therefore not inconsistent with expectations.

The distributions for levels C and E both peak at $\sim 10^{\circ}$ and strongly suggest $\Delta l=1$. It is very likely that these are the partially resolved

analogues of the giant dipole resonances in ^{12}C, and, if so, will have $J^{\pi} = 1^-$.

The distribution for level D peaks at $\sim 32^{\circ}$ and, using a DWBA calculation (see section 7.8), the data were fitted best with a $\Delta l=3$ angular distribution. Such a transition would lead to a 2^-, 3^- or 4^- level in ^{12}N. There is a 3^-, T=1 level in ^{12}C at 20.64 MeV and it is possible that D is its analogue. However there are a number of other nearby states in ^{12}C with unknown J^{π}.

7.5 Oxygen

Fig. 7.5.A shows the 0° lithium hydroxide spectrum. The main peak is from the lithium in the lithium hydroxide, and most of the remainder of the excitation is from the oxygen. The contribution from lithium was subtracted before fits were attempted.

It is known (Zafiratos, 1965) that the ground state and first three excited states of ^{16}F (A) lie within a few hundred keV of each other and are 0^-, 1^-, 2^- and 3^- (though not necessarily respectively). The first peak in the oxygen spectrum therefore presumably consists of unresolved transitions to these levels. There is also evidence for excitation of the 1.30 MeV level, B, but the excitation is weak and its identification dubious.

No other level was resolved at small angles and it was only possible to obtain cross-sections for the total excitation of the extensive group of levels, C. However, at 25°, 30° and 35° (lab.) a sharp peak at 4.2 ± 0.1 MeV was clearly seen above the general excitation. This is clear evidence that its angular distribution peaks at much higher angles than those of the other levels suggesting $\Delta l \geq 2$. Values of the cross-sections for the three spectra in which D was resolved are shown in fig. 7.5.D.

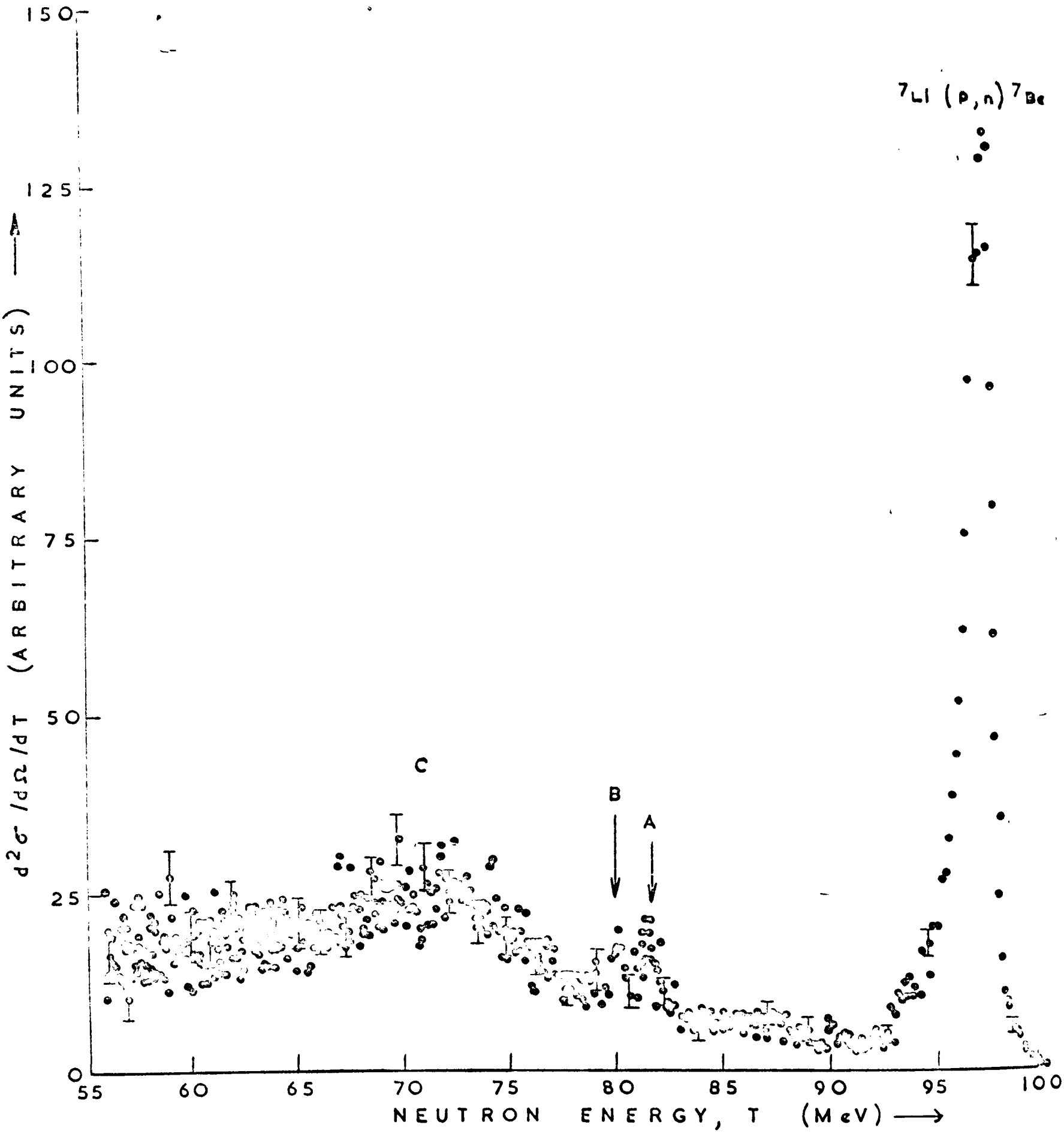

FIG. 7·5.A. 0° ENERGY SPECTRUM FROM LITHIUM HYDROXIDE

^{16}O (p, n) ^{16}F

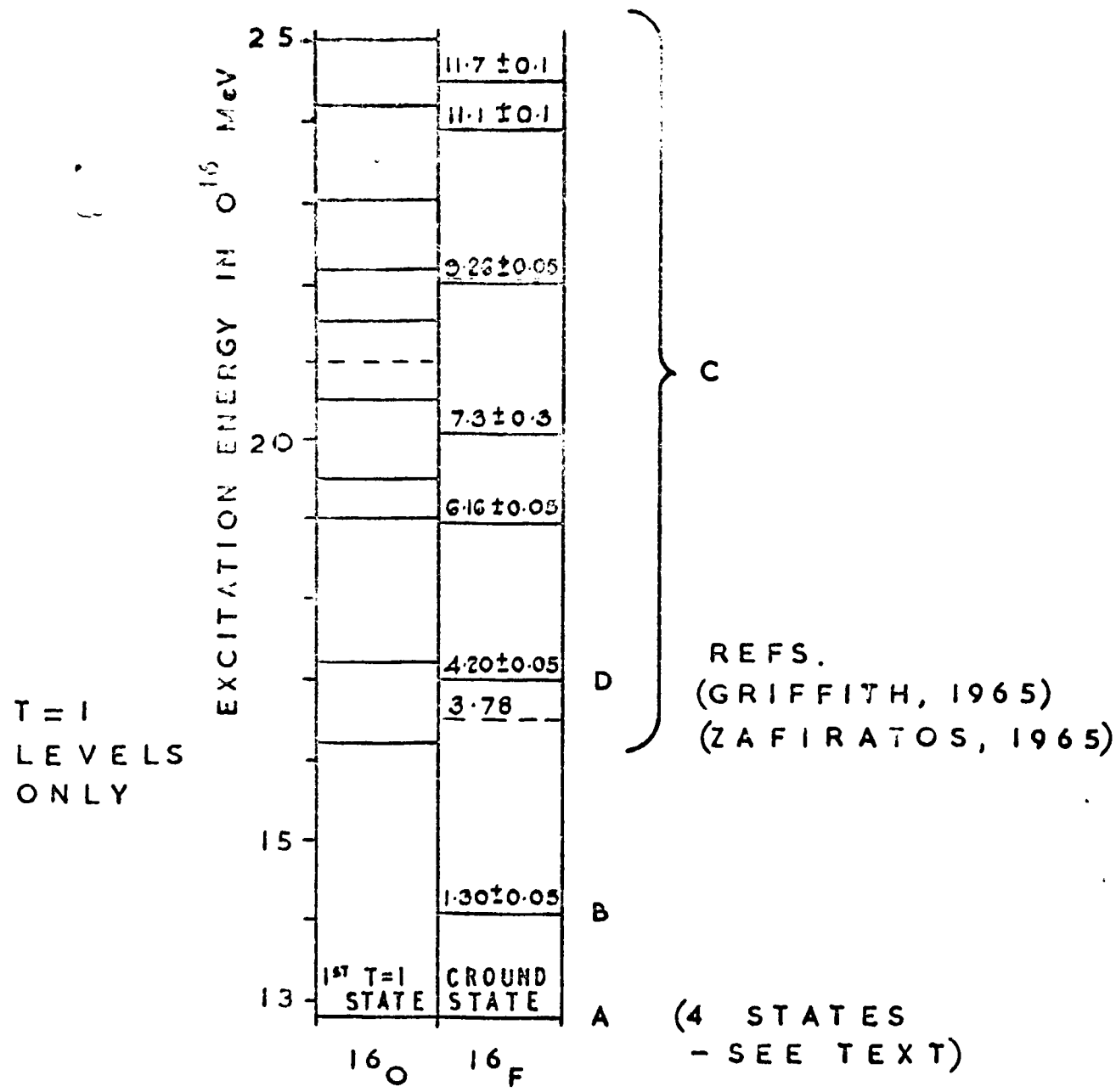

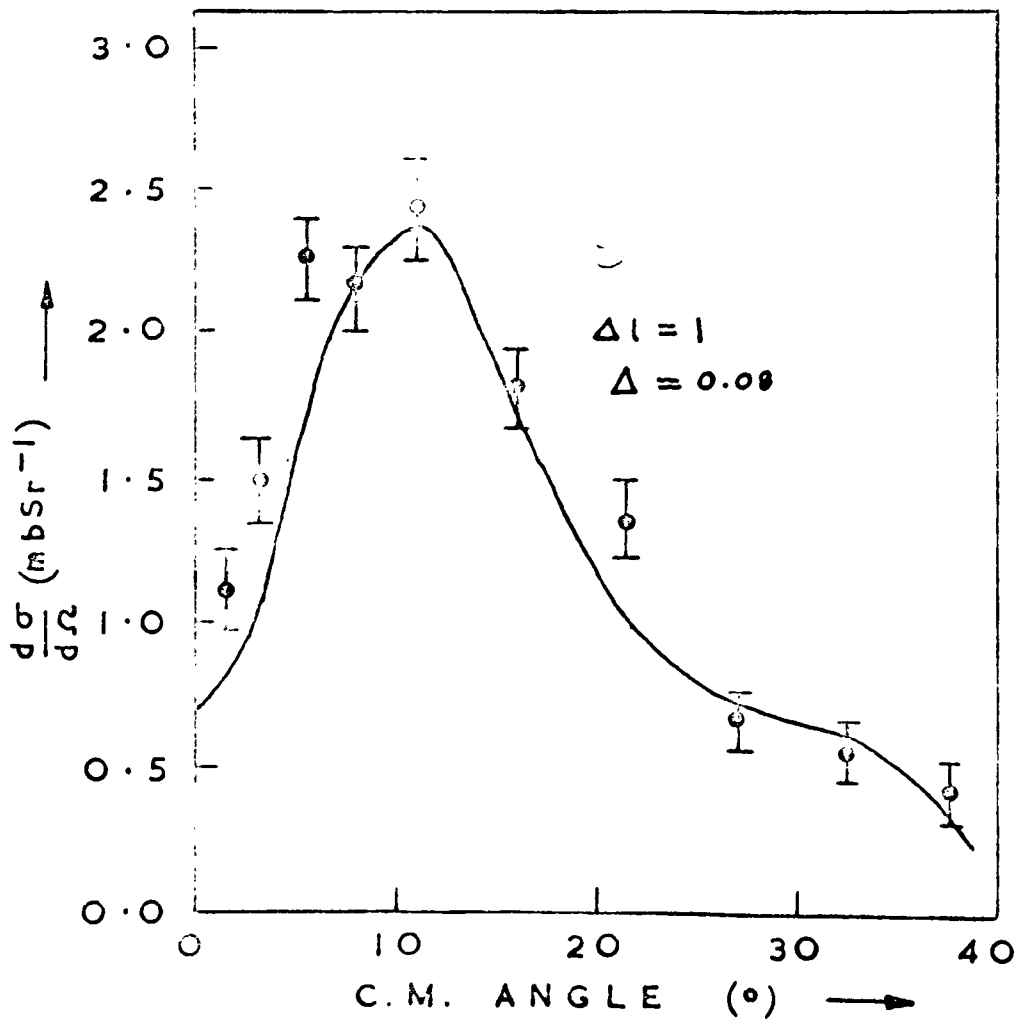

C.M. ANGLE (°)	CROSS SECTION (mbsr^{-1})	ERROR
1·5	1·10	0·13
3·2	1·47	0·14
5·5	2·26	0·14
8·1	2·11	0·14
10·9	2·43	0·15
10·2	1·79	0·14
21·6	1·84	0·12
27·0	0·67	0·10
32·3	0·54	0·09
37·7	0·43	0·12

GROUP A

FIG. 7·5. B.

^{16}O (p, n) ^{16}F

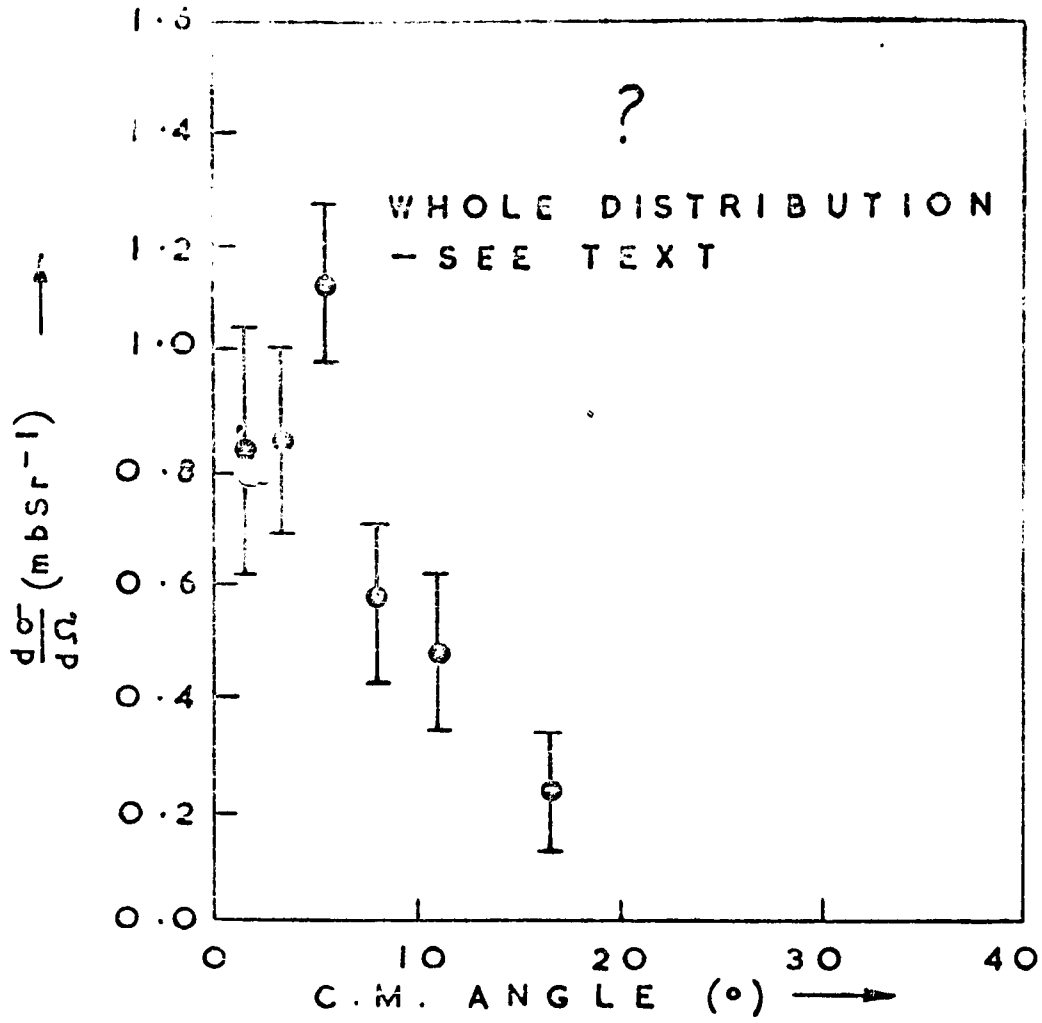

C.M. ANGLE (°)	CROSS SECTION ($mb\,sr^{-1}$)	ERROR
1·5	0·83	0·21
3·2	0·84	0·15
5·5	1·15	0·14
8·1	0·56	0·14
10·9	0·48	0·14
16·3	0·24	0·11
21·6	—	—
27·0	—	—
32·3	—	—
37·7	—	—

LEVEL B

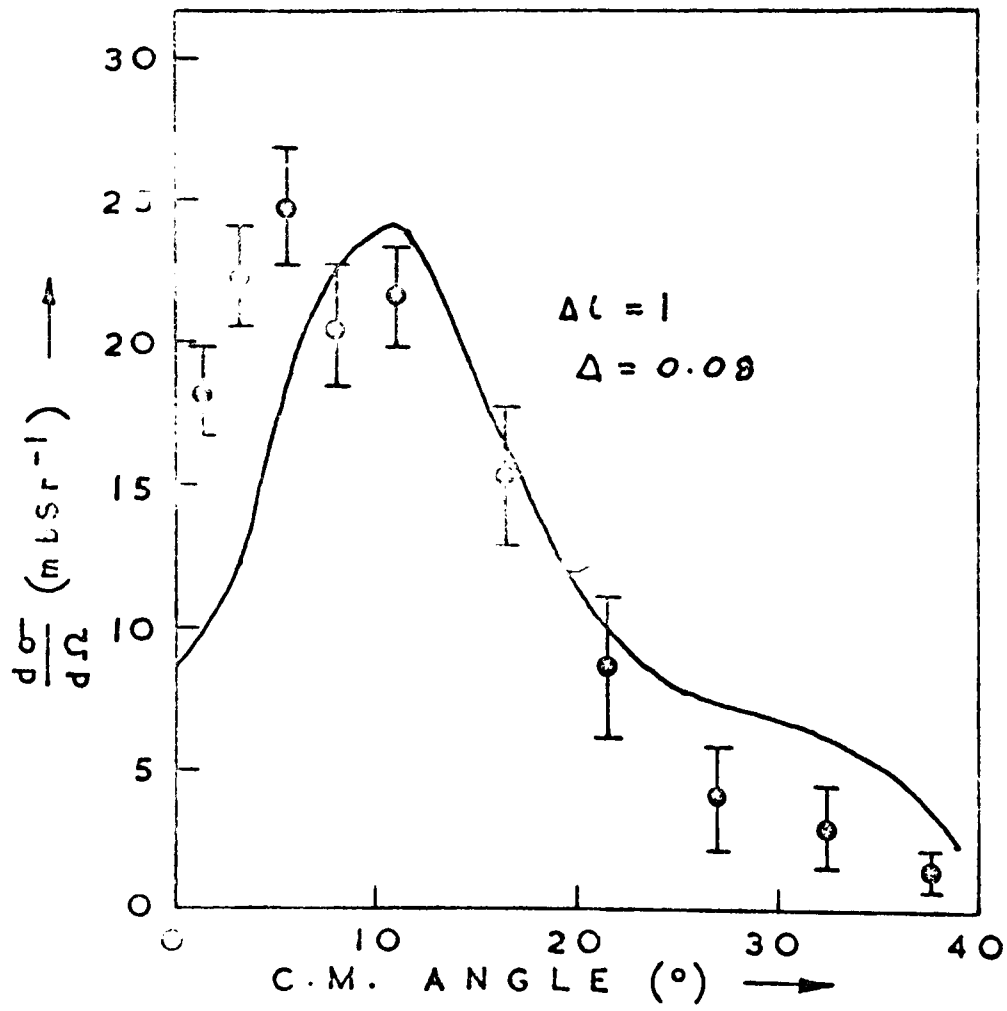

C.M. ANGLE (°)	CROSS SECTION ($mb\,sr^{-1}$)	ERROR
1·5	17·9	1·9
3·2	22·2	1·9
5·5	24·8	2·1
8·1	20·7	2·1
10·9	20·6	1·9
16·3	15·3	2·4
21·6	8·4	2·4
27·0	3·9	1·9
32·3	3·0	1·4
37·7	1·2	0·8

GROUP C

FIG. 7.5.C.

$^{16}O\ (p,n)\ ^{16}F$

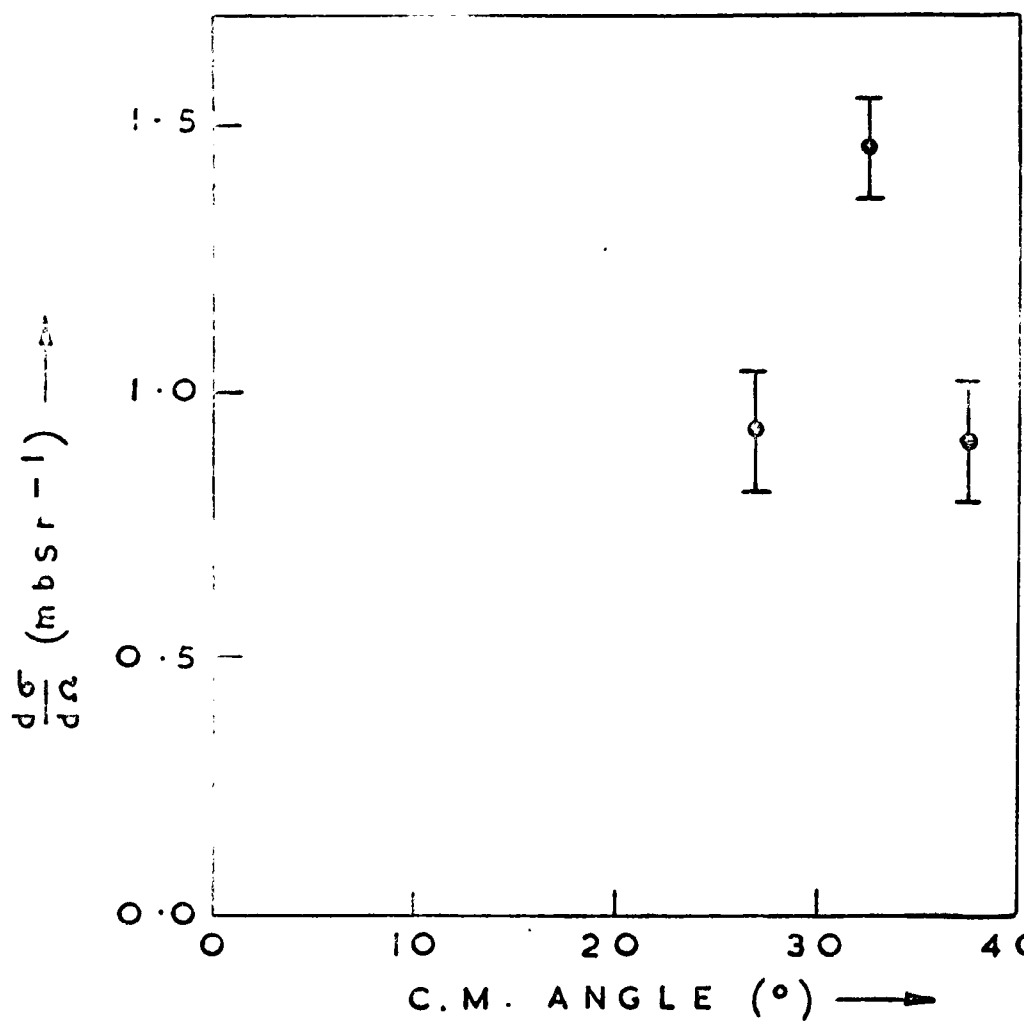

C.M. ANGLE (°)	CROSS SECTION ($mbsr^{-1}$)	ERROR
1·5	—	—
3·2	—	—
5·5	—	—
8·1	—	—
10·9	—	—
16·3	—	—
21·6	—	—
27 0	0·92	0·11
32·3	1·46	0·10
37·8	0·91	0·11

LEVEL D

FIG. 7·5.D.

Distributions for A and C clearly indicate $\Delta l=1$. That for B is more inconclusive. It is therefore likely that the transition A proceeds to the 0^-, 1^- or 2^- states rather than to the 3^- state since this would require $\Delta l=2$. It is also likely that the analogue in ^{16}F of the giant dipole resonance in ^{16}O constitutes a large part of C.

7.6 Comparison with other data

This section makes two sorts of comparisons of the present results with other data. The first two sub-sections contain a comparison with (p,n) reactions at the same, and different energies, and sub-section 7.6.3 compares the results with a (p,p') reaction whose results have been normalized to the energy of this experiment.

7.6.1 Comparison with the previous 100 MeV data

Comparison of the present results with those of Saltmarsh (Saltmarsh, 1965) are shown in table 7.6.A. Saltmarsh used the same absolute normalization technique as was used with the present data and errors from this source have not been included in the comparison. However the random errors have been increased to take account of Saltmarsh' 6% and the present 10% monitoring error.

The magnitudes of the cross-sections agree reasonably within experimental error, and show no evidence for a "one-way" deviation from each other. However Saltmarsh' angular distributions for ^{7}Li and ^{9}Be are narrower than those from the present experiment, though those for ^{12}C and ^{16}O agree quite well. In view of the admitted possibility of angular normalization error in the present experiment, it might be thought that Saltmarsh' distributions are to be preferred. However, there are two pieces of evidence which counter this. First, the DWBA angular distribution shown in fig. 7.1.C (see section 7.8 for DWBA) was predicted using the same parameters as had been found by Clough (Clough, 1969,A) to fit his data for the same reaction at

SITION	MAXIMUM CROSS-SECTION (mb Sr^{-1})		WIDTH* (°)	
	SALTMARSH	PRESENT	SALTMARSH	PRESENT
n) ^{7}Be(A+C)	25·3 ± 1·8	27·9 ± 2·8	9 ± 1	12 ± 1
n) ^{9}B (A)	6·0 ± 2·2	13·0 ± 1·3 [redacted]	8 ± 2	11·5 ± 1·5
n) ^{11}C (A)	NOT OBSERVED	5·73 ± 0·53	NOT OBSERVED	11·0 ± 0·5
n) ^{12}N (A)	6·31 ± 0·63	5·02 ± 0·50	10 ± 2	9·5 ± 0·5
n) ^{16}F (A)	1·75 ± 0·26	2·4 ± 0·3	10 ± 2†	12 ± 2†

R $\Delta l=0$ DISTRIBUTIONS, WIDTH IS THE
E CORRESPONDING TO THE HALF HEIGHT

R THE $\Delta l=1$ TRANSITION, WIDTH IS
TION OF FIRST MAXIMUM

LE 7·6.A. COMPARISON WITH
EVIOUS (p,n) DATA AT 94 MeV

NSITION		MAXIMUM CROSS-SECTION (mbSr^{-1})		
		CLOUGH et al 30 MeV	50 MeV	PRESENT 98·5 MeV
,n) ^{7}Be	(A + B)	24·0	24·0	[redacted] 27·9
,n) ^{9}B	(A)	19·3	12·5	13·0
	(C + D)	7·3	8·6	9·0
,n) ^{11}C	(A)	11·2	12·7	5·7
	(B)	1·6	4·3	4·0
	(C + D)	5·9	8·3	7·8
,n) ^{12}N	(A)	0·67	1·58	5·02

BLE 7·6.B. COMPARISON WITH
N REACTIONS AT 30 AND 50 MeV

50 MeV, and this prediction fits the present data much better than it fits Saltmarsh'. Secondly, it is expected that as the radius of the nucleus increases, the width of the angular distribution should decrease. This prediction is confirmed very well with the present results, but is in conflict with Saltmarsh' data. It is therefore possible that the present distributions represent an improvement over Saltmarsh' distributions.

7.6.2 Comparison with (p,n) reactions at 30 and 50 MeV

Clough et al (Clough, 1969; Clough, 1970) have studied (p,n) reactions at 30 and 50 MeV on all the nuclei studied in the present experiments with the exception of oxygen. A comparison of their 0° differential cross-section with those from the present experiment are shown in table 7.6.B.

The general expectation is that between 50 MeV and 100 MeV, the angular distribution for a $\Delta l=0$ transition should become narrower and the 0° cross-section should rise somewhat, the total cross section remaining approximately constant. The regrettably large normalization error on the present data makes it difficult to draw firm conclusions, but one or two points stand out:

1) The $^{12}C(p,n)^{12}N(g.s.)$ is very much higher at 100 MeV - this may be explained simply in terms of a reduction of phase space at 50 MeV due to the low Q-value (- 18.124 MeV) of the reaction.
2) The $^{11}B(p,n)^{11}C(g.s.)$ cross-section is low at 100 MeV, but cross-sections for transitions to the excited states are quite comparable in magnitude.

Clough's analysis of his data is discussed further in section 7.8.

7.6.3 Comparisons with (p,p') reactions

It may be shown, e.g. (Clegg, 1965) on the direct interaction model simply on the assumption that "knock-out" processes may be ignored, that for an even-even spin zero target nucleus,

$$\frac{\frac{d\sigma}{d\Omega_{cm}}(p,n)}{\frac{d\sigma}{d\Omega_{cm}}(p,p')} = 2,$$

where the transitions are to analogous levels. Thus the $^{12}C(p,p')^{12}C^*$ reaction to the first T=1 state at 15.1 MeV (the analogue of the ground state of ^{12}N) should exhibit the same angular distribution at 100 MeV as the (p,n) reaction, but with half the cross-section. No (p,p') data exist at 100 MeV, but the reaction has been studied at 185 MeV (Hasselgren, 1965) and 155 MeV (Jacmart, 1964). On the direct interaction model, the cross section is equal to the product of the square of the nucleon-nucleon scattering amplitudes and the overlap integral. The overlap integral may be assumed the same for the two reactions, so that the (p,p') data may be normalized to 100 MeV using the appropriate nucleon-nucleon scattering amplitudes. This has been done by Langsford (Langsford, 1969) who used the free nucleon-nucleon scattering amplitudes (impulse approximation) calculated from the MacGregor phase shifts (MacGregor, 1968). He compared the results with Saltmarsh' (p,n) data (Saltmarsh, 1965) and found that the angular distributions were the same within experimental error, but that the (p,n) cross-section was only 1.4 times the (p,p'). The present $^{12}C(p,n)^{12}N$ (g.s.) angular distribution is the same as Saltmarsh' within experimental error, but the absolute cross-sections are a little lower. This exacerbates the discrepancy yielding a ratio 1.3 ± 0.2. Langsford suggests that the discrepancy

is due to the neglect of absorption effects in normalizing the high energy data to 100 MeV, but the size of the discrepancy seems rather great to be accounted for in this way. However, a precise comparison must await a suitable $^{12}C(p,p')$ experiment at 100 MeV, and preferably a better absolute normalization of the (p,n) cross sections.

7.7 The analogue transitions

Analogue transitions were observed in the present experiment for ^{7}Li, ^{9}Be and ^{11}B. They have already been compared with Saltmarsh' data in section 7.6.

Saltmarsh studied a very much wider range of analogue transitions than was observed in the present experiment, and an optical model analysis has been done by Thurlow (Thurlow, 1968). It is therefore only worthwhile to note how the points of difference of the present data may affect her conclusions.

The main difference is that the present angular distributions are wider than those found by Saltmarsh, and therefore if the present data are to be preferred as suggested is possible in section 7.6, this would reduce the rather high radii which Thurlow deduced for the nuclei concerned.

7.8 D.W.B.A. analysis

The methods by which direct reactions may be analysed were reviewed briefly in Chapter 1, where it was established that though DWIA is relatively simple, and directly predicts the cross-sections, DWBA, which assumes an effective interaction between the nucleons is likely to produce better fits - certainly below ~100 MeV. Some evidence was presented in section 7.1 that PWIA predicted too high a value for the $^{7}Li(p,n)^{7}Be$ (g.s.) transition, though there is little

doubt that refinements to the IA approach would improve the situation.

The present data were fitted with a microscopic DWBA computer code written by E. Friedman (Friedman, 1966). In the present instance, shape fits only were obtained, but a discussion is presented about possible approaches to the analysis of the magnitudes of the cross-sections.

7.8.1 Theoretical framework

In DWBA, the transition amplitude is written as (Madsen, 1966; Satchler, 1966)

$$T_{if} = \int \chi_f^*(\underline{k}_f, \underline{r}) \langle \psi_f | V_{eff} | \psi_i \rangle \chi_i(\underline{k}_i, \underline{r}) \, d\underline{r}$$

where χ_i and χ_f are distorted waves describing the incoming and outgoing particles with momenta $\underline{k}_i$ and k_f, ψ_i and ψ_f are nuclear wave-functions and V_{eff} is the effective interaction causing the transition.

In the microscopic approach used here, V_{eff} is written in terms of nucleon-nucleon potentials. The general nucleon-nucleon potential is written as

$$V_{N-N} = \left[V_{00} + V_{10}\, \underline{\sigma}\cdot\underline{\sigma}_I + (V_{01} + V_{11}\, \underline{\sigma}\cdot\underline{\sigma}_I)\, \underline{\tau}\cdot\underline{\tau}_i\right] f(\underline{r}-\underline{r}_I)$$

where $\underline{\sigma}$ and $\underline{\tau}$ are the spin and isospin vectors, and $f(\underline{r}-r_I)$ is the radial variation. For a (p,n) reaction, necessarily involving "isospin flip", only the isospin dependent terms V_{01} and V_{11} can contribute if "knock-out" processes are neglected (see e.g. (Atkinson, 1968)), so that V_{eff} may be written as

$$V_{eff} = \sum_{I=1}^{N} (V_{01} + V_{11}\underline{\sigma}\cdot\underline{\sigma}_I)\, \underline{\tau}\cdot\underline{\tau}_I \, f(\underline{r}-\underline{r}_I)$$

where the free particle is unsubscripted and the summation is over

all the target nucleons which can take part in the reaction.

The nuclear wave-function is then separated, to yield

$$\Psi_f = \frac{1}{r_I} R_f(r_I)\, \phi_f(\Omega_I, \underline{\sigma}_I)$$

and similarly for Ψ_i.

The transition amplitude then also separates:

$$T_{if} = \int \chi_f^* \chi_i \sum_I \frac{1}{r_I^2} R_f(r_I) R_i(r_I) f(\rho_I)\, dr \times \int \sum_I \phi_f(\Omega_I, \underline{\sigma}_I)(V_{01} + V_{11}\underline{\sigma}_I \cdot \underline{\sigma}_I)\underline{\tau}_I \cdot \underline{\tau}_I \phi_i(\Omega_I, \underline{\sigma}_I) d\Omega$$

$$= P(r)\, Q(\Omega)$$

In the present formulation the shape of the angular distribution depends only on P, and the magnitude depends in addition on Q. A preliminary attempt to fit the shape of the angular distributions of the present data is discussed in sub-section 7.8.2 and the way in further analysis may be carried out to determine V_{01} and V_{11} is discussed in subsection 7.8.3.

7.8.2 Shape fits

The shape of the angular distribution is determined by the term

$$P(r) = \int \chi_f^* \chi_i \sum_I \frac{1}{r_I^2} R_f(r_I) R_i(r_I) f(\rho_I)\, dr$$

The distorted waves χ_f and χ_i were calculated by distorting the incoming and outgoing plane waves by an averaged optical potential derived from elastic scattering studies. The potentials given by Satchler et al (Satchler, 1964) were used for all the nuclei since it was shown that the dependence of the shape on the optical parameters was slight.

A Yukawa form is taken for the nucleon-nucleon potential

$$f(\rho_I) = \frac{e^{-\alpha \rho_I}}{\alpha \rho_I} \quad ,$$

where $\rho_I = |\underline{r}_I - \underline{r}|$, and harmonic oscillator wavefunctions for the nuclear wave-functions. For the 1p-shell (deShalit, 1963)

$$R_i(r) \propto r^2 e^{-(\delta_i/2)r^2}$$

and similarly for R_f, where δ_i and δ_f are the oscillator parameters.

$$\therefore \quad R_f R_i \propto r^4 e^{-\Delta r^2}$$

where $\Delta = \frac{1}{2}(\delta_f + \delta_i)$.

Therefore, neglecting the slight dependence on the optical parameters, the shape is determined by α and Δ. For the present analysis, α was kept fixed at the value

$$\frac{1}{\alpha} = 1.414 \text{ fm}$$

given by one pion exchange (though this has been criticized (Mani, 1970) on the grounds that at 100 MeV, two pion exchange and more complicated processes enter into the nucleon-nucleon interaction), and only Δ was varied.

The results of the fits are presented along with the experimental results in sections 7.1 - 7.5 and the values of Δ used are indicated. The value of Δ used for the $^7Li(p,n)^7Be$ was the same as that used by Clough (Clough, 1969,A) in a similar analysis at 50 MeV, and it may be seen that a reasonable fit is obtained. Values of Δ were kept constant for a particular element.

It is possible to obtain information about the nuclear radius from the values of Δ, but since the shape of the angular distribution depends also on α, and since the harmonic oscillator wave-functions do not accurately represent the shape of the nuclei, it was not thought worthwhile to do this. (The justification for using oscillator wavefunctions is that it has been shown that (Jaques, 1970),

provided the appropriate size parameter is suitably adjusted, the angular distribution shape is not sensitive to details of the nuclear wave-function).

7.8.3 Determination of V_{01} and V_{11}

Having determined the parameters of P(r), the magnitude of the transition amplitude is determined by

$$Q(\Omega) = \int \sum_{I} \phi_f(\Omega_I, \sigma_I)(V_{01} + V_{11}\, \underline{\sigma}\cdot\underline{\sigma}_I)\, \underline{\tau}\, \underline{\tau}_I\, \phi_i(\Omega_I, \sigma_I)\, d\Omega,$$

and a detailed analysis of experimental data can yield values of V_{01} and V_{11} and sometimes details of ϕ_f and ϕ_i.

In the first instance, ϕ_f and ϕ_i may be taken as extreme L-S or j-j coupled shell model wavefunctions (Jahn, 1951; Edmonds, 1952) and V_{01} and V_{11} determined accordingly. In a "no spin-flip" transition, both V_{01} and V_{11} can contribute and cannot be separately determined, but in a "spin-flip" transition, only V_{11} contributes allowing its value to be determined. The best example from the present data is the $^{11}B(p,n)^{11}C(1.99\ MeV)$ transition, which on a L-S coupled description is

$$^2P_{3/2} \longrightarrow {}^2P_{1/2} \quad .$$

Using this value of V_{11}, the value of V_{01} may then, for example be determined from the analogue transition $^{11}B(p,n)^{11}C(g.s.)$ which is

$$^2P_{3/2} \longrightarrow {}^2P_{1/2}$$

Such an analysis has been carried out by Clough (Clough, 1969; Clough, 1970) for a range of 1p-shell nuclei at 30 and 50 MeV and he found that values of V_{01} and V_{11} were the same throughout the 1p-shell and that while V_{11} was fairly constant with energy, V_{01} showed a considerable energy dependence. It would, therefore, be particularly

interesting to extend the analysis to the present 100 MeV data, and it is unfortunate that the absolute normalization errors are so large (14%).

A further aspect of Clough's analysis is worthy of mention in view of the already mentioned strong excitation of states in the $^{11}B(p,n)^{11}C$ reaction and the relative absence of excitation in the $^{7}Li(p,n)^{7}Be$ reaction. Both the 4.305 and 4.794 MeV levels in ^{11}C are found to be strongly excited, the angular distribution clearly indicating $\Delta l=0$. However on the pure L-S coupling scheme, the states are

$$^{2}D_{3/2} \text{ and } ^{2}D_{5/2}$$

and the transition from a pure $^{2}P_{3/2}$ ground state could only proceed via $\Delta l=2$. Clough takes this as evidence of a considerable admixture of $^{2}D/_{3/2}$ in the ground state wave-function, and calculates that, taking the excited states of ^{11}C to be pure ^{2}D states, a first approximation to the ground state wave-function is

$$\psi(^{11}B_{g.s}) = 0.6\ ^{2}D_{\frac{3}{2}} + 0.8\ ^{2}P_{\frac{3}{2}} .$$

A similar situation exists in ^{7}Be. Transitions to the 4.55 and 6.51 MeV levels, presumed to be $^{2}F_{7/2}$ and $^{2}F_{5/2}$ levels cannot proceed via $\Delta l = 0$ since there can be no F admixture in the $J = 3/2$ ground state of ^{7}Li. However if there were an admixture of $^{2}D_{3/2}$ in the ground state of ^{7}Li the levels at 7.2 and 9.9 MeV (presumed to be $^{2}D_{5/2}$ and $^{2}D_{3/2}$) would be expected to be excited via a $\Delta l=0$ transition, and the observed absence of such excitations may be taken as evidence of the relative purity of the $^{2}P_{3/2}$ ground state of ^{7}Li. The only $\Delta l=0$ transition possible for this state is the

$$^{2}P_{3/2} \longrightarrow {}^{2}P_{1/2}$$

transition to the first excited state of ^{7}Be, in agreement with the observations.

7.8.4 Discussion

The shape fits discussed in sub-section 7.8.2 are relatively easy to produce and only provide some indication of the nuclear size. The shape is not sensitive to details of the reaction model, and may be reproduced quite adequately using PWIA, and reasonably simply by taking a δ-function for the nuclear wave-function. Fits to the absolute magnitudes are of much more significance as discussed in sub-section 7.8.3.

CHAPTER 8

CONCLUSIONS

This Chapter takes a broad view of the experiment, and an overall assessment is given in section 8.1. The way in which research into these reactions could usefully be developed in the future is considered in section 8.2.

8.1 Assessment of the experiment

Although it is believed that many worthwhile experimental results have been obtained, the experiment was only partially successful. The investigations into the performance of the new time of flight spectrometer were particularly disappointing as it proved impossible to improve the energy resolution beyond 1.2 MeV (f.w.h.m.) as opposed to the expected 0.5 MeV. However there is some hope for future improvement.

Nevertheless, the resolution of 1.2 MeV obtained was considerably better than the 2 MeV achieved in previous work (Saltmarsh, 1965) at this energy, and permitted the determination of the angular distributions of the cross-sections for a considerably extended range of transitions. However, a number of problems remain which could probably have been answered with a resolution of 0.5 MeV. For example, only a little new evidence of a purely experimental nature has been obtained with respect to the excitation of levels in ^{9}B other than the ground state in the $^{9}Be(p,n)^{9}B$ reaction, and the limits of error on the degree of excitation of the 0.431 MeV level in ^{7}Be in the $^{7}Li(p,n)^{7}Be$ reaction are still rather large.

Another unhappy feature of the experiment was the failure of the absolute monitoring system and this led to the possibility of error in the angular distributions which varied systematically with angle. Although it is thought likely that these errors are small, the only direct experimental conclusion was that they were probably less than 10% out to a laboratory

angle of 12.5°. Furthermore the overall absolute normalization of the cross-sections was subject to a ± 14% error.

The results are, nevertheless, felt to justify further theoretical analysis. Detailed angular distributions in the range 0-40° (lab.) have been obtained with a random error for the small angle points typically ± 5% for a wide range of transitions in the nuclei concerned.

Shape fits to the angular distributions have been successfully made using a DWBA computer code, and it is felt that the data justify further analysis along these lines to determine the isospin dependent and spin-isospin dependent terms in the nucleon-nucleon effective interaction at 100 MeV, and to compare the results with similar analyses at 30 and 50 MeV. In this context, the absolute normalization error is particularly unfortunate since it limits the accuracy with which the effective interaction can be found.

It would also be of considerable interest to determine whether the DWIA would give good fits to the results, and possibly to extend the analysis to determine the "off the energy shell" term in the nucleon-nucleon interaction.

8.2 Future developments

A wide range of (p,n) transitions to the ground states of the residual nucleus have been studied at 100 MeV by Saltmarsh (Saltmarsh, 1965), and the present experiment has performed a more penetrating study of transitions to excited states as well as the ground states of a relatively small series of 1p-shell nuclei. Consequently, there seems little scope for simply extending the range of nuclei and levels studied without making some major improvements in the experimental technique.

Future developments in the experimental study of (p,n) reactions in the region of 100 MeV may therefore be expected to concentrate on two major features:

1) a considerable improvement in energy resolution, and

2) the precise determination of absolute cross-sections.

8.2.1 Improvement in energy resolution

A significant improvement in energy resolution would considerably extend the range of transitions which could be studied. In particular many of the transitions involving $\Delta l \geq 0$ which are only weakly excited in (p,n) reactions at this energy, could be adequately separated from the background only if a considerable improvement in resolution, say to less than 0.2 MeV, were achieved. For the detailed study of these reactions, observations at wider scattering angles would be desirable.

With the present time of flight system on the synchrocyclotron, the problems which limited the resolution in the present experiment to 1.2 MeV can probably be overcome, but there seems little prospect of reducing the resolution beyond 0.5 MeV since to do this would involve either reducing the time spread of the internal proton beam to below 2ns which is likely to be impossible, or of considerably lengthening the flight path beyond the present 100m which is, at least for the present, impractical. Achieving a resolution of 0.5 MeV would be worthwhile and would justify some further experiments (in particular study of the $^{9}Be(p,n)^{9}B$ reaction), but to achieve a resolution of $\leq$ 0.2 MeV would require a timing resolution of $\leq$ 0.8 ns for a 100m flight path. Such a time spread could probably be achieved using an accelerator with very high intrinsic phase stability such as the isochronous sector-focussed cyclotron at Maryland.

8.2.2 Determination of absolute cross-sections

It was made clear in section 7.8 that there is little further point in the precise determination of the shapes of the angular distributions for the $\Delta l=0$ transitions easily observed in (p,n) reactions, but that a precise knowledge of the magnitudes of the cross-sections can enable a considerable amount of information about the nucleon-nucleon interaction within the nucleus and the nature of the wave-functions of the nuclear levels to be obtained.

The experimental difficulty in determining absolute cross-sections lies in the problem of measuring the intensity of the internal beam of the synchrocyclotron, and it was seen how an attempt to do this in the present experiment failed (Chapter 5). However, there is no reason in principle why this should be impossible, and it is strongly hoped that the problems will be overcome-perhaps along the lines suggested in Chapter 5.

Appendix A

Construction of the boron and lithium hydroxide targets

This Appendix describes the technique used for the manufacture of the boron and lithium hydroxide targets. Section A.1 discusses the difficulties involved, considers some available techniques, and explains why most were rejected. The technique finally adopted is described in section A.2.

A.1 Some available techniques

Boron

Boron is not readily available in sheet form because of its brittleness and very high melting point (2300°C). The high melting point also makes it impossible to cast in the form of a target using ordinary laboratory apparatus. Sintering is an alternative technique to casting, and requires lower temperatures, but, again, special equipment is required.

Vacuum deposition is a routine technique used for making boron targets, but the maximum thickness which can be achieved is ~50 μm, to be compared with the ~200 μm required for this experiment.

None of these techniques was as simple as the slurry method described in section A.2.

Lithium hydroxide

Lithium hydroxide is also brittle and not available in sheet form. It can, however, be melted (m.p. = 450°C) using a bunsen burner, and casting is a practical technique. This was tried, but problems were encountered as follows.

1) The low surface tension of the liquid caused it to creep up the sides of the mould, and the thickness of the resulting casting was very non-uniform. With the size (30 x 100 mm) and mean thickness (~250 μm) required, there was usually a large hole in the middle!

2) The casting tended to adhere to the 630 μm thick gold mould used, and it was usually impossible to remove in one piece. A platinum mould might have been better, but was not tried. An attempt was made to use a 50 μm thick gold mould as this could have been left adhering to the lithium hydroxide to form the gold backing mentioned in Chapter 3, section 3.3, but this mould buckled seriously on being heated.

These problems could almost certainly have been overcome by designing suitable apparatus, but, again, the slurry method was simpler.

A.2 The slurry method

Essentially this technique consists of mixing the finely powdered material with a solution of some suitable binding material to form a slurry, depositing the slurry in a mould, and allowing the solvent to evaporate. The powder is then held together by the binding material. The technique is not original, and the author is indebted to M.A. Tuplin for explaining it to him.

In the present instance, Zapon, an industrial lacquer (78 parts $C_{12}H_{16}O_6(ONO_2)_4$ + 22 parts $C_{10}H_{16}O$), was used as the binder. The boron used was already in very finely powdered form, but the lithium hydroxide was ground further using a mortar and pestle. A suitably weighed quantity (~ 2g) of boron or lithium hydroxide was then mixed with a quantity (~ 50 ml) of acetone, and 0.30 ml of a 125.6 gl^{-1} solution of Zapon in acetone was added to form the slurry mix.

The target frame with gold backing was itself used as the mould. The 50 μm thick gold foil was sandwiched between the frame and a rigid slab of aluminium, and the three were bolted together to make the assembly leakproof. The assembly was then clamped in a horizontal position and the slurry added using a bulb pipette.

It was essential, particularly with the boron target, to deposit the slurry in thin layers at a time, since if the whole amount were deposited at

once, a network of wide cracks appeared on drying, and the target tended to disintegrate. Deposition of a thin layer minimised the cracking, and any cracks which did appear could be "healed" by the deposition of further slurry inside them.

When drying was complete, the aluminium slab was carefully removed, leaving the boron or lithium hydroxide (+ Zapon) in place adhering to the gold. A thin frame was then bolted to the target frame to hold the gold firmly in place.

The thickness of the resulting targets was adequately uniform, being estimated to fluctuate by $\sim 10\%$ on a small scale, but when averaged over an area ~ 1 cm^2 to vary by $\leq 5\%$ from one part of the target to another.

The targets were fragile, but, provided they were handled carefully, were sufficiently strong for use in the experiment.

The contamination of the targets with Zapon was not serious as the Zapon constituted only 2% of the total. In the case of the boron target, the contamination did not contribute to the spectrum at all over the main region of interest since the Q-values for the (p,n) reactions on ^{12}C, ^{14}N and ^{16}O were all considerably lower than that on ^{11}B.

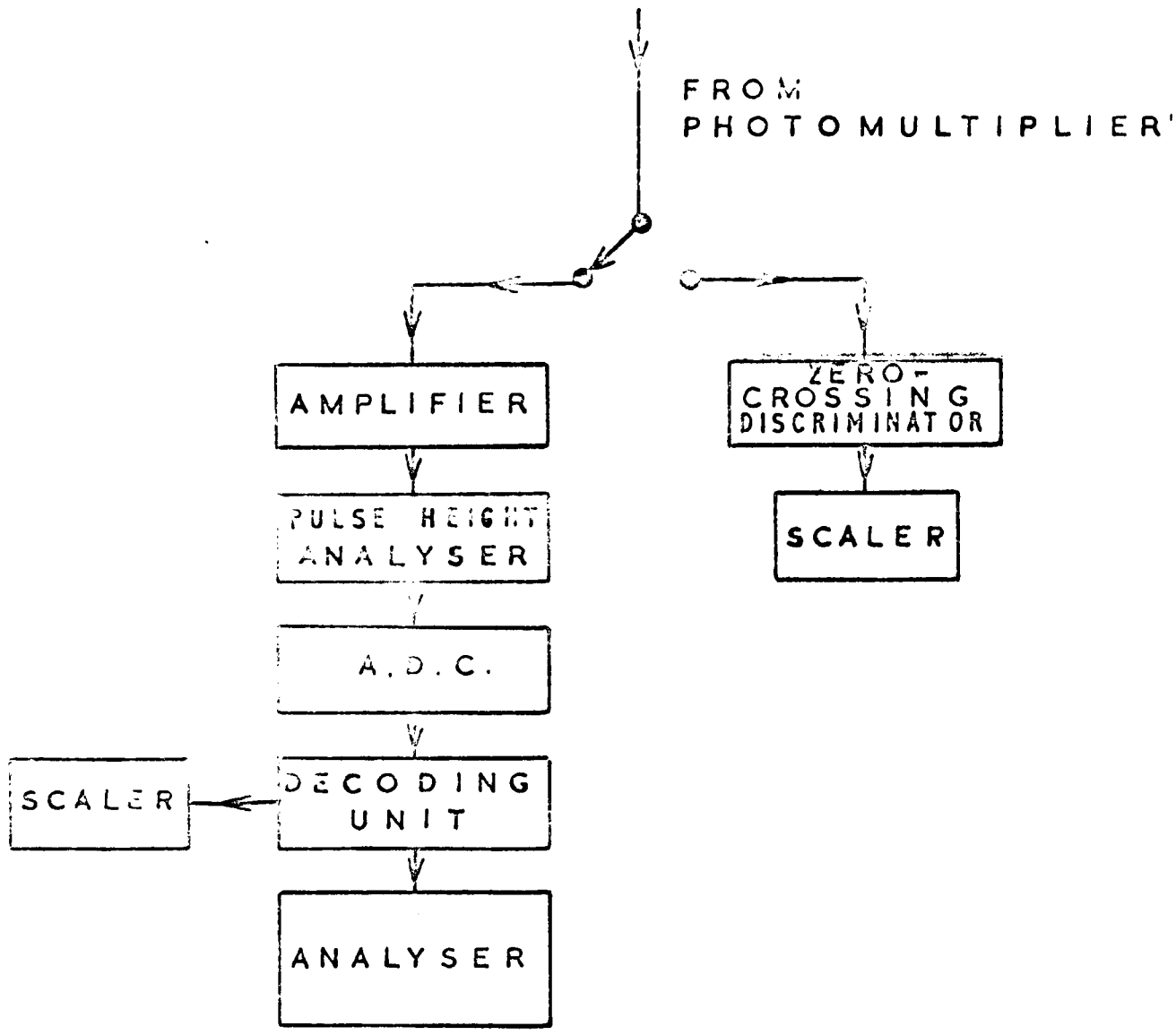

FIG. B·A. SYSTEM FOR SETTING COUNTER GAIN

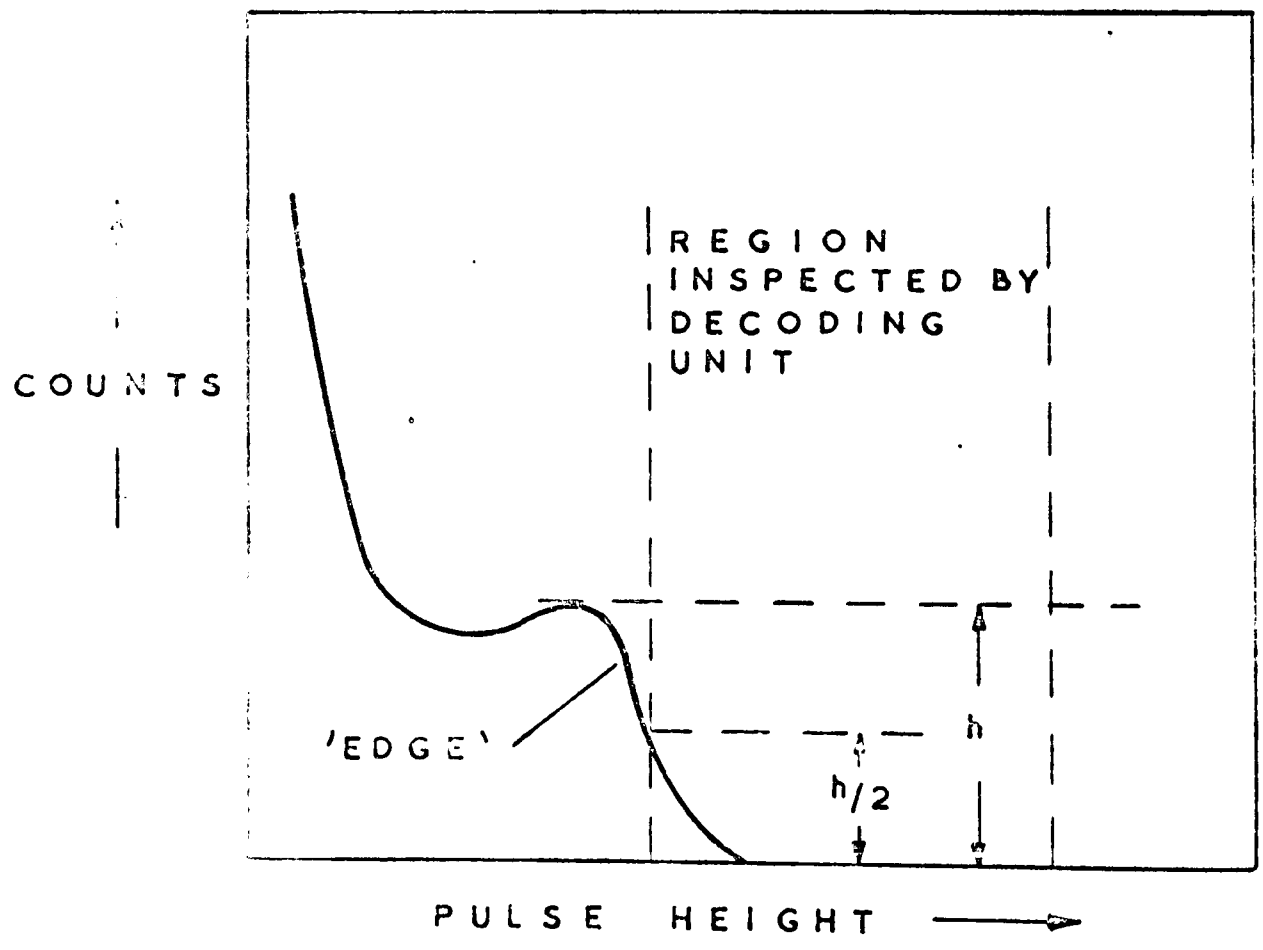

FIG. B·B. A COMPTON RECOIL SPECTRUM

Appendix B

Setting the counter gain

Since the light pulses produced in a scintillator by neutrons of a given energy can vary in height from zero to a certain maximum, it is necessary to set the gain of the photomultiplier/discriminator system by reference to a conveniently reproducible standard. This is usually done by setting the detection threshold to correspond to pulse heights produced by Compton recoil electrons from a suitable γ-decay with energies corresponding to the high energy "edge".

The γ source used in the present experiment for the main counter was ^{137}Cs, and the electronics used are shown in fig. B.A. The Compton recoil spectrum was displayed on the analyser by replacing the time of flight electronics by an amplifier, pulse height analyser, and analogue to digital converter. A typical spectrum is shown in fig. B.B. The high counting rate at low pulse heights is due to electronic "noise" in the photomultiplier tube, and the "edge" is considerably rounded. However the "half-height" position was accurately reproducible, and the counting rate from the source for pulses above this height was determined by using the decoding unit to inspect a block of the store of the analyser as indicated in the figure (B.B.)

The output from the photomultiplier was then switched to the input of the zero-crossing discriminator, and the bias level adjusted until the counting rate became the same as that above the half height.

Appendix C

Measurement of the energy variation of the detection efficiency

The variation with neutron energy of the detection efficiency of the main detector was measured during the D69 run by comparing it with that of a standard detector using a cylindrical scintillator 76 mm in diameter and 178 mm long, whose response had been previously determined (Bowen, 1962). For a given "gain" setting (see Appendix B), the energy variation of detection efficiency for a scintillation detector depends only on the geometry and nature of the scintillator, so that it was possible to use a different photomultiplier from that used in the original experiment.

The target changer was replaced inside the synchrocyclotron by a 100 mm thick block of aluminium which produced a smooth spectrum of neutron energies between 0 and 95 MeV. The main detector and the standard detector were placed side by side on a plinth in front of the beam stop in the 100 m access area. As there was only one collimator close to the target, the neutron beam was quite wide enough to encompass both detectors at this point and the areas of the aluminium block "seen" by each detector were displaced by only 0.7 mm. As a check on the uniformity of the beam intensity, the detectors were interchanged with no measurable effect.

The gain of the standard detector was set to the half height of the Compton recoil edge from the beta decay of ^{60}Co, as had been used in the original experiment, and of the main counter to that from ^{137}Cs as was used throughout the present experiment (see Appendix B).

The spectrum from only one detector at once could be stored in the analyser since the timing electronics could not be duplicated, but the total counting rates from both detectors were recorded on scalers, and these scalers constituted a continuous monitor of the beam level whichever counter

was storing in the analyser.

The experimental procedure consisted simply of storing the spectrum from first one counter and then the other for suitable lengths of time and noting the scaler contents after each count. This was repeated a number of times, and also with the positions of the detectors interchanged, to permit consistency checks. All the data were self-consistent.

The results were calculated by first applying the dead-time correction to each spectrum (Chapter 6, section 6.1) normalizing to a fixed number of "monitor" counts from the scalers, and calculating the ratios of the contents of each channel.

The fitting program (Chapter 6, section 6.4) was used to fit an analytic function to the results. The ratio varied very slowly with energy, and, multiplying by the ratios of the cross-sectional areas of the scintillators, the ratios of the efficiencies was found to be

$$\frac{\text{main counter}}{\text{standard counter}} = \frac{1.385}{1 - 6.916 \times 10^{-4}\ (T-90)}$$

where T MeV is the neutron energy.

A similar function had previously been fitted to the energy variation of the standard counter by Saltmarsh, viz.

$$\varepsilon_{\text{standard}} = \frac{0.2082}{1 + 7.245 \times 10^{-3}\ (T-90)} ,$$

so that the efficiency of the main counter was found to be given by

$$\varepsilon_{\text{main}} = \frac{0.2884}{(1 - 6.916 \times 10^{-4}\ (T-90))(1 + 7.245 \times 10^{-3}\ (T-90))}$$

REFERENCES

Ajzenberg-Selove, 1968.	F. Ajzenberg-Selove and T. Lauritsen.	Nuc. Phys. A114 (1968)1
Atkinson, 1968.	J.A. Atkinson and V.A. Madsen.	Phys. Rev. Lett. 21 (1968) 294.
Baz, 1958	A.J. Baz.	Sov. Phys. -JETP 6 (1958) 709.
Bell, 1968	R.A. Bell, P.J. Clements and A. Langsford.	AERE - R5732
Bethe, 1958	H. Bethe	Ann. of Phys. 3 (1958) 190.
Blair, 1961	J.S. Blair	Phys. Rev. 123 (1961) 2151.
Bohm, 1946	D. Bohm and L.L. Foldy.	Phys. Rev. 70 (1946)249.
Bohm, 1947	D. Bohm and L.L. Foldy	Phys. Rev. 72 (1947)649.
Bonner, 1970	B.E. Bonner.	Private communication.
Bowen, 1962	P.H. Bowen, G.C. Cox, G.B. Huxtable, A. Langsford, J.P. Scanlon G.H. Stafford and J.J. Thresher.	Nuc. Inst. Meth. 17 (1962) 117.
Bowen, 1970	P.H. Bowen	To be published.
Chew, 1950	G.F. Chew	Phys. Rev. 80 (1950) 196.
Chew, 1952, A	G.F. Chew and G.C. Wick	Phys. Rev. 85 (1952) 636.
Chew, 1952, B	G.F. Chew and M.L. Goldberger	Phys. Rev. 87 (1952) 778.
Clegg, 1965	A.B. Clegg	"High Energy Nuclear Reactions" Clarendon Press, Oxford, 1965.
Clough, 1969	A.S. Clough, C.J.Batty, B.E. Bonner, C. Tschalär, L.E. Williams and E. Friedman.	Nuc. Phys. A137 (1969) 222.
Clough, 1970	A.S. Clough, C.J. Batty B.E. Bonner, L.E.Williams	Nuc. Phys. A143 (1970) 385.

Edmonds, 1952	A.R. Edmonds, B.H. Flowers	Proc. Roy. Soc. 214 (1952) 514.
Francis, 1953	N. Francis and K.M. Watson.	Phys. Rev. 92 (1953)291.
Friedman, 1966	E. Friedman.	RHEL/R 131.
Griffith, 1965	J.A.R. Griffith, C.J. Batty, R.S.Gilmore and G.H. Stafford	Nuc. Phys. 68 (1965) 36.
Guest, 1961	P.G. Guest	"Numerical Methods of Curve Fitting", Cambridge University Press, Cambridge (1961)
Hasselgren, 1965	D. Hasselgren, P.V.Renberg O. Sundberg and G. Tibell	Nucl. Phys. 69 (1965) 81.
Hughes, 1955	D.J.Hughes and J.A.Harvey	BNL - 325(1955)
Inglis, 1962	D.R. Inglis	Nuc. Phys. 301 (1962) 1.
Jacmart, 1964	J.C. Jacmart	Thesis, University of Paris (1964).
Jahn, 1951	H.A. Jahn and H. van Wieringen	Proc. Roy. Soc. 209 (1951) 502.
Jaques, 1970	D. Jaques	Private communication.
Kerman, 1959	A.K. Kerman, H. McManus, and R.M. Thaler	Ann. of Phys. 8 (1959) 551.
König, 1962	L.A. König, J.H.E. Mattauch and A.H. Wapstra	Nuc. Phys. 31 (1962) 18.
Kretzsman, 1961	Kretzsman	Ann. Rev. Nuc. Sci. 11 (1961) 1.
Kurath, 1956	D. Kurath	Phys. Rev. 101 (1956) 216.
Lane, 1962	A.M. Lane and J.M. Soper	Nuc. Phys. 37 (1962) 663.
Langsford, 1965, A	A. Langsford, P.E. Dolley and G.B. Huxtable	Nuc. Inst. Meth. 33 (1965) 57.
Langsford, 1965, B	A. Langsford	Synchrocyclotron Group Internal Report. SCI/TP(65) 5.
Langsford, 1967, A	A. Langsford and P.E. Dolley	AERE - R5381.

Langsford, 1967, B	A. Langsford, P.H. Bowen G.C. Cox, P.E. Dolley, R.A.J. Riddle and M.J.M. Saltmarsh	Nuc. Phys. A99 (1967) 246.
Langsford, 1969	A. Langsford and M.J.M. Saltmarsh	AERE - R 6089.
Lauritsen, 1966	T. Lauritsen and F. Ajzenberg-Selove	Nuc. Phys. 78 (1966) 1.
Macefield, 1969	B.E.F. Macefield, B. Wakefield and D.H. Wilkinson	Nuc. Phys. A131 (1969) 250.
MacGregor, 1968	M.H. MacGregor R.A. Arndt and R.M. Wright	Phys. Rev. 173 (1968) 1272.
Madsen, 1966	V.A. Madsen	Nuc. Phys. 80 (1966) 177
Mahalanabis, 1964	J. Mahalanabis	Thesis, London University, 1964.
Mani, 1970	G.S. Mani	Private communication.
Nguyen Ngoc, 1963 - see below.		
Powell, 1965	M.J.D. Powell	Computer Journal 7 (1965) 303
Riesenfeld, 1958	W.B. Riesenfeld and K.M. Watson	Phys. Rev. 102 (1956) 1157.
Saltmarsh, 1965	M.J.M. Saltmarsh	Thesis, Oxford University, 1965.
Sanada, 1970	J. Sanada.	Journ. Phys. Soc. Japan 28 (1970) 524.
Satchler, 1964	G.R. Satchler, R.M. Drisko and R.H. Bassel.	Phys. Rev. 136 (1964) B637.
Satchler, 1966	G.R. Satchler	Nuc. Phys. 77 (1966) 481.
Scanlon, 1957	J.P. Scanlon, G.H. Stafford, J.J. Thresher and P.H.Bowen	Rev. Sci. Inst. 28 (1957) 191.
Scanlon, 1970, A	J.P. Scanlon	To be published.
Scanlon, 1970, B	J.P. Scanlon	Private communication.
Nguyen Ngoc, 1963	H.Nguyen Ngoc, M.Hors, and J.Perez y Jorba	Nuc. Phys. 42 (1963) 62

de-Shalit, 1963	A. de-Shalit and I. Talmi.	"Nuclear Shell Theory" Academic Press, New York and London, 1963.
Spencer, 1960	R.R. Spencer, G.C. Phillips, and T.E. Young.	Nuc. Phys. 21 (1960) 310.
Taylor, 1970	A.E. Taylor	AERE - R 6448
Thurlow, 1968	N. Thurlow	Nuc. Phys. A109 (1968) 471.
Watson, 1953	K.M. Watson	Phys. Rev. 89 (1953) 575.
Wigan, 1967	M.R. Wigan	Thesis, Oxford University, 1967.
Wigan, 1968	M.R. Wigan, R.A. Bell, P.J. Martin, O.N. Jarvis and J.P. Scanlon.	Nuc. Phys. A114 (1968)
Zafiratos, 1965	C.D. Zafiratos, F. Ajzenberg-Selove, and F.S. Dietrich.	Phys. Rev. 137 (1965)